INFORMATION TO USERS

This manuscript has been reproduced from the microfilm master. UMI films the text directly from the original or copy submitted. Thus, some thesis and dissertation copies are in typewriter face, while others may be from any type of computer printer.

The quality of this reproduction is dependent upon the quality of the copy submitted. Broken or indistinct print, colored or poor quality illustrations and photographs, print bleedthrough, substandard margins, and improper alignment can adversely affect reproduction.

In the unlikely event that the author did not send UMI a complete manuscript and there are missing pages, these will be noted. Also, if unauthorized copyright material had to be removed, a note will indicate the deletion.

Oversize materials (e.g., maps, drawings, charts) are reproduced by sectioning the original, beginning at the upper left-hand corner and continuing from left to right in equal sections with small overlaps. Each original is also photographed in one exposure and is included in reduced form at the back of the book.

Photographs included in the original manuscript have been reproduced xerographically in this copy. Higher quality 6" x 9" black and white photographic prints are available for any photographs or illustrations appearing in this copy for an additional charge. Contact UMI directly to order.

UMI

A Bell & Howell Information Company
300 North Zeeb Road, Ann Arbor MI 48106-1346 USA
313/761-4700 800/521-0600

Université d'Ottawa · University of Ottawa

HYDROTHERMAL ACTIVITY IN A CORAL REEF ECOSYSTEM, TUTUM BAY, AMBITLE ISLAND, PAPUA NEW GUINEA

Thomas Pichler

A Thesis submitted to the School of Graduate Studies and Research in partial fulfillment of the requirements for the Ph.D. Degree: Science

Ottawa-Carleton Geoscience Centre
University of Ottawa

ABSTRACT

Previous research on sea floor hydrothermal activity has focused primarily on deep-sea, polymetallic sulfides found along volcanically active portions of the mid-ocean ridges or in deep back-arc basins. There is, however, not much known about either hydrothermal venting or its petrologic definition within shallow-water (nearshore or shallow shelf) carbonate settings associated with volcanic islands.

The fringing reef around Ambitle Island, Papua New Guinea is possibly the only present day coral reef exposed to the extensive discharge of a hot, mineralized hydrothermal fluid. Venting occurs in shallow (5-10 m) water along the inner shelf that contains a patchy distribution of coral-algal reefs. Two types of venting are observed: (1) focused discharge of a clear, two-phase fluid from discrete orifices, 10-15 cm in diameter with discharge temperatures from 89 to 98°C and estimated flow rates as high as 300 to 400 L/min; (2) dispersed or diffuse discharge that consists of streams of gas bubbles ubiquitous throughout area. The composition of the gas is mainly CO_2 (92.6 - 97.9 %) with minor amounts of N_2, O_2, CH_4 and He. Compared to seawater the hydrothermal fluids are depleted in Cl, Br, SO_4, Na, K, Ca, Mg and Sr and enriched in HCO_3, B, Si, Li, Mn, Fe, Rb, Cs, Sb, Tl and As. Although some elements are significantly enriched, they do not have a clear impact on ambient seawater composition because their concentration is buffered by mixing and uptake into secondary minerals. Only the surface water in Tutum Bay carries a clear imprint of the hydrothermal fluids.

Fluid evolution and final chemical composition is controlled by a two- or possibly three-step process: (1) Phase separation in the deep reservoir beneath Ambitle Island produces a high temperature vapor that rises upward and subsequently reacts with cooler ground water to form a low pH, CO_2-rich water of approximately 150-160°C. (2) The steep topography causes lateral movement of this CO_2-rich fluid towards the margin of the hydrothermal system where it mixes with the marginal upflow from the deep reservoir. This produces a dilute chloride water of approximately 165°C. A third step may be the entrainment by minor amounts of ground or

seawater during its final ascent. Based on a B-Rb/Cs mixing model, it has been estimated that approximately 10% of the deep reservoir fluid reaches the surface.

Aragonite, ferroan calcite and Fe(III) oxyhydroxide are the prominent hydrothermal precipitates in Tutum Bay. Aragonite encrusts dead coral fragments, volcaniclastic boulders and pebbles, and fills secondary fracture and remaining primary intergranular porosity within volcaniclastic arenite. Microcrystalline (0.1 mm) ferroan, low-Mg calcite occurs as crusts commonly interlaminated with Fe(III) oxyhydroxides and also locally replacing aragonite adjacent to Fe(III) oxyhydroxides. Precipitation from the hydrothermal solution is caused by CO_2 degassing (aragonite) and mixing with seawater (Fe(III) oxyhydroxide). Hydrothermal deposits are unique in their chemical composition. Compared to "normal-marine" shallow-water carbonate the Ambitle aragonite displays anomalous Sr isotope ratios (~0.70415) that are closer to island-arc basalt than to seawater (~0.7092). Fe(III) oxyhydroxide shows very low Mn values (Fe/Mn>600) and elements which are usually enriched in Fe(III) oxyhydroxide, such as Co and V, are below crustal abundances and well below their concentrations in island-arc volcanics.

The hydrothermal fluids contain extremely high arsenic concentrations of more than 800 ppb. Seven individual vents in four different areas within Tutum Bay discharge an estimated 1500 g of arsenic per day into an area of approximately 50 by 100 m with an average depth of 6 m. These values are the highest arsenic concentrations reported from any marine setting including black smoker fluids from mid-ocean ridges. Despite the amount of arsenic released into the bay, corals, clams and fish do not show a direct response to the elevated values. Fish have been observed to hover over vent orifices bathing in the hydrothermal fluid. The diversity and health of the coral reef is indiscernible from reefs that are not exposed to hydrothermal discharge.

Two mechanisms efficiently control and buffer the arsenic concentration: (1) dilution by seawater and (2) incorporation in and adsorption on Fe(III) oxyhydroxides that precipitate when the hydrothermal fluids mix with ambient seawater. The hydrothermal fluids have a pH

of ~6 and are slightly reducing. These conditions are ideal for the removal of As by way of coprecipitation and/or adsorption onto Fe(III) oxyhydroxide. The Fe(III) oxyhydroxides that precipitate in Tutum Bay can contain up to 75,000 ppm As, by an order of magnitude the highest As values found in a natural system.

The skeletons of scleractinian corals and the shells of *Tridacna gigas* clams do not show elevated concentrations of arsenic when compared to specimens collected from outside Tutum Bay. When compared to a "non-hydrothermal" coral, Tutum Bay corals, however, they possess a distinct $\delta^{13}C$, $\delta^{18}O$, $^{87}Sr/^{86}Sr$ and Sr signature. $\delta^{13}C$ ranges from -4.5 to -1.0‰ and $\delta^{18}O$ from -6.0 to -3.8‰ for corals from Tutum Bay, while the "non-hydrothermal" sample has $\delta^{13}C$ values ranging from -1.8 to -0.5‰, and $\delta^{18}O$ values of -5.4 to -4.6‰. Strontium isotope ratios are very close to seawater values, but the three samples from Tutum Bay have $^{87}Sr/^{86}Sr$ lower than the "non-hydrothermal" sample. The observed isotope and elemental Sr patterns indicate that the hydrothermal input into Tutum Bay clearly influences the coral growth in the surrounding reef. Of the various direct and indirect hydrothermal effects recorded by the corals, thermal stress is likely the single most important.

RÉSUMÉ

Les études antérieures sur l'activité hydrothermale dans les hautes mers concernaient en premier lieu les sulfures polymetalliques des fonds océaniques rencontrés le long des zones rides midio-océaniques volcaniques actives ou bien dans les bassins arrière arc. Cependant, peu est connu sur les vents hydrothermaux et leurs définitions pétrologiques à l'intérieur des zones des carbonates de faible profondeur (plateau de faible profondeur) associées aux îles volcaniques.

Le récif frangeant autour de l'île Ambite, Papua , Nouvelle Guinée, est possiblement le seul récif corallien exposé à une décharge extensive de fluide hydrothermal minéralisé. La décharge a lieu dans les eaux de faible profondeur (5-10 m) lelong du plateau intérieur qui contient des algues et des récifs coralliens dispersés. Deux types de vents sont observés; 1°) ceux présentant une décharge ponctuelle à partir d'orifices discrets (10-15 cm de diamètre). Dans ce cas deux types de liquides sont rencontrés et dont les températures varient entre 89 et 98°C, ils pr.sentent un flux pouvant atteindre 300 à 400 L/min et 2°) ceux présentant une décharge diffuse et dispersée consistant en des bulles de gas. La composition du gaz est principalement CO_2 (92.6-97.9 %) avec de faible teneurs en N_2, O_2, CH_4 et He. En comparaison avec l'eau marine, les fluides hydrothermaux sont appauvris en , Cl, Br, SO_2, Na, K, Mg, et Sr et enrichis en HCO_3, B, Si, Li, Mn, Fe, Rb, Cs, Sb, Tl et As. Même si certains éléments présentent des concentrations élevées, ils ne présentent aucun impact sur la composition de l'eau marine car leur concentration est stabilisée par le mélange avec l'eau marine et le fractionnement dans les minéraux secondaires. Seule l'eau de surface à la Baie de Tutum présente la signature des fluides hydrothermaux.

L'évolution et la composition finale des fluides hydrothermaux sont contrôlées par deux ou possiblement trois processus pendant trois étapes; la première étape représente la phase de séparation dans le réservoir profond sous l'île Ambite produisant une vapeur de haute température qui progresse vers le haut en réagissant avec des eaux souterraines de température

plus basse formant ainsi des eaux de faible pH et riche en CO_2, cette eau présente une température variant entre 150-160°C. Dans la deuxième phase, la topographie escarpée provoque un mouvement latéral de ce fluide riche en CO_2 vers la marge du système hydrothermal où il se mélange avec le flux marginal montant du réservoir. Ceci produit une eau de température approximativement de 165°C et de faible teneur en chlore. La troisième étape peut être expliquée par le transport par de faible quantité d'eau souterraine dans sa montée finale. En se basant sur les rapports B-Rb/Cs dans le modèle de mélange, on estime qu'à peu près 10% du fluide du réservoir profond atteint la surface.

L'aragonite, la calcite ferrugineuse et les oxydes et hydroxydes de fer (Fe(III)) sont lescplus importants précipités dans la Baie Tutum. L'aragonite encroûte les fragments de coraux morts, des galets et des fragments volcanoclastiques. Elle remplie les fractures secondaires et la porosité primaire intergranulaire dans l'arénite volcanoclastique. La calcite microcrystalline ferrugineuse et de faible teneur en Mg se présente comme une croûte communément interlaminée avec des oxydes et hydroxydes de Fe(III) et des fois remplaçant l'aragonite adjacente en oxydes et hydroxydes de Fe(III). La précipitation à partir des solutions hydrothermales est due au dégazage de CO_2 (aragonite) et au mélange avec l'eau marine (oxydes et hydroxydes de Fe(III)). Les dépôts hydrothermaux présentent une composition unique. Comparés avec les carbonates de faible profondeur des eaux marines (normales), l'aragonite de l'île Ambitle montre une signature isotopique du Sr (~0.70415) proche de celle des basaltes des îles océaniques que de celle de l'eau marine (~0.7092). Les oxydes et hydroxydes de Fe(III) montrent une faible teneur en Mn (Fe/Mn>600) et en éléments qui sont souvent très abondants dans les oxydes et hydroxydes de Fe(III) telsque le Co et V qui présentent des concentrations inférieures à celle de la croûte et très faible par rapport à leur concentrations dans les îles volcaniques.

Les fluides hydrothermaux présentent des concentrations extrêmement élevées d'arsenic pouvant aller au-delà de 800 ppb. Sept vents individuels dans quatre zones différentes dans la région de la Baie Tutum déchargent environ 1500 g d'arsenic par jour dans une région

d'environ 50 par 100 m et de profondeur moyenne de 6 m. Ces valeurs correspondent aux concentrations d'arsenic les plus élevées jamais notées dans un environnement marin y compris les fluides dérivant des cheminées noires dans les rides midio-océaniques. Malgré cette décharge massive d'arsenic dans la Baie, les coraux, les mollusques et les poissons ne montrent aucune réponse. La diversité faunistique et la bonne conservation du récif corallien est indiscernable des récifs qui ne sont pas exposés aux décharges hydrothermales.
Deux mécanismes contrôlent et stabilisent la concentration en arsenic: 1) dilution par l'eau marine et 2) l'incorporation et l'adsorption sur les oxydes te les hydroxydes de Fe (III) qui précipitent lorsque les fluides hydrothermaux se mélangent avec l'eau marine environnante. Les fluides hydrothermaux ont un pH de ~6 et sont peu réducteurs. Ces conditions sont idéales pour l'élimination de l'arsenic par coprecipitation et/ou adsorption sur les oxydes et hydroxydes de Fe(III). Les hydroxydes de Fe(III) qui précipitent à la Baie Tutum peuvent contenir jusqu'à 75,000 ppm d'arsenic représentant ainsi les teneurs en As jamais rencontrées dans un système naturel.

Les squelettes des madréporaires et les coquilles de *Tridacna gigas* ne montrent pas des concentrations élevées en As lorsque ceux-ci sont comparés aux spécimens collectés de l'extérieur de la Baie Tutum. La comparaison des coraux de Tutum Baie avec des coraux (non hydrothermaux) montre que ces derniers possèdent des signatures isotopiques $\delta^{13}C$, $\delta^{18}O$, $^{87}Sr/^{86}Sr$ différentes. Pour les Coraux de la Baie Tutum $\delta^{13}C$ varie de -4.5 à -1.0‰ et $\delta^{18}O$ varie de -6.0 à -3.8‰, alors que pour les coraux (non hydrothermaux) $\delta^{13}C$ présente des valeurs allant de -1.8 à -0.5‰ et des valeurs $\delta^{18}O$ allant de -5.4 à -4.6‰. Les rapports isotopiques de Sr sont très proches de ceux de l'eau marine, mais les trois échantillons de la Baie Tutum ont un $^{87}Sr/^{86}Sr$ inférieur à celui du coral (non hydrothermal). Les profils d'isotopes de Sr et de l'élément Sr montrent que les décharges hydrothermales dans la Baie de Tutum influencent la croissance des coraux dans les récifs coralliens qu'ils l'entourent. Des effets hydrothermaux directs et indirects enregistrés par les coraux, le stress thermique est le plus important.

ACKNOWLEDGMENTS

WOW, it's done! Looking back and realizing how many have contributed and helped, seems to make it impossible to thank everybody without letting this part become longer than the thesis itself. I would like to apologize to all I cannot or forgot to mention, but to whom I am very grateful for their help and support. However, there were some who went out of their way in order to help me to achieve my goals and those I would like to mention individually.

First of all thanks to Manfred Grün, who talked me into getting the type of high school degree necessary to study science at a German University. Otherwise, I would have ended up studying most likely accounting or something similarly exciting. When I was still at Carleton University George Dix sparked the interest that eventually led to this study and Claudia Schröder-Adams is thanked for her spiritual, financial and intellectual support. I thank the professors, staff, graduate and undergraduate students at the Earth Sciences Department, University of Ottawa, for providing a truly pleasant working atmosphere. Technical support was excellent. In particular, I would like to mention Ian Clark, Danielle Fortin and Keiko Hattori for the fruitful discussions we had. Larbi El Bilali translated my abstract into French - THANKS! Gwendy Hall and her staff at the Geological Survey of Canada did a great job analyzing my (difficult) water samples. Mike Risk and Jeff Heikoop, McMaster University, are thanked for their collaboration and in particular for their patience, while teaching me all about corals. My field assistants, Stan, Daniel, Donna and Yannick, had to work insane hours and endure my company while in the field. The inhabitants of Ambitle Island were always friendly and supportive during my visits. Philip Tolain is thanked for his company and our trips to the jungle.

Most of the thesis research was funded by an American Chemical Society, Petroleum Research Grant (No. 31585-AC8) and Natural Sciences and Engineering Research Council of Canada operating grant to Jan Veizer. But I would also like to acknowledge the support of two

Geological Society of America, Student Research Grants (No. 5681-95 and 5904-96) and a Society of Economic Geologists Mc Kinstry Scholarship that were awarded to me.

For the quality of the final copy I am in debt to my committee, Claudia Schröder-Adams, Keiko Hattori, John Blenkinsop and Robin Renaut. Their input improved the quality of my work. Now, how do I feel about my supervisor (Super-Veizer)? Imagine a little bird that fell out of its nest. Now it sits screaming and hungry on the road just waiting to be run-over by a car or digested by a cat. The end is almost inevitable, but suddenly this nice little old lady comes by, picks up the bird and takes it home to provide food and shelter. The way that little bird must feel towards the nice old lady that is exactly how I feel about my supervisor. When I was all alone, with nothing but a crazy idea to study shallow-water hydrothermal springs in a coral reef, he picked me up and provided everything necessary to successfully complete my work.

A very big share in the success of this study belongs to my parents, Josef and Helene, my aunts, Edda and Martha, my grandmothers Elisabeth and Theresia, and my grandfather Josef. They always supported me and made it possible for me to study abroad. A big share in the final success of this work, however, belongs to my wife Cristina. Her love and understanding have little limits; she endures my unusual working hours and long absence during fieldwork without complain (almost no complain). But most of all she believed in me and whenever I had lost that belief myself, she gave me the necessary strength to go on.

TABLE OF CONTENTS

LIST OF TABLES

LIST OF FIGURES

ORIGINAL CONTRIBUTION

The original contributions of this thesis to the scientific body include:

1. First scientific description of the shallow-water hydrothermal system in Tutum Bay, Papua New Guinea.
2. A database of chemical and isotopic analyses based on laboratory and field work for the hydrothermal fluids.
3. Petrographic description and database of chemical and isotopic analyses based on laboratory work for the hydrothermal carbonates and Fe(III) oxyhydroxides.
4. A database of chemical and isotopic analyses based on laboratory work for Tutum Bay *Porites* corals.
5. A model for the origin and subsurface history of Tutum Bay vent waters.
6. Precipitation model for carbonate minerals and Fe(III) oxyhydroxides based on $^{87}Sr/^{86}Sr$ ratios.
7. Evaluation of $\delta^{18}O$ and $\delta^{13}C$ equilibrium during carbonate precipitation from the hydrothermal fluid.
8. Qualitative reconstruction of physico-chemical vent processes based on the nature of hydrothermal precipitates.
9. Estimated influence of vent discharges on ambient seawater in Tutum Bay using silica concentration as a tracer.
10. Demonstration that corals are capable to record the hydrothermal influence in their trace element and isotope composition.

1. INTRODUCTION

1.1 GENERAL STATEMENT

Most studies of seafloor hydrothermal activity have focused primarily on deep-sea hydrothermal systems found along volcanically active portions of the mid-ocean ridges or in deep back-arc basins. Submarine hydrothermal activity and hydrothermal alteration of oceanic crust, however, is not confined to deep-water environments. Additional locations are found in much shallower water at the flanks of volcanic islands and on the tops of seamounts (e.g., Butterfield et al., 1990; Dando and Leahy, 1993; Heikoop et al., 1996a; Hodkinson et al., 1994; Pichler et al., 1995; Sarano et al., 1989; Sedwick and Stüben, 1996; Varnavas and Cronan, 1991; Vidal et al., 1981; Vidal et al., 1978). Our understanding of these shallower systems is limited and we are only now starting to appreciate their importance on a bigger scale. Much less is known about shallow-water venting in nearshore or shallow shelf coral reef settings associated with volcanic islands, where substantial input of hydrothermal fluids can affect the temperature, salinity and carbonate saturation state of ambient seawater. Shallow venting may cause significant differences in petrologic and chemical properties of marine abiotic and biogenic carbonates, if compared to the well known submarine carbonate diagenesis in shallow-water tropical environments (Tucker and Wright, 1990). Such differences arise from mixing of hydrothermal fluids and seawater, a process that exerts physical and chemical impact superimposed on the usual oceanographic controls that regulate biological productivity and sedimentation (Tucker and Wright, 1990). This "new" carbonate environment may be more applicable to the understanding of submarine diagenesis in ancient shallow-water carbonates from tectonically active regions, oceanic islands, or basins with high heat flow.

This thesis is a broad reconnaissance study of newly discovered vents that discharge in a tropical, shallow-water coral reef ecosystem. Its purpose is to develop a descriptive model for physical and chemical vent processes (Chapter 2), to examine in detail the style of

hydrothermal precipitation (Chapters 3 & 4), to document temporal changes (Chapter 5), to investigate the hydrothermal effect on ambient seawater (Chapter 6) and to describe biological response to hydrothermal influences (Chapter 7). A study of this location is the first step to evaluate the global and historical importance of hydrothermal activity in coral reef settings and to expand our basic understanding of carbonate diagenesis.

1.2 LOCATION AND GEOLOGICAL SETTING

The study area lies along the southwest margin of Ambitle Island, one of the Feni islands in the southernmost island group of the Tabar-Feni chain, Papua New Guinea (Fig. 1-1). The islands of the Tabar-Feni chain are Pliocene-to-Recent alkaline volcanoes that occur in the forearc region of the former ensimatic New Hanover-New Ireland-Bougainville island arc (Fig. 1-1). The volcanoes erupt an unusual suite of silica-undersaturated, high-K calc-alkaline lavas generated during adiabatic decompression melting during the uplift of the New Ireland forearc basin (McInnes and Cameron, 1994). Subaerial volcanic rocks have wide-ranging compositions from primary basanites and alkali olivine basalts to fractionated phonolites (Wallace et al., 1983). The last stage in the volcanic evolution of the volcanic islands is the emplacement of silica-saturated cumulodomes of trachyte.

The Tabar-Feni volcanoes stand apart from the surrounding arc volcanoes of New Ireland and New Britain in that they have a proclivity towards producing Au mineralization as epitomized by the world-class Ladolam Au deposit (40 million oz) on Lihir Island (Fig. 1-1) (Davies and Ballantyne, 1987). The deposit is hosted within the geothermally active 4 x 6 km diameter Luise Caldera, which is thought to have suffered sector collapse and partial inundation by seawater. In addition to Lihir every other island group has been or currently is an exploration target for epithermal gold deposits. The Kabang prospect on Ambitle Island, for

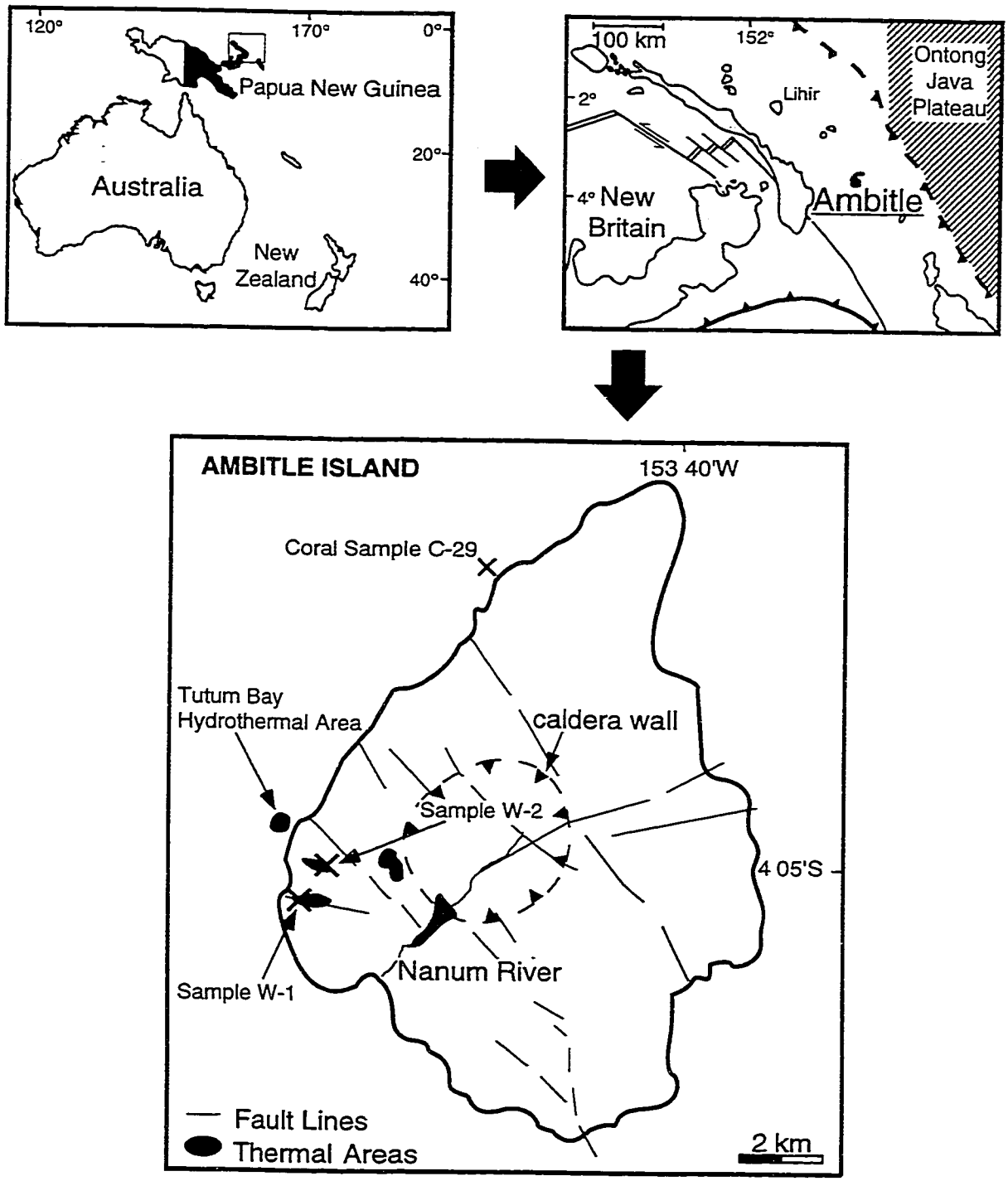

Fig. 1-1 Location of Ambitle Island, one of the Feni islands in eastern Papua New Guinea (modified after Licence et al., 1987). Geothermal areas indicated in dark are primarily along the western side of the island.

example, contains ore grades up to 5 g/t with concentrations as high as 50 g/t in silica sinters (Licence et al., 1987).

Ambitle is part of a Quaternary stratovolcano, characterized by a steep topography, with a central eroded caldera built on poorly exposed Oligocene marine limestone (Wallace et al., 1983). Volcanic strata (interbedded lava flows, lahar deposits, tuffs, and scoriae) dip radially from the island, presumably extending beneath the shelf. Several geothermal areas are located primarily along the western coast and in the western part of the caldera near breaches in the caldera wall (Fig. 1-1). Hot mud pools, springs of chloride and acid sulfate waters, and a few low temperature fumaroles are present, with temperature and pH values ranging from 67 to 100 °C and 1.9 to 9.1, respectively (Wallace et al., 1983). Except for the southern coast, where extensive fresh water input inhibits reef development, the island is completely surrounded by a fringing coral reef that can extend up to several hundred meters offshore.

1.3 THE TUTUM BAY SUBMARINE HOT SPRINGS

Submarine hydrothermal venting occurs at Tutum Bay (Figs. 1-2 and 1-3) in shallow (5-10 m) water along the inner shelf that contains a patchy distribution of coral-algal reefs surrounded by medium to coarse-grained mixed carbonate-volcaniclastic sand and gravel. The site is located along a fault trace that intersects several of the onland geothermal areas (Fig. 1-1).

Two types of venting are observed. (1) Focused discharge of a clear, two-phase fluid occurs from discrete orifices, 10-15 cm in diameter, with phase separation (boiling) at the sea floor. There is no associated topographic edifice. This type of discharge produces a roaring sound underwater and has an estimated flow rate as high as 300 to 400 L/min (comparable to that of a fire hose). Shimmering and a whitish coloration, indicative of hot water and water vapor, extend several meters above vent orifices (Fig. 1-4a). Fluid temperatures at vent orifices

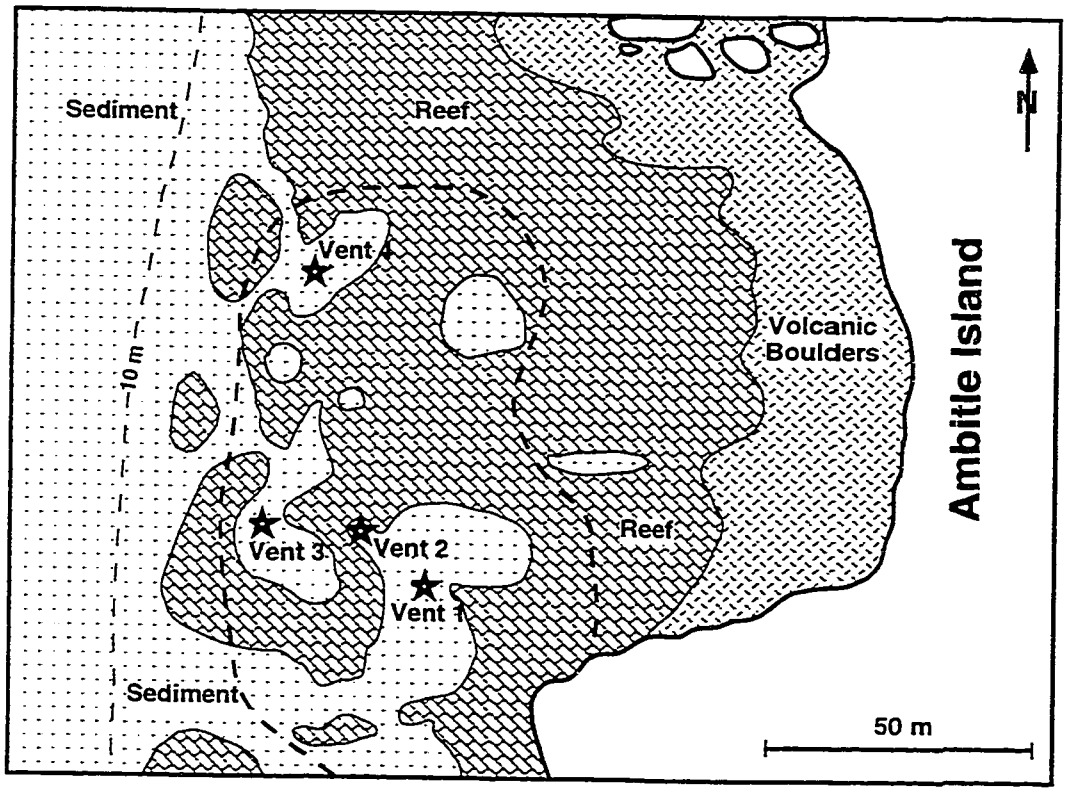

Fig. 1-2 Location of hydrothermal vents within Tutum Bay on the west side of Ambitle Island. The bold dashed line indicates the extent of gaseous discharge."

Fig. 1-3 Location of Tutum Bay. (a) Aerial view of the southwest corner of Ambitle Island; Tutum Bay is indicated by the arrow. (b) Looking south across Tutum Bay. The white buoy indicates the location of vent 2. Vents 1 and 3 can be recognized on the surface by relatively flat water to the right and left of vent 2.


a


b

Fig. 1-4 Underwater photographs of focused discharge in Tutum Bay. (a) Vent 1. Hydrothermal fluids discharge at an approximate rate of 400 L/min. Mixing with ambient seawater is minimal at the vent orifice, but increases as the fluid rises. The discharge of gas is present in form of bubble streams. The field of view is ~18 m at a water depth of ~ 7 m. (b) Vent 3. Three individual vents discharge a mixture of hydrothermal fluid and gas. Bubble streams are not as dense as around vent 1 and the immediate area around vent sites is devoid of corals. The field of view is ~ 8 m at a water depth of 9 m.

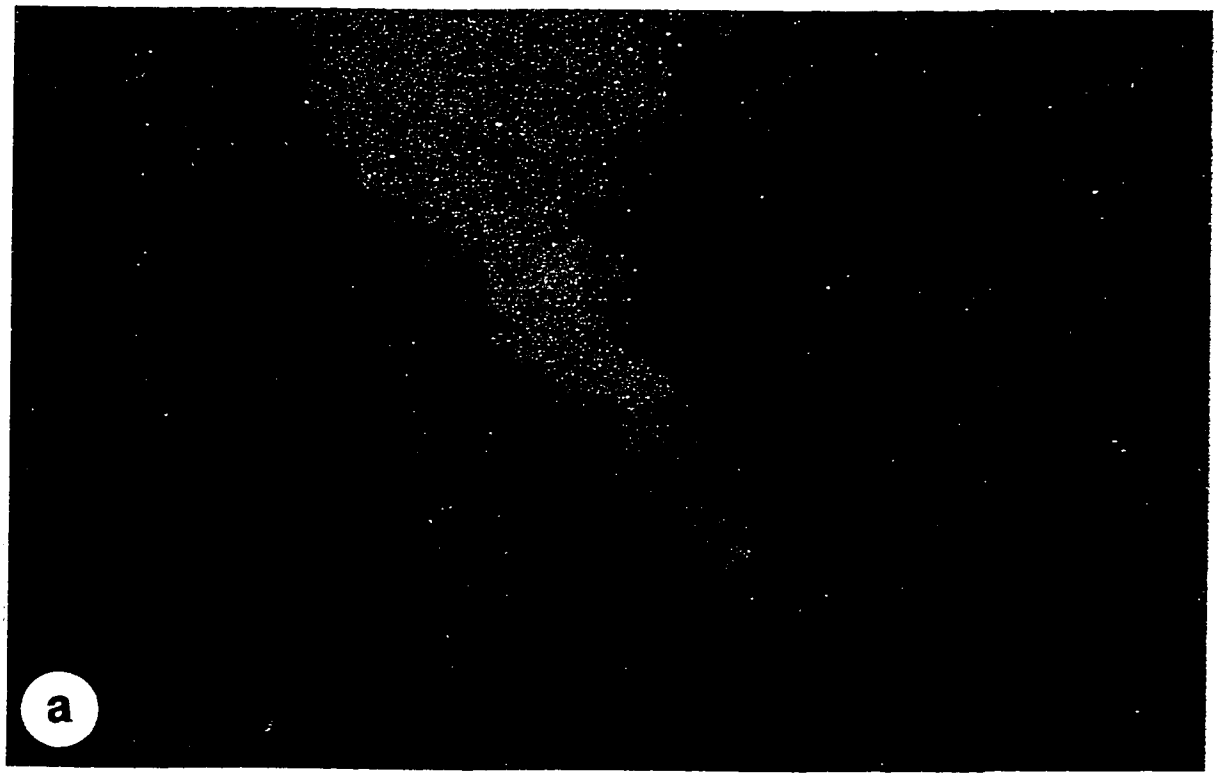
a


b

are between 89 and 94 °C. (2) Dispersed or diffuse discharge consists of streams of gas bubbles emerging directly through the sandy to pebbly unconsolidated sediment and through fractures in volcanic rocks (Fig. 1-5b). This type of venting appears to be itinerant, with shifts in locations on the order of tens of centimeters, possibly related to tortuous migration through the surface sediment.

Four locations of focused venting are present in Tutum Bay (Fig. 1-2). Vents 1 and 2 are single vents with hydrothermal discharge from only one orifice (Fig. 1-4a) and vent 3 is an assemblage of three vents that are very close together in an area of approximately 2 x 2 m (Fig. 1-4b). Vent 4 is located some distance north of these vents (Fig. 1-2) and it is closely associated with an area of massive gas emanation (Fig. 1-5a). Vent 4 is slightly different from the other vents; there shimmering hot water discharges at low rates through several small orifices (1 to 5 cm in diameter) in an area of approximately 1 x 3 m. Based on their geographic position the vents have been divided into two groups A and B; area A consists of vents 1, 2 and 3 and area B of vent 4 (Fig. 1-2).

Hydrothermal precipitates accumulate on dead coral substrate and rock fragments surrounding vent portals and include euhedral aragonite crystals and microcrystalline crusts of Fe(III) oxyhydroxide, aragonite, and ferroan calcite.

Visually, the coral reef in Tutum Bay seems to be indiscernible from its neighboring reefs to the north or south. Several bleached corals are present, but partly or wholly bleached corals are common to all reefs along the west coast of Ambitle and can be found in most reefs in the equatorial region of the western Pacific. There is no correlation between coral bleaching and distance from vent sites, and healthy corals can be found very close (< 1 m) to vent orifices. Rather than by the discharge of hydrothermal fluids the distribution of corals vs. sand is controlled by seafloor temperature. Seafloor temperatures in sandy areas can be as high as 98°C and are generally more than 35°C, rapidly increasing with depth. A similar phenomenon can be observed in on-land geothermal areas. In Wairakei, New Zealand, for example, the

Fig. 1-5 Underwater photographs of diffuse and gaseous discharge in Tutum Bay. (a) Vent 4. Here several vents discharge at a low rate and can be recognized by shimmering in-between the bubble streams. Similar to vent 3, no reef building corals are present in the area. Volcanic boulders, however, are colonized by flower corals (*Xenia sp.*). The field of view is ~8 m at a water depth of 9 m. (b) View across the reef to the southwest of vent 1. Gas discharge is ubiquitous, but the health of the surrounding corals is obviously not compromised.

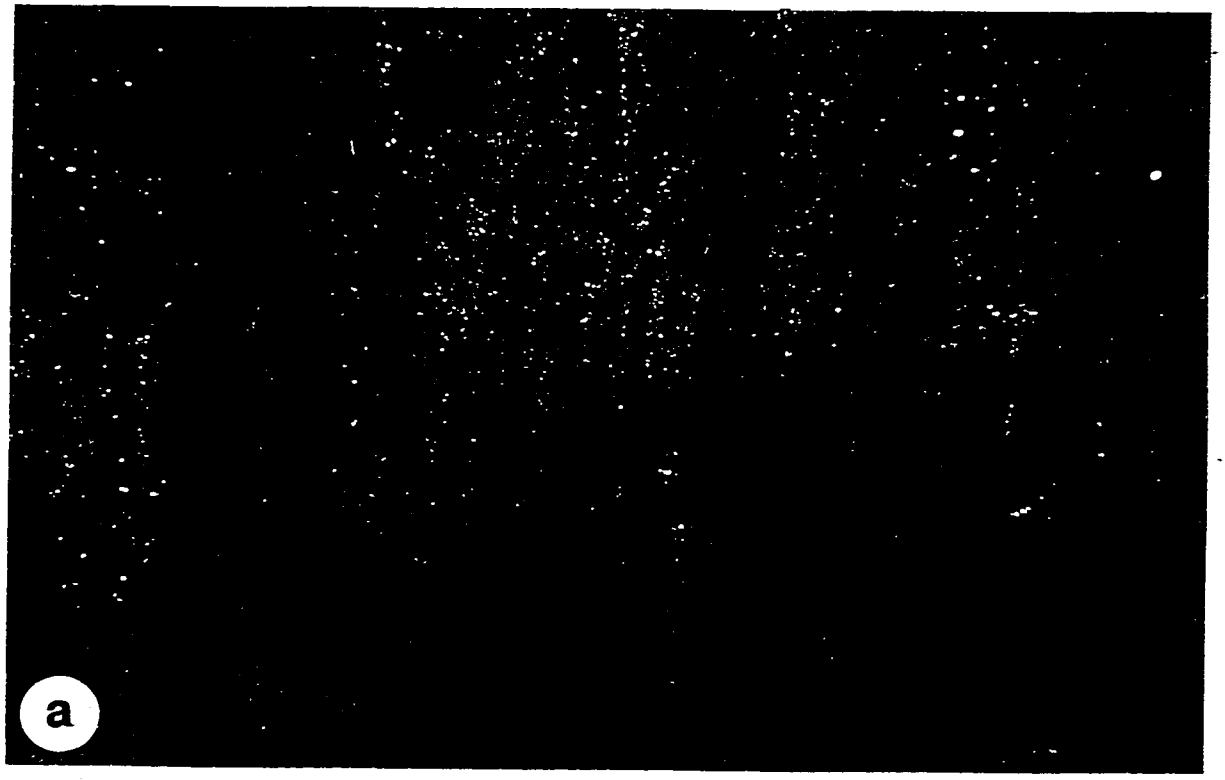
a

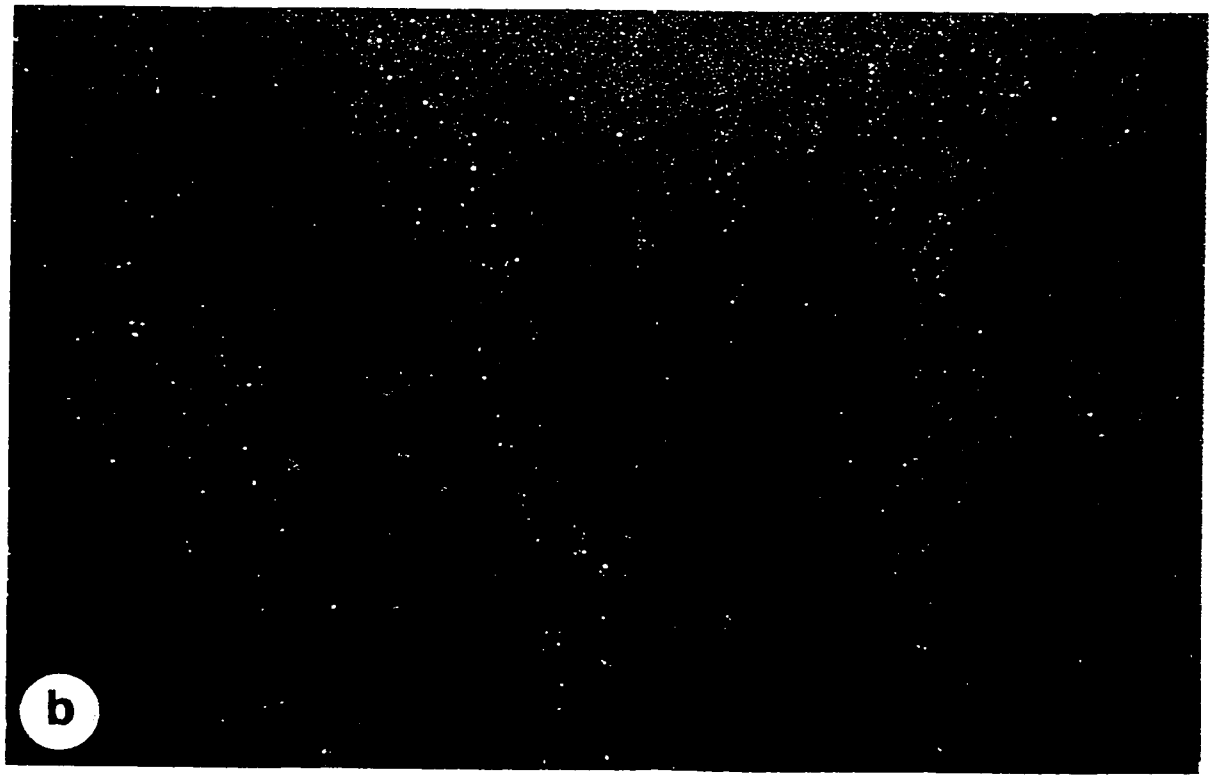
b

distribution and height of vegetation is closely controlled by ground temperature (Burns, 1997). *Tridacna* clams are omnipresent throughout Tutum Bay and include *T. gigas, T. maxima, T. crocea* and *T. squamosa.*

2. THE HYDROTHERMAL FLUID

2.1 INTRODUCTION

The chemical composition of seawater is controlled through a combination of processes, such as low and high temperature seafloor alteration, fluvial and atmospheric input, and sedimentation. In near shore environments, anthropogenic input in the form of municipal, agricultural and industrial waste water may cause a significant alteration of seawater composition. This holds true particularly for poorly flushed coastal waters in the Mediterranean, whereas in remote and under-developed regions, such as the Tabar-Feni islands, anthropogenic influences are generally of little importance. In areas of volcanic activity and/or high heat flow, however, the discharge of fluids from shallow marine hydrothermal systems may have a considerable impact on the chemical composition of the often biologically-important coastal surface waters.

The chemical composition of hydrothermal fluids can vary significantly between subaerial and submarine hydrothermal systems. Seafloor hydrothermal fluids are generally acidic, reducing and metal-rich (e.g., Von Damm, 1990), whereas on-land hot spring waters are generally neutral and metal-poor (e.g., Giggenbach, 1995a). Known shallow-water hydrothermal systems, although submarine, have many of the attributes of their on-land counterparts and are transitional in character between deep-sea hydrothermal vents and terrestrial hot springs.

The submerged flanks of island arc volcanoes provide an exceptional opportunity to study the essential differences and similarities between subaerial and submarine venting and the transition from one to the other. In the near-shore, shallow-water setting along the western shore of Ambitle Island the physico-chemical conditions may not be drastically different from the on-shore hydrothermal systems (for example in terms of pressure and temperature), but their discharge into seawater sets them apart. Mixing with cold oxidizing seawater right at the

seawater-seafloor interface for an impermeable seafloor, or in the subsurface if local sediments are saturated with seawater, causes Eh, pH and temperature to change in the hydrothermal fluid, in pore water and in ambient seawater.

2.2 SAMPLING AND ANALYTICAL PROCEDURES

Generally the chemical analysis of water samples is more accurate under well controlled laboratory conditions than in the field. Some parameters, however, are unstable and must be therefore measured immediately after sampling. In this study I used sample containers, preservation techniques and holding times recommended for water analysis by the US Federal Registry (Hach Company, 1993). Vent temperatures were measured with a maximum thermometer. Due to inherent difficulties when working underwater, however, these measurements should be regarded as minimum temperatures. Vent water samples were collected over a period of 10 days either by inserting a Teflon® tube as far as possible into the vent orifice or covering the vent orifice with a Teflon® funnel. Medical syringes (60 mL) were connected to the Teflon tube or funnel via three-way stopcock. Using this setup, generally 15 syringes were filled at a time and brought to the surface. While sampling vents 2, 3 and 4 minor amounts of water vapor, indicative of phase separation, were observed during filling of the syringes. On-board, aliquots were taken and immediately analyzed for pH, conductivity and alkalinity. Total alkalinity (A^T) was measured as equivalent $CaCO_3$ and expressed as HCO_3^-, using a Hach digital titrator and titrating to an endpoint of pH 4.5 (Hach Company, 1993). The remaining solution was filtered to <0.45 µm and subsequently separated into subsets for later analyses. Samples were stored in high density polyethylene bottles. Aliquots for cation and trace element analyses were acidified with ultra pure HNO_3. Additionally, 60 mL aliquots of selected samples were acidified with double distilled HCl (35%) for determination

of As^{3+}/As^{5+}. Samples for $\delta^{13}C$ analyses were filled into brown glass bottles (118 mL), poisoned with $HgCl_2$ and capped with phenolic screw caps with Polyseal® liners to avoid headspace.

The single orifice vents 1 and 2 were sampled twice and duplicate samples are indicated by a capital letter following the sample number, i.e., 1B. Two of the three orifices at vent 3 were sampled, i.e., 3-1 and 3-2. A duplicate of 3-1 was taken. At vent 4 three samples were taken from three different orifices within a single mound, i.e., 4, 4B, 4C. A sample of ambient seawater (SW) and the samples W-1 and W-2 from the on-shore hot springs (Fig. 1-1) were obtained by submerging a 1 L high density polyethylene bottle. These sample were treated exactly as the Tutum Bay vent waters.

Throughout the sampling period several samples of de-ionized water were treated in the same way as the vent samples, i.e., filtered, acidified and filled into high density polyethylene bottles. These samples were later analyzed together with the vent samples in order to check for possible contamination. In order to assure data quality for analyses that were not performed by myself, I always submitted blind duplicate samples.

Major cations, trace elements, ultra trace elements and rare earth elements (REE) were determined at the Geological Survey of Canada: Li, Rb, Sr, Sb, Cs, and Tl by direct ICP-MS and Fe and Mn by chelation ICP-MS following a tenfold dilution with de-ionized water. REEs were analyzed by chelation ICP-MS without dilution and the following isotopes were used to minimize isobaric interference: ^{139}La, ^{140}Ce, ^{141}Pr, ^{144}Nd, ^{147}Sm, ^{153}Eu, ^{160}Gd, ^{159}Tb, ^{163}Dy, ^{165}Ho, ^{166}Er, ^{169}Tm, ^{174}Yb and ^{175}Lu. A more detailed description of the direct and chelation inductively coupled plasma mass spectrometry (ICP-MS) methodology and associated figures of merit can be found elsewhere (Hall et al., 1995; Hall et al., 1996). Ca^{2+}, Mg^{2+}, Na^+ and K^+ were measured by flame atomic absorption spectrometry (FAA). Prior to analyses for Ca^{2+}, Mg^{2+}, Na^+ and K^+ a Cs/La buffer solution was added to a suitable aliquot of the sample to suppress ionization. Si and B were analyzed by ICP-ES. The total arsenic (As^T) concentration was measured by AAS at a solution pH <2 as As-hydride. As^{3+} was determined by AAS as

As^{3+}-hydride, generated at pH 5 (citrate buffer). Finally, As^{5+} was calculated from the difference between As^T and As^{3+}. Anion (Cl^-, Br^-, SO_4^{2-}) concentrations were measured at the University of Ottawa with a DIONEX 100 High Pressure Liquid Chromatograph. Calibration curves were constructed using a control blank and DIONEX standard solutions. The overall completeness and quality of each analysis was checked by performing a charge balance according to:

$$\Sigma\text{anions (meq)} = \Sigma\text{cations (meq)}. \qquad [2\text{-}1]$$

The difference was always less than 5%.

Gas samples were collected into 600 mL bottles through an inverted Teflon® funnel that was placed over the vent. In order to estimate the total gas flux from Tutum Bay more than 100 flux measurements were carried out by timing the replacement of a known water volume from a graded cylinder. All flux measurements were normalized to 1 bar (i.e., atmospheric pressure at sea level). The chemical composition was analyzed at the Institute of Geological and Nuclear Sciences in Lower Hutt, New Zealand following Giggenbach and Gogoul (1989).

Oxygen and hydrogen isotope ratios were determined at the University of Ottawa and are reported in delta notation (δ) relative to VSMOW. Oxygen was analyzed following CO_2 equilibration at 25°C on a triple collector VG SIRA 12 mass spectrometer. The CO_2-water fractionation factor used is 1.0412 (Friedman and O'Neil, 1977). The routine precision (2σ) on the analyses is 0.10‰. Hydrogen isotopes were determined on H_2 generated by zinc reduction in an automated double collector VG 602D mass spectrometer. The routine precision (2σ) for these analyses is 1.5‰. The isotopic composition of dissolved inorganic carbon (DIC) was determined on a triple collector VG SIRA 12 mass spectrometer by analysis of CO_2 generated by reaction with H_3PO_4. The routine precision (2σ) on the analyses is 0.10‰.

$^{87}Sr/^{86}Sr$ were measured on a five collector Finnigan MAT 262 solid source mass spectrometer at the Institut für Geologie, Ruhr Universität, Bochum following Buhl et al.

(1991) and Diener et al. (1996). The average of 100 repeat measurements for the NBS 987 standard was 0.710224±0.000008.

2.3 RESULTS

2.3.1 General Statement

The samples collected from the submarine vents in Tutum Bay are mixtures of hydrothermal fluid and seawater (Table 2-1). Entrainment of ambient cool seawater may have happened in the shallow seafloor or during sampling. Assuming conservative behavior during mixing, several chemical species can be used to trace the mixing process if the concentration difference between seawater and hydrothermal fluid is sufficient. The best case scenario is if the element under consideration is absent in one of the mixing partners. The early laboratory study of Bischoff and Dickson (1975) showed that high temperature (>200°C) hydrothermal fluids have lost all their Mg due to precipitation of Mg-rich minerals in the subsurface. Although the fluids that discharge in Tutum Bay are quite different from those studied by Bischoff and Dickson (1975), Mg is used as an indicator for seawater entrainment. Given their chemical composition and proximity to shore, Tutum Bay hydrothermal fluids most likely derived from meteoric waters that are already much lower in Mg when compared to seawater. In addition, most studies of deep circulating geothermal waters that are meteoric derived, show very low concentrations of Mg (< 1 mg/l) (e.g., Nicholson, 1992), as confirmed by the analyses of samples W-1 and W-2 (Table 2-1). The assumption of complete Mg absence in the vent fluids is most likely not correct, but given the enormous concentration difference between seawater and vent fluid, it is well within any analytical uncertainty. Another option to correct for seawater entrainment is to use Si as a tracer of mixing (e.g., Sedwick and Stüben, 1996). Both alternatives have been explored in Fig. 2-1, where Si and Mg^{2+} are plotted vs. Cl^- with

TABLE 2-1
LOCATION, TEMPERATURE, PH AND MAJOR ELEMENT COMPOSITION OF TUTUM BAY VENT WATERS, AMBIENT SEAWATER AND ONSHORE GEOTHERMAL SPRINGS.

No.	Location	T	pH	Cl	Br	SO_4	HCO_3	B	Si	Na	K	Ca	Mg	Li	Mn	Fe	Rb	Sr	Cs	Sb	Tl	As^{3+}	As^{T}
Unit		(°C)		(ppm)	(ppm)	(ppm)	(ppm)	(ppm)	(ppm)	(ppm)	(ppm)	(ppm)	(ppm)	(ppb)	(ppb)	(ppb)	(ppb)	(ppb)	(ppb)	(ppb)	(ppb)	(ppb)	(ppb)
1	Vent 1	90	6.2	1200	4.7	1033	796	8.2	103	1250	97	205	60	1009	463	1600	340	6700	59	7.6	4.7	748	820
1B	Vent 1	90	6.2	1250	7.4	1012	805	8.0	104	1185	92	207	650	999	447	1500	335	6600	59	8.3	4.5	799	801
2	Vent 2	80	6.3	2300	11	1141	766	8.3	96	1705	106	225	135	935	434	1570	328	6900	53	6.8	3.9	774	779
2B	Vent 2	80	6.2	2900	13	1132	798	n.d.	93	1915	109	228	160	914	434	1400	318	6900	50	7.3	3.9	701	701
3-1	Vent 3	88	6.3	3100	7.1	1192	769	7.9	92	2025	112	233	175	877	421	1500	314	6900	49	7.2	3.7	689	689
3-1B	Vent 3	88	6.2	1760	8.5	1109	764	8.1	100	1375	96	219	90	933	474	1680	336	7000	53	7.7	3.9	712	732
3-2	Vent 3	89	6.2	190	6.8	1059	769	7.8	99	1465	102	218	100	933	475	1640	331	7000	53	7.7	4.2	736	743
4	Vent 4	90	6.2	1600	8.4	1004	801	8.2	99	1350	110	195	85	941	355	990	353	6400	59	8.6	5.1	806	880
4B	Vent 4	90	6.4	1900	9.1	1037	824	8.4	97	1455	119	198	100	927	349	950	347	6300	58	8.5	4.8	756	830
4C	Vent 4	91	6.7	2960	17	1125	772	8.1	90	1925	125	210	160	862	332	920	330	6400	54	7.7	4.5	718	885
W-1	Waramung Hot Spring	98	8.8	12000	29	6318	559*	44	84	9700	1400	7.4	0.9	4272	2.2	25	2768	2100	440	156	20	1550	1550
W-2	Kapkai Hot Spring	92	8.4	13900	21	7075	667*	54	103	11250	1560	4.7	0.8	5052	1.8	25	3345	2600	550	31	16	2900	2900
SW	Seawater	28	8.0	19500	45	2748	154	4.1	0.2	10450	354	405.0	1235	137	1.6	15	104	7900	0.6	0.5	0.3	n.d.	3.7

Notes: n.d. not determined; * values represent total alkalinity because they include HS^- alkalinity. Repeat standard deviations in % are as follows: Cl, Br, SO_4, B, Si, Na, Ca , Fe, Mn, Rb, Sr, < 5 %; K = 7 %; Sb = 16 %; As = 17 %.

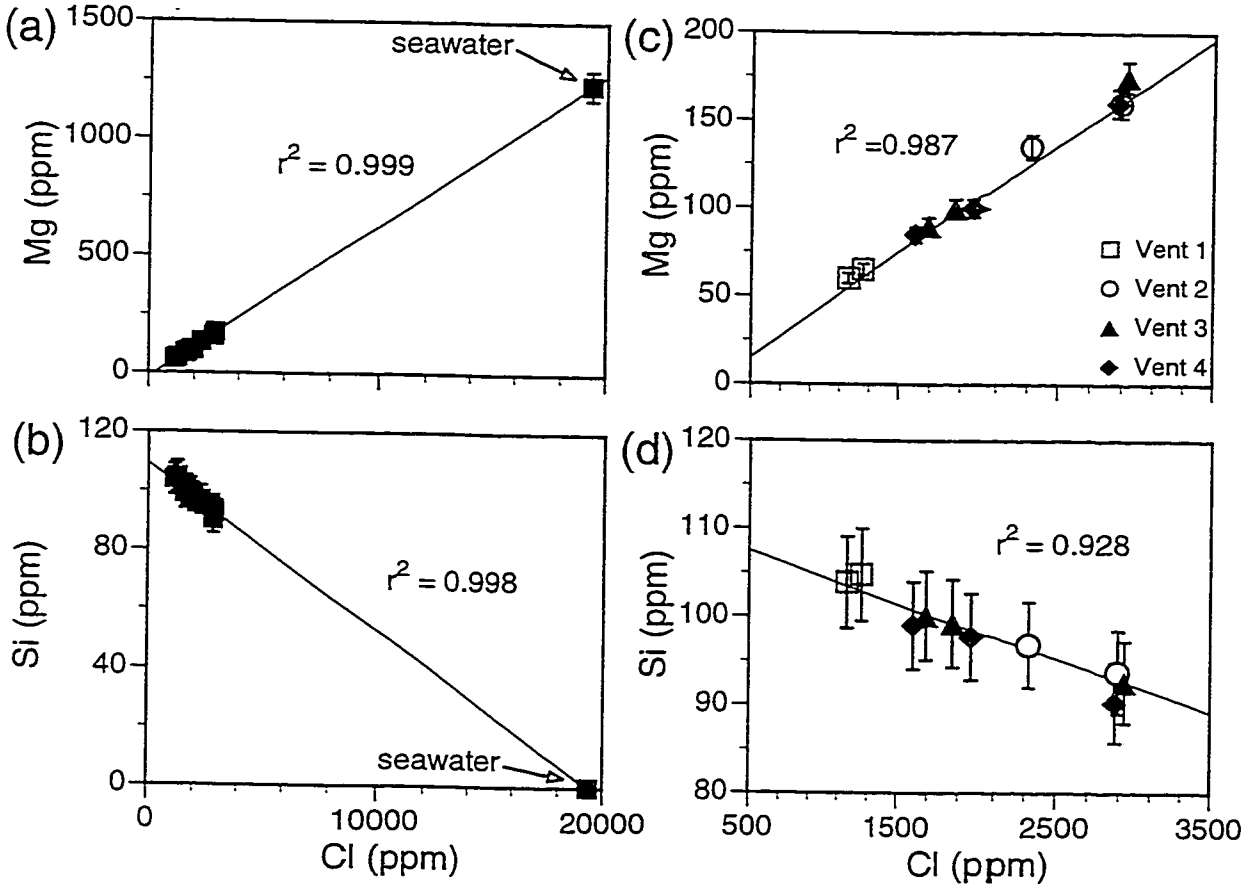

Fig. 2-1 (a) Dissolved Mg vs. Cl in Tutum Bay vent waters and seawater. (b) Dissolved Si vs. Cl in Tutum Bay vent waters and seawater. (c) Dissolved Mg vs. Cl for individual vents. (d) Dissolved Si vs. Cl for individual vents.

their respective linear regression fits. The Si values, although, consistently decreasing with an increase of seawater component (i.e., Cl^- concentration) deviate barely beyond their analytical error (Fig. 2-1b, d). Relative to ambient seawater, Mg^{2+} is depleted and Si is enriched and both show almost perfect correlation ($r^2 > 0.99$) with Cl^- (Fig. 2-1a, b). This high correlation, however, is due to the outlier effect (Swan and Sandilands, 1995) caused by the seawater data point. Excluding this outlier (Fig. 2-1c, d), the correlation, although still high, is somewhat less for Si ($r^2 = 0.928$) than for Mg^{2+} ($r^2 = 0.987$). It is assumed therefore that for Tutum Bay samples Mg^{2+} is a more reliable tracer of mixing. The poorer correlation for Si may be due to its higher susceptibility to changes in temperature and its greater inclination to post-sampling concentration changes due to adsorption on to container walls.

The data presented in Table 2-2 are endmember compositions that have been calculated according to the following formula:

$$X_{hf} = \frac{X_m - X_{sw}(Mg_m/Mg_{sw})}{1-(Mg_m/Mg_{sw})} \qquad [2\text{-}2]$$

where X_{hf} is the calculated endmember concentration, X_m the measured concentration, X_{sw} the concentration in seawater. No correction of chemical composition for phase separation was attempted. In order to account for phase separation, the sampling pressure, steam composition and/or reservoir conditions have to be known (Henley et al., 1984). This information can generally be obtained when sampling in explored on-land geothermal systems, but not when sampling underwater hot-springs. The effect of phase separation on chemical composition for Tutum Bay vent waters, however, seems to be negligible. Only minor amounts of steam were observed while sampling vents 2, 3 and 4 and no steam was observed at vent 1. The impression of heavy boiling seems to be an effect caused by simultaneous discharge of non-condensable gas and water.

TABLE 2-2
CALCULATED ENDMEMBER COMPOSITION FOR pH, MAJOR AND SELECTED MINOR ELEMENTS IN TUTUM BAY VENT WATERS

Sample	Cl	Br	SO_4	B	Si	Na	K	Ca	Mg	Li	Mn	Fe	Rb	Sr	Sb	Cs	Tl	As
Unit	(ppm)	(ppm)	(ppm)	(ppm)	(ppm)	(ppm)	(ppm)	(ppm)	(ppm)	(ppb)	(ppb)	(ppb)	(ppb)	(ppb)	(ppb)	(ppb)	(ppb)	(ppb)
1	263	3.83	945	8.4	109	780	81.2	195	0*	1053	487	1680	352	6636	8.0	62.4	4.9	862
1B	243	6.60	916	8.2	111	670	77.4	197	0*	1047	472	1644	348	6554	8.7	62.8	4.8	845
2	223	9.79	944	8.8	109	632	76.1	203	0*	1033	488	1760	355	6771	7.6	59.8	4.3	874
2B	419	12.72	891	n.d.	108	645	72.5	202	0*	1029	498	1636	350	6811	8.3	58.2	4.4	770
3-1	395	4.67	935	8.6	108	634	72.0	205	0*	999	491	1775	349	6806	8.3	57.2	4.3	786
3-1B	290	7.45	980	8.4	108	662	76.2	205	0*	996	512	1818	354	7019	8.3	57.9	4.1	789
3-2	308	5.48	910	8.2	108	673	79.8	202	0*	1003	518	1783	351	6936	8.3	58.3	4.5	808
4	314	7.41	875	8.5	106	677	91.9	180	0*	1001	382	1070	371	6286	9.2	63.5	5.4	945
4B	362	7.98	886	8.8	106	662	98.8	181	0*	997	380	1041	368	6232	9.2	64.0	5.2	903
4C	398	16.86	883	8.7	104	656	91.4	181	0*	970	382	1065	364	6211	8.8	62.3	5.1	1016

Note: * Mg concentration for these samples is 0 ppm by convention

The samples W-1 and W-2 from the on-land thermal areas were taken from the same springs as samples WA1 and KP in Licence et al. (1987). Their chemical composition is in excellent agreement, indicating stable conditions for these springs during more than 12 years (Table 2-1 and Table 1 in Licence et al., 1987).

2.3.2 The anions: Cl^-, Br^-, SO_4^{2-} and HCO_3^-

The vent waters from Tutum Bay are depleted in Br^-, SO_4^{2-} and Cl^- relative to ambient seawater and SO_4^{2-} and Cl^- are positively correlated with Mg^{2+} (Fig. 2-2). There are no distinct trends for individual vents; all samples either follow the same vent water - seawater mixing trend or plot in one cluster. HCO_3^- is enriched relative to ambient seawater and negatively correlated with Mg^{2+}. The linear regression analysis shows a very high degree of correlation for all three species (> 0.986), but excluding the seawater outlier the correlation for SO_4^{2-} is much less ($r^2 = 0.77$) and for HCO_3^- correlation disappears ($r^2 = 0.165$).

Endmember compositions are listed in Table 2-2. For all samples, SO_4^{2-} values are within their analytical uncertainty. Cl^- and Br^-, however, show a significant spread except for vent 1.

2.3.3 The alkali metals: Li^+, Na^+, K^+, Rb^+ and Cs^+

The alkaline metals Li^+, Rb^+ and Cs^+ are significantly enriched over ambient seawater and negatively correlated with Mg^{2+} (Table 2-1 and Fig. 2-3). Na^+ and K^+ are significantly depleted relative to seawater and positively correlated with Mg^{2+} (Table 2-1 and Fig. 2-3). The Na^+ depletion is similar to the depletion observed for Cl^-. Again, excluding the seawater outlier, only Na^+ maintains the high degree of correlation (Fig. 2-3).

Endmember concentrations are listed in Table 2-2. Except for the Na^+ value in sample 1, which is slightly higher than the rest, all Na^+ and Li^+ estimates are within their analytical

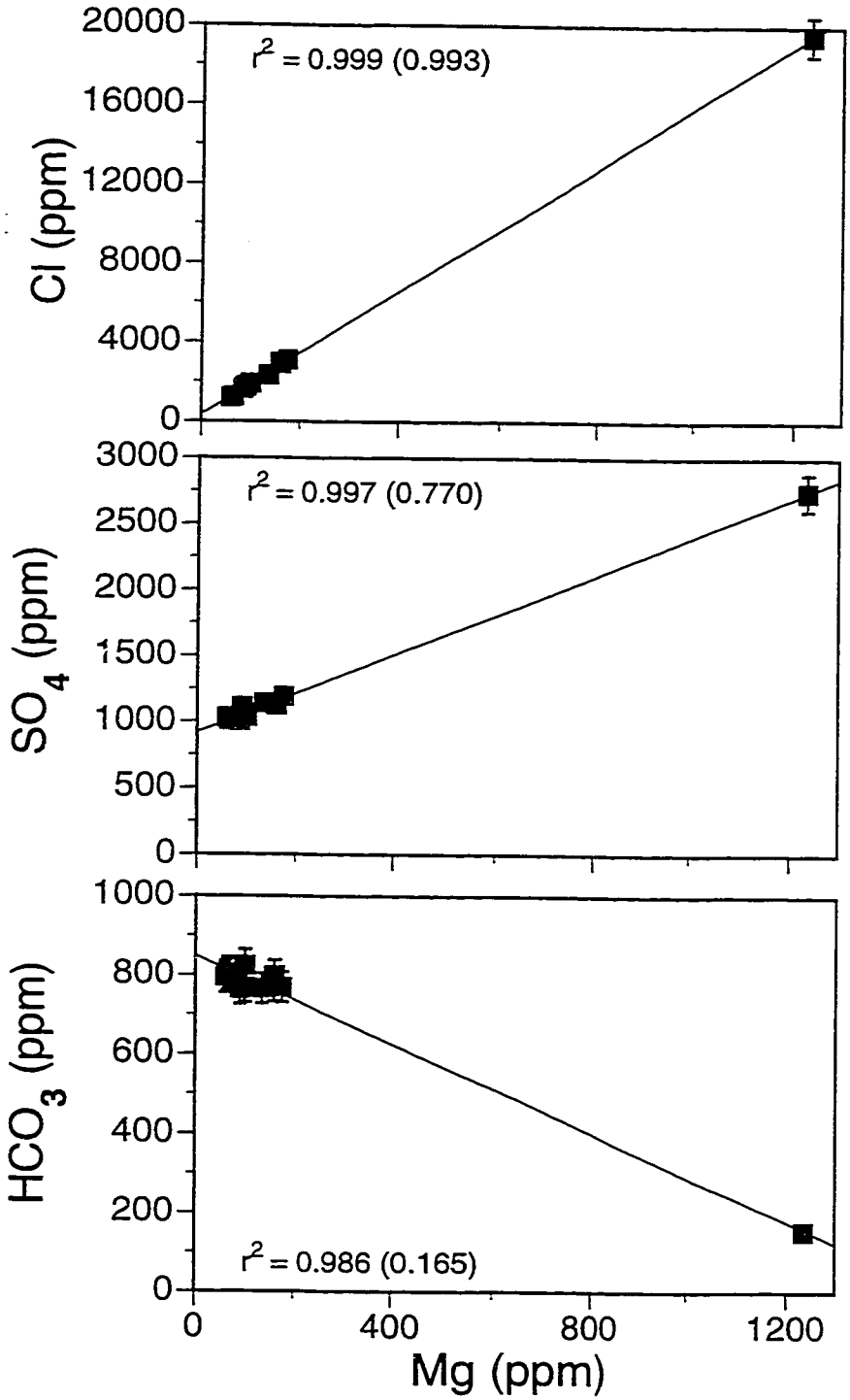

Fig. 2-2 Major anions (Cl, SO_4 and HCO_3) vs. Mg in Tutum Bay vent waters and seawater. r^2 is the correlation coefficient for the linear regression taking into account the whole data set including seawater (Mg ~ 1200 ppm) and r^2 in brackets is the correlation coefficient for the linear regression excluding seawater. See text for more detail.

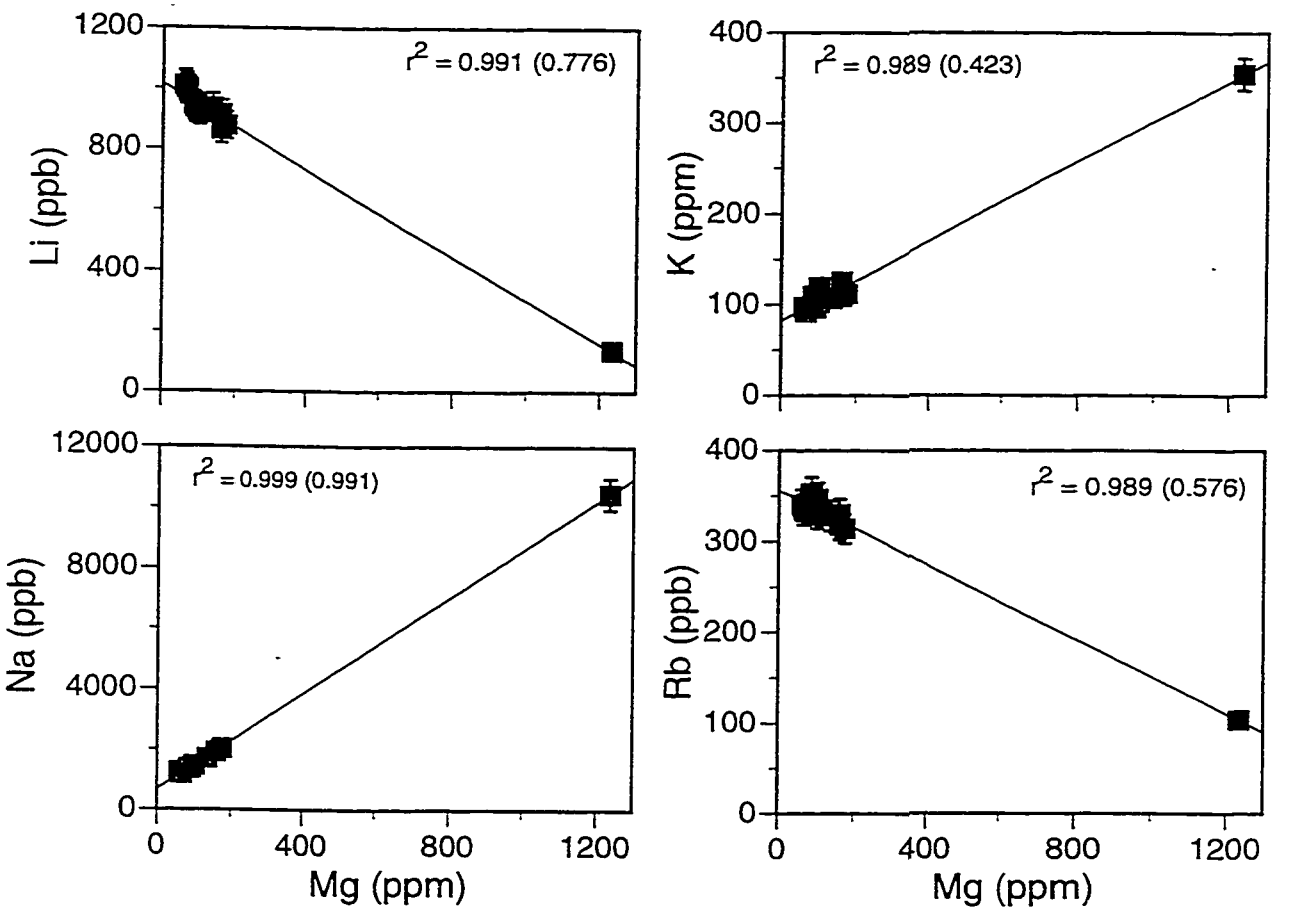

Fig. 2-3 Li, Na, K and Rb vs. Mg in Tutum Bay vent waters and seawater. Explanation of correlation coefficients as in Fig. 2-2. See text for more detail.

error. The K^+ values fall into two distinct groups for area A and area B, with higher concentrations in B. The Rb^+ and Cs^+ concentrations are within their analytical error, the values for area B, however, are consistently higher than those for area A.

2.3.4 The alkaline earths: Mg^{2+}, Ca^{2+} and Sr^{2+}

All Tutum Bay vent waters have Ca^{2+} concentrations that are significantly lower than ambient seawater (Table 2-1 and Fig. 2-4). Values for vents in area A and area B plot in two distinct groups that are both positively correlated with Mg^{2+} (Fig. 2-4). Linear regression analysis shows a high degree of correlation ($r^2 > 0.99$) for both groups which is maintained ($r^2 > 0.93$) after exclusion of the seawater outlier (Fig. 2-4). The Sr^{2+} concentration in vent waters is only slightly lower than in ambient seawater and there is no apparent correlation between Sr^{2+} and Mg^{2+}.

Endmember concentrations for Ca^{2+} are almost identical for individual vents (Table 2-2). Concentrations for both areas are within their respective analytical uncertainty, but area A vents have slightly higher values.

2.3.5 Selected trace elements: Fe, Mn, As, Tl, Sb

The transition metals Fe and Mn are highly enriched over ambient seawater (Table 2-1 and Fig. 2-5). Values for vents in area A are higher than those from area B, but both are positively correlated with Mg^{2+} (Fig. 2-5). After exclusion of the seawater value, correlation for area A drops substantially while for area B it remains high. The values for the individual areas, however, do not deviate beyond their analytical error.

Endmember concentrations for Fe and Mn are almost identical for individual vents (Table 2-2). Concentrations for both areas are within their respective analytical uncertainty, but area A vents have significantly higher values.

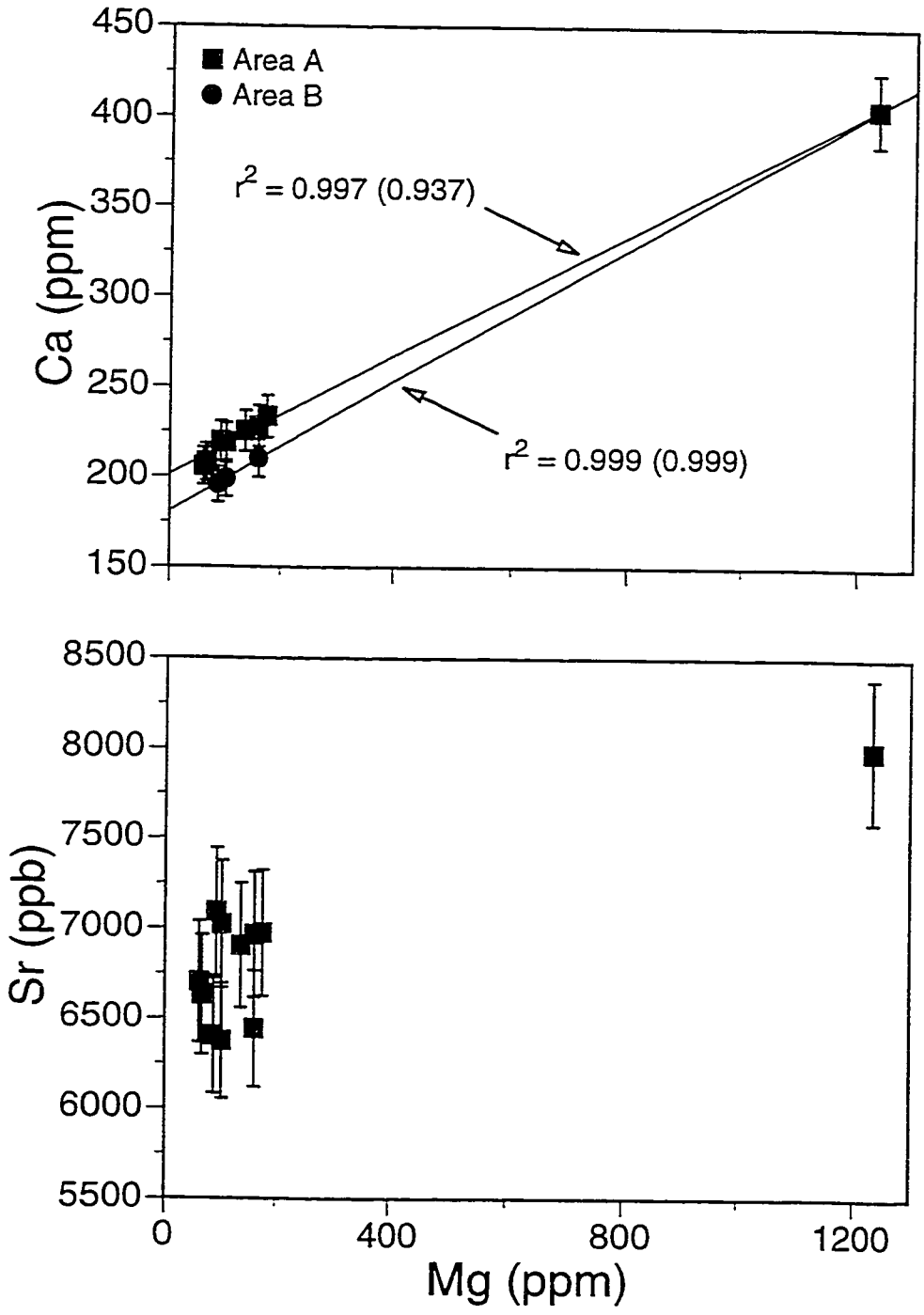

Fig. 2-4 Ca and Sr vs. Mg in Tutum Bay vent waters and seawater. Explanation of correlation coefficients as in Fig. 2-2. See text for more detail.

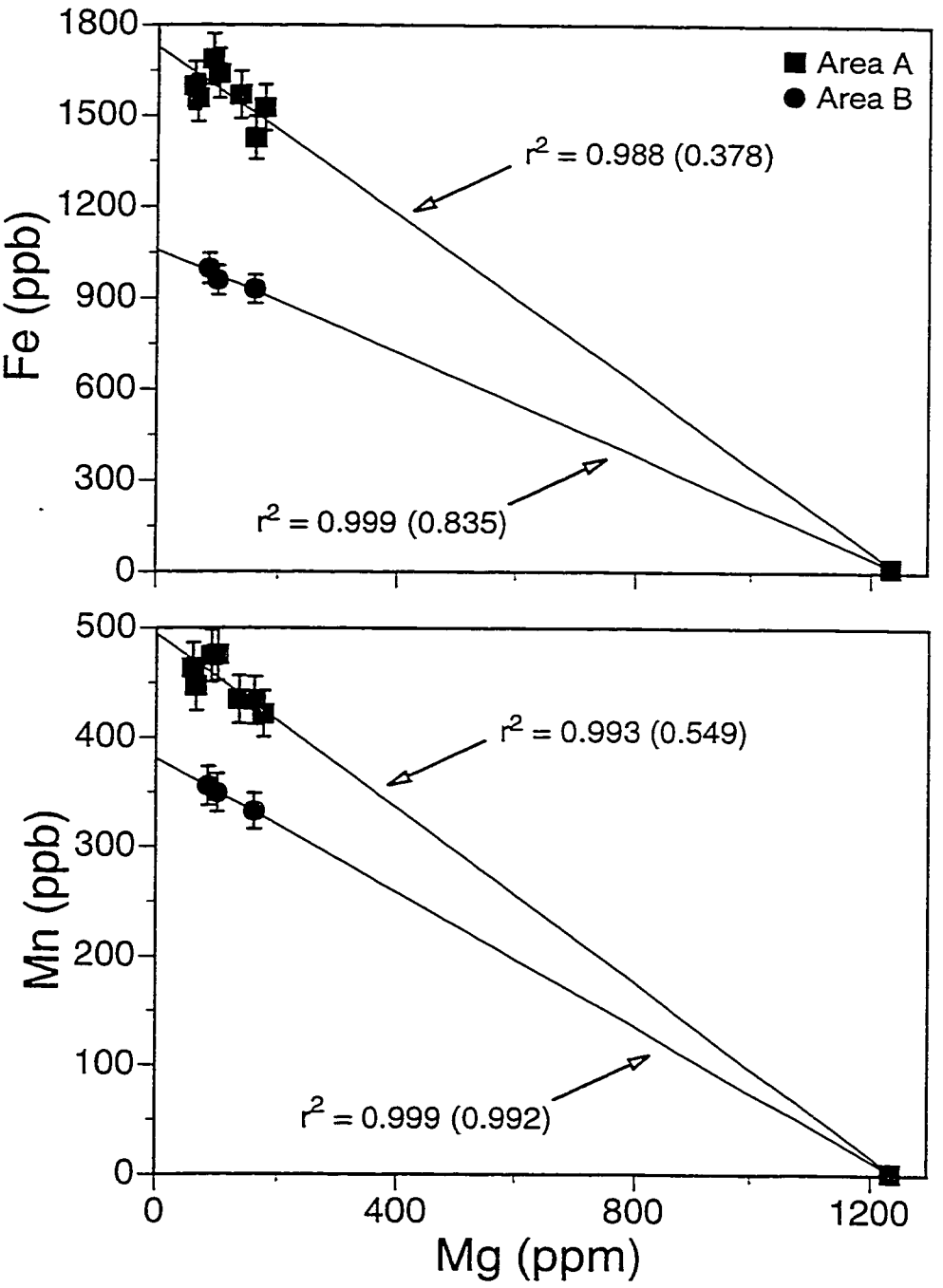

Fig. 2-5 Fe and Mn vs. Mg in Tutum Bay vent waters and seawater. Explanation of correlation coefficients as in Fig. 2-2. See text for more detail.

Relative to ambient seawater, Sb, As and Tl are significantly enriched in all vents (Table 2-1). Arsenic concentrations are up to 275 times above seawater and it is dominantly present in its tri-valent state. Endmember concentrations for Sb, As and Tl fall into groups, as observed for Ca^{2+}, Fe and Mn, except that values for area B are higher than those for area A.

2.3.6 Rare earth elements (REE)

Rare earth element (REE) concentrations in Tutum Bay vents waters are generally one order of magnitude higher than those reported for average seawater (Fleet, 1984). North American Shale Composite (NASC) normalized raw and endmember concentrations are plotted in Fig. 2-6. The pattern geometry for raw and endmember values is effectively the same, except that the endmember patterns plot slightly higher. The samples from vents 1 and 3 (1, 3-1 and 3-2) and their duplicates (1B and 3-1B) plot very closely together, showing the same pattern geometry: an initial drop from La to Ce followed by rise from the Ce minimum to a Eu maximum and a slight decrease towards an intermediate Lu. The pattern geometry for samples from vent 4 (4, 4B and 4C) is quite different; REE concentrations initially drop from La to the Ce minimum, followed by a rise to a Dy maximum and a slight decrease towards Lu.

2.3.7 Isotopes: $\delta^{13}C$, $^{87}Sr/^{86}Sr$, $\delta^{18}O$ and δD

The $\delta^{13}C$ of Tutum Bay vent waters are depleted relative to seawater. They scatter significantly and there is no correlation with Mg (Fig. 2-7). As a result, Mg-corrected values still scatter beyond their analytical error which sets $\delta^{13}C$ apart from the other isotopes (see below) (Table 2-3). This is not surprising considering how pH-dependent the geochemistry of CO_2 and its dissolved species is. Mixing with ambient seawater affects not only the isotope composition but also the pH. $\delta^{13}C$ is thus the isotope value most susceptible to seawater

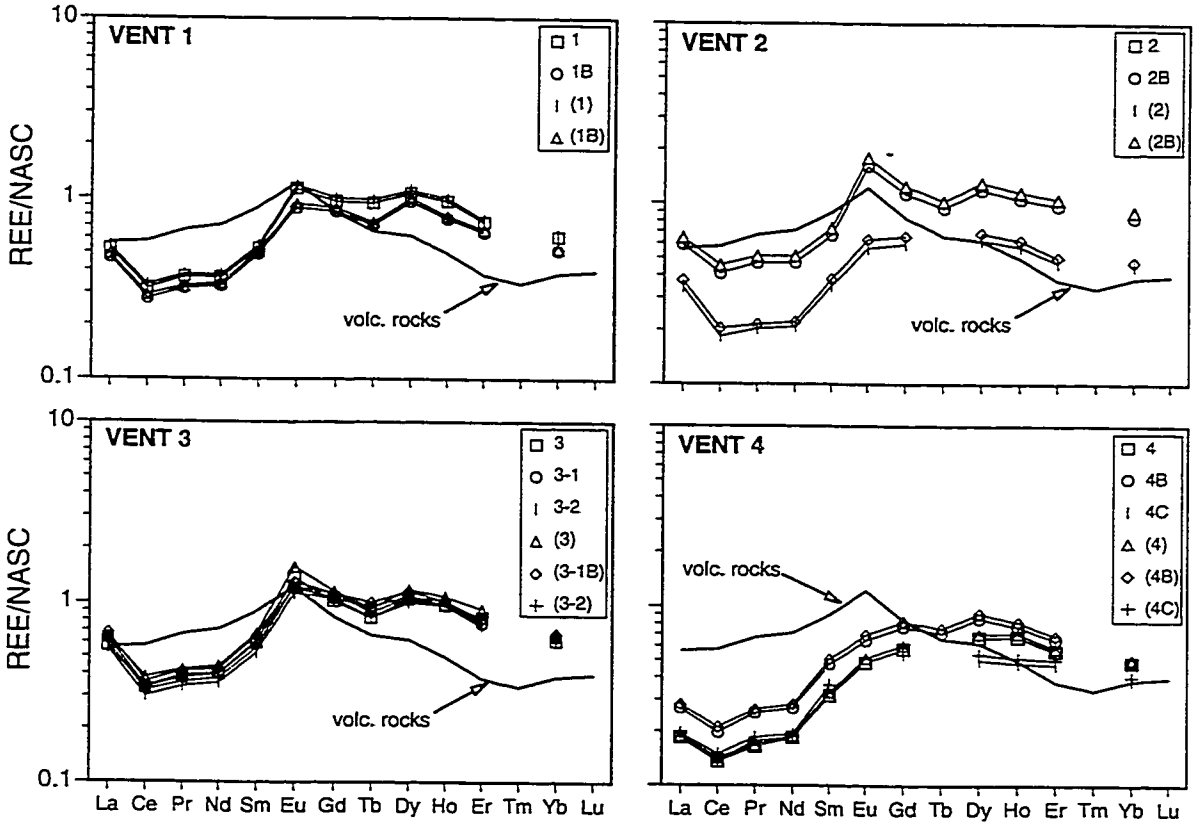

Fig. 2-6 North American Shale Composite (NASC) (Haskin et al., 1968) normalized rare earth element (REE) plots for vents 1, 2, 3 and 4. REE concentrations for vent waters are multiplied by 10^6. The bold pattern without labels represents the average REE composition of volcanic rocks from Ambitle Island; data are from Wallace et al. (1983).

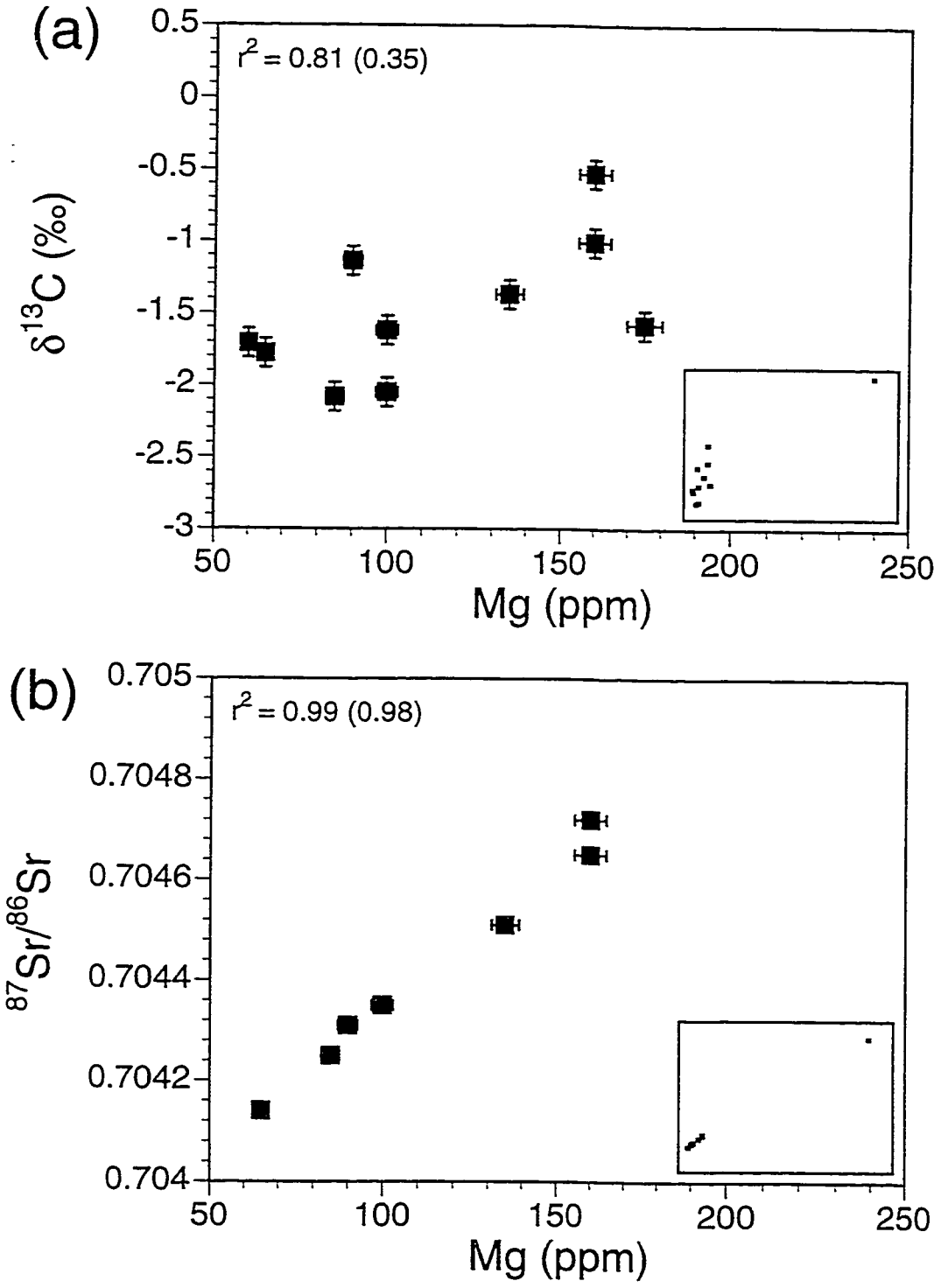

Fig. 2-7 $\delta^{13}C$ and $^{87}Sr/^{86}Sr$ vs. Mg in Tutum Bay vent waters and seawater. The small inset in the lower right corner shows the whole data set including seawater. Explanation of correlation coefficients as in Fig. 2-2. See text for more detail.

TABLE 2-3
OBSERVED AND MG-CORRECTED ISOTOPIC COMPOSITIONS OF TUTUM BAY HYDROTHERMAL FLUIDS

Sample	$\delta^{13}C$ (PDB) ‰		$\delta^{18}O$ (VSMOW) ‰		δD(VSMOW) ‰		$^{87}Sr/^{86}Sr$	
1	-0.11	*-0.13*	-4.78	*-5.05*	-26.3	*-28.0*	n.d.	*n.d.*
1B	0.18	*0.12*	-4.88	*-5.17*	-29.5	*-31.5*	0.70414	*0.70386*
2	-1.37	*-1.69*	-4.52	*-5.13*	-27.0	*-31.1*	0.70451	*0.70394*
2B	-0.53	*-0.80*	-4.41	*-5.13*	-26.0	*-30.9*	0.70465	*0.70398*
3-1	-1.58	*-2.05*	-4.30	*-5.08*	-26.3	*-31.7*	n.d.	*n.d.*
3-1B	-1.14	*-1.33*	-4.71	*-5.11*	-27.4	*-30.1*	0.70431	*0.70393*
3-2	-1.62	*-1.87*	-4.60	*-5.04*	-30.1	*-33.3*	n.d.	*n.d.*
4	-1.75	*-1.97*	-4.74	*-5.12*	-30.7	*-33.5*	0.70425	*0.70388*
4B	-1.30	*-1.53*	-4.70	*-5.15*	-26.0	*-28.9*	0.70435	*0.70393*
4C	-1.01	*-1.35*	-4.40	*-5.12*	-23.8	*-28.3*	0.70472	*0.70406*
W-1	-0.91	*n.a.*	-0.25	*n.a.*	-14.8	*n.a.*	0.70409	*n.a.*
W-2	-2.38	*n.a.*	0.20	*n.a.*	-17.7	*n.a.*	0.70394	*n.a.*
SW	1.26	*n.a.*	0.41	*n.a.*	6.6	*n.a.*	0.70918	*n.a.*

Notes: n.d. not determined; n.a. not applicable; raw values are in normal font and Mg-corrected values are in italics. Max. error for strontium isotope values is ±0.000009 2 Standard Errors.

contamination. The samples with the lowest values, therefore, should most likely be the best estimates of $\delta^{13}C$.

The $^{87}Sr/^{86}Sr$ ratios of vent waters are considerably lower than those of local seawater (Table 2-3). Values for the whole data set (including seawater) are positively correlated with Mg^{2+} ($r^2 > 0.99$) and the degree of correlation remains high after exclusion of the seawater value ($r^2 > 0.96$) (Fig. 2-7b). After Mg-correction for seawater contamination all ratios are within their analytical uncertainty of ±0.000009. Their mean (0.70394) is almost identical to the X-axis intercept of the linear regression, i.e., zero-Mg ratio (0.703933). Both ratios (mean and x-axis intercept) are in very good agreement with the $^{87}Sr/^{86}Sr$ ratio of on-land samples (W-1 and W-2, Table 2-3) and of subsurface rocks at Ambitle Island (0.703813, M. Perfit, pers. comm.) and, therefore, strengthen the assumption of a zero-Mg endmember and the use of Mg^{2+} as a tracer of seawater mixing.

$\delta^{18}O$ and δD are relatively depleted compared to local seawater (Table 2-3). $\delta^{18}O$ is positively correlated with Mg^{2+} ($r^2 > 0.99$) and the degree of correlation remains high after exclusion of the seawater value ($r^2 > 0.98$) (Fig. 2-8a). δD seems to be positively correlated with Mg^{2+} ($r^2 > 0.97$), but values hardly deviate beyond their analytical uncertainty (Fig. 2-8b). This correlation, however, is invalidated ($r^2 > 0.37$) after exclusion of the seawater value (outlier). After Mg-correction for seawater contamination all values for $\delta^{18}O$ and δD are within their analytical uncertainty and they plot on the local meteoric water line (LMWL) (Fig. 2-9). The means of $\delta^{18}O$ (-5.11 ‰) and δD (-30.73 ‰) of Mg-corrected Tutum Bay vent water are almost identical to the means of $\delta^{18}O$ (-5.18 ‰) and δD (-30.71) of local precipitation (see Fig. 2-9 for more explanation).

2.3.8 Gas composition and flux

The chemical and isotopic compositions of non-condensable gases collected from submarine vents in Tutum Bay are listed in Table 2-4. In all samples, CO_2 is the dominant

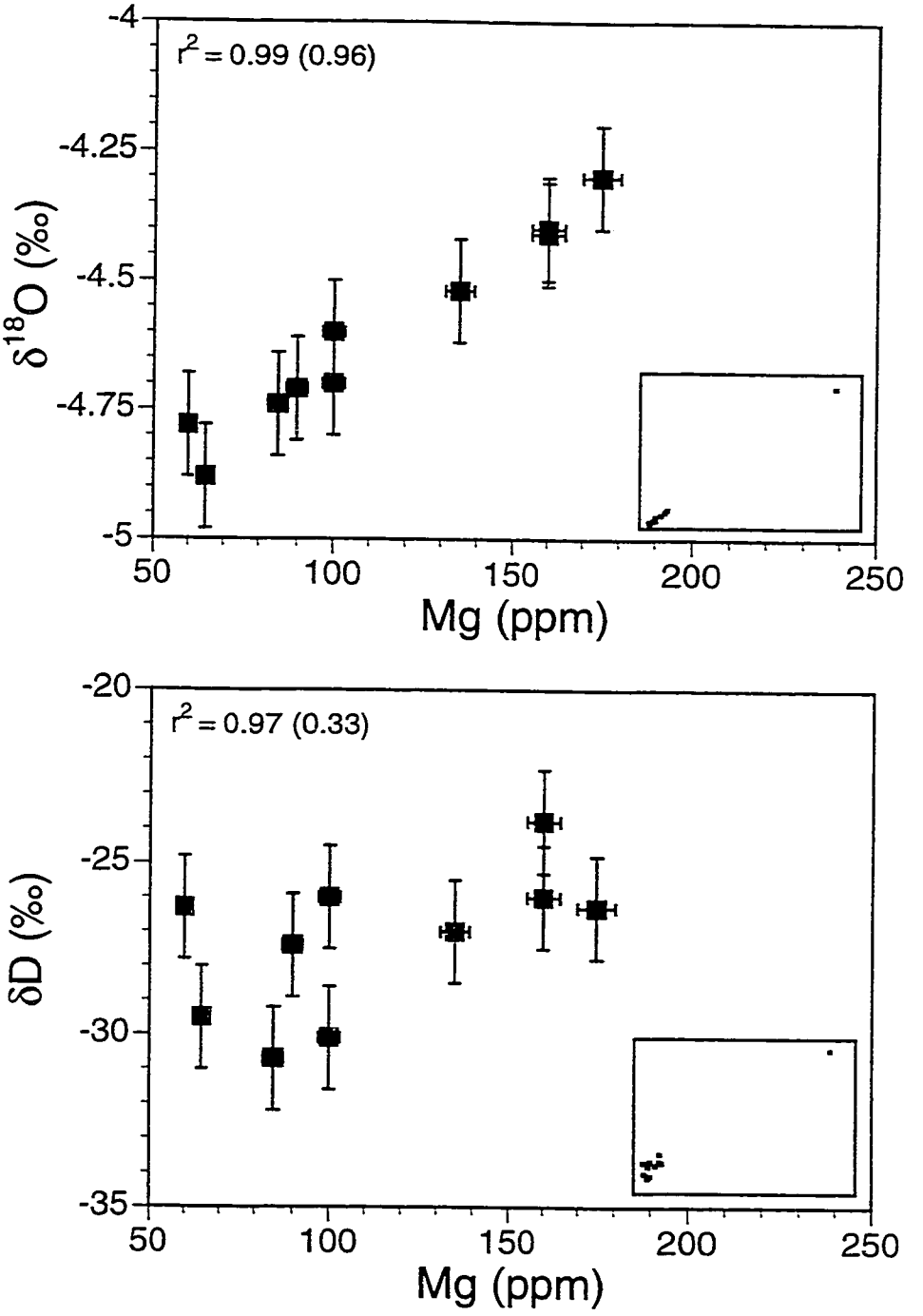

Fig. 2-8 $\delta^{18}O$ and δD vs. Mg in Tutum Bay vent waters and seawater. The small inset in the lower right corner shows the whole data set including seawater. Explanation of correlation coefficients as in Fig. 2-2. See text for more detail.

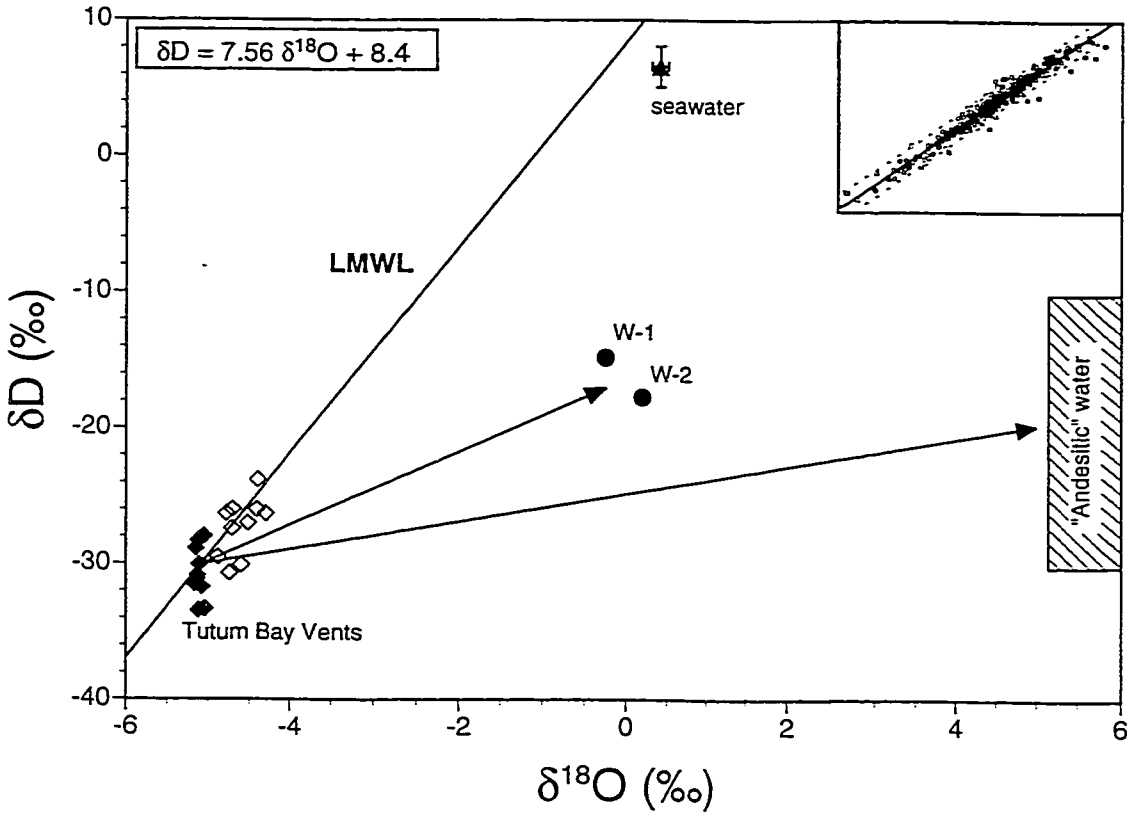

Fig. 2-9 $\delta^{18}O$ and δD plot of Tutum Bay vent water, seawater and two onland hot springs, W-1 (Waramung) and W-2 (Kapkai). The box for "andesitic water" is from Giggenbach (1992). The small inset in the upper right corner shows the whole data set for the local meteoric water line (LMWL). Data are from the website (http://www.iaea.or.at) of the International Atomic Energy Agency (IAEA) and represent the four closest monitoring stations to Ambitle Island whose elevation is sea level. Filled diamonds are Mg-corrected values and open diamonds are as analyzed.

TABLE 2-4
CHEMICAL AND ISOTOPIC COMPOSITIONS OF DRY GASES FROM TUTUM BAY, AMBITLE ISLAND IN ‰ AND MMOL/MOL, RESPECTIVELY; T(°C) IS THE CH_4/CO_2 EQUILIBRATION TEMPERATURE

Sample	CO_2	H_2S	He	H_2	O_2	N_2	$N_2(c)$	CH_4	T(°C)	$\delta^{13}C_{(CO_2)}$	$\delta^{13}C_{(CH_4)}$	$\delta D_{(CH_4)}$
TB-1	927	<0.3	0.021	<0.01	7.3	44	29	20	257	-2.23	-17.1	-112
TB-2	966	<0.3	0.012	<0.01	5.4	22	11	6	291	n.d.	n.d.	n.d.
TB-3	979	<0.3	<0.01	<0.01	6.1	36	24	14	268	n.d.	n.d.	n.d.
TB-4	949	<0.3	<0.01	<0.01	4.3	35	23	14	267	-2.55	n.d.	n.d.
TB-5	926	<0.3	0.011	<0.01	5.8	47	35	20	257	n.d.	n.d.	n.d.

Note: $N_2(c) = N_2 - 2O_2$; n.d. is not determined

component, but all the submarine gases contain significant amounts of O_2, representing either an inherent component of these gases, dissolved air stripped from seawater by the rising gas bubbles, or introduction during sampling. In the absence of any information on the origin of O_2 and N_2, their concentrations can be corrected by subtracting 2 * O_2 from measured values of N_2 to obtain N_2(c) (corrected) (W. Giggenbach, pers. comm.). The factor of 2 is the approximate value of the N_2-O_2 ratio in air-saturated water.

Submarine environments offer the unique opportunity to study and measure the gas flux from a hydrothermal area. The presence of gas bubbles allows for precise location and account of every gas vent, which, in theory, permits the precise, quantitative determination of the amount of discharge. The total gas flux from the Tutum Bay hydrothermal area is approximately 20 L/s and the amount of CO_2 released is approximately 18-19 L/s.

2.3.9 Redox potential

In addition to the sampling for chemical analyses, I also sampled a limited amount of water from each vent during a single dive for simultaneous on-board Eh and pH measurements. This was done in order to assess a possible significant redox difference between the individual vent fluids. The pH measurement was used to monitor seawater contamination and the quality of the Eh measurement was checked against Ouinhydrone solution (e.g., Clark and Fritz, 1997). All vent fluids were found to be reducing and have similar Eh values; vent 1 = -0.175v, vent 2 = -0.171v, vent 3 = -0.173v and vent 4 = -0.175v. These values are similar to those obtained from As^{3+}/As^{5+} calculations (Fig. 2-10).

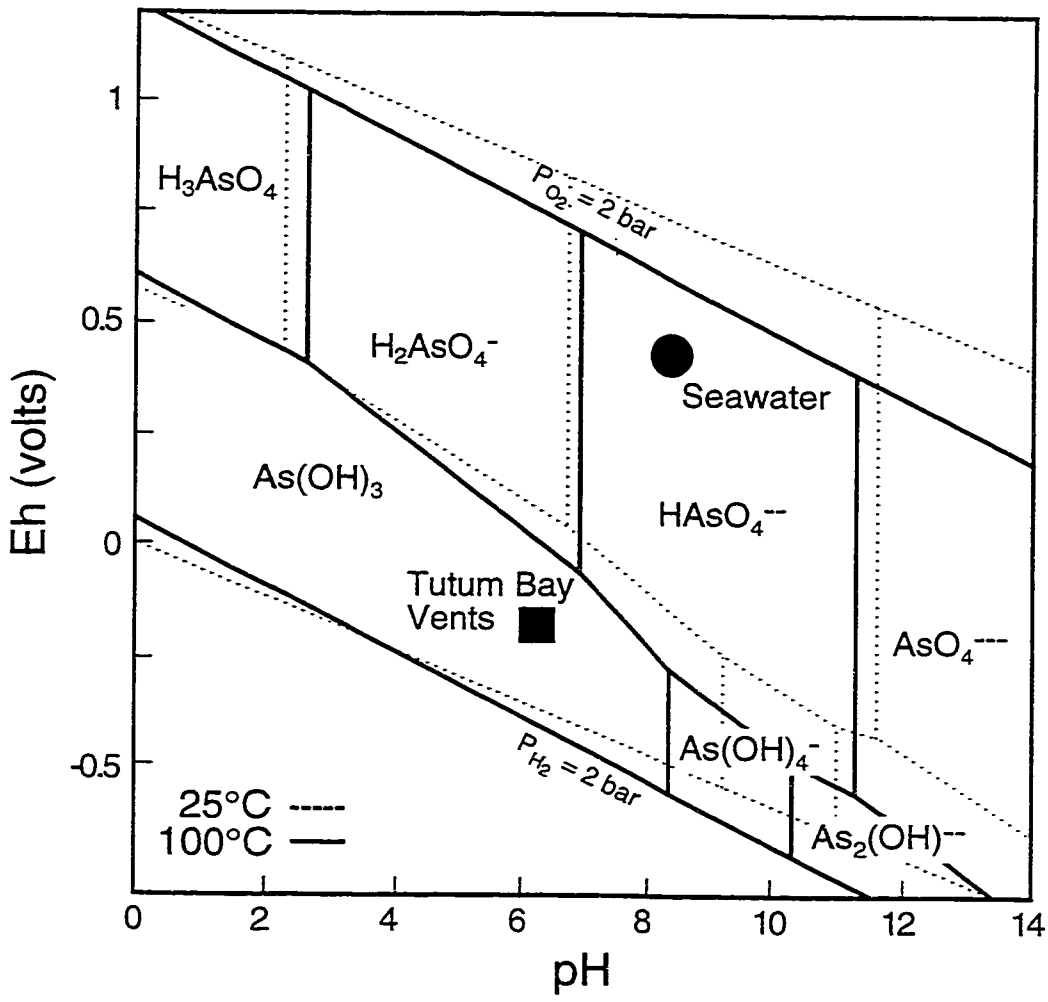

Fig. 2-10 Eh-pH diagram for the system As-O-H at 30°C (dashed lines) and 100°C (solid lines) at a pressure of 1.013 bars. Activities of As^{3+} and HCO_3^- are assumed to be 10^{-3} and 10^{-4}, respectively. Thermodynamic data are from Brookins (1988) and references therein.

2.4 DISCUSSION

The discharge composition of thermal springs is controlled by two sets of processes: 1) deep reservoir conditions, and 2) secondary processes during ascent. In the deep reservoir, host rock composition, temperature, direct magmatic contributions and residence time are the controlling factors. During ascent a drop in pressure and temperature can initiate phase separation and mineral precipitation, causing a dramatic change in fluid composition. Mixing with other hydrothermal fluids and/or groundwater is possible at any depth. In near-shore and submarine environments mixing with seawater cannot be ruled out. The chemical composition of a hydrothermal fluid, sampled at the surface, generally contains an imprint of its subsurface history. Chemically inert constituents (tracers) provide information about their source, whereas chemically reactive species (geoindicators) record physico-chemical changes (e.g., Ellis and Mahon, 1977; Giggenbach, 1991; Nicholson, 1992). Examples of widely used solute tracers and geoindicators are Cl, B, Li, Rb, Cs and Na, K, Mg, Ca, SiO_2, respectively. The boundary between the two groups, however, is not rigid and depending on the physico-chemical conditions of the hydrothermal system tracers may participate in chemical reactions and geoindicators can behave inertly.

The division into area A and B, based initially on geographic location, has been reinforced by chemical composition. Although the chemical composition of all Tutum Bay vent waters is quite alike, compared to area A, area B has higher K, Rb, Sb, Cs, Tl and As and lower Ca, Li, Mn, Fe and Sr concentrations (Table 2-5). This seems to be directly related to the composition of samples W-1 and W-2 that also have elevated concentrations of K, Rb, Sb, Cs, Tl, and As and lower Ca, Li, Mn, Fe, and Sr concentrations (Table 2-1). Thus the slight chemical difference in area A and B vent waters may be attributed to varying subsurface addition of a hydrothermal fluid similar in composition to W-1 and W-2.

The rare earth element (REE) patterns (Fig. 2-6) are as expected for hydrothermal fluids with a pH of ~ 6 (Michard, 1989). The pattern geometry is similar to that of the host rocks

TABLE 2-5
AVERAGE CHEMICAL AND ISOTOPIC COMPOSITIONS FOR AREA A AND AREA B HYDROTHERMAL FLUIDS COMPARED TO SEAWATER

Sample	Unit	Area A	Area B	Seawater
pH		6.1	6.3	8.03
Cl	(ppm)	295	360	19520
Br	(ppm)	6.8	10.7	45
SO_4	(ppm)	930	880	2748
HCO_3^-	(ppm)	840	860	154
B	(ppm)	8.4	8.6	4.1
Si	(ppm)	108	105	0.2
Na	(ppm)	650	665	10450
K	(ppm)	76	94	350
Ca	(ppm)	201	180	405
Mg	(ppm)	0*	0*	1235
Li	(ppb)	1020	990	136
Mn	(ppb)	495	380	1.6
Fe	(ppb)	1720	1050	15
Rb	(ppb)	351	367	104
Sr	(ppb)	6790	6240	7990
Sb	(ppb)	8.2	9.1	0.6
Cs	(ppb)	59	63	0.5
Tl	(ppb)	4.4	5.2	0.3
As	(ppb)	820	954	3.7
$\delta^{13}C$	‰	-1.5	-1.6	1.3
$\delta^{18}O$	‰	-5.1	-5.1	0.4
δD	‰	-30	-30	6.6
$^{87}Sr/^{86}Sr$	ratio	0.70392	0.70395	0.70918

Note: *Mg concentration is assumed to be 0 ppm by convention.

(Fig. 2-6) but Ce, Pr, Nd and Sm are relatively depleted, reflecting their greater immobility during hydrothermal alteration (Thompson, 1991). Some of the Ce may also have been lost due to adsorption onto or co-precipitation with Fe(III) oxyhydroxides prior to sampling. Ce^{3+} is easily oxidized to Ce^{4+} and may directly precipitate as CeO_2 while the other REEs still remain in their trivalent state (Goldberg et al., 1963). In addition, Ce forms colloidal ceric hydroxide (Carpenter and Grant, 1967) which is readily scavenged by Fe(III) oxyhydroxides. The slight difference in pattern geometry between areas A and B could be caused as well by varying degrees of subsurface mixing. This, however, does not account for the difference in vent 2 samples.

2.4.1 Origin of the hydrothermal fluid and probable mixing trends

A fluid in a hydrothermal system may be derived from any, or any combination, of the following sources: meteoric water, seawater, connate water, magmatic water and juvenile water. Mixing of waters from different sources affects many aspects of the geochemistry of a hydrothermal system, such as chemical composition, isotopic composition, temperature profile and gas content. Deep sea hydrothermal systems active along mid-oceanic ridges, in back-arc basins and on the flanks of seamounts likely derive all their fluid from seawater, although a minor magmatic contribution cannot be completely ruled out (De Ronde, 1995). In contrast, on-land hydrothermal areas derive most of their fluid from meteoric sources, but a significant magmatic contribution is likely (e.g., Giggenbach, 1992). Determination of the fluid origin is an important step in order to constrain subsurface processes and reservoir conditions. While the source determination is relatively straightforward in deep marine and inland settings, the subject becomes more complex in coastal regions (off-shore and on-shore) where seawater incursion can significantly alter the fluid composition in a hydrothermal system. For example, seawater mixing is present in the Savusava (Fiji), Puna (Hawaii) and Reykjanes (Iceland) hydrothermal systems (Nicholson, 1992). Similarly, meteoric water may be the source for

submarine hydrothermal systems in coastal areas where a steep topography and ample supply of rainwater can force the Ghyben-Herzberg boundary substantially offshore (Chuck, 1967; Nahm, 1966). Tropical and subtropical island-arc volcanoes are good examples for these conditions. Subsurface sealing of a hydrothermal systems, as argued for White Island, New Zealand (Giggenbach et al., 1989), can be another mechanism to prevent seawater from entering the nearshore environment, thus allowing for a meteoric water dominated submarine hydrothermal system.

The deuterium and oxygen isotopic composition of water is generally a good indicator of its origin. All Tutum Bay vent waters plot very close to the local meteoric water line (LMWL) whose equation is (Fig. 2-9):

$$\delta D = 7.56 * \delta^{18}O + 8.4 \qquad [2\text{-}3]$$

and their mean δD and $\delta^{18}O$ is almost identical to mean local precipitation, thus indicating that they are of a local meteoric origin, although discharging in a submarine environment. Hydrothermal fluids normally plot to the right of the LMWL due to exchange of ^{18}O with rock that came into contact with the fluid (e.g., Craig, 1966) or caused by subsurface mixing with an "andesitic water" (Giggenbach, 1992). Tutum Bay vent waters did not shift to the right of the LMWL indicating that they have undergone only little water-rock isotope exchange or mixing with an "andesitic water". Neither process, however, can be completely ruled out because an initial ^{18}O-shift to the right may have been later reversed by a subsequent isotope exchange between CO_2 and H_2O. Isotope shifts to the left have been observed in several CO_2-rich aquifers and hydrothermal waters (e.g., Fritz and Frape, 1982; Vuataz and Goff, 1986). The two on-land hot springs, Waramung and Kapkai, show a significant diagonal shift to the right which is contrary to the isotope exchange model by Craig (1963) but in support of the "andesitic water" model by Giggenbach (1992). The somewhat steeper mixing slope is to be

expected and can be explained by underground steam separation at a shallow level prior to discharge.

The $^{87}Sr/^{86}Sr$ ratios of Tutum Bay vent waters are quite different from local seawater, although their Sr concentrations are similar (Table 2-3). In contrast to the absolute Sr concentration, which in a hydrothermal fluid is controlled by host rock composition, pH (CO_2 content) and temperature, the $^{87}Sr/^{86}Sr$ ratios are independent of physico-chemical effects and similar or identical to those of the host rocks at isotopic equilibrium (e.g., Barnes et al., 1981). Based on their work at the Valles caldera, New Mexico, Vuataz et al. (1988) found that isotopic equilibrium for $^{87}Sr/^{86}Sr$ between a hydrothermal fluid and its host rock is rapidly attained. The same authors also noted that low Sr concentrations are generally characteristic of high temperature volcanic hosted hydrothermal systems, while high Sr concentrations are characteristic of low temperature and/or a Paleozoic sedimentary aquifer/reservoir. If seawater is considered as a possible source then the $^{87}Sr/^{86}Sr$ composition of Tutum Bay vent waters can only be explained by a complex and unlikely process of complete removal of seawater Sr, followed by Sr addition from volcanic rock.

Additionally, a seawater source or substantial seawater dilution can be ruled out on the basis of rather low total dissolved solids (TDS) (< 3000 mg/l) and molecular ratios indicative of a seawater source or seawater dilution, such as Cl/Mg, Cl/Br, Cl/SO_4 and Ca/Mg (Nicholson, 1992), that are quite different from those caused by seawater mixing.

After the meteoric origin of Tutum Bay vent fluids has been established, their physico-chemical history is best explored in a set of diagnostic ternary diagrams (e.g., Chang, 1984; Giggenbach, 1991; Giggenbach, 1997; Nicholson, 1992). Hydrothermal waters are generally divided into neutral chloride, acid sulfate and bicarbonate waters, but mixtures between the individual groups are common. They are classified on the basis of their major anions: Cl, SO_4 and HCO_3 (Fig. 2-11a). Tutum Bay vents plot close to the ΣCO_3 corner along the upper boundary for steam heated waters. Waters that plot in this area generally form due to condensation of vapors separated from a deeper neutral chloride water into cooler

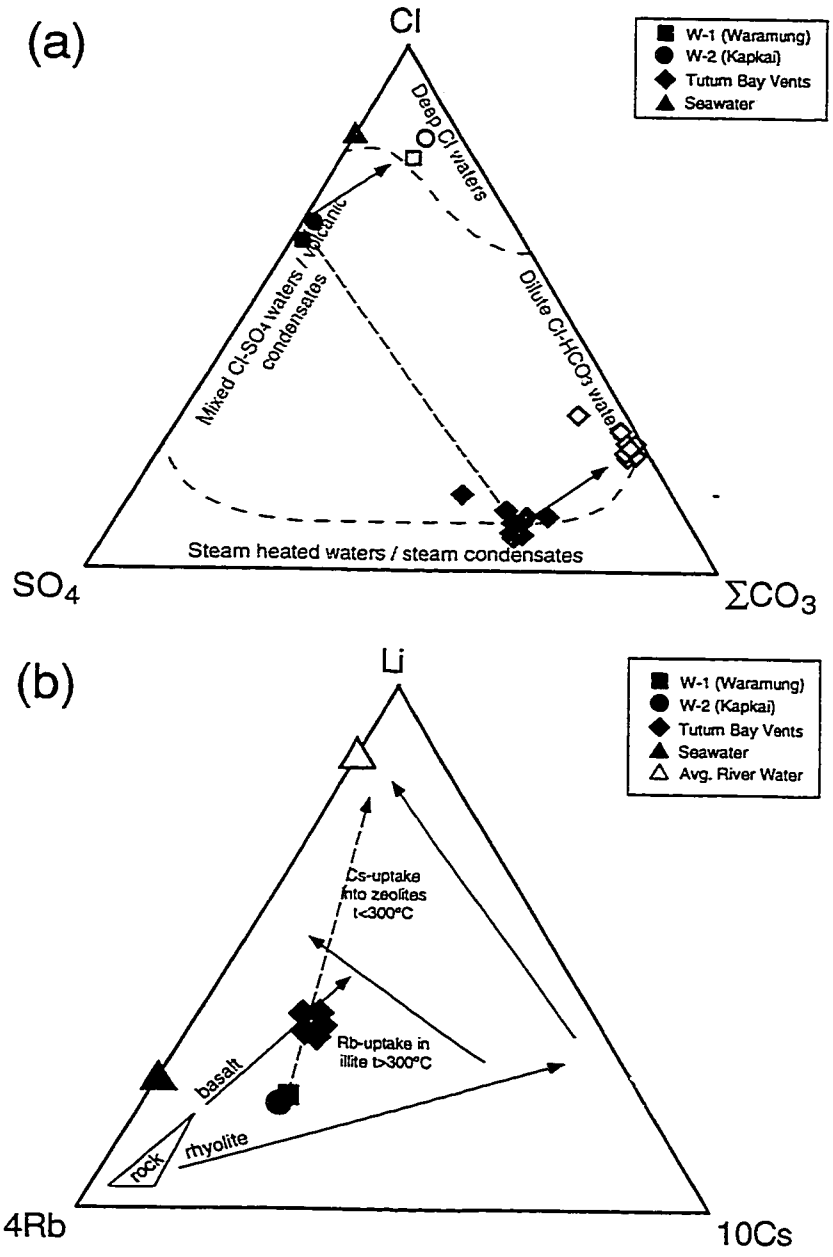

Fig. 2-11 (a) Relative Cl, SO_4 and ΣCO_3 contents of Tutum Bay, Waramung and Kapkai hot-springs. Empty symbols indicate SO_4 corrected position (see text). ΣCO_3 has been corrected for seawater contamination and includes H_2CO_3 and HCO_3. (b) Relative Li, Rb and Cs contents of Tutum Bay, Waramung and Kapkai hot-springs. Arrows indicate fluid evolution due to Rb and Cs-loss into alteration minerals. The dashed line indicates relative Li uptake by the hydrothermal fluid due to shallow processes (see text) and possible entrainment of meteoric water. The Rb-Cs ratio remains relatively constant.

ground water at a shallow level. There, based on the gas content of the vapor and redox conditions, either acid sulfate or bicarbonate waters are formed (e.g., Ellis and Mahon, 1977; Giggenbach, 1997; Hedenquist, 1990; Henley and Ellis, 1983). Based on their relative position in the ternary diagram the Tutum Bay waters are classified as bicarbonate waters, although the sulfate content of is too high for a true bicarbonate water. The high SO_4 content can be attributed to subsurface contribution from a SO_4-rich neutral chloride water, thus shifting the samples away from their original field along the Cl-ΣCO_3 mixing line (Fig. 2-11a). The SO_4-rich neutral chloride water is represented by samples W-1 and W-2 (Fig. 2-11a) that were collected at the Waramung (W-1) and Kapkai (W-2) thermal areas. The waters discharged from these hot-springs are interpreted to represent the deep reservoir fluid of the extensive hydrothermal system that is present under the west side of the island (Licence et al., 1987). Their high sulfate concentration may be due to absorption of magmatic vapors (e.g., Giggenbach, 1997) or simply result from leaching of marine sedimentary rocks that underlie the Ambitle volcano (Wallace et al., 1983). Their position on the Cl-ΣCO_3 mixing line, however, can be projected by simply drawing a mixing line between Tutum Bay, Waramung and Kapkai samples and shifting it parallel until W-1 and W-2 are in the field of deep chloride waters. Now they plot at a position indicative of a CO_2-rich dilute chloride waters which form by way of mixing with a shallow CO_2-rich water (e.g., Hedenquist, 1990). They can also form by mixing with groundwater, but then they would plot closer to the deep chloride water field (Fig. 2-11a). Dilute chloride waters are generally found above boiling zones and on the margins of high temperature hydrothermal systems.

Based solely on major anion composition, mixing between a bicarbonate water and seawater cannot be entirely ruled out (Fig. 2-11a) and less reactive elements, such as the rare alkalis Li, Rb and Cs (Giggenbach, 1991), must be utilized as additional criteria for fluid origin. These elements are added to the hydrothermal fluid at depth due to water-rock interaction and they are generally not affected by shallow processes. Relative Li, Rb and Cs contents (Fig. 2-11b) more or less exclude the possibility of a substantial seawater component.

All samples plot away from the compositional field of crustal rocks, indicating that secondary processes must have affected their composition. The crystallization of illite at high temperature must have removed some of the initial Rb from fluids W-1 and W-2 explaining their relative position in Fig. 2-11b. The Li/Cs ratios is dependent on lithology and the intermediate position between basalt and rhyolite is in good agreement with the andesitic composition of the Ambitle volcano (Wallace et al., 1983). The relatively higher Li content of the Tutum Bay samples may be due to the Cs-uptake into secondary zeolites during cooling, Li-uptake due to shallow processes, or mixing with meteoric water (Fig. 2-11b). The loss of Cs to zeolites is most likely not of any importance considering that the Rb/Cs ratio remains constant. In Tutum Bay waters the ratios of all alkalis, except for Li, are almost identical to those in samples W-1 and W-2. Butterfield et al. (1990), who studied the boiling hydrothermal fluids at Axial seamount on the Juan de Fuca ridge, also noted unexpectedly high levels of Li in the vapor-enriched phase and attributed this to water-rock interaction subsequent to phase separation. This would argue that at least some of the relative Li increase has to be attributed to shallow leaching, a proposition contrary to the belief that Li is the alkali probably least affected by secondary processes (e.g., Giggenbach, 1991).

Two other important elements, Cl and B, are widely used to trace the origin and the subsurface flow of hydrothermal fluids. In the case of the Tutum Bay samples, however, Cl cannot be applied successfully because the concentration gradient between seawater and hydrothermal fluid is enormous and the error introduced due to seawater contamination is therefore substantial. Boron, on the other hand, seems to be an excellent tracer for subsurface conditions at Ambitle Island (Fig. 2-12). Regardless of their concentrations Li/B, Rb/B and Cs/B ratios remain constant in all samples, indicating a common source reservoir. The subsurface flow direction from W-2 over W-1 to Tutum Bay is indicated by decreasing B and alkali contents which record dilution of the deep reservoir fluid by either groundwater or bicarbonate water (Fig. 2-12), in accord with their geographic and topographic location. The vents in Tutum Bay are topographically lowest and furthest away from the center of the

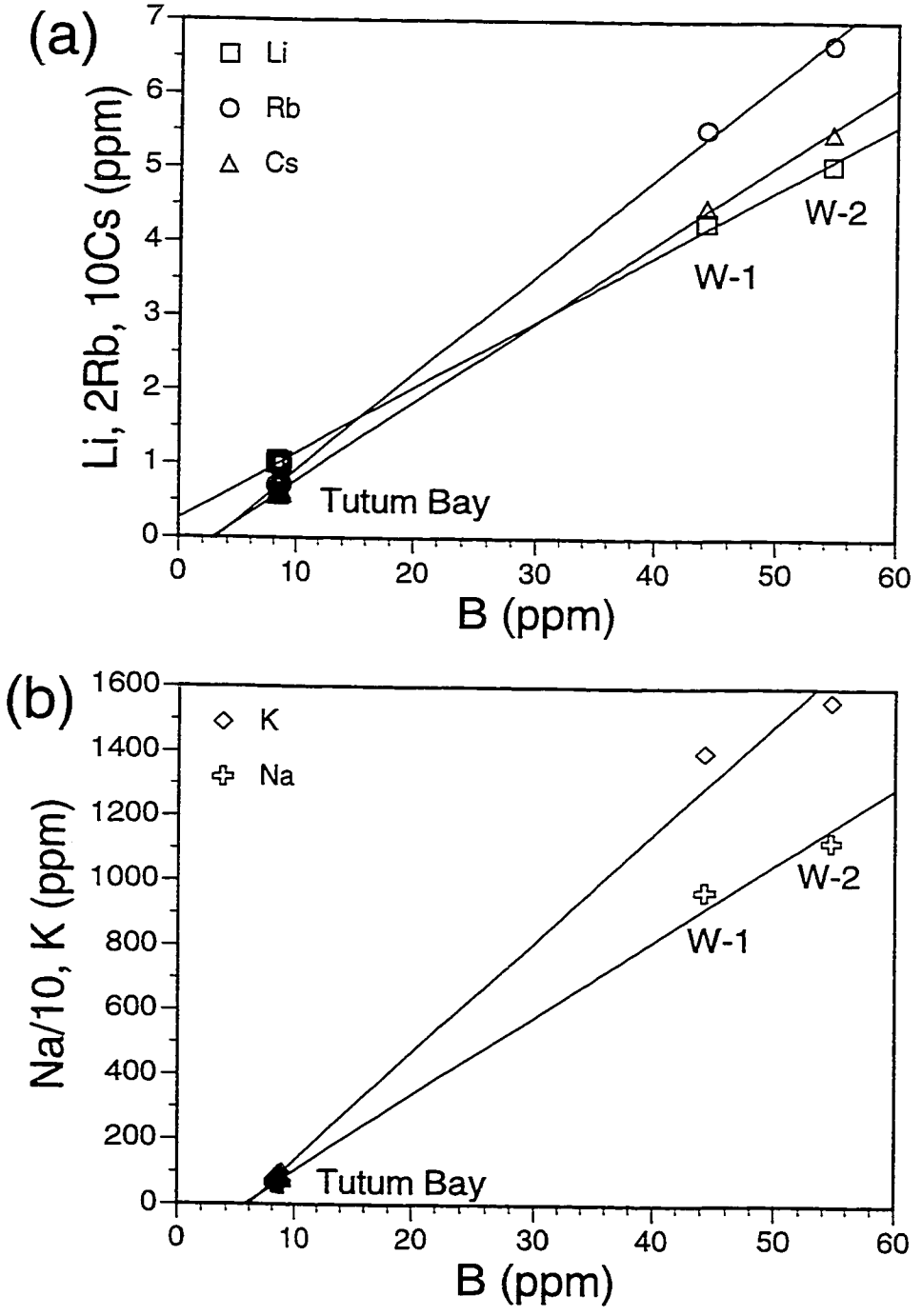

Fig. 2-12 (a) Li, Rb and Cs vs. B in Tutum Bay, Waramung (W-1) and Kapkai (W-2) hot-springs. $r^2 > 0.99$ for all linear regression lines. (b) Na and K vs. B in Tutum Bay, Waramung (W-1) and Kapkai (W-2) hot-springs. $r^2 > 0.91$ for all linear regression lines.

hydrothermal system, whereas the sample from the Kapkai thermal area (W-2) is relatively higher (approximately 30 m above sea level) and closer. The linear regression lines for Rb and Cs and for Na and K converge exactly at that point where they intercept the x-axis (Fig. 2-12). Assuming that the regression lines represent mixing between deep neutral chloride and shallow bicarbonate water, the intercept of the x- or y-axis represents one endmember. This endmember, based on Rb and Cs would have a boron excess of approximately 3 ppm, whereas the one based on Li would have a Li excess of approximately 0.25 ppm. The former is a much more likely alternative for a process that forms bicarbonate water. Boron occurs largely as boric acid (H_3BO_3), its volatile form, and can be easily carried in the vapor phase even at lower temperatures (Tonani, 1970). Using a simple mass balance equation, based on the 3 ppm boron excess, bicarbonate and chloride water fractions were calculated to be 0.89 and 0.11, respectively. Based on the Na-K boron excess bicarbonate and chloride water fractions would be 0.93 and 0.07, respectively. This deep reservoir component is in good agreement with that found in waters of similar origin in other hydrothermal systems. Hedenquist (1990), for example, estimated that at the Broadlands-Ohaaki geothermal system most of the marginal upflow mixes with steam-heated waters and only little deep fluid (~ 10 %) rises to the surface.

Additional insight into potential processes controlling the fluid composition and subsurface processes may be provided by the chemical composition of the gases, as listed in Table 2-4. An initial classification of the gases is carried out in terms of relative concentrations of N_2(c), He and CO_2 contents (Giggenbach, 1995b). On the basis of gas discharges from a wide range of tectonic environments, the compositions of volcanic and geothermal vapors were found to represent essentially mixtures of two endmember components: a mantle derived component, very low in N_2 with CO_2/He ratios of 20 000 to 40 000, and an arc-type component with much higher CO_2/He ratios of $> 10^6$ and a quite uniform CO_2/N_2 ratio of 100±60 (Giggenbach, 1995b). The data points for the gases plot at the upper boundary of the compositional area outlined for volcanic and geothermal vapors (Fig. 2-13) and across the middle of the triangle, suggesting a major input of mantle-derived gases. The increased relative

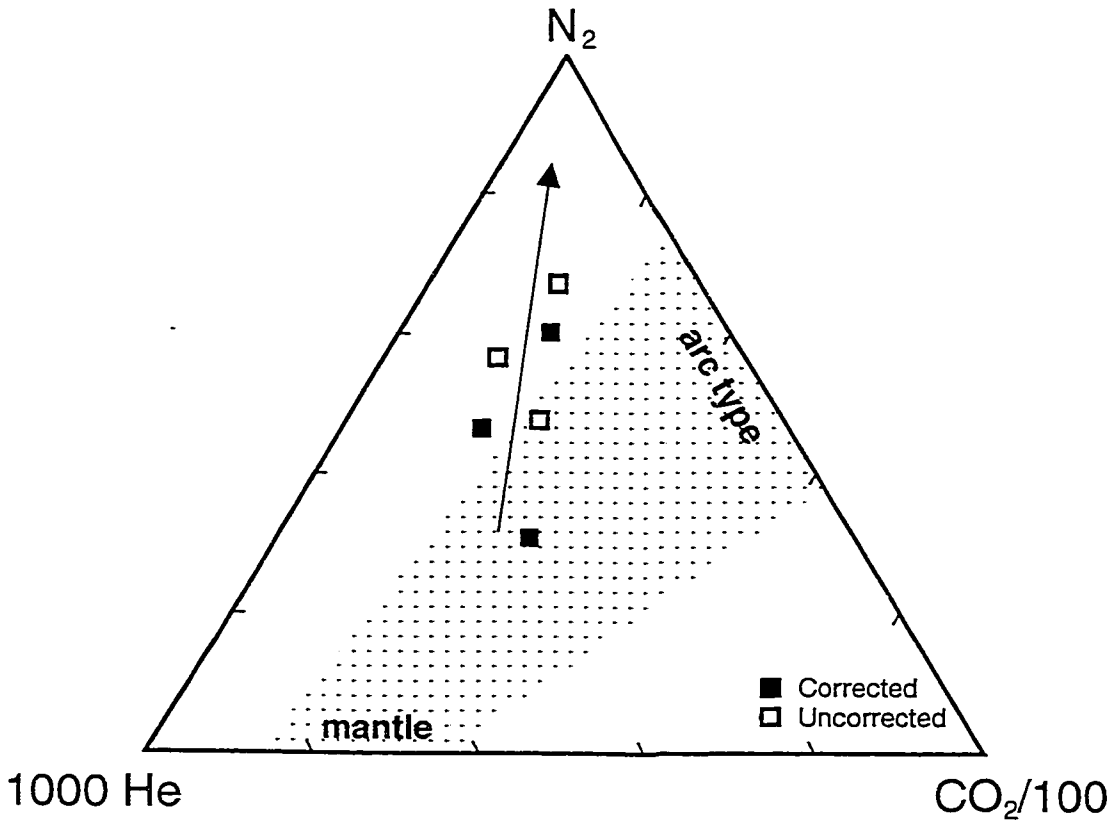

Fig. 2-13 Ternary plot of relative CO_2, N_2 and He contents of non-condensable gases collected from submarine discharges in Tutum Bay (after Giggenbach, 1995b). The shaded area indicates the relative position for mantle and arc type gases. The arrow indicates N_2 uptake due to sample contamination with air.

N_2 contents may reflect increased stripping of N_2 during the rise of the gases through air-saturated seawater. Increased interaction of the gases with water can be expected to lead to removal of soluble components, an assumption supported by the absence of H_2S, the most soluble component (Table 2-4).

The $\delta^{13}C$ isotopic composition of the CO_2 could be reconciled with a predominantly mantle origin, but could also point to the addition of carbon from marine carbonates. The later is in good agreement with the assumption that the high SO_4 content of the hot spring waters is due to leaching of marine sedimentary rocks that underlie the Ambitle volcano (see above). The $\delta^{13}C$ value of approximately -2.35 ‰ lies intermediate between the known range for marine carbonate derived (Welhan, 1988) and mantle derived CO_2 (Hoefs, 1997). At Ambitle, which is located on top of the West Melanesian trench, the mantle-derived CO_2 may be as heavy as -3 ‰ due to a possible contribution from subducted sediments. The value of -3 ‰ is based on work of Poorter et al. (1991), who reported isotopic compositions of volcanic gases from the East Sunda and Banda arcs, Indonesia which is a similar tectonic setting on the west side of Papua New Guinea. The carbon and hydrogen isotopic compositions of methane (CH_4) are similar to values reported for abiogenic CH_4 (Fig. 2-14). Due to the very steep geothermal gradient in Tutum Bay, subsurface temperatures are immediately above 100°C which excludes bacterial fractionation. In particular, the distinct enrichment of heavy carbon isotopes leads to the conclusion that inorganic process such as the Fischer-Tropsch reaction are responsible for the CH_4 formation (e.g., Botz et al., 1996; Lyon and Hulston, 1984).

2.4.2 Geothermometry

Solute geothermometers, such as listed in Table 2-6, provide powerful tools to estimate subsurface conditions. Their successful application has been extensively discussed in the geothermal literature and relies on five basic assumptions: 1) exclusively temperature dependent

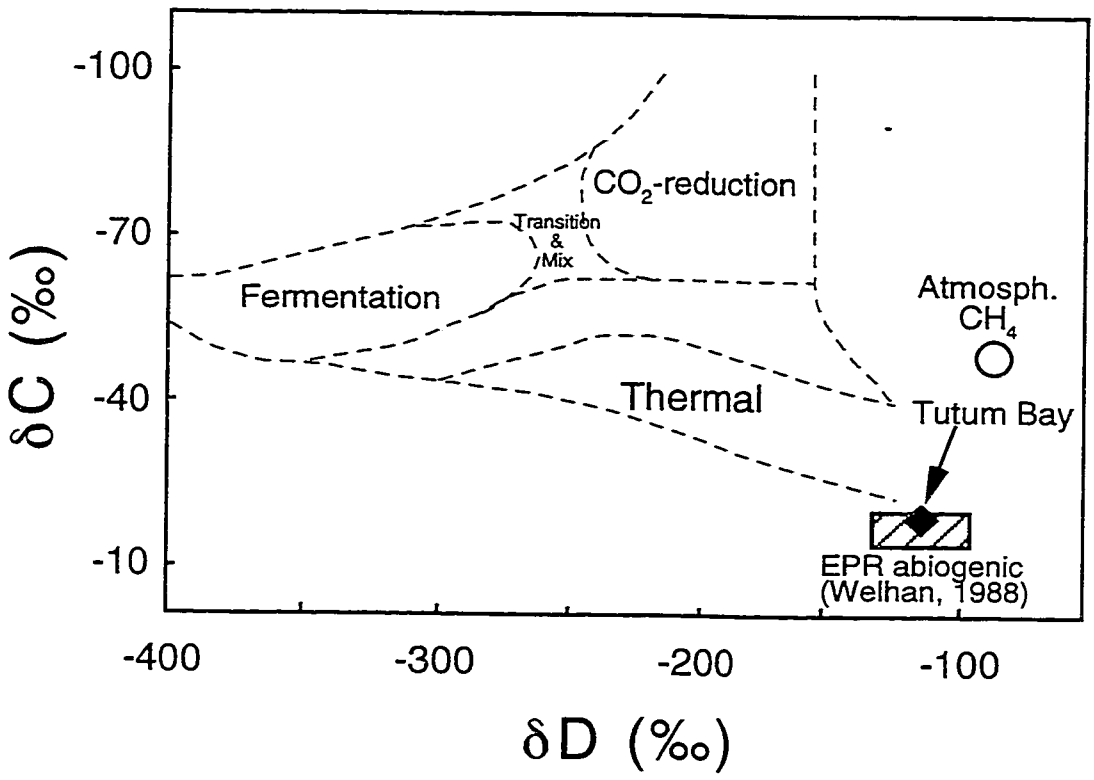

Fig. 2-14 Characterisic isotope fields for CH_4 formed by different processes (after Botz et al., 1996). The compositional field for East Pacific Rise (EPR) abiogenic CH_4 is from Welhan et al. (1988).

TABLE 2-6
CALCULATED RESERVOIR TEMPERATURES FOR KAPKAI, WARAMUNG AND TUTUM BAY VENT FLUIDS

Thermometer	Vent 1	Vent 2	Vent 3	Vent 4	W-1	W-2	Ref.*
	T°C	T°C	T°C	T°C	T°C	T°C	
Amorphous Silica	9	8	8	7	-3	6	1
Chalcedony	100	99	99	98	86	97	1
Quartz	128	127	127	126	114	125	1
Quartz steam loss	125	124	124	123	113	122	1
K/Mg	n.d.	n.d.	n.d.	n.d.	306	310	2
Li/Mg	n.d.	n.d.	n.d.	n.d.	203	209	3
Na/Li	166	172	169	168	111	112	4
Na/K	246	253	252	273	276	271	5
Na/K	240	245	244	262	264	260	2
Na-K-Ca	191	192	192	206	312	320	6

Note: *References: (1) Fournier (1977), (2) Giggenbach (1988), (3) Kharaka and Mariner (1989), (4) Kharaka et al. (1983), (5) Fournier (1979), (6) Fournier (1973).

mineral-fluid reaction; 2) abundance of the mineral and/or solute; 3) chemical equilibrium; 4) no re-equilibration; and 5) no mixing or dilution (Nicholson, 1992). The no mixing or dilution assumption, however, can be circumvented if their extent and/or influence on solute ratios (e.g., Na/K) is known (see above).

The calculated temperatures in Table 2-6 differ quite drastically. This is not surprising considering that most problems in the use of geothermometers arise from application to unsuitable samples. Different geothermometers, however, record different equilibria and disagreement does not immediately eliminate the use of one or the other. Careful application and evaluation of calculated temperatures may provide important clues to the overall hydrology of the hydrothermal system.

The temperatures calculated with the silica geothermometers (Fournier, 1977) are too low to represent a reliable estimate of the reservoir condition. This is to be expected in particular for the samples W-1 and W-2, since these springs are fed from reservoirs with temperatures in excess of ~230°C and have, therefore, lost some of their initial silica due to precipitation of quartz, chalcedony, or amorphous silica during ascent (Fournier, 1985; Rimstidt and Barnes, 1980). The application of the silica thermometer to Tutum Bay samples (V-1 to V-4) is problematic because they are a mixture of at least two fluids and the thermometer is based on absolute silica concentration.

The quality of reservoir temperatures calculated with one of the following thermometers: K/Mg (Giggenbach, 1988), Mg/Li (Kharaka and Mariner, 1989), Na/Li (Kharaka and Lico, 1982), Na/K (Fournier, 1979; Giggenbach, 1988) and Na-K-Ca (Fournier and Truesdell, 1973) depends strongly on the equilibrium between fluid and host lithology. Attainment of reservoir equilibrium has been verified for samples W-1 and W-2 based on their relative Na, K and Mg concentrations (e.g., Giggenbach, 1988). Unfortunately, this method cannot be directly applied to the Tutum Bay samples because they have zero-Mg by definition, but equilibrium conditions would apply for Mg concentrations between approximately 0.2 and 2 ppm. Temperatures obtained from the Li/Mg and Na/Li thermometers are substantially lower

than those form the other ionic solute thermometers (Table 2-6). Exchange reactions with Mg seem to be expeditious at lower temperatures and Mg-based thermometers may, therefore, record the last equilibrium prior to discharge (e.g., Nicholson, 1992). The low Li/Mg temperature, however, is in contrast with the K/Mg thermometer. Considering that the relative Mg, Na and K concentrations of W-1 and W-2 indicate deep reservoir equilibrium, it is rather the Li concentration that must have been affected during ascent or at a shallower level. The temperature obtained from K/Mg, Na/K and Na-K-Ca are in good agreement and indicate a reservoir temperature of approximately 300°C. Na/K temperatures are slightly lower which is to be expected given the slightly peripheral location of the thermal areas. The Na/K ratio of a hydrothermal fluid generally increases during lateral flow (Ellis and Mahon, 1977). The Tutum Bay samples, although mixed with water of a different origin, still carry a significant Na/K imprint of the deep reservoir. Temperatures for vents 1, 2 and 3 are slightly lower, while vent 4 has identical temperatures to W-1 and W-2 (Table 2-6). This would confirm that the discharge from vent 4 has a relatively greater proportion of the deep reservoir fluid (see above). The notable disagreement between Tutum Bay and on-land Na-K-Ca temperatures is a result of the high pCO_2 and, therefore, higher Ca concentration in Tutum Bay fluids.

The Na/Li temperatures obtained for Tutum Bay samples may be representative of shallow reservoir conditions that postdate mixing between deep reservoir and bicarbonate fluid. When compared to Mg, Na, K, Rb and Cs, Li seems to be the element most affected by shallow reservoir processes, but the calculated Na/Li temperatures appear to be in good agreement with theoretical considerations. Let us consider one more time the process that leads to the formation of a CO_2 or bicarbonate water. Isenthalpic expansion of steam, separated from a deeper liquid phase at close to atmospheric pressure, is accompanied by a drop in temperature to about 160°C (Giggenbach, 1997). Bicarbonate waters, formed due to interaction between groundwater and this 160°C steam, have generally temperatures in the vicinity of 150°C (e.g., Cioni and D'Amore, 1984; Hedenquist, 1990). Mixing of this 150°C bicarbonate water with a 300°C deep reservoir fluid at a ratio of ~ 9:1, as obtained from the boron mixing model (see

above), leads to a final shallow reservoir temperature of 165°C which is in perfect agreement with the calculated Na/Li temperatures (Table 2-6). Calculated ^{13}C equilibrium temperatures for the system $CO_{2(g)}$ - $HCO_{3(l)}^-$ (Friedman and O'Neil, 1977) are also in good agreement with the proposed process of Tutum Bay vent water formation. For the $\delta^{13}C$ range of CO_2 gas (-2.55 to -2.23 ‰) and HCO_3^- (-1.06 to -2.2 ‰) temperatures are between 145 and 170°C.

Assuming equilibration of the gases dissolved in a liquid phase and preservation of equilibrium CH_4/CO_2 ratios in the samples (Giggenbach and Matsuo, 1991), the CH_4-CO_2 equilibrium temperatures are between 257 and 291°C (Table 2-4). Depth of separation, therefore, should be at approximately 1000 m, providing that the deep reservoir fluid is on the boiling curve. These CH_4-CO_2 equilibrium temperatures are in good agreement with reservoir fluid estimates based on the Mg/Li, Na/K and Na-K-Ca solute geothermometers (Table 2-6). While there is apparent chemical equilibrium between CO_2 and CH_4, carbon isotopic equilibrium is not attained. This is not surprising considering that equilibration time may be as long as 20000 years at a temperature of 400°C and 10^7 years at 300°C (Giggenbach, 1982). A temperature calculated with the carbon isotope thermometer of Lyon and Hulston (1984):

$$t°C = -173 + 15790/(\,^{13}C + 9) \qquad [2\text{-}4]$$

of 488°C is too high to represent reservoir conditions. This temperature most likely represents an earlier equilibrium at greater depth (e.g., Botz et al., 1996; Lyon and Hulston, 1984).

2.5 SUMMARY AND CONCLUSIONS

Compared to seawater, the hydrothermal fluids from Tutum Bay are depleted in δD, $\delta^{18}O$, $\delta^{13}C$, ^{87}Sr, Cl, Br, SO_4, Na, K, Ca, Mg and Sr and enriched in HCO_3, B, Si, Li, Mn, Fe, Rb, Cs, Sb, Tl and As. They seem to be dominantly of meteoric origin, although they

discharge in a marine environment. Their final chemical composition is the outcome of a two- or possibly three-step process (Fig. 2-15): (1) Phase separation in the deep reservoir beneath Ambitle Island produces a high temperature vapor that rises upward and subsequently reacts with cooler ground water to form a low pH, CO_2-rich water of approximately 150-160°C. This fluid is highly reactive and pH-Eh sensitive elements such as Fe, Mn, Ca and Sr are leached form the host rock in the shallow reservoir. (2) Caused by the steep topography, this CO_2-rich fluid moves laterally towards the margin of the hydrothermal system where it mixes with the marginal upflow of the deep reservoir fluid. This produces a dilute chloride water of approximately 165°C. A third step may be the entrainment of minor amounts of ground or seawater during its final ascent. Based on a B-Rb/Cs mixing model it has been estimated that approximately 10% of the deep reservoir fluid reaches the surface.

The definite chemical composition of Tutum Bay vent fluids may be slightly different from the values reported in Table 2-2, because of phase separation during ascent from the shallow reservoir and the Mg-correction for seawater contamination. (Single-step phase separation during flashing of a liquid from 160°C to 100°C produces approximately 12% vapor, which would represent the maximum error for elements that preferentially remain in the liquid phase) Thermometry and mixing calculations, however, are not affected, because they are based on element ratios rather than on absolute concentrations.

The gas phase present in Tutum Bay is predominantly of magmatic/mantle origin with a minor contribution from subducted sediments. The total discharge from all vents is approximately 20 L/s. Carbon dioxide and methane are apparently in chemical equilibrium with a liquid phase in the deep reservoir, although ^{13}C isotopic equilibrium has not been attained.

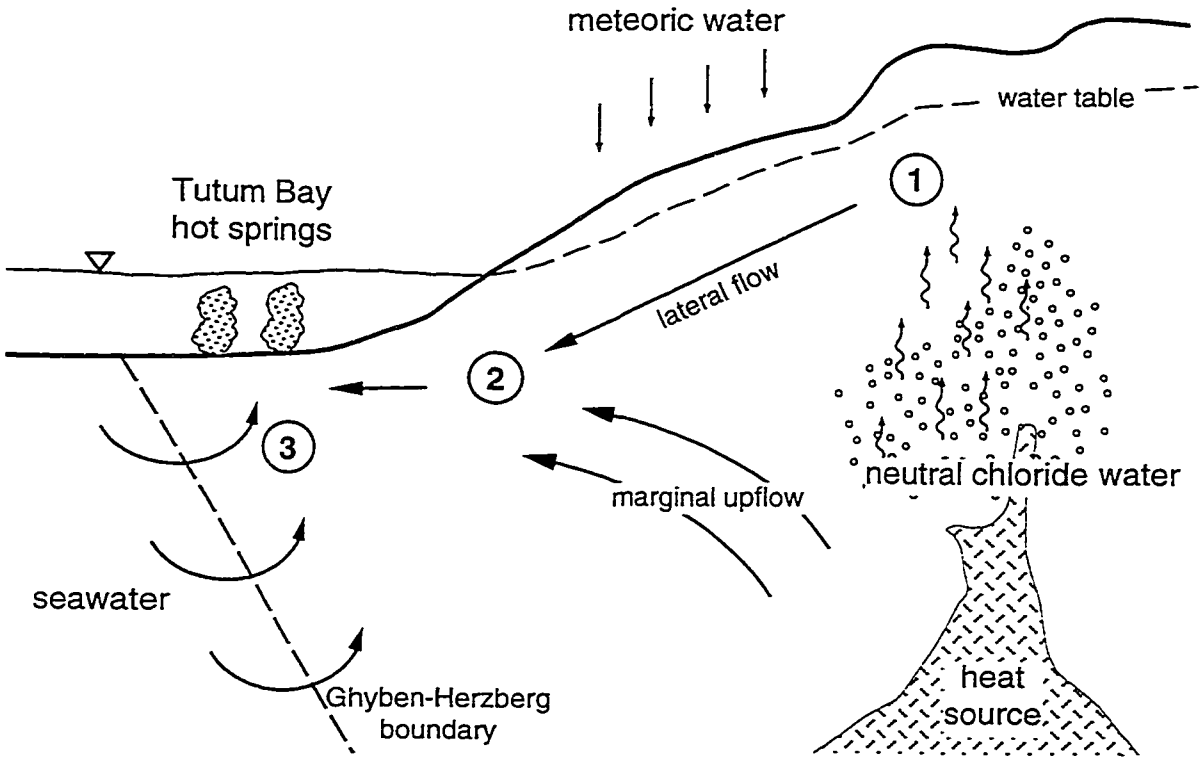

Fig. 2-15 Hypothetical cross section through Tutum Bay and the west side of Ambitle Island. The circled numbers (1, 2 and 3) indicate the approximate location of subsurface reaction zones: (1) Formation of a steam heated bicarbonate water, (2) gravity driven lateral flow and mixing with marginal upflow from deep reservoir neutral chloride water, and (3) possible mixing with seawater near the Ghyben-Herzberg boundary.

3. THE PRECIPITATION OF HYDROTHERMAL ARAGONITE

3.1 INTRODUCTION

Throughout the geological record several occurrences of hydrothermally precipitated carbonate minerals have been reported from sedimentary sequences. Precipitation was inferred to be from hydrothermally modified meteoric waters (e.g., Derochers and Al-Aasm, 1993) or due to venting of methane rich fluids (cold and hot) (e.g., Hovland, 1990; Kaufman et al., 1996). The fringing reef on the west side of Ambitle Island is the only known present-day location where purely hydrothermally-driven carbonate deposition is extensively co-occurring with a natural biogenic calcifying community and "normal" marine carbonate cementation. Hydrothermal fluids affect adjacent scleractinian corals and the local benthic foraminifera population (Switzer, 1997).

3.2 ANALYTICAL METHODS

Hand specimens, polished thin and thick sections were examined using standard light, cathodoluminescence, and fluorescence microscopy. Several thin sections were stained with a mixture of 0.2% hydrochloric acid and 0.2% potassium ferricyanide to visualize Fe-content. Mineral identification was confirmed by scanning electron microscope (SEM) analysis and powder and single-crystal X-ray diffractometry (XRD). Small sample chips were carbon coated and mounted on aluminum stubs for SEM analysis on a Cambridge Stereoscan 360 scanning electron microscope, fully integrated with an Oxford Instruments (Link) eXL-II energy dispersive x-ray (EDX) microanalyzer. XRD analyses were performed on a Philips PW 3710, stepping 0.02 °2θ from 2.00° to 88.00 °2θ using copper x-radiation generated at 45 kV and 40 mA.

The chemical composition of aragonite and calcite was determined by micro-beam analyses on carbon-coated polished thin sections and bulk chemical methods on powdered sample material. Electron microprobe analyses were performed on a CAMECA SX-50, operating at 15 kV accelerating voltage, 2 nA beam current and beam diameters varying from <1μm to 5μm. The quality of the microprobe data was estimated from calculated structural formulae based upon the chemical analyses. Proton microprobe analyses were carried out on the Ruhr University, Bochum micro-PIXE, on spots of approximately 5 μm diameter, using a 3 MeV beam (Bruhn et al., 1995) and element concentrations were evaluated with the GUPIX software package (Maxwell et al., 1989; Maxwell et al., 1995).

Trace element concentrations in carbonates are generally minor (e.g., Veizer, 1983) and, therefore, below the detection limit of conventional microbeam methods. In order to obtain a more detailed chemical and isotopic composition of the hydrothermal carbonate, the samples V-2(x), V-2(m), V-3a, V-4.1a and V-4.2a were separated from coral and or volcanic material (e.g., Fig. 3-1). For these samples major elements were obtained by x-ray fluorescence (XRF) and wet chemical methods. As, Au, Br, Hg, Sb, Se and W were determined by neutron activation analyses (NAA). Ag, Cd, Cs, Hf, In, Mo, Nb, Pb, Rb, Ta, Th, Tl, U, Y, and Zr were determined by inductively coupled plasma mass spectrometry (ICP-MS) and Ba, Be, Co, Cr, Cu, Ni, Sc, Sr, and V were determined by inductively coupled plasma emission spectrometry (ICP-ES). XRD, XRF, SEM, ICP and microprobe analyses were carried out at the Geological Survey of Canada, NAA was performed by Activation Labs in Ancaster, Ontario. Analytical errors are as follows: < 2% for XRD, < 5% for wet chemical analyses, < 5% for ICP-ES (except < 10% for Ag, Ba and Sr), < 10% for ICP-MS and ~ 20 % for INAA. In order to assure data quality for analyses that were not performed by myself, I always submitted blind duplicate samples.

Carbon and oxygen isotope analyses were performed at the G. G. Hatch Isotope Laboratory, University of Ottawa on a triple collector VG SIRA 12 mass spectrometer. The

Fig. 3-1 Petrography of hydrothermal precipitates. (a) Photograph of a large hand specimen collected from a dead vent in the area of vent 4. A large volcanic boulder embedded in a matrix of volcaniclastic sediment, Fe-oxyhydroxide, biogenic carbonate and hydrothermal aragonite. The Fe-oxyhydroxide lined opening on the lower right (arrow) used to be a channel for the hydrothermal fluid. (b) Photograph of a slab from the above hand specimen. The hydrothermal fluid channel is now to the left and the Fe-oxyhydroxide has already been removed for chemical and isotopic analyses. This sample clearly shows the change (arrow) from coarse (light gray) to fine grained (bright white) aragonite.


Nikon
a


1 cm
b

routine precision was tested using an internal standard and is 0.1‰ for carbon and oxygen. All results are reported in standard delta (δ) notation in per mil (‰) units, relative to the PDB standard for carbon and relative to VSMOW for oxygen, unless otherwise noted. $^{87}Sr/^{86}Sr$ were measured on a five collector Finnigan MAT 262 solid source mass spectrometer at the Institut für Geologie, Ruhr Universität, Bochum following Buhl et al. (1991) and Diener et al. (1996). The average of 100 repeat measurements for the NBS 987 standard was 0.710224±0.000008. Six samples (V-2(x), V-2(m), V-4.1(x), V-4.1(m), V-4.3(x), V-4.3(m)) for O, C and Sr isotope analyses were taken by micro-drilling to allow for a direct comparison between fine grained and coarse grained aragonite within one sample.

Temperature and salinity of fluid inclusions were determined using a Fluid Inc gas-flow heating/freezing stage. Geochemical calculations were carried out with the computer programs SOLMINEQ, GEOCHEMIST'S WORKBENCH and PHREEQC (Parkhust, 1995).

3.3 SAMPLE DESCRIPTIONS

A complete listing of all carbonate samples and short description is presented in Table 3-1. The precipitation of hydrothermal carbonates in Tutum Bay is not restricted to, but mainly occurs in the immediate vicinity of vent sites. Throughout the bay hydrothermal fluids seep slowly through the seafloor and cause precipitation of aragonite in intergranular spaces in the bottom sediment or in open spaces in the skeletons of dead corals (Fig. 3-2). The bulk precipitation, however, is in the proximity of the four vent sites (Fig. 1-2). There aragonite forms isopachous rims, monomineralic layers and splays of euhedral (pseudohexagonal) crystals that encrust dead corals and volcaniclastic boulders and pebbles (Fig. 3-1). The growth direction of individual crystals is parallel to each other and normal to their substrate and they can be up to 2 cm long. Crystals are generally terminated by scalloped surfaces that do not represent the internal structure and an abrupt change of crystal habit and size (Fig. 3-3). The

TABLE 3-1
DESCRIPTION OF TUTUM BAY HYDROTHERMAL CARBONATE PRECIPITATES

Sample	Location	Description	XRD analyses
V-1A	Vent 1	white micritic carbonate matrix in open spaces between volcanic sediment	aragonite
V-2D	Vent 2	hydrothermal carbonate big clear crystals (Fig. 3-3) from massive layers in the vent orifice	aragonite
V-2E	Vent 2	hydrothermal carbonate small white crystal ends on top of V-2D (Fig. 3-3)	aragonite
V-3A	Vent 3	white micritic hydrothermal carbonate matrix with some bigger euhedral crystals where space available (Fig. 3-2)	aragonite
FV-3B	Vent 3	dead coral fragment (Fig. 3-2)	aragonite
V-4.1A	Vent 4	white micritic hydrothermal carbonate on top of bigger crystals and below Fe-oxyhydroxides (Fig. 3-1)	aragonite
V-4.1B	Vent 4	big clear/gray euhedral aragonite crystals (Fig. 3-1)	aragonite
V-4.2A	Vent 4	big clear/gray euhedral aragonite crystals	aragonite
V-4.2B	Vent 4	fine grained Fe-calcite crust on top of V-4.2A	aragonite & calcite
V-4.3	Vent 4	alternating layers of coarse and fine grained aragonite	aragonite
FV-4A	Vent 4	big (up to 2 cm) clear/gray euhedral aragonite crystals	
FV-4B	Vent 4	fine grained portion of FV-4A	aragonite
FV-4C	Vent 4	fine grained Fe-calcite crust (Fig. 3-4)	calcite
V-2 (x)	Vent 2	micro-drilled sample of coarse aragonite from sample V-2	aragonite
V-2 (m)	Vent 2	micro-drilled sample of fine grained (micritic) aragonite from sample V-2	aragonite
V-4.1 (x)	Vent 4	micro-drilled sample of coarse aragonite from sample V-4.1	aragonite
V-4.1 (m)	Vent 4	micro-drilled sample of fine grained (micritic) aragonite from sample V-4.1	aragonite
V-4.3 (x)	Vent 4	micro-drilled sample of coarse aragonite from sample V-4.3	aragonite
V-4.3 (x)	Vent 4	micro-drilled sample of fine grained (micritic) aragonite from sample V-4.3	aragonite

Fig. 3-2 Petrography of hydrothermal precipitates. (a) Photograph of a hand specimen collected near vent 2. Poorly sorted rounded to subrounded sand to pebble sized volcaniclastic sediment cemented by hydrothermal aragonite (white); with almost complete filling of primary pore space by aragonite. Some volcanic fragments show centripetal alteration zones. (b) Photomicrograph with crossed polars of a scleractinian coral skeleton. Hydrothermal aragonite (arrow) is starting to occlude open spaces. In plain light or at a slightly different crossed polars setting it is almost impossible to distinguish between coral and hydrothermal aragonite. The scale bar is 10 μm.

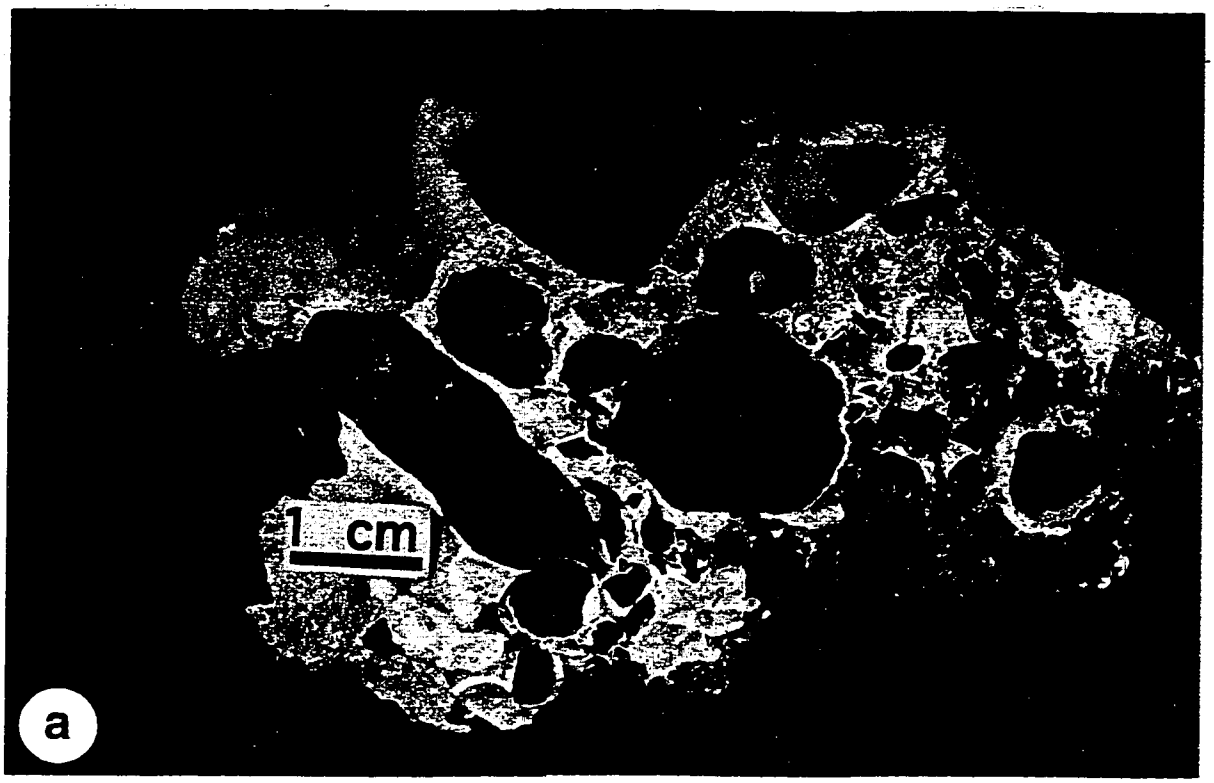
1 cm
a

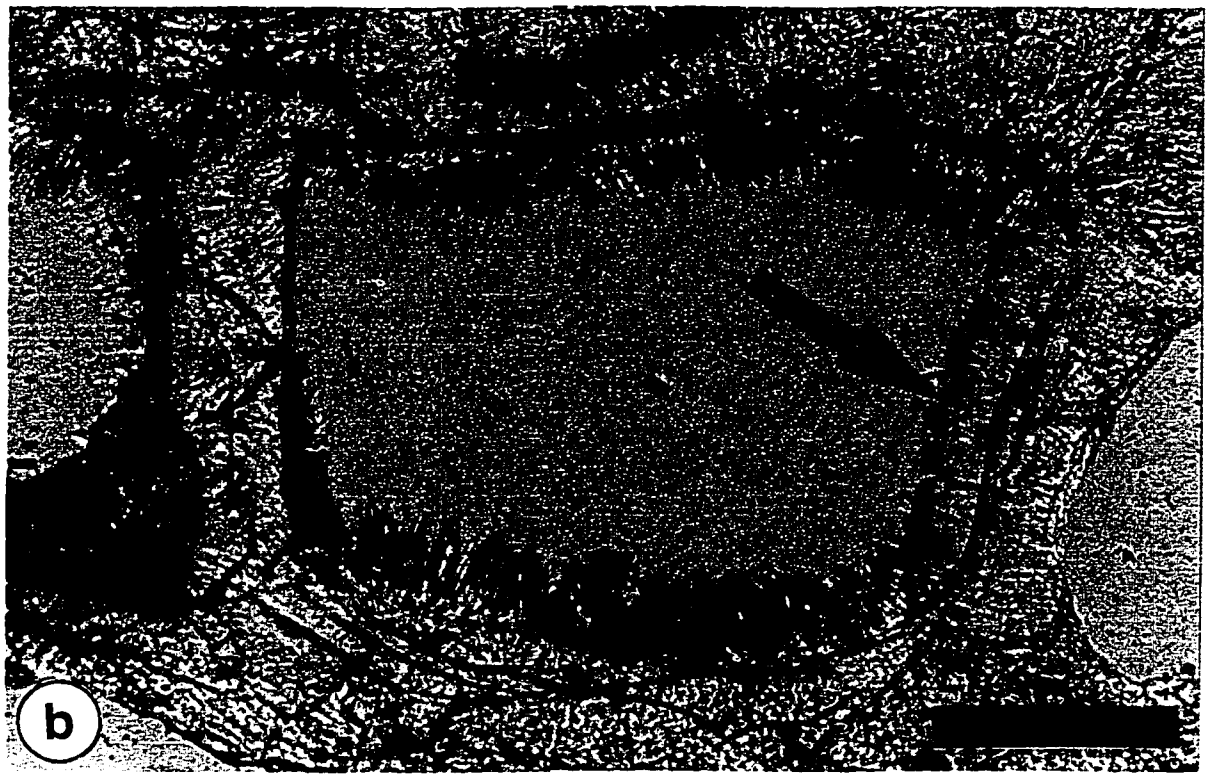
b

Fig. 3-3 Petrography of hydrothermal precipitates. (a) Photograph of euhedral, pseudo-hexagonal coarse aragonite (gray) and fine grained aragonite (white). Crystals grow approximately normal to the volcaniclastic substrate. (b) Photomicrograph of two pseudo-hexagonal aragonite crystals and radiating fine grained aragonite (feather dendrites). The feather dendrites are terminated by a thin layer of Fe-oxyhydroxide. The two spots where proton microprobe analyses were performed are indicated by squares. The scale bar in the lower left represents 200 μm.

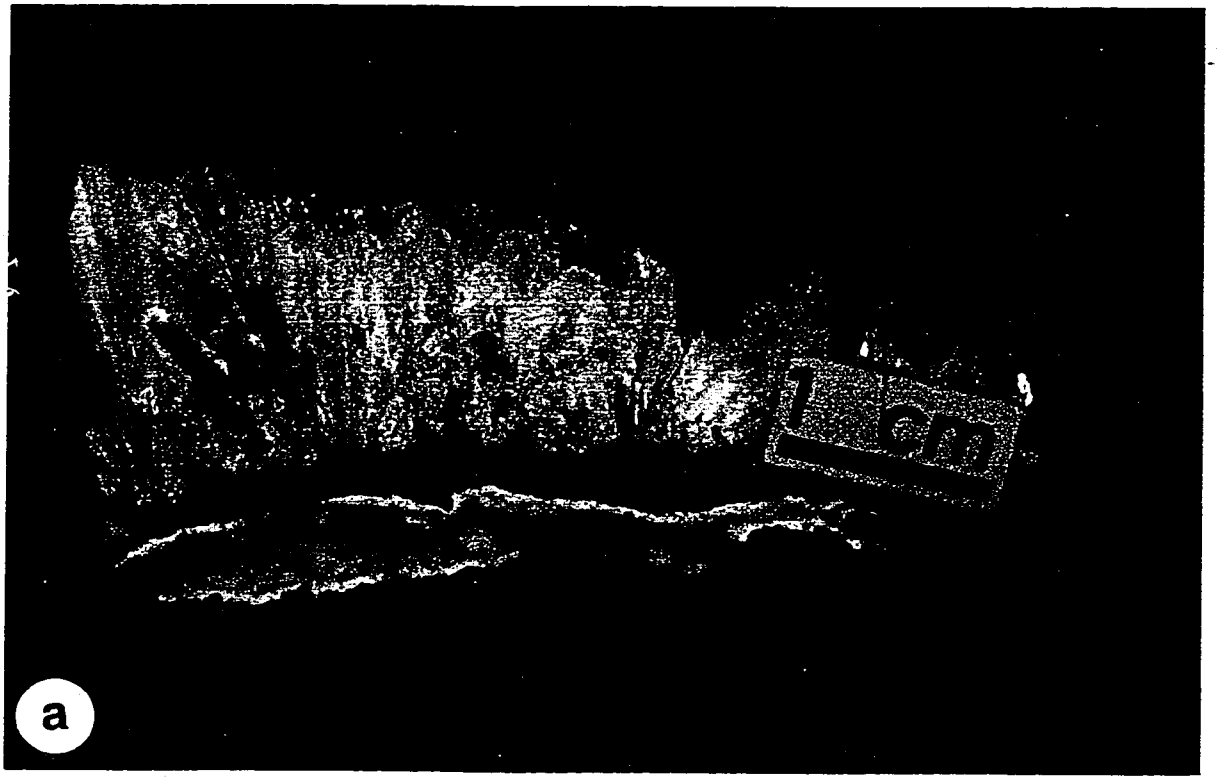
1 cm
a

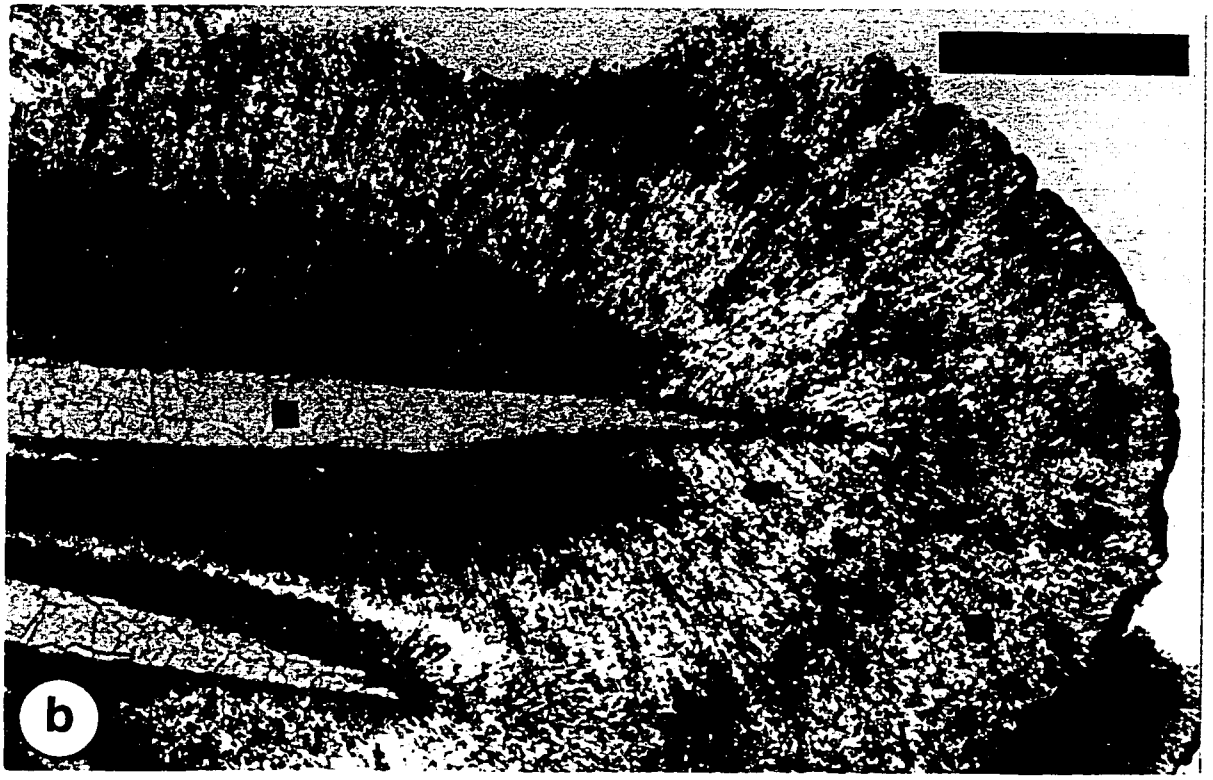
b

irregularity of crystal tops may indicate episodes of dissolution (e.g., Jones and Renaut, 1996).

Microcrystalline (0.1 mm) ferroan, low-Mg calcite (Fe-calcite) occurs as crusts most commonly interlaminated with Fe(III) oxyhydroxides (Fig. 3-4). From microscopic observation alone it is unclear if the Fe-calcite is directly precipitated or a replacement of aragonite. It was not possible to separate enough Fe-calcite for bulk chemical analyses and even the material separated for isotope analysis may be slightly contaminated with aragonite. Based on macroscopic, microscopic and XRD observations it has been estimated that the abundance of Fe-calcite is < 1% of the total amount of hydrothermal carbonate in Tutum Bay.

3.4 RESULTS

3.4.1 Chemical composition

Except for Y and Si (Table 3-2 and 3-3), aragonite shows no anomalous concentrations of trace elements and values are as for normal marine abiotic aragonite (Veizer, 1983). In contrast, ferroan, low-Mg calcite has unusually low Mg concentrations relative to Sr when compared to other marine calcite cements and significantly higher Fe and Mn than Tutum Bay aragonite (Fig. 3-5, Table 3-3). Relative to micro-crystalline aragonite (V-2(m)), coarse aragonite (V-2(x)) is slightly enriched in Ca, Ba, Ga, Pb, Ta and Y, and slightly depleted in Fe, Mn, Rb, Th and Zr. The concentration of these elements is close to their respective detection limits. Thus these values are subject to an increased analytical error and actual differences are likely very small. For Ca, Sr, Fe and Mn, however, the difference could be verified by proton probe analysis (see Fig. 3-3). Analysis of the coarse aragonite (V-2(x)) by proton probe yielded the following concentrations: Ca 360000 ppm, Sr 11000 ppm, Fe 80 ppm

Fig. 3-4 Petrography of hydrothermal precipitates. (a) Photograph of a hand specimen from vent 4. Volcaniclastic sediment cemented by hydrothermal aragonite is covered by a very thin yellowish layer of Fe-calcite. (b) Photomicrograph of alternating laminae of Fe-oxyhydroxide (upper arrow), ferroan calcite (dark gray to blue), and aragonite (yellowish white) cementing volcanic clasts. Calcite may be partially replacing aragonite at the border between them (lower arrow). For scale, the length of the lower arrow represents approximately 4 mm.

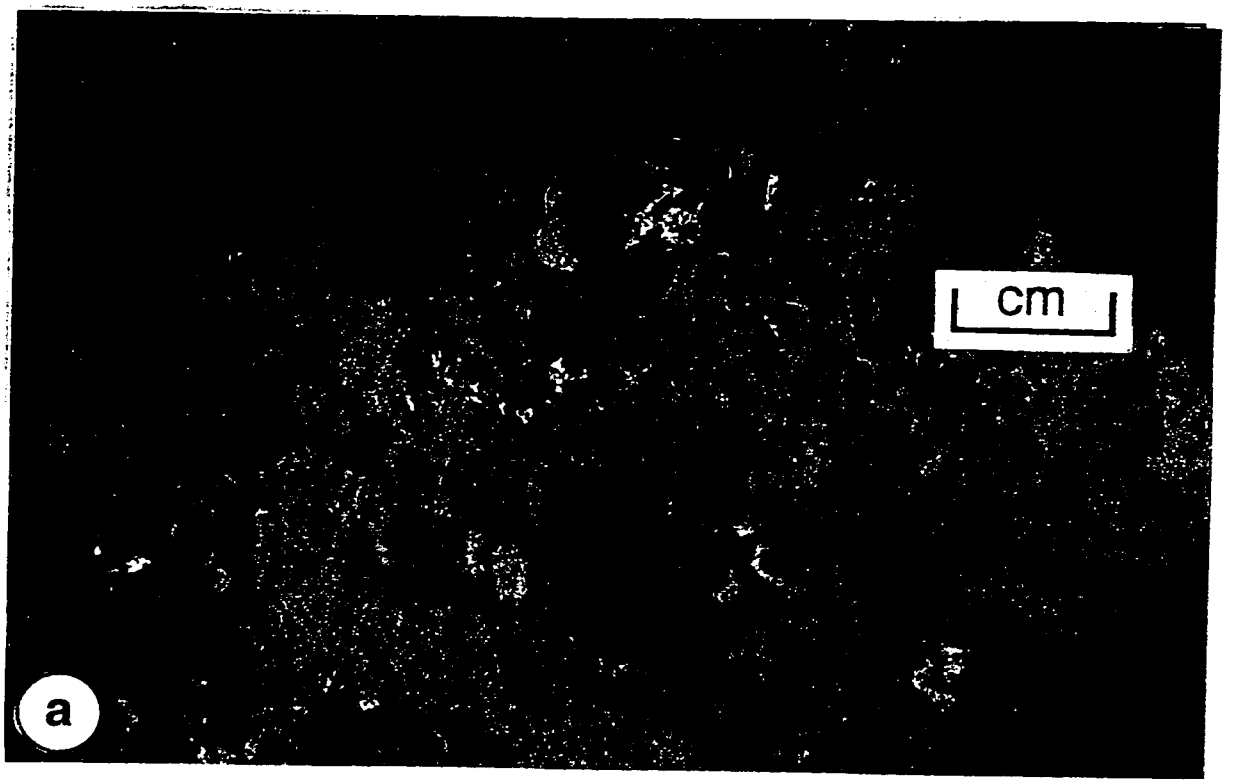
cm
a

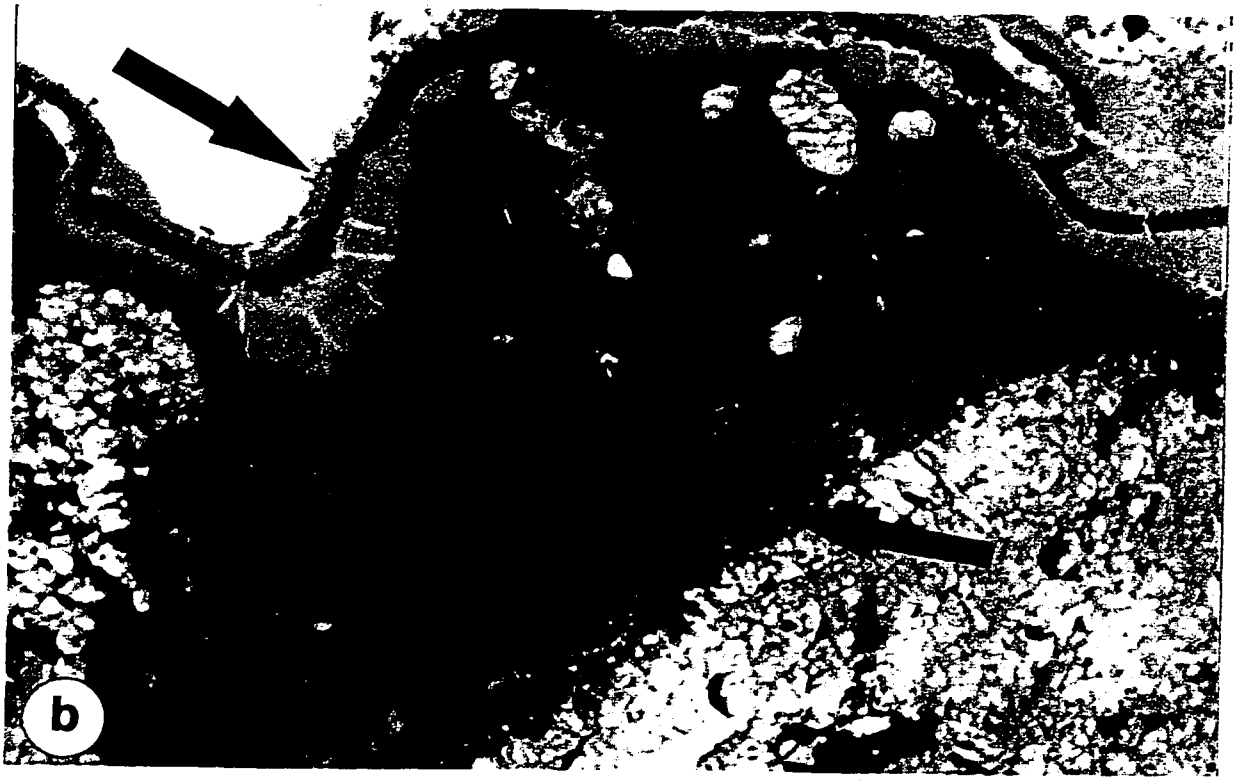
b

TABLE 3-2
MAJOR, MINOR AND TRACE ELEMENT COMPOSITION OF SELECTED TUTUM BAY HYDROTHERMAL CARBONATE PRECIPITATES

Sample	Unit	V-2D	V-2E	V-3A	V-4.1A	V-4.2B
SiO_2	%	<0.01	1.01	<0.5	<0.01	1.04
TiO_2	%	0.01	<0.02	<0.02	0.01	0.02
Al_2O_3	%	0.10	<0.2	<0.2	0.10	0.34
$Fe_2O_3^T$	%	<0.01	0.07	0.18	<0.01	0.15
MnO	%	<0.01	0.01	0.07	<0.01	0.01
MgO	%	0.05	0.05	0.09	0.04	0.07
CaO	%	53.84	51.60	52.20	53.63	51.00
Na_2O	%	<0.01	0.05	0.05	<0.01	0.08
K_2O	%	<0.01	<0.05	<0.05	<0.01	<0.05
CO_2	%	44.15	44.1	44.0	44.1	n.d.
P_2O_5	%	0.02	0.02	0.02	0.01	<0.01
S^T	%	<0.02	<0.02	<0.02	<0.02	n.d.
Total	%	99.20	97.9	97.9	99.0	53.7
Ag	ppm	0.20	0.2	0.7	0.4	0.1
As	ppm	<2	<2	n.d.	<2	<2
Au	ppm	<5	<5	n.d.	<5	<5
Ba	ppm	47	<30	<30	<30	<30
Be	ppm	<0.5	<0.5	<0.5	<0.5	<0.5
Br	ppm	<1	<1	n.d.	<1	<1
Cd	ppm	<0.2	<0.2	<0.2	<0.2	0.4
Co	ppm	<5	<5	<5	<5	<5
Cr	ppm	<10	<10	<10	<10	<10
Cs	ppm	0.04	0.08	0.17	0.05	14
Cu	ppm	<10	<10	<10	<10	18
Ga	ppm	0.7	0.3	1.6	0.3	16
Hf	ppm	0.08	<0.05	0.15	0.12	1.4
Hg	ppm	<1	<1	n.d.	<1	<1
In	ppm	<0.05	<0.05	0.1	<0.05	<0.05
Mo	ppm	<0.2	<0.2	<0.2	0.4	3.8
Nb	ppm	0.10	0.10	0.2	0.34	3.0
Ni	ppm	<10	<10	<10	<10	<10
Pb	ppm	9.5	7	10	10	27
Rb	ppm	0.43	0.76	1.00	0.48	49
Sb	ppm	<0.2	<0.2	n.d.	<0.2	<0.2
Sc	ppm	<0.5	<0.5	1.6	<0.5	<0.5
Se	ppm	<5	<5	n.d.	<5	<5
Sr	ppm	10900	11000	10000	10800	9500
Ta	ppm	0.50	<0.2	<0.2	0.8	0.7
Th	ppm	<0.02	0.03	0.1	0.03	0.97
Tl	ppm	0.04	<0.02	<0.02	0.16	0.70
U	ppm	0.03	0.03	0.05	0.05	1.10
V	ppm	<5	<5	<5	<5	6
W	ppm	<4	<4	n.d.	<4	<4
Y	ppm	67	24	90	18	47
Zn	ppm	<5	<5	<5	<5	<5
Zr	ppm	<0.5	0.7	0.9	3.1	49

TABLE 3-3
REPRESENTATIVE ELECTRON MICROPROBE ANALYSES FOR HYDROTHERMAL PRECIPITATES

Sample	FV-4A	FV-4A	FV-4A	FV-4A
Mineral	Aragonite	Aragonite	Calcite	Calcite
CaO	55.04	54.83	43.83	37.45
MgO	0.00	0.04	1.04	1.14
FeO	0.00	0.20	5.26	7.66
MnO	0.09	0.14	2.23	3.64
SrO	1.14	0.81	0.11	0.16
BaO	0.00	0.09	0.01	0.18
ZnO	0.00	0.04	0.07	0.18
SO_3	0.08	0.09	0.94	0.76
As_2O_5	0.01	0.02	0.00	0.10

Note: All analyses are reported in wt%.

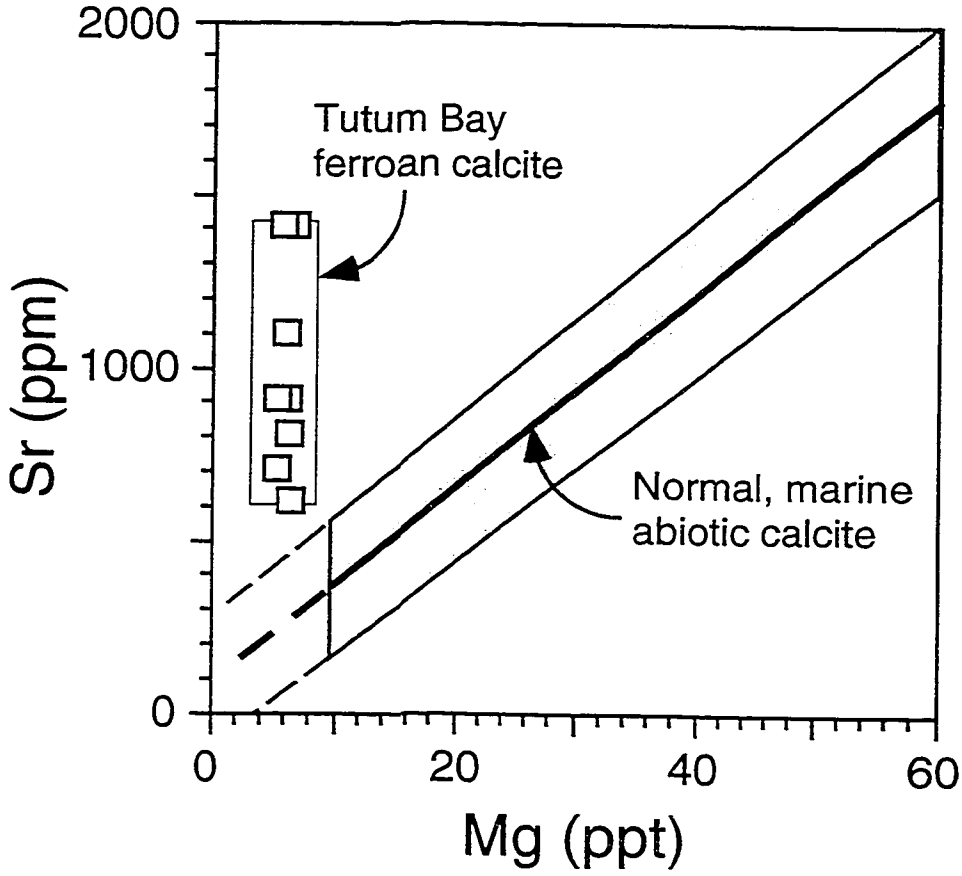

Fig. 3-5 Strontium concentrations in ferroan calcite are higher than expected relative to Mg when compared to the average (black line) and general range (stippled area) of Sr concentrations in marine low-temperature abiotic calcite (Carpenter and Lohmann, 1991).

and Mn 50 ppm, while V-2(m) had lower Ca (340000 ppm) and Sr (12000 ppm) and higher Fe (100 ppm) and Mn (80 ppm).

North American Shale Composite (NASC) normalized rare earth element (REE) concentrations for hydrothermal aragonite are presented in Fig. 3-6. The patterns of samples V-2 and V-3 show an initial drop from La to Ce, followed by a rise from the Ce minimum to an Eu maximum and a constant decrease towards a Lu minimum. From La to Tb the pattern geometry closely resembles that of the parent hydrothermal fluid (Fig. 3-6a, b). The hydrothermal fluid pattern has a small increase in Dy before it decreases towards an intermediate Lu. The patterns for coarse and micro-crystalline aragonite in sample V-2 are effectively the same, except that the coarse aragonite shows significantly higher concentrations. The two samples from vent 4 are different and more closely resemble the pattern of the parent hydrothermal fluid (Fig. 3-6c). REE concentrations initially drop from La to a Ce minimum which is followed by a rise to a Eu (V-4.2) or Dy (V-4.1) maximum and a slight decrease towards Lu.

3.4.2 Isotopic composition

C and O isotope values of aragonite crystals and Fe-calcite are plotted in Fig. 3-7. Collectively, $\delta^{18}O$ and $\delta^{13}C$ values are more negative than those expected for abiotic aragonite precipitated at low (25 °C) temperatures characteristic of shallow-water, tropical settings (Fig. 3-7b). $\delta^{13}C$ values, however, are within the ranges expected for marine carbon (Anderson and Arthur, 1983) and slightly higher than for abiotic aragonite from Lake Tanganyika that is interpreted to have incorporated hydrothermal CO_2 (Stoffers and Botz, 1994). Ferroan calcite has an oxygen isotope composition similar to those of aragonite samples, but its $\delta^{13}C$ value is depleted relative to aragonite by about 1‰. This is near to the shift predicted and observed between low-temperature aragonite and Mg-calcite cements (Gonzalez and Lohmann, 1985). The $\delta^{18}O$ value of a scleractinian coral that was dead at the time of sampling, is distinct from

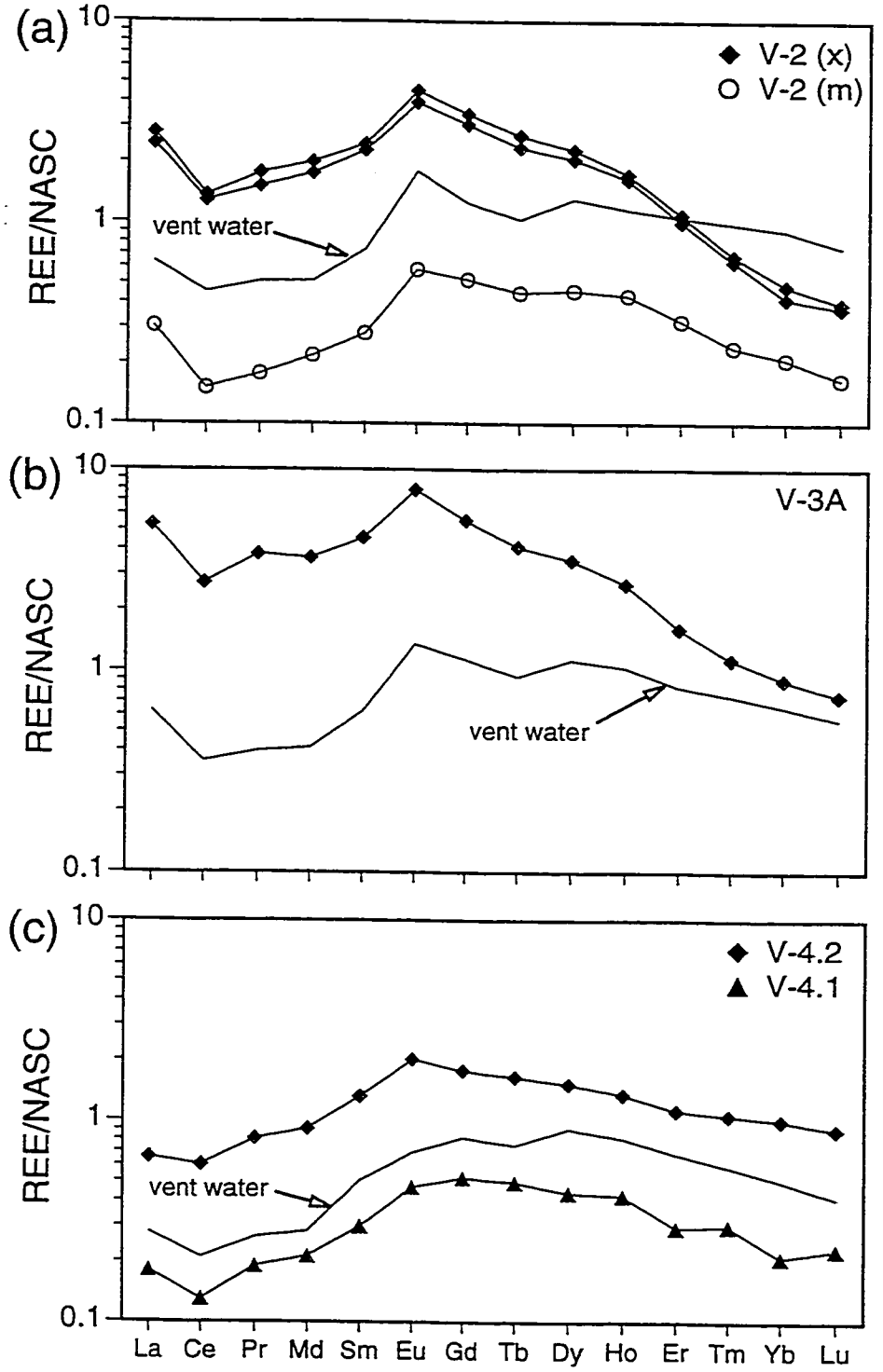

Fig. 3-6 North American Shale Composite (NASC) (Haskin et al., 1968) normalized rare earth element (REE) plots for hydrothermal aragonite precipitates from vents 2, 3 and 4. REE concentrations for vent waters (Fig. 2-6) are multiplied by 10^6 and the values for Tm and Lu are interpolated and extrapolated.

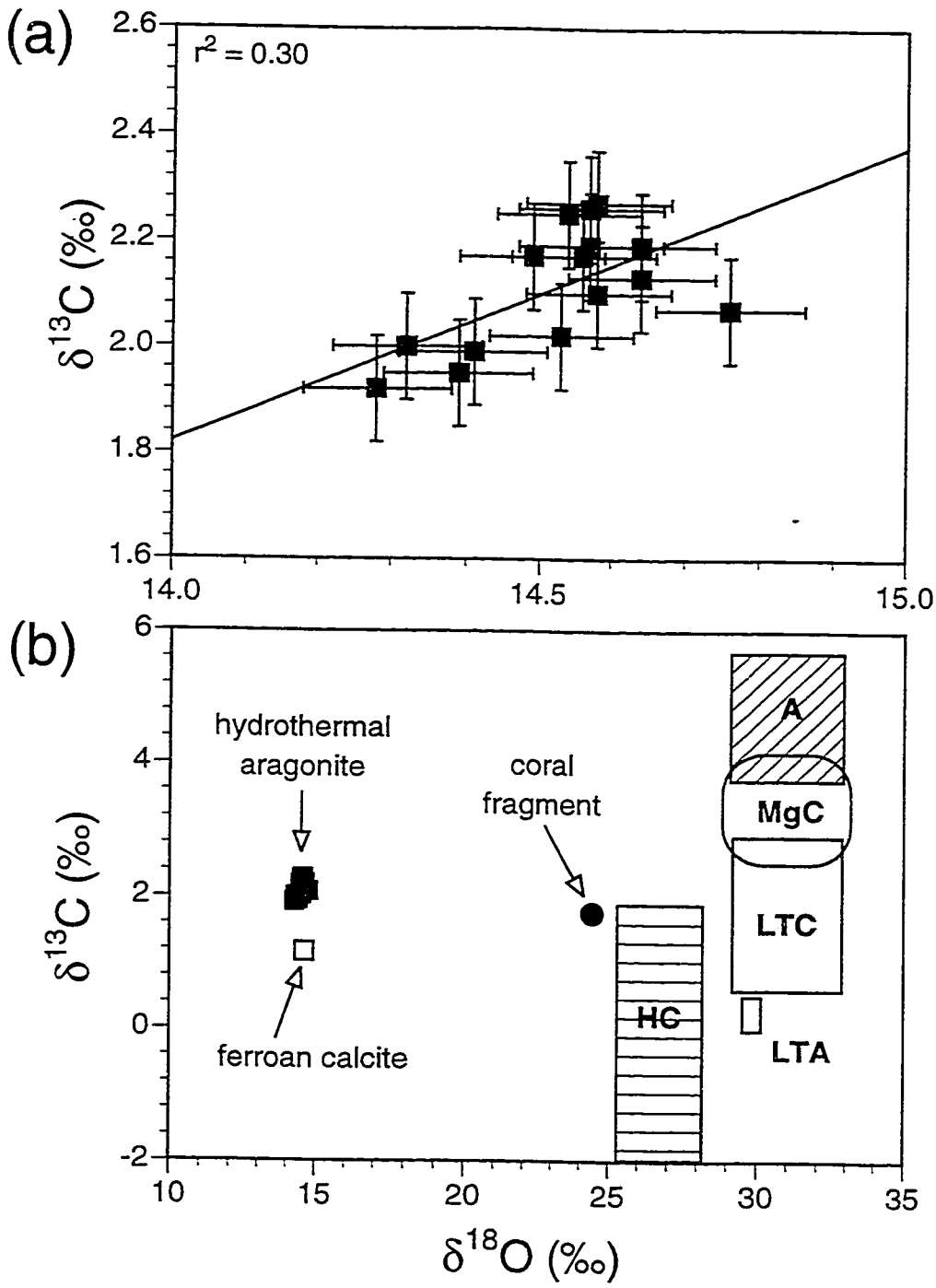

Fig. 3-7 Carbon and oxygen isotope values for abiotic aragonite, coral aragonite, and ferroan calcite at Ambitle Island. (a) Tutum Bay aragonite data only. (b) Comparison between Tutum Bay aragonite, ferroan calcite and other carbonates. Sources for other data are as follows: hermatypic corals (HC) (Tucker and Wright, 1990); low temperature aragonite (LTA), experimentally determined (Tarutani et al., 1969); aragonite (A) and Mg-calcite (MgC) cements (Gonzalez and Lohmann, 1985); and Lake Tanganyika hydrothermal aragonite (LTC) and Mg-calcite (Stoffers and Botz, 1994).

the value of encrusting microcrystalline aragonite and falls just below the lower limit of the field defined by hermatypic corals (Fig. 3-7b).

A closer look at the samples that were collected by micro-drilling reveals that micro-crystalline and coarse-crystalline aragonite have a slightly different isotope signature. Micro-crystalline aragonite has lighter $\delta^{18}O$ and $\delta^{13}C$ (Fig. 3-8), but a higher $^{87}Sr/^{86}Sr$ (Table 3-4). Assuming isotopic equilibrium, the lighter $\delta^{18}O$ and $\delta^{13}C$ values would indicate that the micro-crystalline aragonite precipitated either at higher temperatures or from a distinctively lighter fluid.

$^{87}Sr/^{86}Sr$ values for hydrothermal aragonite are similar to values for submarine volcanic rocks that were dredged ~2 km southwest of Tutum Bay (Johnson et al., 1988) and to volcanic rocks collected on the island (M. Perfit, 1997 pers. comm.) (Fig. 3-9). Skeletal aragonite of a dead scleractinian coral, however, has a value intermediate between values of oceanic crust and modern seawater (Table 3-4 and Fig. 3-9). This intermediate $^{87}Sr/^{86}Sr$ value is caused by precipitation of hydrothermal aragonite in the coral skeleton after its demise (Fig. 3-1b).

3.4.3 Fluid inclusions

Few fluid inclusions appear within aragonite crystals, and no measurable inclusions were found in Fe-calcite. Inclusions are elongate (5-10 μm) and oriented parallel to the crystal's c-axis. From three crystals, six inclusions have high liquid to vapor ratios, no daughter products, and define homogenization temperature range of 80 - 110°C. These values are similar to field measurements (see above). Freezing experiments show ice-melting temperatures between -2.5 and 0 °C. Eutectic temperatures could not be determined.

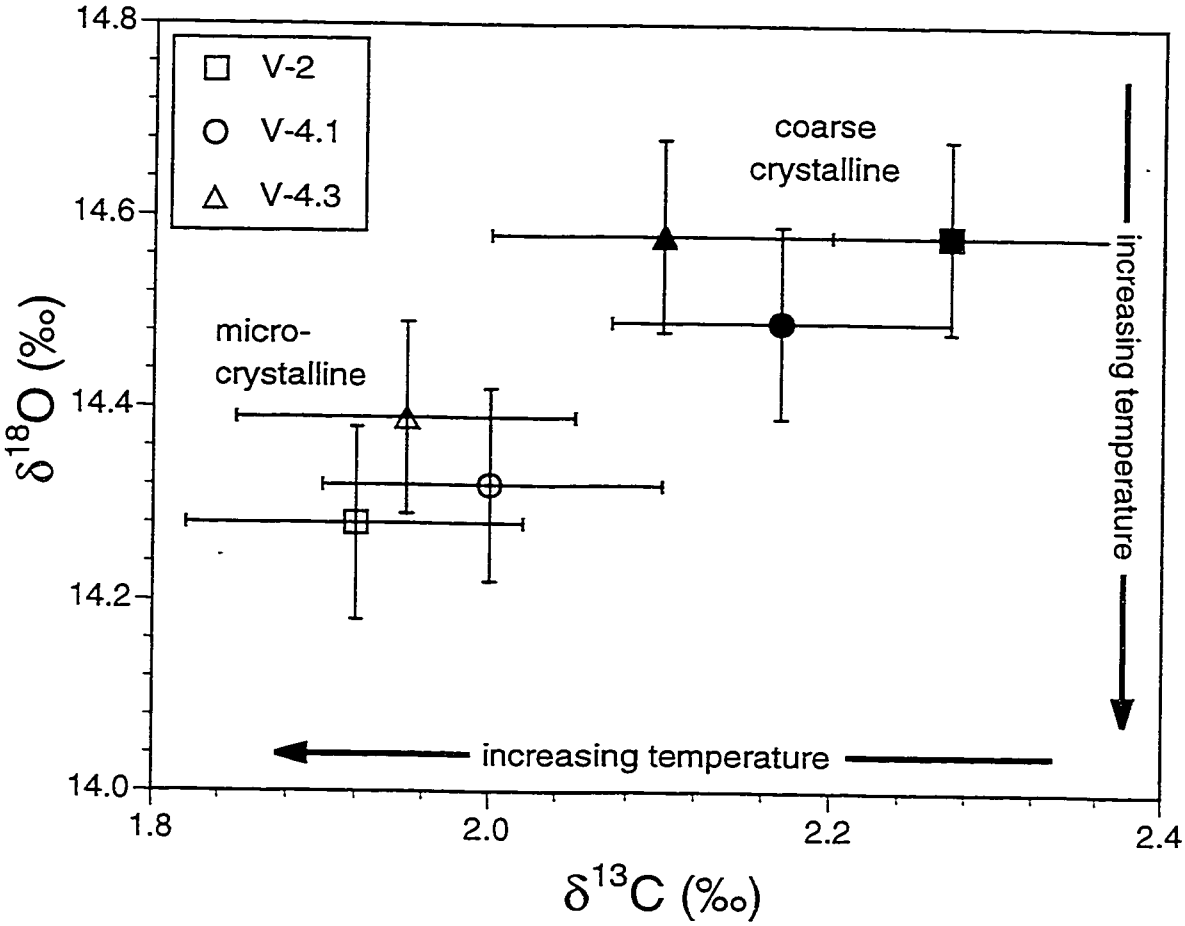

Fig. 3-8 $\delta^{13}C$ and $\delta^{18}O$ plot for micro crystalline and coarse crystalline aragonite. The arrows indicate the temperature trends for equilibrium precipitation. Based on equilibrium fractionation calculations (Friedman and O'Neil, 1977), the lower $\delta^{18}O$ and $\delta^{13}C$ values suggest precipitation at higher temperature.

TABLE 3-4
ISOTOPIC COMPOSITION OF HYDROTHERMAL ARAGONITE AND IRON-CALCITE FROM TUTUM BAY

Sample	$\delta^{18}O$ (VSMOW) ‰	$\delta^{18}O$ (PDB) ‰	$\delta^{13}C$ (PDB) ‰	$^{87}Sr/^{86}Sr$ ± 2 Standard Errors	Mineral
V-2D	14.57	-15.85	2.26	0.704142 ±13	aragonite
V-2E	14.53	-15.89	2.02	n.d.	aragonite
V-2D	14.64	-15.79	2.19	0.704097 ±10	aragonite
V-3A	14.57	-15.85	2.19	0.704097 ±08	aragonite
V-4.1A	14.41	-16.00	1.99	n.d.	aragonite
V-4.2B	14.56	-15.86	2.17	n.d.	aragonite
FV-4A	14.64	-15.78	2.13	n.d.	aragonite
FV-4B	14.76	-15.66	2.07	n.d.	aragonite
FV-4C	14.54	-15.88	2.25	n.d.	aragonite
V-2 (x)	14.58	-15.84	2.27	n.d.	aragonite
V-2 (m)	14.28	-16.13	1.92	n.d.	aragonite
V-4.1 (x)	14.49	-15.93	2.17	0.704131 ±14	aragonite
V-4.1 (m)	14.32	-16.09	2.00	0.704551 ±08	aragonite
V-4.3 (x)	14.58	-15.84	2.10	n.d.	aragonite
V-4.3 (m)	14.39	-16.02	1.95	n.d.	aragonite
FV-4B	14.70	-15.72	1.14	n.d.	Fe-calcite

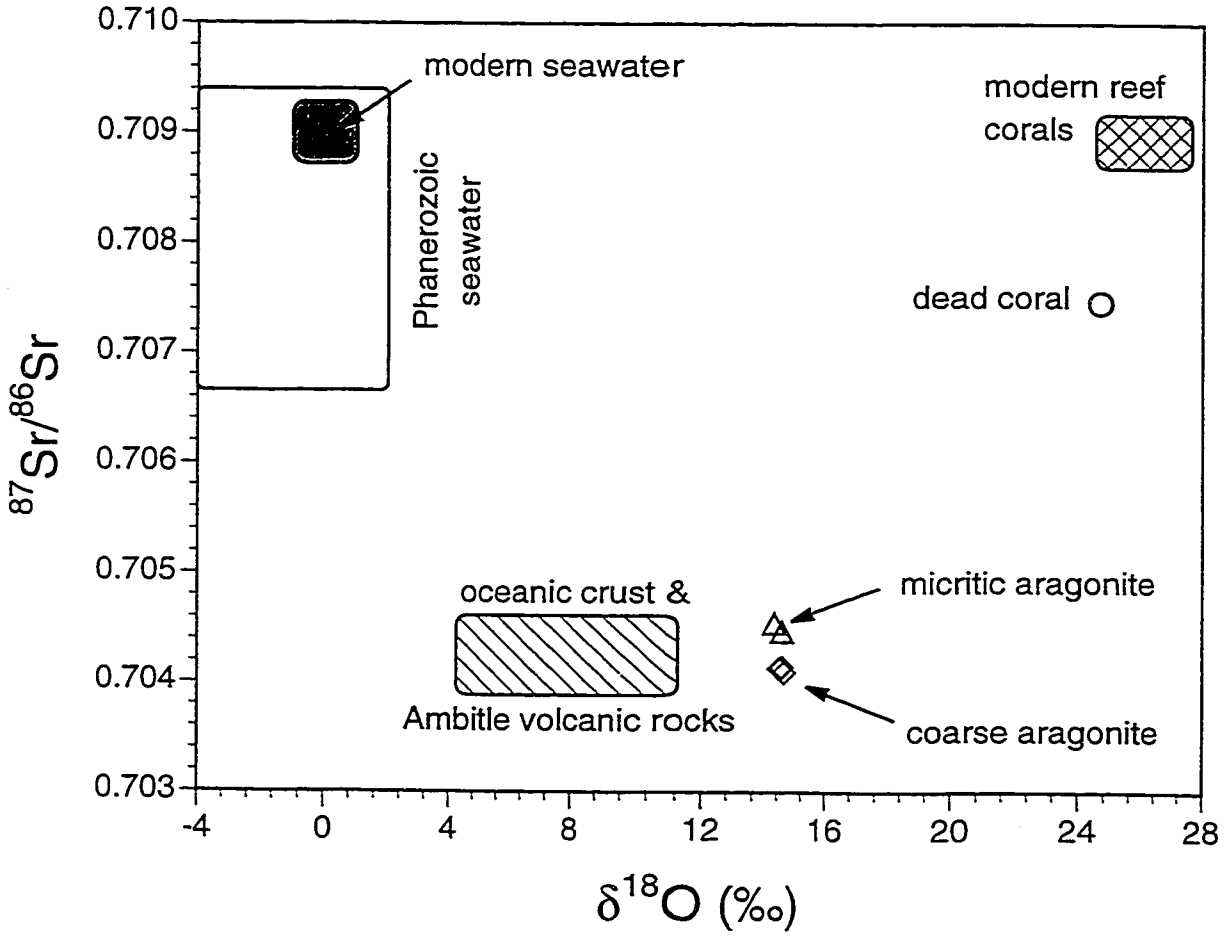

Fig. 3-9 $^{87}Sr/^{86}Sr$ ratios for abiotic aragonite crystal, crust, and coral aragonite. Samples of crust and coral are from the same hand specimen. Heavy stippled area is present-day seawater, and lighter stippled area is an approximate range of seawater compositions through Phanerozoic times. Sources for volcanic rock are from Hoefs (1997) and M. Perfit (pers. comm., 1997).

3.5 DISCUSSION

The precipitation of a carbonate phase from solution is primarily controlled by pCO_2, pH, temperature, ion activity and microbial activity. These factors are closely related and they often compete with each other. The formation of travertine deposits in CO_2-rich springs, for example, is a result of CO_2 degassing due to a drop in pressure. At the same time, however, cooling of the spring water may increase carbonate solubility and whether precipitation takes place is determined by the respective intensity of the competing processes. Hydrothermal fluids in Tutum Bay are CO_2-rich ($pCO_2 > 2$ atm) and either boiling or are close to boiling as they enter seawater; this combined with a drop in pressure causes a rapid loss of CO_2. Mixing with seawater causes a drop in temperature and an increase in pH, the latter favoring carbonate precipitation. To further investigate the precipitation process it is necessary to assess the amount of mixing between hydrothermal fluid and seawater prior to and during precipitation.

$^{87}Sr/^{86}Sr$ ratios are a widely used tracer in mixing processes (Faure, 1986). The mass difference between the two strontium isotopes, ^{87}Sr and ^{86}Sr, is too small to cause a measurable fractionation during precipitation. Thus the $^{87}Sr/^{86}Sr$ ratio in aragonite can be used as a direct measure of its ratio in the parent fluid. $^{87}Sr/^{86}Sr$ values in hydrothermal aragonite indicate that some mixing with seawater occurs during its precipitation (Fig. 3-10). Assuming seawater and hydrothermal fluid to be 30°C and 100°C, respectively, the temperature of the mixture can be calculated with the mass balance equation:

$$t_M = (1-y) * t_{HF} + y * t_{SW} \qquad [3\text{-}1]$$

where t is the temperature in °C and y is the seawater fraction. The calculated maximum seawater fraction is 11%, which corresponds to a maximum temperature drop by approximately 7°C to 93°C. The corresponding maximum change in pH is about 0.2 units. The

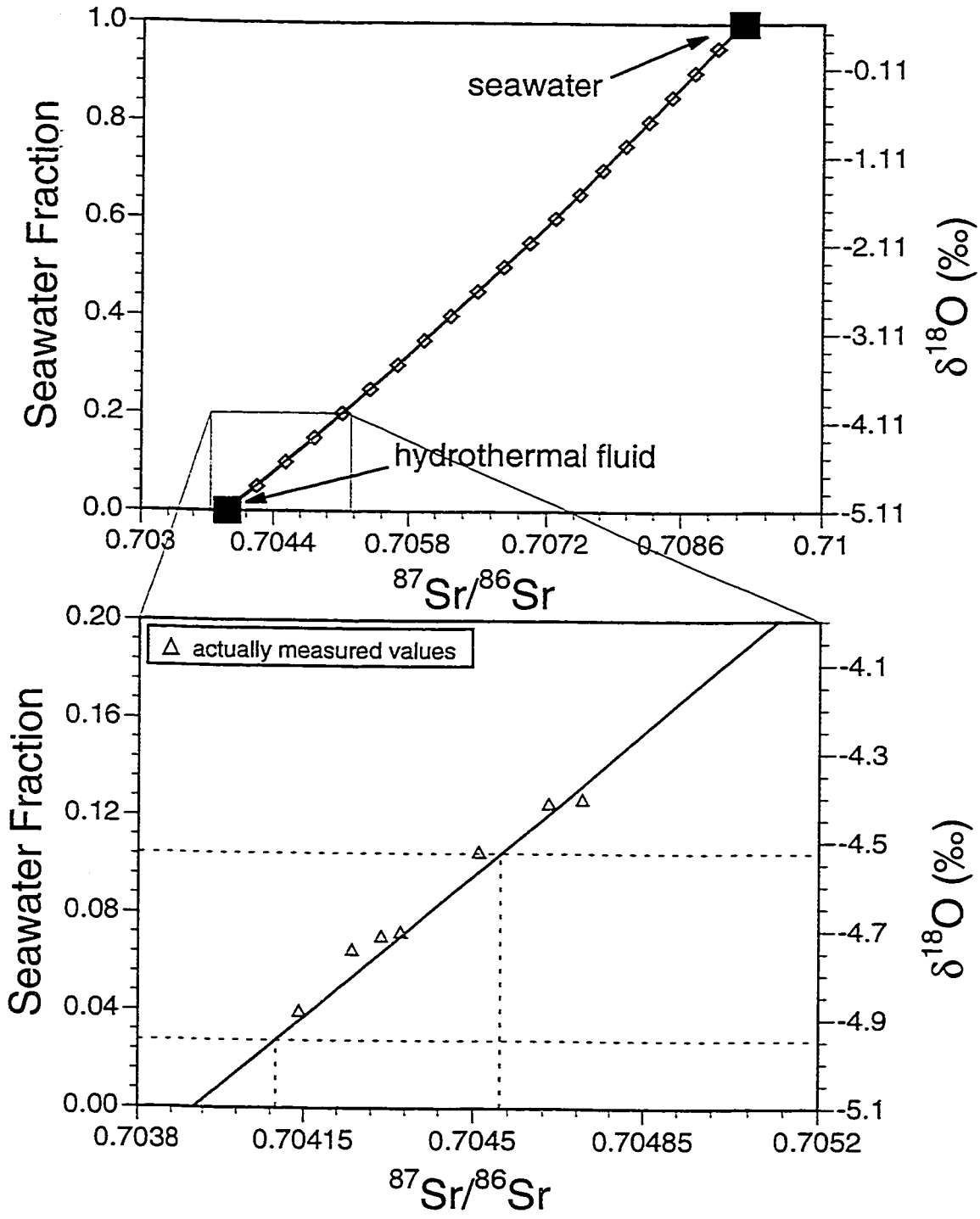

Fig. 3-10 Mixing curve between the hydrothermal fluid and seawater endmember (Table 2-5) based on $^{87}Sr/^{86}Sr$ ratios and $\delta^{18}O$ values. The curve was calculated following Faure (1986). The open triangles represent actually measured $^{87}Sr/^{86}Sr$ and $\delta^{18}O$ in hydrothermal fluids.

calculated extent of mixing, although very small, may prevent precipitation if one of the mixing partners is dramatically undersaturated with respect to calcium carbonate. In Tutum Bay, however, both seawater and hydrothermal fluid are supersaturated with respect to calcium carbonate and the relatively elevated activity of Ca^{2+} in seawater may actually be the trigger that initiates nucleation (Dandurand et al., 1982).

Microbial activity can greatly enhance the precipitation of carbonates in warm-springs ($t < 70°C$) (e.g., Folk, 1994), but the temperatures of Tutum Bay vents are probably too high to allow for extensive microbial activity and precipitation should be controlled mainly by inorganic factors.

Of the factors that control precipitation in most on-land hot-springs and in Tutum Bay, CO_2 degassing is arguably the single most important (e.g., Dandurand et al., 1982; Renaut and Jones, 1997; Simmons and Christenson, 1994; Usdowski et al., 1979). CO_2 degassing increases the pH and subsequently increases supersaturation, leading to the precipitation of calcium carbonate:

$$Ca^{2+} + 2HCO_3^- \Rightarrow CaCO_3 + H_2O + CO_2\uparrow. \qquad [3\text{-}2]$$

The hydrothermal carbonate in Tutum Bay is almost completely in the form of aragonite which is surprising considering that the parent hydrothermal fluid is slightly more supersaturated with respect to calcite ($SI_{cacite} = 0.65$ and $SI_{aragonite} = 0.55$). The formation of either aragonite or calcite is still poorly understood, but it is clear that no single fluid parameter is likely to be the sole or dominant control in natural environments (Burton, 1993).

Precipitation of aragonite rather than calcite is a common process in tropical shallow-water submarine environments (Tucker and Wright, 1990). In hydrothermal systems, however, calcite is the primary carbonate precipitate, and the presence of aragonite is usually attributed to rapid precipitation rates, elevated Mg/Ca, and stabilizing effects of Ba, Sr and possibly Mg on the orthorhombic crystal structure (Browne, 1973; Folk, 1994). Folk (1994)

suggested that aragonite is the preferential precipitate relative to calcite in hot springs at temperatures > 40°C or with a mMg/mCa of > 1 at temperatures below 40°C. Mg/Ca ratios in Tutum Bay vent fluids are rather low, but temperatures are > 40°C and precipitation rates, although unknown, should be high considering the amount of CO_2 released. The alternation between aragonite and calcite in hot spring travertine at Lake Bogoria, Kenya (Renaut and Jones, 1997), for example, has been attributed to pCO_2 and precipitation rate. There Mg/Ca ratios are also low, but precipitation of aragonite is favored under conditions of high pCO_2 and rapid precipitation. The change in mineralogy at Lake Bogoria is accompanied by a change in crystal habit and size (Fig. 3 in Renaut and Jones, 1997) from coarse crystalline aragonite to fine grained calcite (feather dendrite). The same change in crystal habit and size can be observed in Tutum Bay aragonite (Fig. 3-3), but without any change in mineralogy. Relatively higher $^{87}Sr/^{86}Sr$ ratios in the fine grained portion (Table 3-4) may indicate a higher seawater fraction during its precipitation, thus leading to a lower pCO_2 and, therefore, lower precipitation rate. Slightly more oxidizing conditions, also indicative of a higher seawater fraction, may be hinted at by relatively higher Fe and Mn concentrations in fine grained aragonite (PIXE analysis and Table 3-2). $\delta^{18}O$ and $\delta^{13}C$ equilibrium temperatures, however, are higher than those for the bigger crystals (Fig. 3-8), an observation at odds with the advocated higher seawater fraction. For an explanation of this enigma see the next section.

The change in mineralogy from aragonite to ferroan calcite probably signals an abrupt change of physical and/or chemical conditions at and near vents. Replacement of aragonite by Fe-calcite during times of no direct precipitation is possible, but there is no clear evidence for either the Fe-calcite replacing the aragonite or for its direct precipitation from the hydrothermal fluid. A very drastic change in temperature can account for the change in mineralogy. In a compilation of data from several hot springs, Folk (1994) has shown that aragonite is the preferential precipitate relative to calcite at temperatures > 40°C or with a mMg/mCa of > 1 at a temperature of < 40°C. Relative Sr^{2+} and Mg^{2+} concentrations in ferroan calcite are anomalous compared to "normal-marine" shallow-water abiotic cements (Fig. 3-5) (Carpenter and

Lohmann, 1992). Two factors may be important. First, an elevated Sr distribution coefficient may arise adjacent to the vents due to increased temperature (Lorens, 1981). Second, Sr may be retained during local aragonite replacement by calcite (e.g., Sandberg, 1985).

The generally low trace element concentrations in hydrothermal aragonite are as expected for orthorhombic carbonates (Speer, 1983; Veizer, 1983). This results from their low distribution coefficients and low concentrations in the hydrothermal fluid (Table 2-1). Among the processes that directly incorporate minor and trace elements into orthorhombic carbonate minerals, substitution for Ca in the $CaCO_3$ structure is the most important. Incorporation is generally limited by the necessary charge and the size of the metal cation and, therefore, aragonite preferentially incorporates divalent cations larger than Ca (Speer, 1983). Despite the charge difference (except for Eu^{2+}), rare earth elements (REEs) in Tutum Bay hydrothermal aragonite are also highly concentrated relative to the vent fluid (Fig. 3-6). The REE pattern for samples V-2 and V-3 clearly demonstrates the ionic radius dependence for substitution in the orthorhombic structure. The concentration of REEs with ionic radii larger than or similar to Ca (La to Tb) is controlled by their concentration in the hydrothermal fluid, while those with ionic radii smaller than Ca (Dy to Lu) are relatively depleted (Fig. 3-6a, b). The difference in pattern geometry between the above mentioned samples and those from vent 4, V-4.1 and V-4.2 (Fig. 3-6c) is enigmatic and cannot be conclusively explained. The pace of precipitation and subtle differences in fluid chemistry, pH and redox potential, however, may account for the observed disagreement. The obvious difference in concentration and the slight difference in pattern geometry between the coarse crystalline (V-2 (x)) and fine crystalline aragonite (V-2 (m)) (Fig. 3-6a) is probably a result of seawater mixing during precipitation (see above). The addition of small amounts of seawater may be sufficient to change precipitation rate and to affect the complex stability of the heavy REEs, resulting in lower total concentrations and in a flatter slope between Eu and Lu.

3.5.1 Isotopic Equilibrium - Yes or No?

Attainment of isotopic equilibrium between a hydrothermal precipitate and its parent solution is a prerequisite to the application of any isotope geothermometer. The reconstruction of physico-chemical conditions in fossil hydrothermal systems can be aided by analyses of $\delta^{18}O$ and $\delta^{13}C$ in carbonate minerals (e.g., Ohmoto and Rye, 1979; Simmons and Christenson, 1994), although the existence of isotopic equilibrium is uncertain. Modern hot spring travertines provide natural laboratories to study isotope systematics and to assess equilibrium conditions. Several studies (e.g., Amundson and Kelly, 1987; Dandurand et al., 1982) found that carbonates were not in $\delta^{18}O$ equilibrium with the parental waters, while at the same time $\delta^{13}C$ equilibrium between CO_2 and carbonate was attained.

Following Friedman and O'Neil (1977), and assuming isotopic equilibrium, a precipitation temperature of approximately 78°C was calculated for the hydrothermal fluid using the mean $\delta^{18}O$ of aragonite (14.5‰) and hydrothermal fluid (5.1‰). In the absence of any fractionation factor for abiotic aragonite at temperatures above 40°C, the calcite-water fractionation factor from Friedman and O'Neil (1977) was used because the differences between these two fractionation factors appear to be insignificant above 30°C (Anderson and Arthur, 1983). The possible range of temperatures is shown in Fig. 3-11 (Area A). These temperatures are lower than those estimated from $^{87}Sr/^{86}Sr$ mixing calculations by about 18°C (Fig. 3-11, Area C). Based on $^{87}Sr/^{86}Sr$ ratios, the amount of seawater present during precipitation of aragonite ranged from approximately 3 to 11%. Assuming seawater and hydrothermal fluid to be 30°C and 100°C, respectively, the temperature of the mixtures and, hence, the possible range of precipitation temperatures can be calculated. These temperatures range from 92.3 to 97.9°C corresponding to a $\delta^{18}O$ of approximately -3‰ in the hydrothermal fluid. This value is at odds with the measured hydrothermal fluid $\delta^{18}O$ (Table 2-5).

Some of the discrepancy between the $\delta^{18}O$ and the $^{87}Sr/^{86}Sr$ precipitation temperatures can be explained by the inverse effect of seawater mixing. On one hand, mixing with ambient

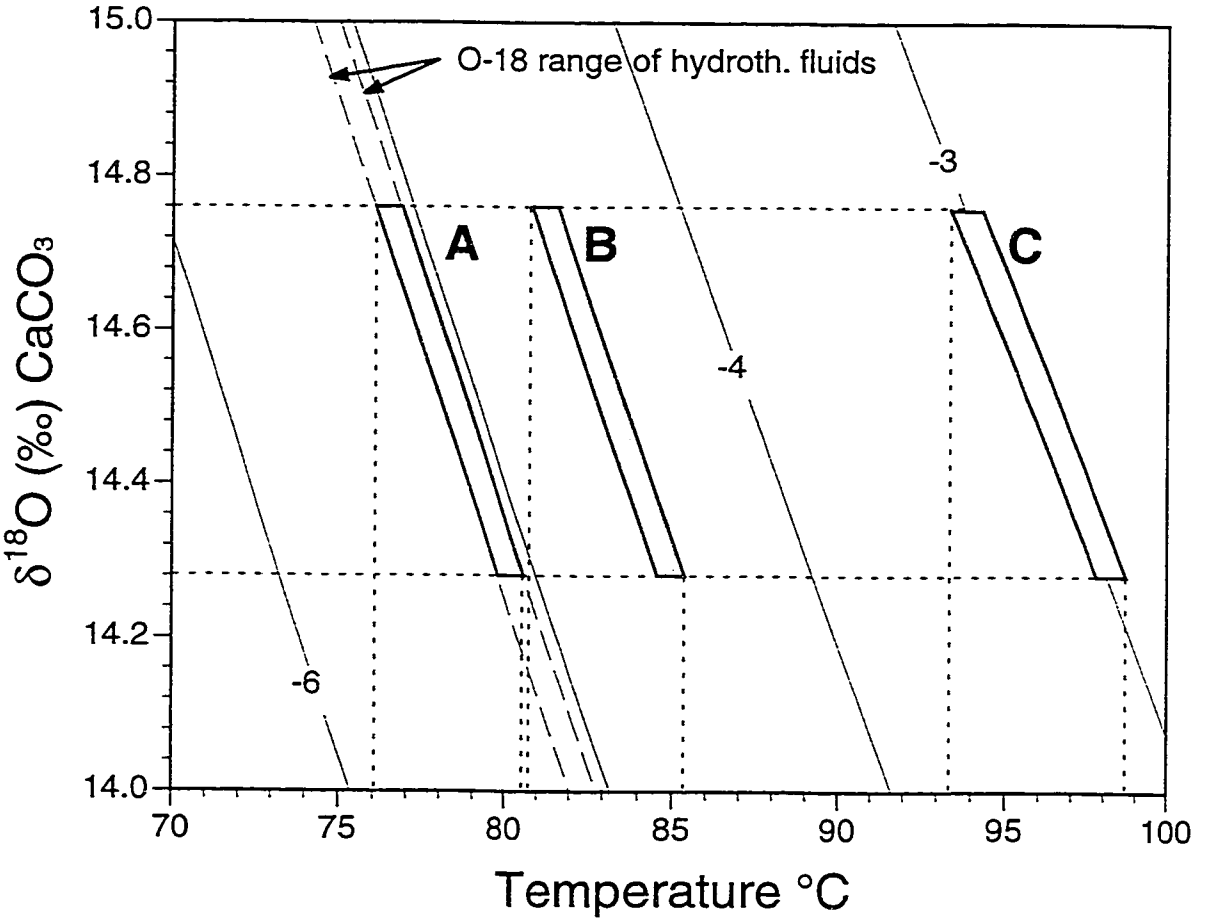

Fig. 3-11 Plot of $\delta^{18}O$ equilibrium temperatures in the system calcite-H_2O. The curves (solid lines) represent the calculated isotopic composition of calcite in equilibrium with water of -3, -4, -5 and -6 ‰ as a function of temperature using the fractionation factors from Friedman and O'Neil (1977). The dashed curves represents the range of $\delta^{18}O$ in Tutum Bay vent waters. The stippled area A represents the possible range of isotopic equilibrium for Tutum Bay hydrothermal aragonite. The stippled area B represents the possible range of isotopic equilibrium for the maximum seawater component during precipitation (see the text for more explanation). The stippled area C represents the expected range of isotopic equilibrium and $\delta^{18}O$ of the hydrothermal fluid based on temperatures derived from mixing considerations for $^{87}Sr/^{86}Sr$ (see the text).

seawater cools the hydrothermal fluid, while on the other addition of ^{18}O leads to the calculation of higher precipitation temperatures. For example, aragonite with a $\delta^{18}O$ of 14‰ is in equilibrium with water of -6 and -4‰ at ~75 and ~91.5°C, respectively (Fig. 3-11). If the maximum amount of seawater is added, the $\delta^{18}O$ of the hydrothermal fluid increases to approximately -4.5‰ (Fig. 3-10) which results in precipitation temperatures between 80.5 and 85°C (Fig. 3-11, Area B). This temperature range, although higher than the pre-mixing $\delta^{18}O$ equilibrium temperatures, is still too low compared to the $^{87}Sr/^{86}Sr$ mixing temperatures.

The $\delta^{13}C$ calcite-CO_2 geothermometer has been successfully applied in many studies of hydrothermal ore deposits and temperatures of precipitation can be determined within ±20°C (Ohmoto and Rye, 1979). The calcite-CO_2 geothermometer has the advantage that mixing with ambient seawater can be neglected due to the immense concentration difference. Equilibrium temperatures were evaluated using two different data sets, (1) the theoretical computations by Bottinga (1968) and (2) those by Chacko et al. (1991). At high temperature (>300°C) both data sets are in good agreement, but below 300°C their fractionation factors become increasingly different with decreasing temperature (Fig. 3-12 and Fig. 5 in Chacko et al. (1991)). Equilibrium precipitation temperatures for the range of Tutum Bay CO_2 are 82 to 91°C and 87.5 to 98°C for the fractionation factors from Chacko et al. (1991) and Bottinga (1968), respectively (Fig. 3-12). Both temperature ranges are larger than those based on $\delta^{18}O$, but they are in better agreement with the $^{87}Sr/^{86}Sr$ mixing temperatures. The $\delta^{13}C$ temperatures calculated with the fractionation factors from Bottinga (1968) are identical to those obtained from $^{87}Sr/^{86}Sr$ mixing calculations (Fig. 3-12b), while those using the fractionation factors from Chacko et al. (1991) are lower but closer to the $\delta^{18}O$ temperatures (Fig. 3-12a).

Seawater mixing during precipitation may explain the apparent increase in temperature between coarse and micro crystalline aragonite (Fig. 3-8). Precipitation rate is not a factor because it has no influence on the oxygen isotopic composition of purely inorganic carbonates (Kim, 1997; Tarutani et al., 1969). The difference in $\delta^{13}C$ on the other hand may be caused by

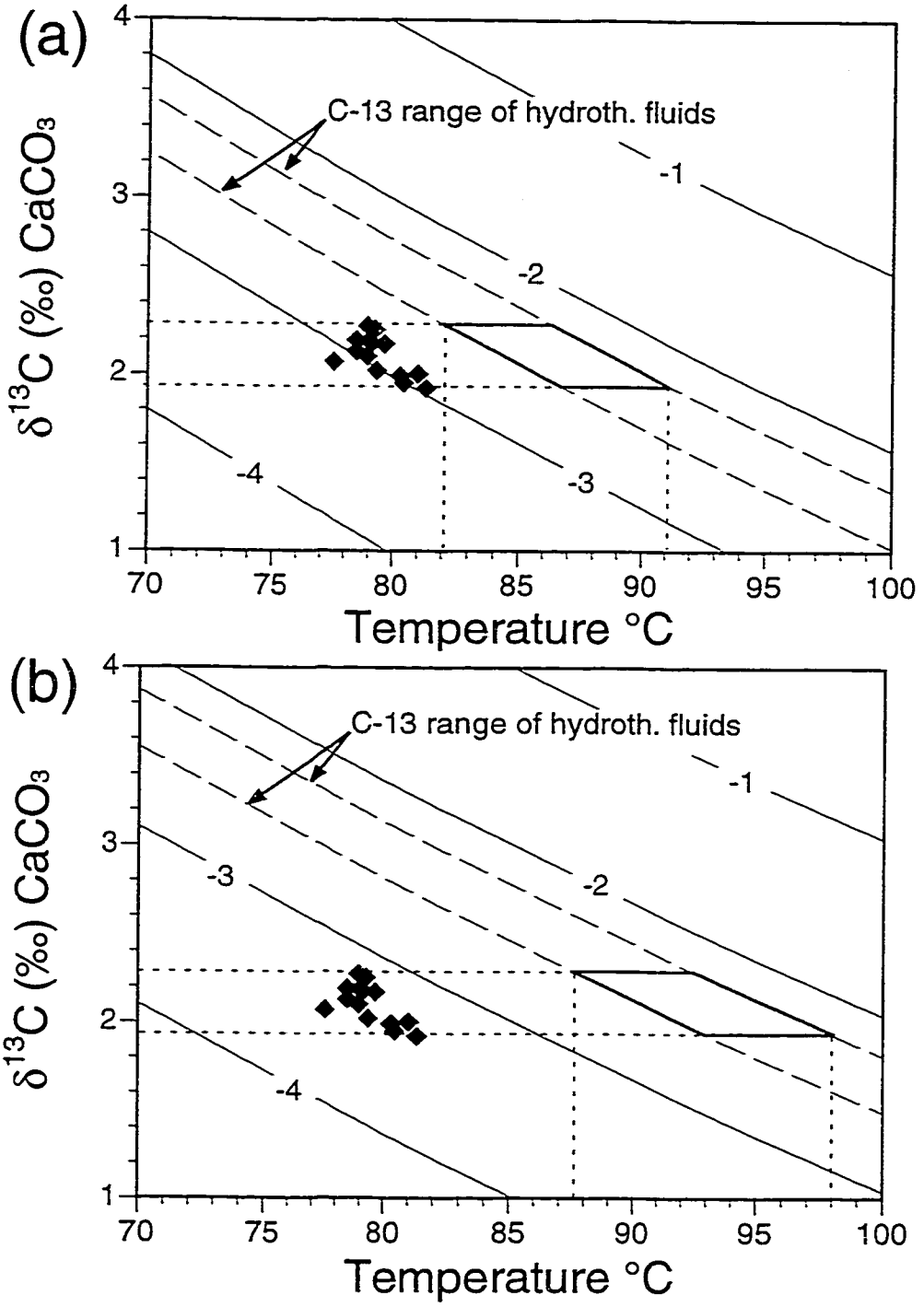

Fig. 3-12 Plot of $\delta^{13}C$ equilibrium temperatures in the system calcite-CO_2 (a) based on data from Chacko et al. (1991) and (b) based on data from Bottinga et al. (1968). The curves (solid lines) represent the calculated isotopic composition of calcite in equilibrium with CO_2 of -1, -2, -3 and -4 ‰ as a function of temperature. Diamonds represent $\delta^{18}O$ equilibrium temperatures.

a change in precipitation rate. Romanek et al. (1992) noted a small positive relationship between precipitation rate and fractionation factor at 40°C.

The temperatures obtained from isotope geothermometry are in good agreement with those from fluid inclusions and those measured in the field (Table 2-1). Similar to observations from onland hot springs (e.g., Amundson and Kelly, 1987; Dandurand et al., 1982), it seems that in Tutum Bay the aragonite precipitated in $\delta^{13}C$ equilibrium with CO_2, while $\delta^{18}O$ equilibrium with water was apparently not attained. However, the bottom line is that once the $\delta^{18}O$ values are corrected for seawater mixing, the difference between minimum and maximum precipitation temperature is only about 10°C. This difference in calculated equilibrium temperature is surprisingly small considering the difficulties associated with obtaining accurate isotope fractionation factors under laboratory conditions (e.g., Chacko et al., 1991; Kim, 1997; Romanek et al., 1992).

3.6 GEOLOGIC IMPLICATIONS OF HYDROTHERMAL CARBONATE PRECIPITATION

3.6.1 Implications for diagenetic processes

Carbonate diagenesis encompasses the chemical, physical and biologic changes that a sediment has undergone after its initial deposition up to the realms of incipient metamorphism. It includes six major processes: cementation, microbial micritization, neomorphism, dissolution, compaction and dolomitization (Tucker and Wright, 1990). Hydrothermal activity present in a carbonate depositional environment, such as the coral reef at Ambitle Island, directly affects cementation, neomorphism and dissolution.

With regard to reef growth and reef preservation, cementation is the most important, and certainly the most studied diagenetic process (Tucker and Wright, 1990). Ambitle Island is

the only known location in which purely geochemically-driven carbonate deposition is extensively co-occurring with a natural biogenic calcifying community. Carbonate minerals, cements and/or hydrothermal precipitates, from this unique environment are different from carbonate minerals found in on-land hot springs and normal reef environments.

Relative Sr^{2+} and Mg^{2+} concentrations in ferroan low-Mg calcite are anomalous compared to "normal-marine" shallow-water abiotic cements (Fig. 3-4). In contrast, most present day carbonate cements consist mainly of high-Mg calcite, whereas the cements that accumulate around the hydrothermal vents near Ambitle Island are composed of aragonite and low-Mg calcite which renders their interpretation in a classical sense impossible. Studies of ancient skeletal carbonates that may have accumulated near hydrothermal vents (e.g., Von Bitter et al., 1990) need to carefully establish temporal and spatial relationships to prove coexistence of abiotic and skeletal carbonate.

Another diagenetic process that is directly affected is neomorphism. Neomorphism describes processes of replacement and recrystallization with a change in mineralogy and increasing crystal size (Folk, 1965). As a result, although geologically not very likely, the big crystals of hydrothermally precipitated aragonite (Fig. 3-2, 3-3) could be interpreted as recrystallized calcite, although exactly the opposite may be the case; ferroan calcite replaces aragonite (Fig. 3-4).

3.6.2 Implications for petroleum exploration

Although the formation and preservation of primary and secondary porosity in carbonates is closely controlled by diagenetic processes such as cementation and dissolution, it is mentioned separately because of its immense importance for petroleum exploration and recovery. Porous limestone and dolomite contain about 50% of the world's known reserves of oil and gas (Choquette and Pray, 1970). Cretaceous carbonate platforms alone contain approximately 16% of the world hydrocarbon reserves (Klemme and Ulmishek, 1991). The

main factors in evaluating carbonate reservoirs are lithofacies, pore types, shelf setting, sequence stratigraphy and diagenetic overprint (Jordan and Wilson, 1994). Cementation and dissolution mechanisms in a hydrothermally influenced carbonate environment are most likely different from those expected under non-hydrothermal conditions.

The formation and preservation of primary porosity in carbonate platforms that were subject to "normal" depositional and diagenetic processes are fairly well understood and, as a result, the inner shelf, outer shelf and slope are the prime petroleum exploration targets (Jordan and Wilson, 1994; Roehl and Choquette, 1985). The occurrence of hydrothermal activity, however, is not confined to any one location within a reef complex and subsurface processes may completely change the reef hydrogeology (Oberdorfer and Buddemeier, 1985) relative to non-hydrothermal settings. Consequently, early occlusion of pore space may have occurred in areas that are generally thought to have high primary pore space (Tucker and Wright, 1990).

The final porosity of a carbonate rock, however, depends on processes following deposition, such as the preservation of primary and formation of secondary pore space. In general, primary porosity decreases with increasing depth as a result of compaction and cementation, while secondary porosity is due to dissolution. It is of great importance, therefore, to assess how much dissolution is produced at depth (Mazzullo and Harris, 1992) and to know the chemical composition and distribution of various pore fluids in the subsurface (Jordan and Wilson, 1994). The degree of carbonate solubility in a water rock system is controlled by a variety of factors (Fig. 3-13), of which most are directly implicated by the input of hydrothermal fluids. As a result of high hydrostatic pressure, high pCO_2 and low pH at depth, carbonate minerals are easily leached from the country rocks and transported upwards with the hydrothermal fluid (increasing pore space). At a later stage, higher in the stratigraphy, pCO_2 and pH will change drastically due to fluid boiling and/or mixing with seawater, subsequently leading to precipitation and occlusion of early pore space. In light of the chemical composition of Tutum Bay hydrothermal fluids one possible consequence could be a

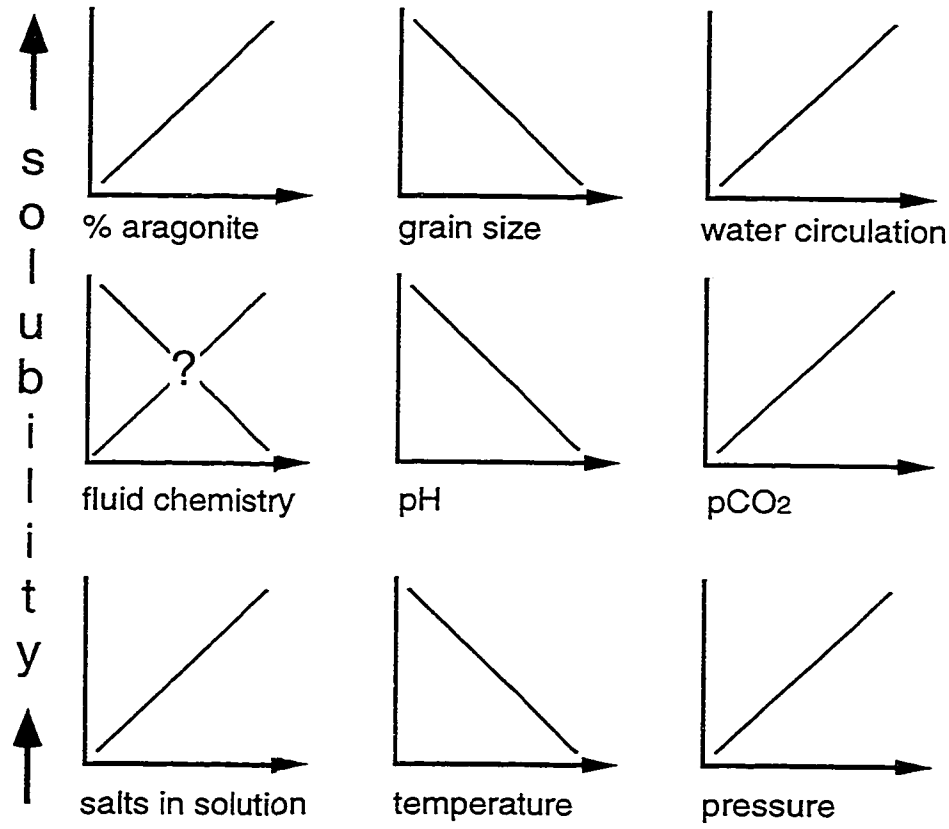

Fig. 3-13 Schematic display of the relationship between various factors that control carbonate solubility in a water-rock system (after Longman, 1982).

considerable porosity transfer from stratigraphically older to younger sections already during eogenetic stages. The bottom line is that thick sequences of carbonate rocks that were exposed to hydrothermal fluids may have increasing pore space with depth - which is in contrast to the general diagenetic model of porosity decrease with increasing depth (Moore, 1989).

3.6.3 Implications for $^{87}Sr/^{86}Sr$-dating of marine carbonates

Throughout Phanerozoic time the $^{87}Sr/^{86}Sr$ of marine carbonates has varied between 0.7067 and 0.7092 and these time-dependent variations have been used to date marine carbonates (Burke et al., 1982; Veizer, 1989). Until recently, it has been believed that $^{87}Sr/^{86}Sr$ values in marine carbonates reflect seawater values. At Ambitle Island, however, carbonate minerals precipitate in a mixed seawater-hydrothermal fluid environment and their $^{87}Sr/^{86}Sr$ values are primarily controlled by hydrothermal strontium. This has implications for marine carbonates that may have accumulated in a similar environment, if the time-dependent variations of $^{87}Sr/^{86}Sr$ were utilized for dating. According to its $^{87}Sr/^{86}Sr$, the coral aragonite from Ambitle Island would have an improbable Late Cretaceous age.

3.7 SUMMARY AND CONCLUSIONS

Tutum Bay vent waters are actively depositing substantial amounts of aragonite as massive layers of euhedral, pseudo-hexagonal crystals up to 2 cm long and as fine grained aragonite (feather dendrite). Pseudo-hexagonal crystals are often terminated by feather dendrite (Fig. 3-3). Near vent sites, primary pore space in volcaniclastic sediment and in skeletons of dead corals is almost completely occluded by hydrothermal aragonite.

Hydrothermal aragonite has a distinctively different isotopic composition when compared to "normal" marine carbonate. This difference arises from precipitation at high

temperature from a mixture of seawater and hydrothermal fluid that has lower $^{87}Sr/^{86}Sr$, $\delta^{18}O$ and δD values than seawater. Based on $^{87}Sr/^{86}Sr$ mixing calculations, the maximum seawater fraction is approximately 11%. Apparently, carbon isotopic equilibrium has been reached, while for oxygen complete equilibrium was not attained. Calculated equilibrium temperatures, nevertheless, are in good agreement with those directly measured and those obtained from fluid inclusion experiments.

Trace element concentrations, except for the REEs, Y and Sr are low. Only Fe-calcite shows distinctive Sr and Mg concentrations compared to "normal" marine carbonate. The REE pattern geometry of aragonite is similar to that of the hydrothermal fluid and concentrations are higher in coarse aragonite than in fine grained examples. This may be caused by higher precipitation rates.

4. THE NATURE AND COMPOSITION OF FE(III) OXYHYDROXIDE DEPOSITS

4.1 INTRODUCTION

The fate of iron in aqueous solutions is a close consequence of redox conditions, because Fe^{2+} is the mobile species and upon contact with oxygen, it is readily oxidized to Fe^{3+} and removed via precipitation of a ferric oxide or hydrous oxide. The oxidation kinetics of Fe^{2+} in seawater are more or less the same as in fresh water (Millero et al., 1987), resulting in similar deposits in the marine and non-marine environment. The most common minerals are hematite, goethite, lepidocrocite, ferrihydrite and protoferrihydrite, and their preferential precipitation depends on the set of physico-chemical conditions. For brevity, these minerals are referred to collectively as Fe(III) oxyhydroxides.

The natural occurrences of Fe(III) oxyhydroxides include gossans, ironstones, soils, hot springs, hydrothermal vents and stream beds. Many Fe(III) oxyhydroxide deposits are of economic interest, either directly for mining or for geochemical prospecting. The ochers, ironstones and gossans on the island of Cyprus, for example, were among the first ores to be mined commercially, dating back to pre-Roman times (Weisgerber, 1982). Hydrous iron oxides are significant indicator minerals in geochemical exploration because they effectively scavenge important ore metals from the weathering zone (e.g., Chao and Theobald, 1976).

Fe(III) oxyhydroxides are particularly important constituents in the marine environment where they generally form due to hydrogenetic (manganese nodules and crusts) or hydrothermal (hydrothermal sediments) processes (e.g., Murray, 1979). Their high specific surface area allows for ready adsorption of most heavy metals. The mainly amorphous nature of these deposits makes them efficient scavengers of many trace metals and, as a result, they are thought to be the most important removal mechanism from seawater for many trace elements, including the rare earth elements.

Most studies of deep water Fe(III) oxyhydroxide were carried out on samples collected by dredging without visual observation (e.g., Hein et al., 1994), or with limited visual observations if collected by a video camera equipped TV grab (e.g., Puteanus et al., 1991). Their geographic location and relation to vent orifices within a hydrothermal system are, therefore, poorly constrained. For most deep sea deposits, the chemical composition of the parent hydrothermal fluid is unknown and has to be inferred from depositional models. The study of Tutum Bay Fe(III) oxyhydroxides will provide us with new insights into their formation in the marine environment. There, hydrothermal fluids and precipitates were collected at the same time allowing for a direct comparison. Furthermore, visual observations that relate the distribution of vent orifices to the deposits could be made.

4.2 SAMPLE DESCRIPTIONS

A complete listing of all Fe(III) oxyhydroxide samples is given in Table 4-1. Fe(III) oxyhydroxides are present throughout Tutum Bay where they form as very thin layers on sediment grains in areas of high seafloor temperature. Massive layers and extensive filling of sediment pore space, however, are restricted to the vicinity of vent sites. There they form a bright orange coating on volcanic boulders (Figs. 3-2 and 4-1a), form distinct bands on corals skeletons, aragonite and Fe-calcite (Figs. 3-3b and 3-4b) and/or precipitate as massive layers in open spaces (Fig. 4-1b). They can vary in color from a bright orange to very dark brown that is almost black, and in hardness from <1 (talc) to about 2.5 (between gypsum and calcite). Hardness and color are related to each other in such a way that the darker the color the harder the Fe(III) oxyhydroxide. Based on sample hardness, color and general appearance, the relative age of Tutum Bay Fe(III) oxyhydroxide deposits was determined qualitatively and from oldest to youngest is in the order FV-1, V-2, V-1B, V-4.1 and V-2 (97). The younger

TABLE 4-1
DESCRIPTION OF TUTUM BAY HYDROTHERMAL FE(III) OXYHYDROXIDE PRECIPITATES

Sample	Location	Description	XRD Scans
FV-1A	Vent 1	massive layers with alternating colors ranging from dark brown to dark orange; indurated and relatively hard compared to the other Fe-oxyhydroxides	protoferrihydrite, gypsum, hematite, As_2O_5, As_2O_5, Fe-smectite
FV-1B	Vent 1	softer layer of dark orange color from beneath FV-1A	n.d.
V-1B	Vent 1	Fe-precipitate on a volcanic boulder	protoferrihydrite
V-2B I	Vent 2	massive layer of reddish brown relatively hard Fe-oxyhydroxide that precipitated on dead coral fragments and aragonite	protoferrihydrite, Fe-smectite, claudetite (As_2O_3)
V-2B II	Vent 2	soft layer of yellow brown color from beneath V-2B I	protoferrihydrite
V-2B III	Vent 2	very thin intermediate layer between V-2B I and V-2B II; may contain significant amounts of both V-2B I and V-2B II	protoferrihydrite
V-4.1D	Vent 4	Fe-oxyhydroxide coating volcanic fragments and fragments of dead corals, contains some aragonite	protoferrihydrite
V-2 (97) I	Vent 4	very thin hard dark greenish brown layer on a coral skeleton that fell partly over the vent orifice; contains significant amounts of V-2 (97) II, was in contact with mainly seawater at the time of sampling; collected from the side of the coral opposite to the vent	protoferrihydrite, Fe-smectite
V-2 (97) II	Vent 4	very soft orange to orange brown layer on a coral skeleton that fell partly over the vent orifice; collected from the side of the coral that faced the vent	protoferrihydrite

Note: n.d.=not determined

Fig. 4-1 (a) Underwater photograph of Tutum Bay vent 1. Field of view is approximately 1 m. Volcanic pebbles, boulders and fragments of dead corals are coated with a thin layer of Fe(III) oxyhydroxide (bright yellow to orange). The thickness of the Fe(III) oxyhydroxide deposits increases with nearness to the point of discharge. (b) Stereo microscope photo micrograph of massive Fe(III) oxyhydroxide collected from inside the orifice at vent 1 (see photo above). The circles and numbers indicate locations where proton probe analyses were performed and correspond to numbers in Table 4-3. The scale bar represents 2 mm.


a

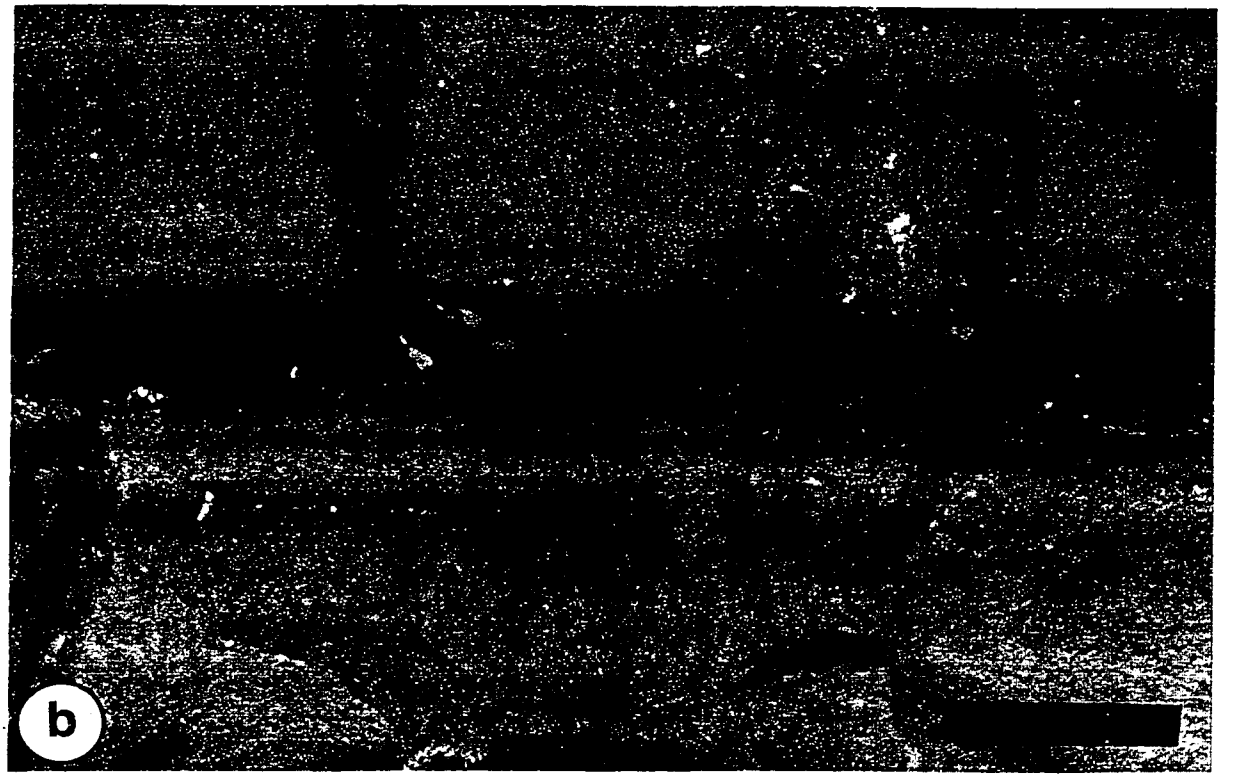
b

samples V-2 (97) and V-4.1 do not show differently colored layers as seen in the two older samples (FV-1 and V-2) (Fig. 4-1b).

The samples V-2 (97) and V-2 were collected from the same vent, except that V-2 (97) was taken approximately 18 months later than V-2. V-2 (97) provides us with the opportunity to estimate the rate of precipitation and to investigate the very early stages of Fe(III) oxyhydroxide precipitation. In February 1997 an unusually strong storm struck Ambitle Island from the southwest (Philip Tolain, 1997 pers. comm.) and heavy seas caused extensive damage to coral reefs and shoreline (pers. observation). In Tutum Bay several large coral heads were tipped over and several colonies of branching corals were destroyed. During that process part of a Staghorn coral (*Agropora robusta*?) must have fallen over the main orifice of vent 2. At the time of sampling, those branches exposed to the hydrothermal fluid were coated with very soft and fragile orange to orange brown Fe(III) oxyhydroxide deposits approximately 5 - 7 mm thick. Given the period between the onset of deposition and sampling, precipitation rates could be as high as 1 cm/year. Precipitation on coral branches continues to roughly 20 cm above the orifice, but deposits gradually become thinner with distance. Those sides of the deposits that were distal to the vent fluid and, therefore, more exposed to seawater than hydrothermal fluid had a very thin greenish brown hard surface layer (V-2 (97) II). Beneath that layer, however, the material was identical to the Fe(III) oxyhydroxides exposed mainly to the hydrothermal fluid.

4.3 ANALYTICAL PROCEDURES AND RESULTS

Bulk Fe(III) oxyhydroxide material was separated from its substrate, rinsed with deionized water to remove halite and carefully crushed in an agate mortar. Sample powders were dried at room temperature to prevent goethite to hematite conversion (Deer et al., 1992), according to:

$$2\ FeOOH + heat\ (> 90°C) => Fe_2O_3 + H_2O. \qquad [4\text{-}1]$$

Chemical, mineralogical and isotopic analytical methods were identical to those described in the analytical section of the previous chapter (3.3).

4.3.1 Mineralogy

A combination of XRD and SEM/EDX analyses was applied to clarify the mineralogical history and composition of the Fe(III) oxyhydroxide deposits. Results are listed in Table 4-1 and representative XRD diffractograms are shown in Figs. 4-2 and 4-3. The two diffractograms in Fig. 4-2 represent the two mineralogical endmembers of Tutum Bay deposits. Sample V-2 has no distinct peaks, except for two broad humps at approximately 38 and 62° 2 theta (d = 2.5 Å and 1.5Å). These two humps may be groups of adjacent diffuse reflections and indicate the presence of hydrous iron oxide (Giessen, 1966; Towe and Bradley, 1967). Chukhrov et al. (1973) proposed the name protoferrihydrite for hydrous iron oxides that give only two reflections (2.5 and 1.5 Å) and ferrihydrite for those that give five reflections (2.52, 2.25, 1.97, 1.72 and 1.48 Å). They also concluded that the lesser amount of reflections for protoferrihydrite indicates the beginning stage of crystallization. The amorphous nature of many Fe(III) oxyhydroxide deposits reflects their very fine grain size and colloidal origin (e.g., Puteanus et al., 1991). Mössbauer spectroscopy confirmed the amorphous nature of any Fe-rich material (mineral) and particle sizes of less than 100 Å for Tutum Bay Fe(III) oxyhydroxides (D. Rancourt, 1997 pers. comm.).

Sample FV-1 also shows the two broad humps at approximately 38 and 62° 2 theta, but several other sharp peaks are clearly observable (Fig. 4-2b). Mineral identification was aided by SEM/EDX analyses and As_2O_5, scorodite ($FeAsO_4*2H_2O$), gypsum and Fe-smectite could be identified. As_2O_4 and hematite are likely, but could not be unequivocally confirmed because

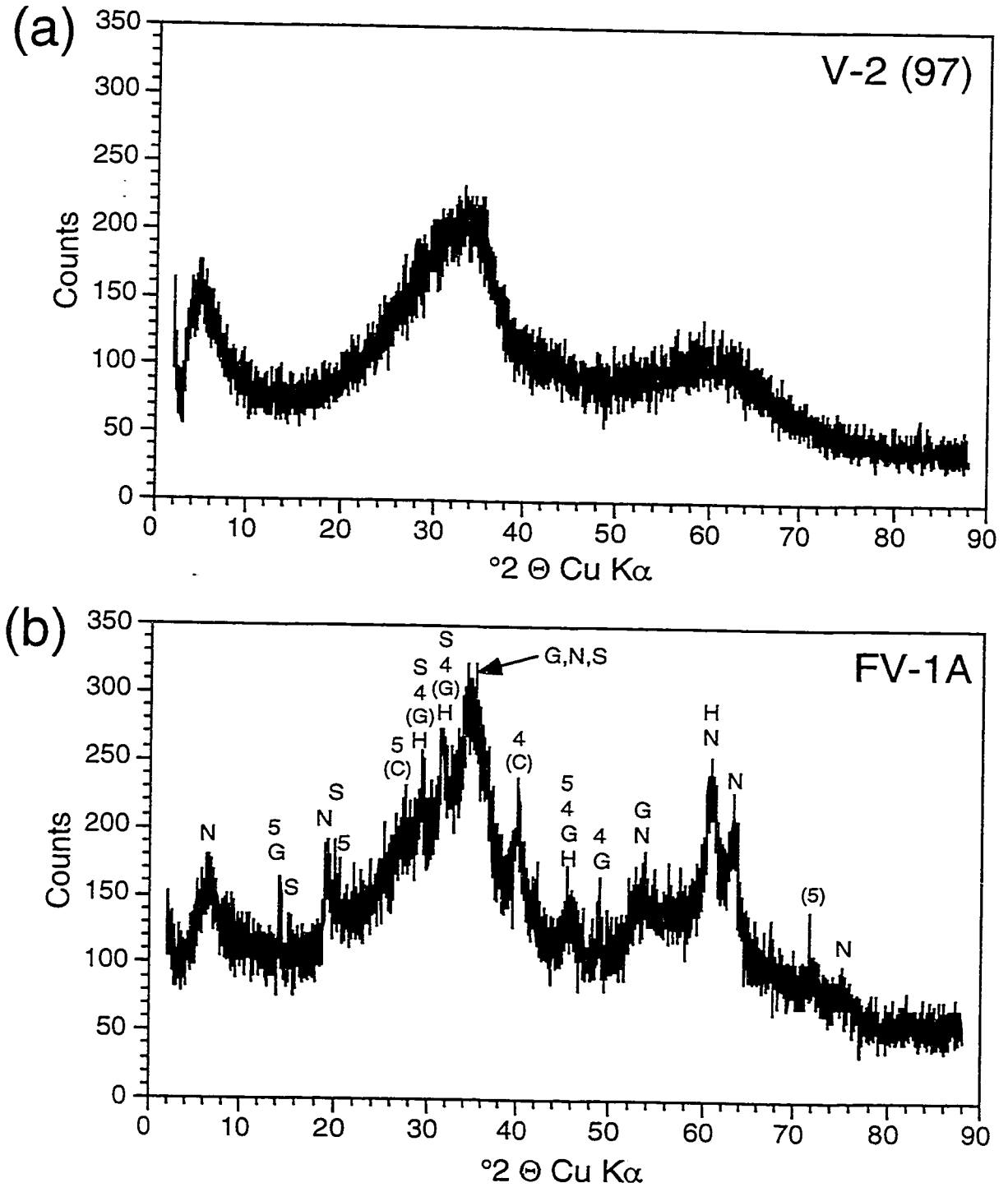

Fig. 4-2 Diffractometer patterns for sample V-2 (97) (a) and FV-1A (b). The two patterns clearly demonstrate the increasing crystallinity with increasing age. V-2 (97) contains only protoferrihydrite, whereas in FV-1A several sharp peaks are superimposed on top of the typical protoferrihydrite pattern: N: smectite (nontronite), G: gypsum, C: claudetite, S: scorodite, H: hematite, 4: As_2O_4 and 5: $A_{s2}O_5$. Letters in brackets indicate doubtful peaks.

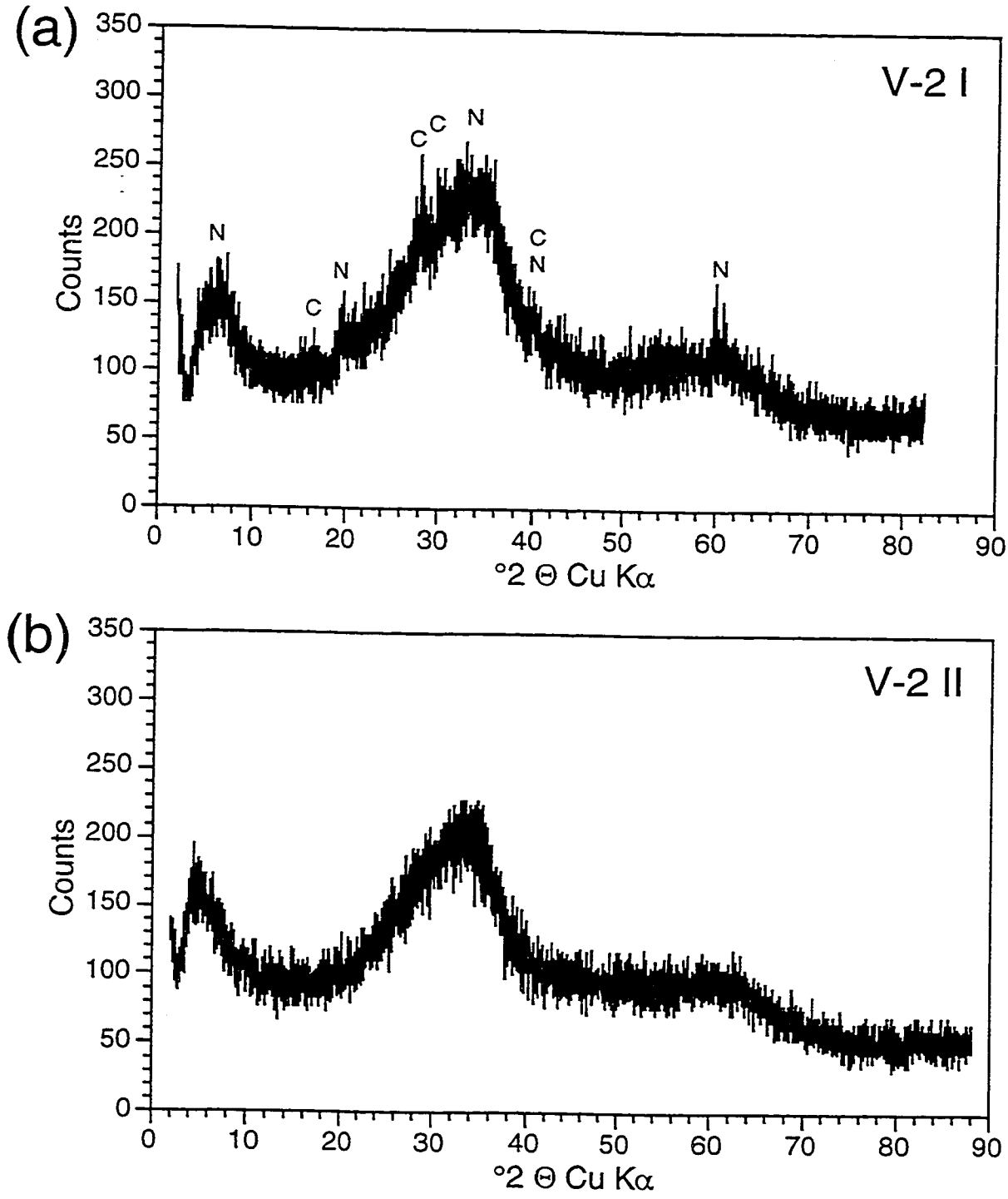

Fig. 4-3 Diffractometer patterns for sample V-2 I (a) and V-2 II (b). The two patterns clearly demonstrate the importance of seawater contact during aging. V-2 I although slightly younger than V-2 II is more crystalline because it remained in contact with either seawater or a mixture of seawater and vent fluid (seawater >> vent fluid). C: claudetite, N: smectite (nontronite).

they share X-ray reflections with As_2O_5, gypsum and Fe-smectite (Fig. 4-2b). The presence of hematite, although hinted at in the XRD pattern, is unlikely because it is contrary to the findings of Mössbauer spectroscopy.

It was not possible to determine the exact variety of Fe-smectite, but circumstantial evidence points towards nontronite, a dioctahedral Fe-smectite. The appearance and greenish color of sample V-2 (97) I is identical to that of a nontronite rich Fe(III) oxyhydroxide deposit in the Woodlark Basin (see Fig. 5 in Binns et al., 1993). Nontronite has been found to be the dominant smectite in other Fe(III) oxyhydroxide deposits in submarine settings (e.g., Alt, 1988; Hekinian et al., 1993; Puteanus et al., 1991; Stoffers et al., 1990) where the presence of oxygenated seawater either prevents the formation of Fe-rich saponite (Fe^{2+}-smectite) or causes the transformation from saponite to nontronite (Andrews, 1980). The presence of kankite ($FeAsO_4*3.5H_2O$), hydrogenarsenate ($H_5As_3O_{10}$) and/or hydrated hydrogenarsenate ($H_3As_4O_4*3H_2O$) is possible but could not be confirmed unambiguously by XRD or SEM/EDX.

The outer layer of sample V-2 (V-2 I, Table 4-1 and Fig. 4-3a) represents a mineralogical composition intermediate between the two samples in Fig. 4-2 (V-2 (97) and FV-1A). Here the presence of a Fe-smectite and claudetite (As_2O_3) could be confirmed. The reflections are not as strong as those for the same mineral in sample FV-1A which may indicate either a lesser amount of mineral present or poorer crystallinity. Claudetite was not conclusively observed in sample FV-1A. The reflections for Fe-smectite and claudetite are absent in the softer and less dark material of sample V-2 II that was collected from beneath V-2 I. This scan is almost identical to that of V-2 (97).

In addition to the two broad humps at 38 and 62° 2 theta (d = 2.5 Å and 1.5Å) a somewhat sharper hump was observed at approximately 4.2° 2 theta (d ~ 20 Å). This hump seems to shift to the right with increasing crystallinity of the Fe(III) oxyhydroxide samples (Figs. 4-2 and 4-3). In samples V-2 (97) and V-2 II it is relatively sharp and located at ~ 4.0 to 4.5° 2 theta, in sample V-2 I it is quite broad and occupies the range from 4.2 to 7.0 4.2° 2

theta and in sample FV-1 it is relatively sharp again and shifted to ~ 6.7 to 7.0 4.2° 2 theta. To my knowledge, this hump (peak) has not been previously mentioned in the literature pertaining to the study of Fe(III) oxyhydroxides and it could not be attributed to the presence of an As-rich mineral, although Tutum Bay Fe(III) oxyhydroxides are unusually high in arsenic. Considering the chemical composition of sample V-2 II (Table 4-2), two minerals may account for this unusual reflection: silhydrite ($3SiO_2*H_2O$) and okenite ($Ca_{10}Si_{18}O_{46}*18H_2O$). These minerals have their 100% reflection at approximately 4.2 and 6° 2 theta (15 to 20 Å). Unfortunately only little is known about these minerals and their presence is entirely a guess that cannot be conclusively confirmed at this time. Given that silhydrite is present in spring deposits (Gude and Sheppard, 1972), while okenite is an alteration product in basaltic rocks (Merlino, 1983), the preference is for the former.

4.3.2 Chemistry

Major, minor and trace element compositions of bulk samples are listed in Table 4-2. Fe(III) oxyhydroxide deposits show approximately the same chemical composition with the exception of Fe, Si, Ca, CO_2^T, and Sr in sample 4.1D. The relatively elevated values for Ca, CO_2^T and Sr are in good agreement with the assumption that this sample is slightly contaminated with aragonite. Fe and Si are related to each other in such a way that samples with high Fe generally have a lower Si concentration. Mössbauer spectroscopic analyses of samples FV-1 and V-2 confirmed that iron is exclusively present in its trivalent state (D. Rancourt, 1997 pers. comm.).

Hekinian et al. (1993) divided Fe and Si oxyhydroxide deposits from south Pacific intraplate volcanoes and East Pacific Rise axial and off-axial regions based on field and compositional variations into four groups: (1) low trace element concentration and Fe from 27 to 45%; (2) high trace element concentration and Fe from 30 to 50 %; (3) low trace element concentration and Fe from 20 to 30% and Si from 7 to 20%, enriched in nontronite; and (4)

TABLE 4-2
MAJOR, MINOR, TRACE ELEMENT AND SR-ISOTOPE COMPOSITION OF TUTUM BAY HYDROTHERMAL FE(III) OXYHYDROXIDE PRECIPITATES

Sample	Unit	FV-1A	FV-1B	V-1B	V-2B I	V-2B II	V-2B III	V-4.1D
SiO_2	%	20.90	14.50	14.10	13.30	12.30	17.20	14.80
TiO_2	%	<0.02	<0.02	<0.02	<0.02	<0.02	<0.02	0.12
Al_2O_3	%	<0.2	<0.2	<0.2	<0.2	<0.2	<0.2	1.04
$Fe_2O_3^T$	%	44.70	52.50	50.90	52.70	54.10	50.80	44.40
MnO	%	0.09	0.08	0.11	0.07	0.07	0.07	0.08
MgO	%	0.83	0.73	1.07	0.78	0.82	1.07	1.28
CaO	%	2.57	1.70	2.51	1.82	1.96	1.63	7.09
Na_2O	%	0.69	0.48	0.67	0.82	1.09	0.76	0.96
K_2O	%	0.20	0.15	0.17	0.12	0.14	0.16	0.33
P_2O_5	%	0.21	0.22	0.19	0.22	0.25	0.20	0.26
CO_2^T	%	0.2	0.2	2.1	1.5	1.6	1.3	7.1
LOI	%	22.4	21.9	18.3	18.3	18.7	19.6	19.2
S^T	%	0.05	0.03	<0.02	0.02	0.04	<0.02	<0.02
Total	%	93.1	91.8	89.8	89.8	90.9	93.2	96.2
Ag	ppm	0.2	0.1	1.5	0.4	0.3	0.4	5.6
Au	ppb	<17	<17	<41	<40	<41	<40	<40
As	ppm	55000	49000	57000	60000	62000	54000	49000
Ba	ppm	180	220	80	110	130	100	70
Be	ppm	35	50	42	39	34	38	28
Br	ppm	<5	11	<4	<5	<4	<5	<4
Cr	ppm	24	30	28	16	26	31	45
Cs	ppm	5.3	3.5	1	1.1	0.98	1.9	3.2
Cu	ppm	33	41	14	15	15	13	160
Ga	ppm	2.1	1	0.9	0.8	0.9	0.9	3.1
Hf	ppm	<0.05	0.06	<0.05	<0.05	<0.05	<0.05	0.17
Hg	ppm	<5	<1	<5	<5	<5	<5	<5
In	ppm	<0.05	<0.05	0.08	0.08	0.06	0.08	0.06
Mo	ppm	3.6	1.7	0.8	0.8	0.7	0.8	1.3
Nb	ppm	<10	<10	<10	<10	<10	<10	18
Ni	ppm	0.08	0.29	0.25	0.18	0.23	0.2	0.55
Pb	ppm	16	35	14	15	16	15	49
Rb	ppm	13	7.1	3.9	3.8	3.9	5.5	9.7
Sb	ppm	240	260	170	180	160	190	190
Se	ppm	<6	<3	<6	<11	<6	<11	<6
Sr	ppm	1100	770	910	940	940	780	1500
Th	ppm	<0.02	0.13	0.03	<0.02	<0.02	<0.02	0.09
Tl	ppm	4.2	3.1	0.82	2	1.9	1.9	0.59
U	ppm	0.92	0.63	0.73	0.34	0.58	0.47	0.88
V	ppm	<5	<5	14	<5	6	<5	80
W	ppm	<12	<7	<10	<10	<11	<11	<10
Y	ppm	10	18	21	9.3	8.1	9.1	20
Zn	ppm	33	56	40	29	24	32	49
Zr	ppm	1	3.2	1.1	1	1	1	6.6
$^{87}Sr/^{86}Sr$		0.70458	n.d.	0.70701	0.70512	0.70478	0.70489	0.70604

Note: n.d.=not determined; Max. error for $^{87}Sr/^{86}Sr$ values is ±0.000009 2 Standard Errors.

very low trace elements and high Si (>35%) and low Fe (<10%). The Si and Fe contents in Tutum Bay Fe(III) oxyhydroxides range between 5.7 and 9.8% and 30.9 and 37.7%, respectively. According to the classification of Hekinian et al. (1993) Tutum Bay deposits are of type 1 and 3, indicating a hydrothermal origin. The sample, FV-1A, that is classified as type 3 (based on Si and Fe concentration), correspondingly contains a significant quantity of nontronite. Manganese (Fe/Mn>600) and combined Co, Ni and Cu values are very low in Tutum Bay Fe(III) oxyhydroxides which places them into the lower left corner of the diagnostic ternary diagram of Bonatti et al. (1972), also indicating a hydrothermal origin (Fig. 4-4). Elements that are usually enriched in Fe(III) oxyhydroxides such as Co and V are below crustal abundance and well below their concentration in island-arc volcanics. Arsenic, on the other hand, is higher than expected by an order of magnitude and clearly sets Tutum Bay Fe(III) oxyhydroxides apart from other deposits (Fig. 4-5). Values are as high as 62,000 ppm if analyzed by neutron activation (Table 4-2) and 76,000 ppm if analyzed by proton probe (Table 4-3). The discrepancy between the two values is a result of different analytical methods. The neutron activation analysis is done on bulk samples and values reflect average sample concentrations. Although values scatter significantly, considering the relatively high analytical uncertainty of this method (~15%) the samples can be regarded as being within the same concentration range (Table 4-2). The As concentrations determined by proton probe, on the other hand, represent only a very small sample area and values scatter well beyond their maximum analytical error of < 5%. This observation is in accord with the heterogeneous nature of Tutum Bay Fe(III) oxyhydroxides deposits. The proton probe analyses listed in Table 4-3 are a traverse across differently colored layers in sample FV-1A (Fig. 4-1B) and darker layers generally have higher As concentrations, but there is no definite inter-element correlation. The same heterogeneity was also observed in the three separates of sample V-2B (Table 4-2).

North American Shale Composite (NASC) normalized rare earth element (REE) concentrations in Tutum Bay hydrothermal Fe(III) oxyhydroxides are plotted in Fig. 4-6. The patterns of samples FV-1A, FV-1B, V1-B and V-2B show an initial drop from La to Ce

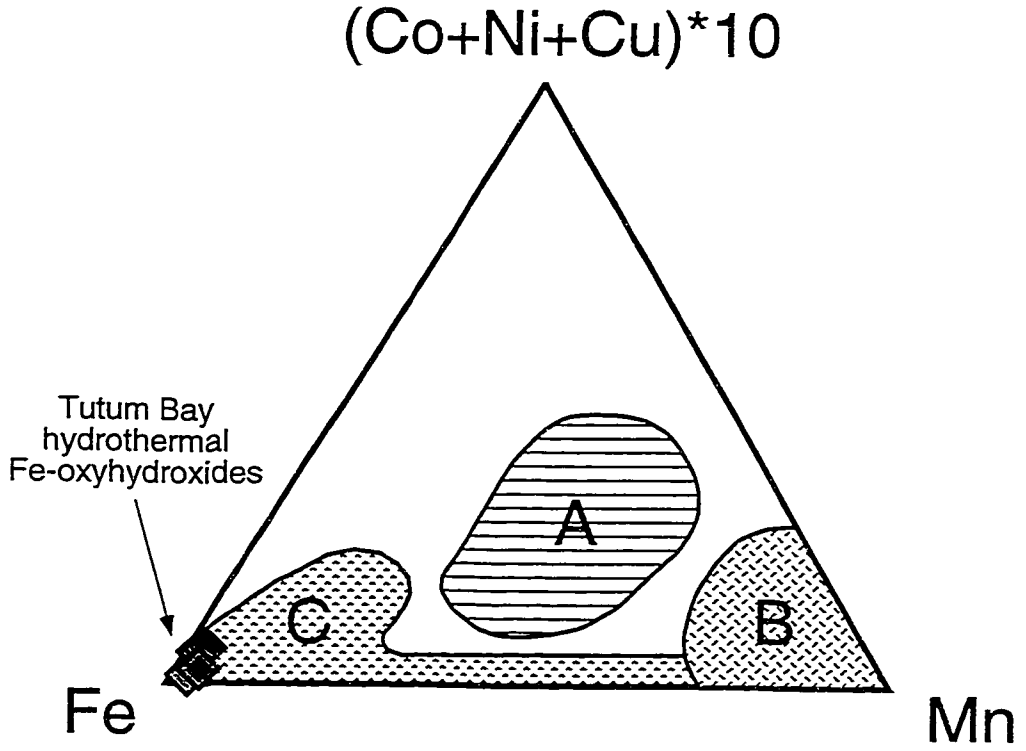

Fig. 4-4 Diagnostic ternary diagram to determine the origin of Fe and Mn-rich oxyhydroxide deposits (after Bonatti et al., 1972). Tutum Bay Fe(III) oxyhydroxides plot at the Fe apex indicating a hydrothermal origin. The fields are as follows: (A) Hydrogenetic cobalt-rich crusts from the central Pacific, from Hein et al. (1994); (B) Diagenetic oxyhydroxides, from Bonatti et al. (1972); (C) Hydrothermal field, from Bonatti et al. (1972).

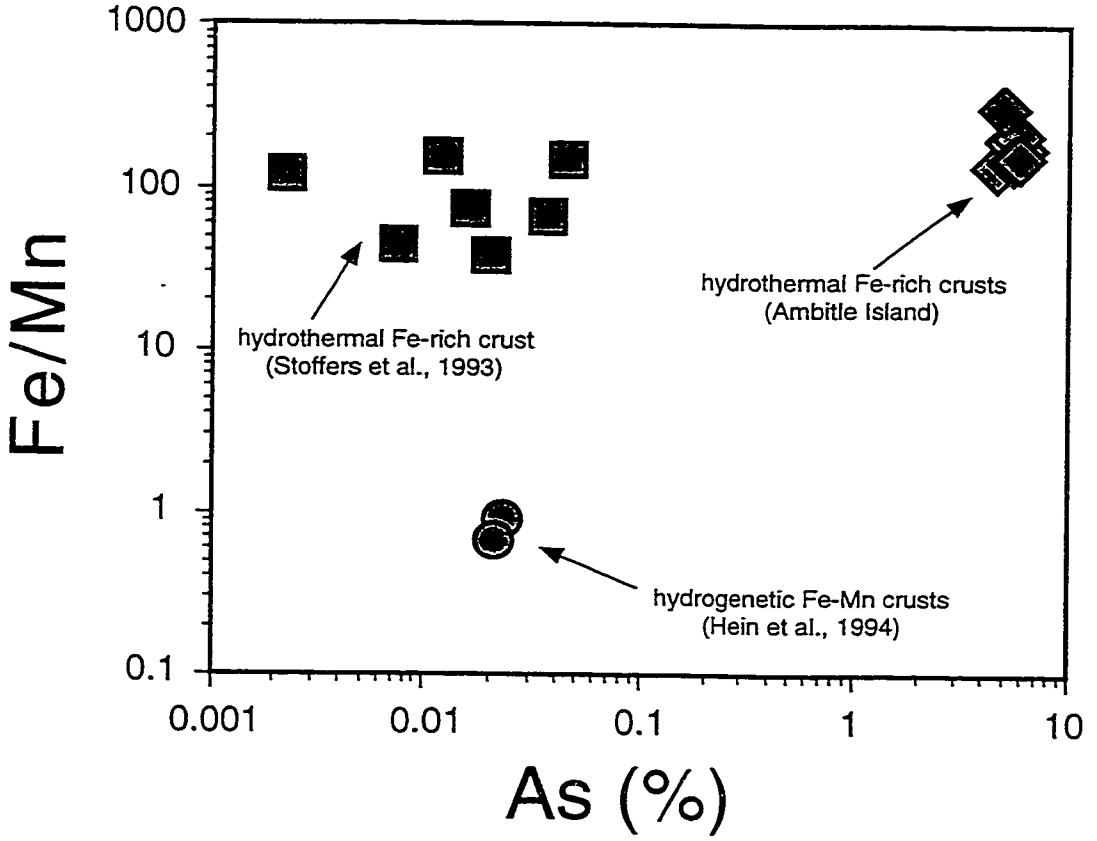

Fig. 4-5 Scatter plot of As concentration vs. Fe/Mn ratio on a log scale. Tutum Bay Fe(III) oxyhydroxide deposits have similar Fe/Mn ratios as hydrothermal Fe-rich crusts from south Pacific seamounts, but As values are more than two orders of magnitude higher.

TABLE 4-3
PROTON PROBE TRAVERSE ACROSS TUTUM BAY FE(III) OXYHYDROXIDE (FIG. 4-1B)

Point	1	2	3	4	5	6	7	8	9
Fe	380000	330000	420000	370000	407000	420000	410000	390000	430000
As	59000	54000	55000	76000	64000	65000	57000	71000	61000
Zn	57	73	76	78	73	70	68	88	63
Sr	350	390	350	1000	700	490	380	700	300
Sb	200	160	220	240	260	290	260	150	220
Ta	160	*<30*	*<30*	190	170	140	130	170	150
Ni	*<24*	*<24*	*<24*	105	*<24*	*<24*	*<24*	*<24*	*<24*
Cu	*<17*	*<17*	*<17*	73	*<17*	72	*<17*	*<17*	80
Y	*<6*	*<6*	20	*<6*	*<6*	*<6*	*<6*	*<6*	20

Note: All analyses in parts per million (ppm); point numbers correspond to those indicated in Fig. 4-1B.

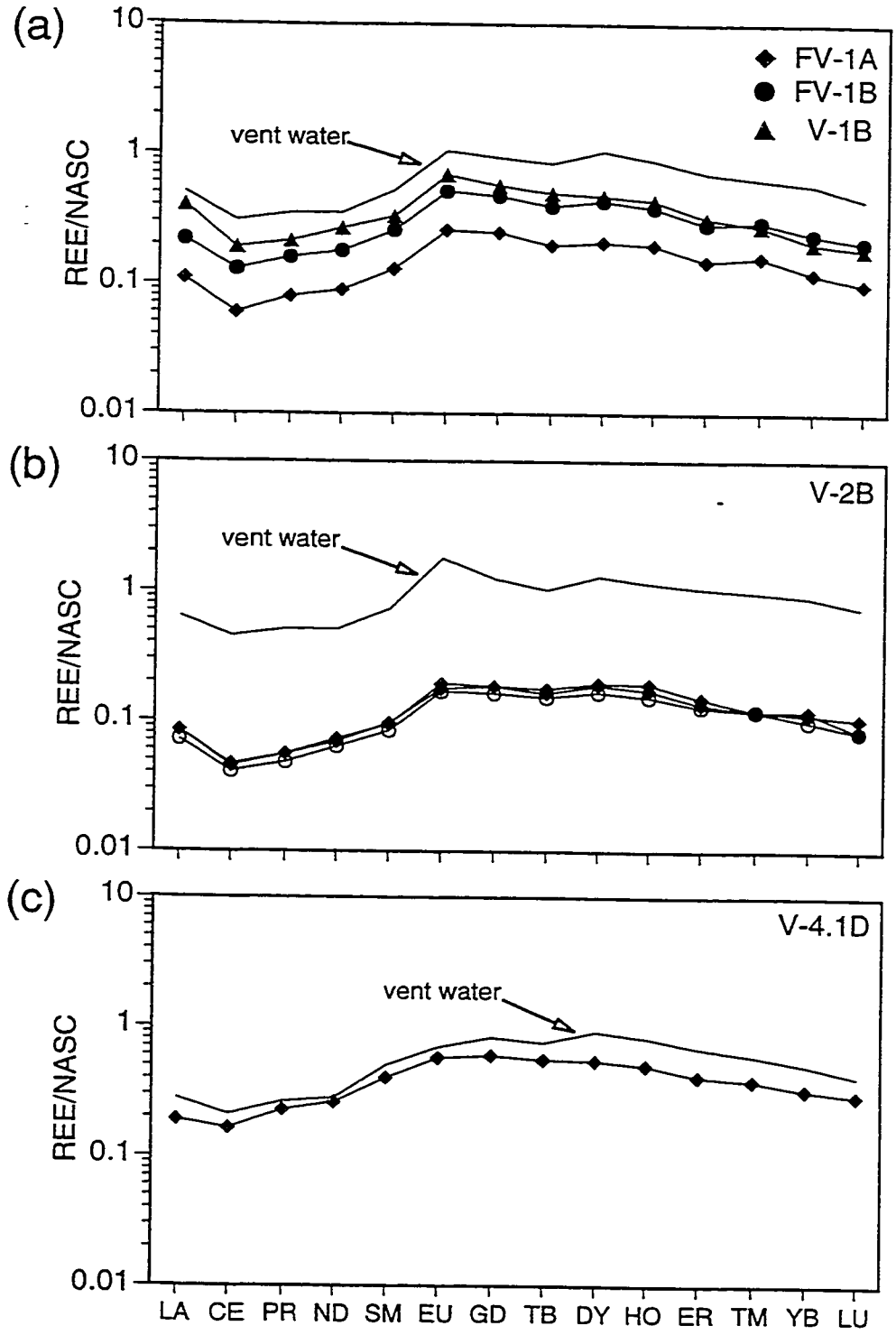

Fig. 4-6 North American Shale Composite (NASC) (Haskin et al., 1968) normalized rare earth element (REE) plots for hydrothermal Fe(III) oxyhydroxide precipitates from vents 1, 2 and 4. REE concentrations for vent waters (Fig. 2-6) are multiplied by 10^6 and the values are interpolated for Tm and extrapolated for Lu.

followed by a rise from the Ce minimum to an Eu maximum and a constant decrease towards a Lu minimum. The pattern geometry approximately resembles that of the parent hydrothermal fluid (Fig. 4-6a, b), except that the Eu peaks in the Fe(III) oxyhydroxides are not as pronounced as in the hydrothermal fluid. The sample from vent 4 is different and more closely resembles the pattern of the parent hydrothermal fluid (Fig. 4-6c). REE concentrations initially drop from La to a Ce minimum which is followed by a rise to a Eu-Gd maximum and a slight decrease towards an intermediate Lu.

4.4 DISCUSSION

Weathering of iron bearing minerals and direct precipitation from solution are the two processes that lead to the formation of Fe(III) oxyhydroxides, such as goethite, lepidocrocite, hematite and ferrihydrite. The final product is dependent on an intricate interplay between bacterial activity, pH, Eh, temperature, precipitation rate and iron concentration (e.g., Alt, 1988; Binns et al., 1993; Chao and Theobald, 1976; Churkhov et al., 1973; Fortin et al., 1993; Hekinian et al., 1993; Murray, 1979; Puteanus et al., 1991; Schwertmann and Fischer, 1973; Stoffers et al., 1993). Direct precipitation from solution occurs either via the slow hydrolysis of Fe^{3+} solution or due to oxidation of Fe^{2+} solutions. The former generally leads to the formation of goethite, except from solutions containing Cl^- which precipitate akageneite (Murray, 1979). Neither mineral was observed in Tutum Bay Fe(III) oxyhydroxides indicating that there, hydrolysis of Fe^{3+} is not an important process. In Tutum Bay vent fluids (Eh ~ -0.17 V and pH ~ 6.1) Fe^{3+} is practically absent and as a result precipitation has to proceed via oxidation of Fe^{2+}. This is easily achieved through mixing with oxygenated seawater (e.g., Millero et al., 1987) and results in an increase of Eh and pH and a decrease in temperature, all of which favor the precipitation of Fe(III) oxyhydroxide (Fig. 4-7). At the same time conditions are not oxidizing enough to cause precipitation of a Mn-rich (Fig. 4-8) and/or

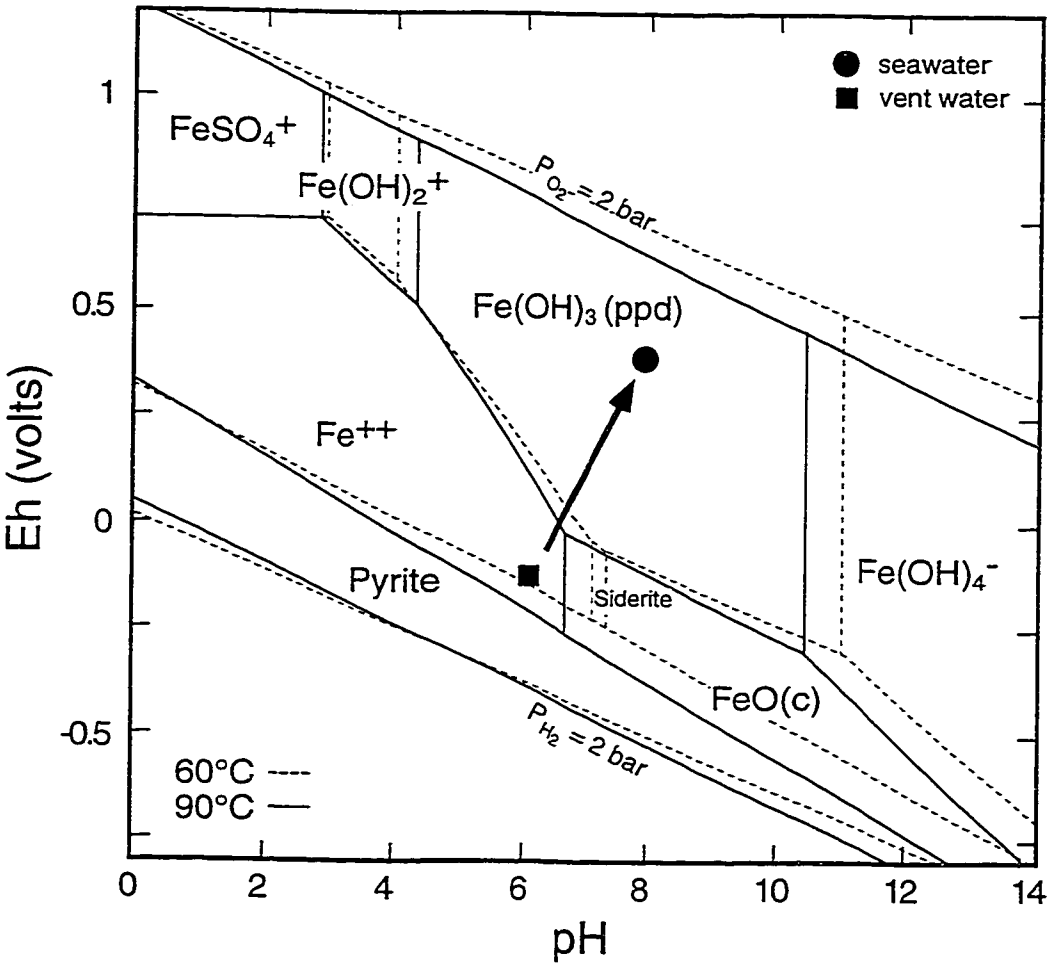

Fig. 4-7 Eh-pH diagram for the system Fe-O-H-SO_4-HCO_3 at 60°C (dashed lines) and 90°C (solid lines) at a pressure of 2.026 bars. Activities for Fe^{2+}, SO_4^{2-} and HCO_3^- are assumed to be 10^{-5}, 10^{-3} and 10^{-3}, respectively. Thermodynamic data are from Brookins (1988) and references therein. $Fe(OH)_3$(ppd) is the field of amorphous Fe(III) oxyhydroxide. The arrow indicates the mixing trend between hydrothermal fluid and seawater.

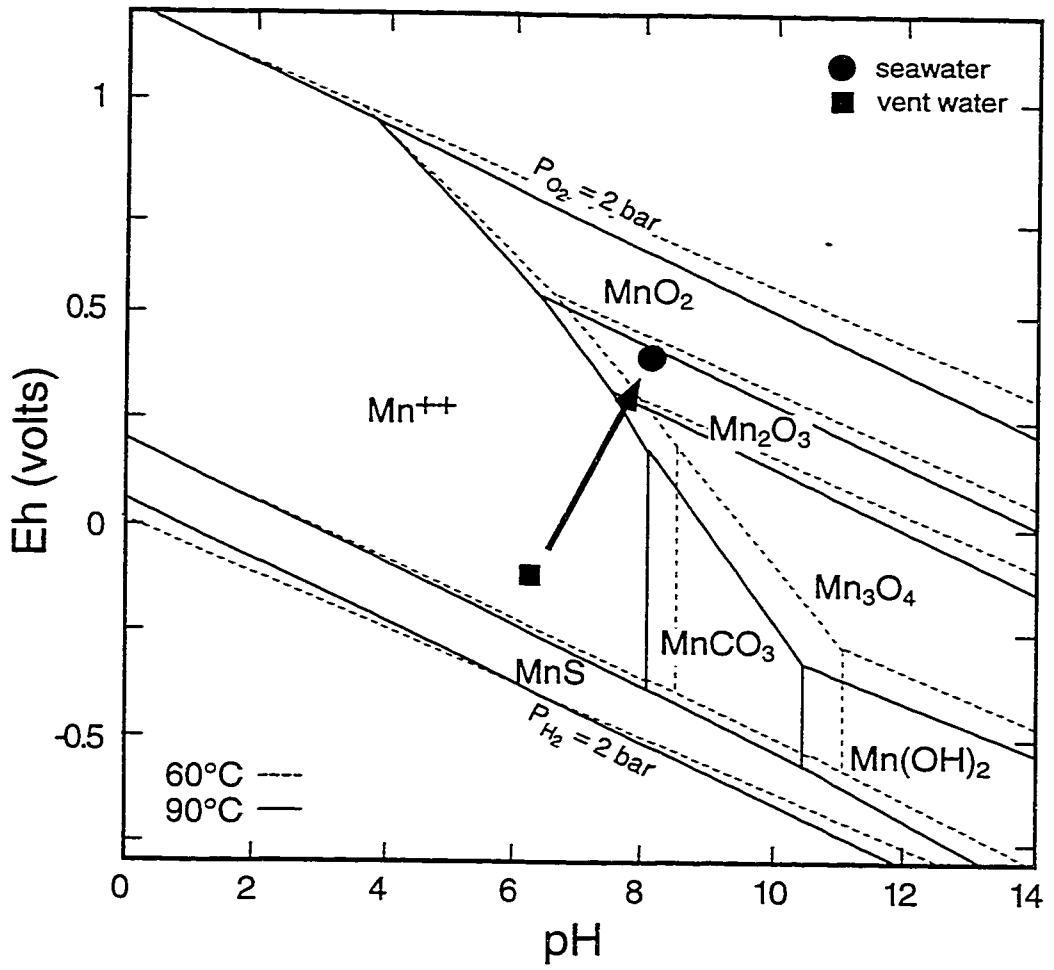

Fig. 4-8 Eh-pH diagram for the system Mn-O-H-SO_4-HCO_3 at 60°C (dashed lines) and 90°C (solid lines) at a pressure of 2.026 bars. Activities for Fe^{2+}, SO_4^{2-} and HCO_3^- are assumed to be 10^{-5}, 10^{-3} and 10^{-3}, respectively. Thermodynamic data are from Brookins (1988) and references therein. The arrow indicates the mixing trend between hydrothermal fluid and seawater. Manganese remains comparably longer in its divalent state and, therefore, in solution than Fe^{2+} (Fig. 4-7), thus explaining its absence in Tutum Bay Fe(III) oxyhydroxides.

As-rich (Fig. 4-9) mineral, explaining their initial absence in Tutum Bay oxyhydroxide deposits. The same process has been called upon to explain the formation of various other Fe(III) oxyhydroxide deposits in submarine settings (e.g., Alt, 1988; Puteanus et al., 1991). Under these conditions X-ray amorphous Fe(III) oxyhydroxides is the preferred material because precipitation is rapid, thus preventing the formation of a crystalline phase. Chukhrov et al. (1973) noted that "with especially rapid deposition of hydrous iron oxides, protoferrihydrite is obtained". Maximum precipitation rates in Tutum Bay are up to three times higher than those measured for Fe(III) oxyhydroxide deposits from Loihi Seamount (Cremer, 1995) and, as a result, protoferrihydrite is the dominant material (Table 4-1).

Oxidation of Fe^{2+} as a mechanism of precipitation is also supported by the use of $^{87}Sr/^{86}Sr$ as a tracer of mixing between hydrothermal fluid and seawater (Fig. 4-10). $^{87}Sr/^{86}Sr$ values in Tutum Bay Fe(III) oxyhydroxide indicate that mixing with seawater occurs during its precipitation (Fig. 4-10). The calculated minimum and maximum seawater fractions are approximately 11 and 57%, respectively. Assuming a temperature of 30°C for seawater and 100°C for the hydrothermal endmember, the temperature of the mixture can be calculated with equation [3-1]. Thus, precipitation of Tutum Bay Fe(III) oxyhydroxides takes place at a temperature range between approximately 60 and 93°C. The corresponding increase in pH, calculated with the same equation, is approximately to 6.3 and 7.2 from the initial pH = 6.1 of the hydrothermal fluid (Table 2-5). This model, however, cannot be used without reservation, because Fe(III) oxyhydroxide is a mixture of different minerals, and the mineral phases represent slightly different physico-chemical conditions. Post-depositional absorption of Sr or exchange with seawater or hydrothermal fluid cannot be excluded due to the extreme reactivity of Fe(III) oxyhydroxide surface areas (e.g., Davis and Kent, 1991). Thus, through time, Fe(III) oxyhydroxides may lose the chemical signature that represents the conditions during precipitation. Nevertheless, the temperatures that were estimated with the $^{87}Sr/^{86}Sr$ mixing model are in good agreement with precipitation temperatures reported in the literature (e.g., Churkhov et al., 1973; Puteanus et al., 1991; Stoffers et al., 1993).

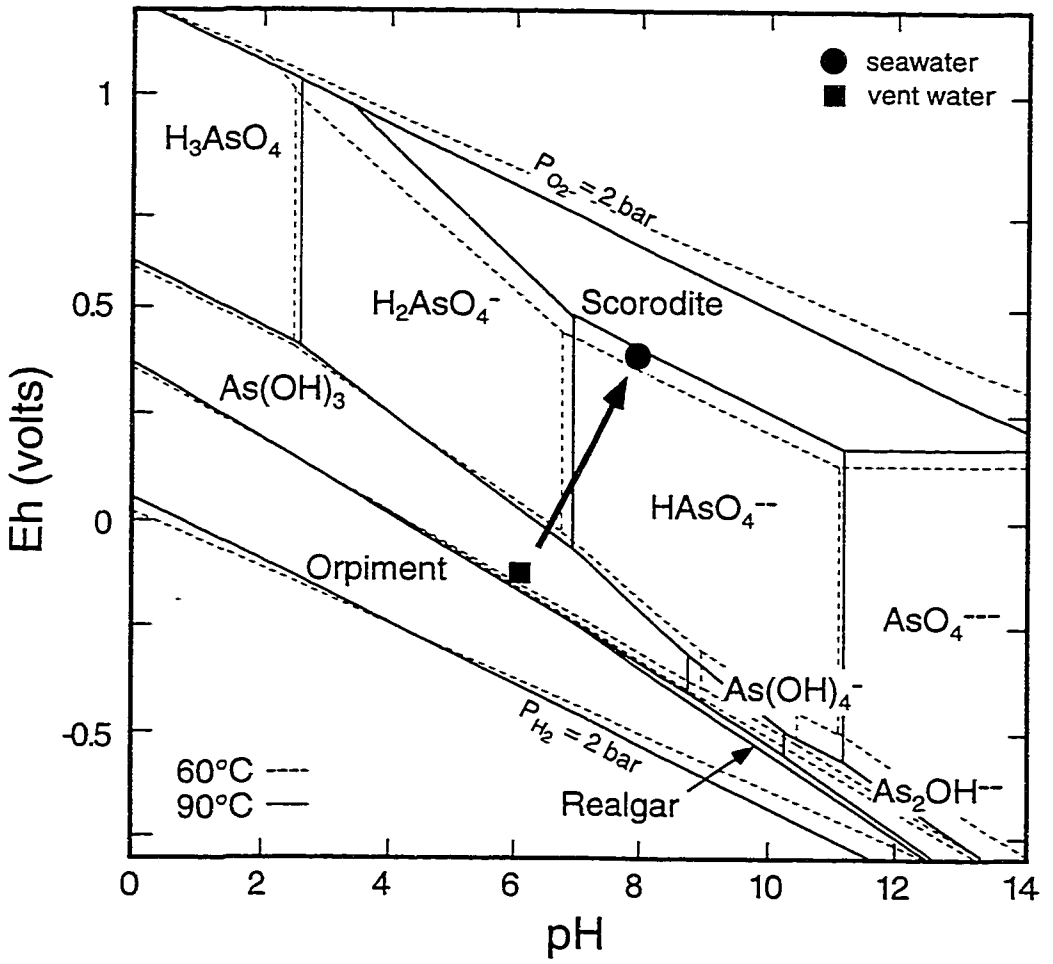

Fig. 4-9 Eh-pH diagram for the system As-Fe-O-H-SO_4-HCO_3 at 60°C (dashed lines) and 90°C (solid lines) at a pressure of 2.026 bars. Activities of As^{3+}, Fe^{2+}, SO_4^{2-} and HCO_3^- are assumed to be 10^{-6}, 10^{-5}, 10^{-3} and 10^{-3}, respectively. Thermodynamic data are from Brookins (1988) and references therein. The arrow indicates the mixing trend between hydrothermal fluid and seawater. At Tutum Bay vent fluid concentrations arsenic remains in solution except for very oxidizing conditions. The conditions necessary for the formation of scorodite, however, cannot be achieved by mixing the hydrothermal fluid with seawater, because respective Fe and As concentrations would be too low.

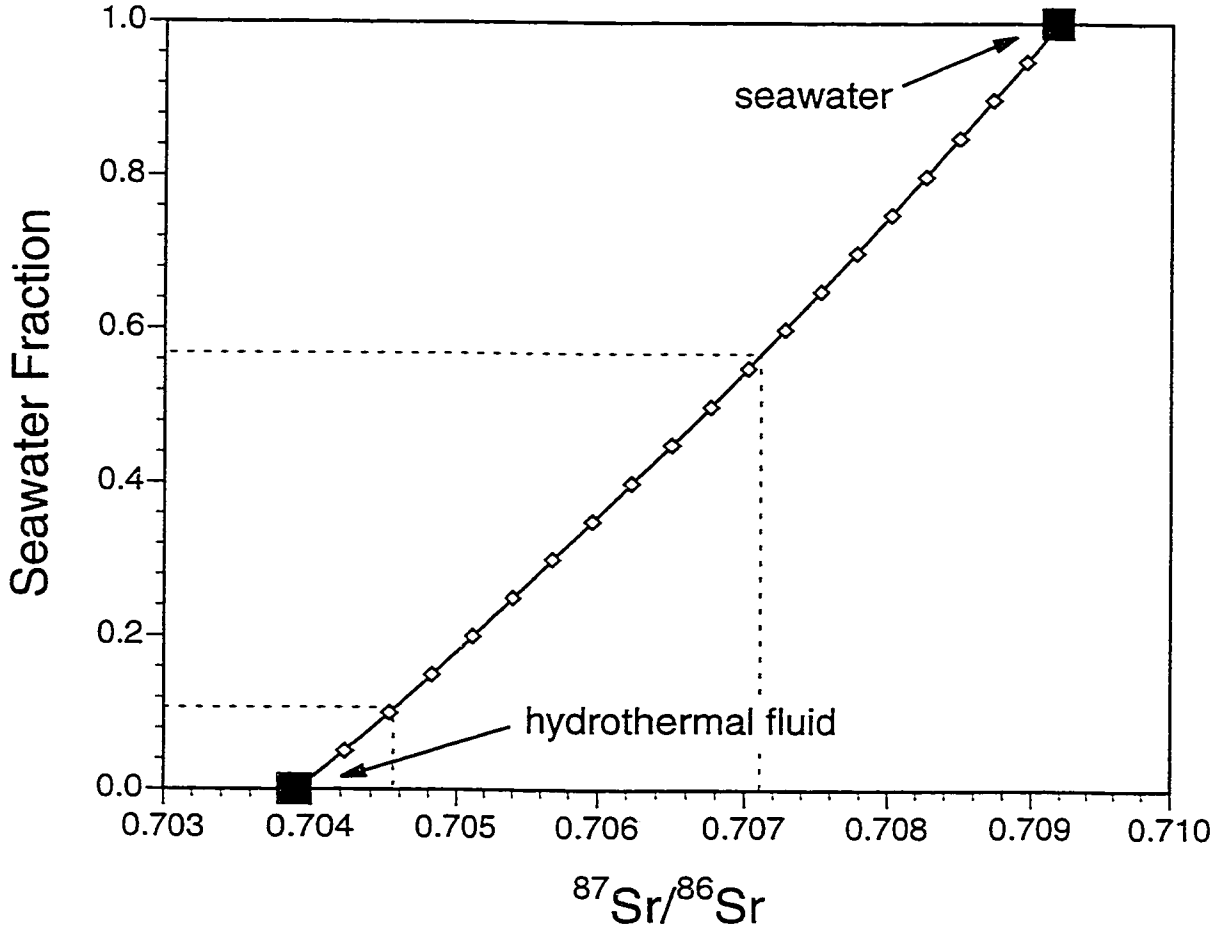

Fig. 4-10 Mixing curve between the hydrothermal fluid and seawater endmember (Table 2-5) based on $^{87}Sr/^{86}Sr$ ratios in Fe(III) oxyhydroxide precipitates. The dashed lines indicate the range of $^{87}Sr/^{86}Sr$ ratios (0.7048 to 0.7071) and the corresponding amount of seawater admixed to the hydrothermal fluid at the time of precipitation.

Bacteria that use the oxidation of Fe^{2+} as an energy source are often involved in the formation of Fe(III) oxyhydroxides (e.g., Churkhov et al., 1973; Fortin et al., 1993; Leblanc et al., 1996). The active participation of bacteria in the precipitation of Tutum Bay Fe(III) oxyhydroxides could neither be confirmed nor disproved. Several rounded to subrounded Fe and Si-rich bodies, approximately 1μm across, were observed by electron microscopy. Transmission electron microscopic (TEM) analyses, however, did not conclusively confirm the presence of bacteria although rounded shapes were observed that could be the mineralized remnants of bacteria (D. Fortin, 1997 pers. comm.).

The very fine grain size and colloidal origin of Fe(III) oxyhydroxide phases is reflected in their amorphous nature. However, once precipitated, aging will increase the crystallinity and generally lead to the formation of either hematite (e.g., Churkhov et al., 1973) or goethite (e.g., Schwertmann and Fischer, 1973). Older seafloor deposits consist almost exclusively of goethite with contents up to 88% (Hein et al., 1994).

The presence of goethite was not confirmed for Tutum Bay Fe(III) oxyhydroxide deposits (Figs. 4-2 and 4-3). The degree of crystallinity as deduced form XRD analyses, however, seems to be directly related to a) relative age of the precipitate and b) exposure to seawater. Samples FV-1A and V-2 I, thought to be older than V-1B, V-2 (97) and V-4.1D, clearly show the more complex XRD patterns. These two samples are the outer layers of their respective Fe(III) oxyhydroxide deposits and were exposed to a mixture of seawater and hydrothermal fluid (seawater >> hydrothermal fluid) at the time of sampling. The two samples, FV-1B and V-2 II, collected from layers just beneath FV-1A and V-2 I, were not directly exposed to seawater and contain only protoferrihydrite.

Rapid precipitation is a process often called upon to explain the amorphous nature of Fe(III) oxyhydroxide precipitates (e.g., Chao and Theobald, 1976; Hekinian et al., 1993). The relatively high silica concentration in Tutum Bay vent fluids may play an additional role. Freshly precipitated Fe(III) oxyhydroxide react very strongly with silicate compounds, thus preventing further crystallization (Schwertmann, 1966; Schwertmann, 1970). Puteanus et al.

(1991) also suggested the presence of an X-ray amorphous nontronite due to rapid precipitation. Nontronite is the first crystalline phase to form up in Tutum Bay Fe(III) oxyhydroxides and its presence in the outer layer of sample V-2 (97) indicates that formation in contact with seawater takes less than six months following precipitation of the Fe(III) oxyhydroxide. Nontronite is a common secondary mineral in many submarine hydrothermal metalliferous deposits (e.g., Bischoff, 1969; McMurtry and Yeh, 1981; Murnane and Clague, 1983) and/or a product of ocean floor weathering of volcanic rocks (e.g., Alt, 1993; Gallahan and Duncan, 1994; Rad et al., 1990; Stakes and Scheidegger, 1981). Puteanus et al. (1991), who extensively reviewed the existing literature on nontronite, found that the temperature of formation, when determined by oxygen isotope thermometry was relatively low (3 - 57°C). These low temperatures are in good agreement with temperatures inferred for its formation in Tutum Bay, based on the assumption that nontronite there forms due to interaction between Fe(III) oxyhydroxide and seawater and/or a very dilute hydrothermal fluid.

The next crystalline phase to appear in Tutum Bay Fe(III) oxyhydroxide deposits is claudetite (As_2O_3), a trivalent arsenic oxide. Claudetite is stable only at extremely high arsenic concentrations ($[As^{3+}] > 10^{-0.8}$ at 25°C) (Fig. 4-11) which were not present at the time of precipitation of the Fe(III) oxyhydroxide (Fig. 4-9). Arsenic compounds are generally soluble and as a result, post depositional interaction with seawater or very dilute hydrothermal fluid should cause the formation of claudetite via dissolution and re-crystallization. This process is imagined to be analogous to the formation of goethite and/or hematite from amorphous Fe(III) oxyhydroxide (e.g., Churkhov et al., 1973; Schwertmann and Fischer, 1973). Under a remaining high $[As^{3+}]$ and increasing oxidizing conditions, claudetite is slowly transformed into pentavalent arsenic oxide (As_2O_5) and scorodite (Fig. 4-11) that are the next minerals to appear in the XRD pattern of sample FV-1A (Fig. 4-2b). The formation of gypsum, which is also present in sample FV-1A, is thought to be caused by interaction between seawater-derived SO_4^{2-} and Ca^{2+} released from Fe(III) oxyhydroxide surfaces.

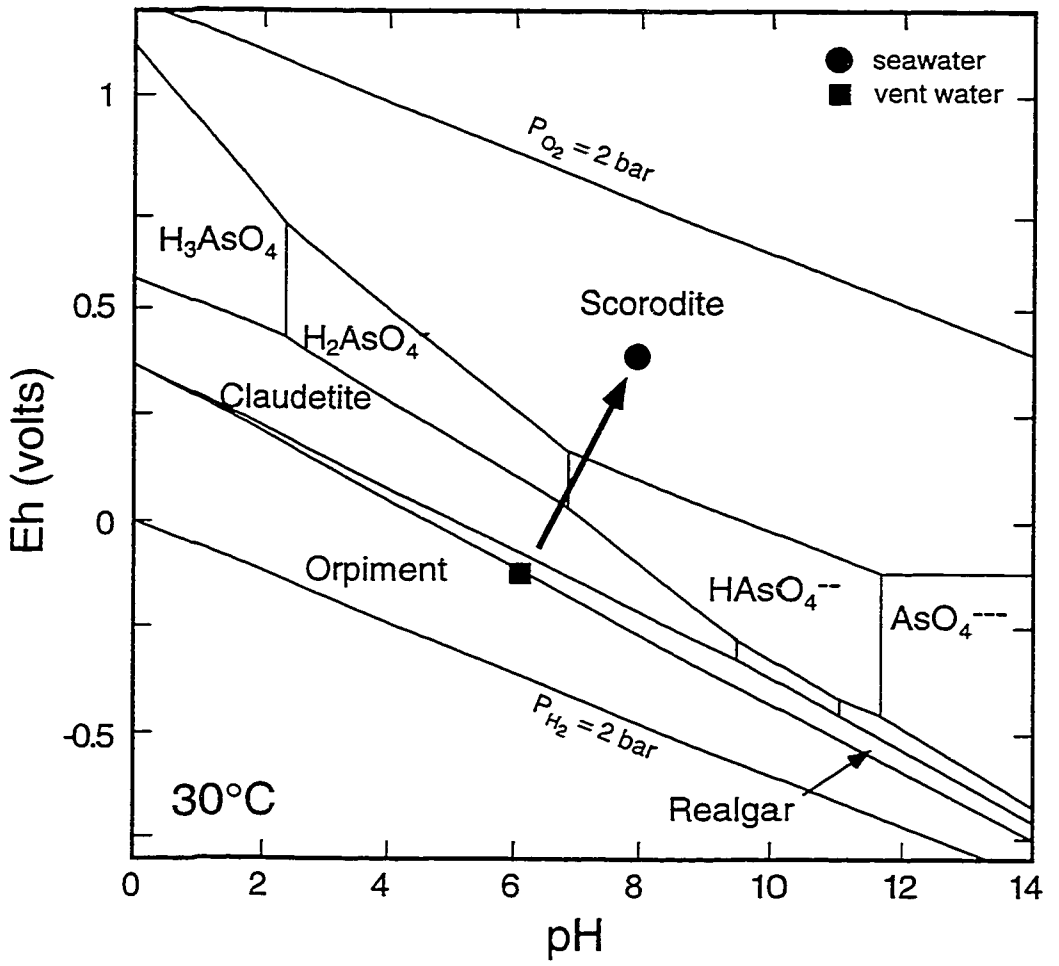

Fig. 4-11 Eh-pH diagram for the system As-Fe-O-H-SO_4-HCO_3 at 30°C (ambient seawater temperature) at a pressure of 2.026 bars and very high As concentration. Activities of As^{3+}, Fe^{2+}, SO_4^{2-} and HCO_3^- are assumed to be $10^{-0.8}$, 10^{-5}, 10^{-3} and 10^{-3}, respectively. Thermodynamic data are from Brookins (1988) and references therein. At such high activity of As, the stability field for $As(OH)_3$ is replaced by claudetite and the field for scorodite increases drastically.

Recrystallization of an amorphous material drastically reduces the specific surface area and, therefore, its capacity to adsorb ions, which is closely related to specific surface area (e.g., Morgan and Stumm, 1964).

4.4.1 The chemical composition of Tutum Bay Fe(III) oxyhydroxide deposits

Scavenging of elements into and onto metal hydroxides results from: 1) coprecipitation, 2) adsorption, 3) surface complex formation, 4) ion exchange, and 5) penetration of the crystal lattice (Chao and Theobald, 1976), but in natural systems it is often impossible to distinguish between coprecipitation and adsorption (Drever, 1982). Adsorption, however, has been observed to be the basis of most surface-chemical reactions (Stumm and Morgan, 1996), making it the most likely cause for the minor and trace element composition in Tutum Bay Fe(III) oxyhydroxides. With the exception of arsenic, trace element concentrations are low and reflect their low concentrations in the hydrothermal fluid (Tables 2-3 and 4-2). Little information exists regarding the intensity of scavenging of elements other than the heavy or ore metals, except that many metals that form strong OH-complexes in water also bind strongly to hydroxide surfaces (Dzombak and Morel, 1990). This is confirmed in Tutum Bay Fe(III) oxyhydroxide deposits where trace metals that form stronger OH-complexes are generally enriched when compared to the alkali elements K, Rb and Cs that form weaker OH-complexes. The Rb/Sb ratio, for example, is 44 in the vent fluid from vent 1 (Table 2-2) and only 0.023 in the corresponding Fe(III) oxyhydroxide sample (V-1B, Table 4-2).

The extent of mixing with seawater during precipitation, as determined by the $^{87}Sr/^{86}Sr$ mixing model, is to some extent also imprinted in the trace element signature of Fe(III) oxyhydroxide, in particular for elements that possess a substantial concentration difference between seawater and hydrothermal fluid. This is evident in the two samples V-1 and FV-1 that were collected at the same vent but from different locations, and experienced therefore different mixing conditions. Sample V-1B, a thin layer coating volcanic boulders adjacent to the orifice

(Fig. 4-1a), has a higher $^{87}Sr/^{86}Sr$ ratio (i.e., higher seawater) and lower concentrations of Cs, Rb, Sb and Tl than FV-1B, a massive layer from within the vent orifice.

Rare earth elements are known to be very effectively scavenged by Fe(III) oxyhydroxides (Koeppenkastrop and De Carlo, 1992; Koeppenkastrop et al., 1991) and as a result Tutum Bay deposits are enriched relative to the hydrothermal fluid by approximately 10^5. Unlike for hydrogenetic Fe and Mn-rich deposits whose pattern geometry is controlled by seawater (e.g., Fleet, 1984), Tutum Bay Fe(III) oxyhydroxide REE concentrations are controlled exclusively by the hydrothermal fluid (Fig. 4-6). In seawater, REEs are undersaturated but can be removed in trace amounts by both inorganic and organic processes and low-temperature alteration. The preferential uptake of light REEs in hydrogenetic Fe and Mn-rich oxyhydroxides is due to the fact that heavy REEs form stronger carbonate complexes in seawater (Lee and Bryne, 1993). The positive Ce anomaly that is generally present in hydrogenetic Fe-rich crusts, contrasts with the negative Ce anomaly in seawater and in Tutum Bay Fe(III) oxyhydroxides (Fig. 4-6). Goldberg (1961) proposed that Ce^{3+} in the ocean is oxidized to Ce^{4+} and precipitated as CeO_2 while the other REEs remain in their trivalent state. In addition, Ce forms colloidal ceric hydroxide (Carpenter and Grant, 1967) which may be scavenged by Fe/Mn-oxyhydroxides.

The ΣREE, although enriched by approximately 10^5 over their concentration in vent fluids, is still relatively low when compared to that in hydrogenetic deposits (Fleet, 1984). Olivarez and Owen (1989) found that the REE/Fe ratio in hydrothermal sediments increases with distance from the ridge axis, i.e., vent site, and argued that REE uptake from seawater is the cause. According to their ideas, low REE/Fe ratios would indicate rapid precipitation, thus preventing adsorption of seawater derived REE, whereas high REE/Fe ratios indicate extended contact with seawater, i.e., low precipitation rate (cf. Stoffers et al., 1993). The high precipitation rates and low REE/Fe ratios observed in Tutum Bay are in general accord with this proposition, but it has to be noted that this model is only valid for a restricted time period. Its validity is compromised once Fe(III) oxyhydroxides start to recrystallize due to extended

contact with seawater. At that time REEs are released from the Fe(III) oxyhydroxide material due to the decrease in specific surface (i.e., adsorption capacity). This is illustrated by the lower ΣREE in the most crystalline sample, FV-1A, when compared to samples FV-1B and V-1B (Fig. 4-6).

4.4.2 The special nature of arsenic in Tutum Bay Fe(III) oxyhydroxides

The oxidation, speciation and solubility of arsenic compounds are largely controlled by inorganic processes (e.g., O'Neill, 1990). Some microbial oxidation, however, is possible despite the fact that arsenic is lethal to most microorganisms (Ahmann et al., 1994; Baldi, 1994; Leblanc et al., 1996). Arsenic compounds exhibit a strong affinity towards adsorption onto and/or coprecipitation with iron hydroxides. The extremely high arsenic concentration in Tutum Bay Fe(III) oxyhydroxides suggests that some may be structurally bound within Fe-oxide, similar to the mineral, schwertmannite, where SO_4^{2-} substitutes for iron. The adsorption of As onto iron hydroxides is controlled by the specific surface area of the adsorbent, which in turn is directly related to its mineralogy, and decreases in the order ferrihydrite > goethite > lepidocrocite > hematite (Bowell, 1994). Several experimental studies have found that adsorption at standard conditions (temperature = 25°C and pressure = 1 bar) is generally rapid and strongest at a pH of approximately 6-7 (e.g., Bowell, 1994; Manning and Goldberg, 1997; Pierce and Moore, 1980). Comparing these experimental conditions with those present in Tutum Bay it is not surprising that there As concentrations are exceedingly high in Fe(III) oxyhydroxides. The strong pH affinity would also explain the relatively low As concentration in deep sea Fe(III) oxyhydroxide deposits (Fig. 4-5). Most deep-sea deposits are thought to precipitate from hydrothermal solutions with a significantly lower pH than Tutum Bay vent fluids (Cremer, 1995). Mixing between seawater and hydrothermal fluid, therefore, would have to be extremely high in order to reach a pH favorable of extensive As adsorption. This

should cause a low As concentration in the mixture because of its low concentration in seawater.

The concentration of arsenic in Tutum Bay Fe(III) oxyhydroxide deposits is actually so high that it cannot be considered a trace element. Following Fe and Si, As is the third most abundant element and its concentration is the highest reported from any marine setting, illustrating the special nature of the Tutum Bay hydrothermal system. Arsenic concentrations in Tutum Bay vent fluids are also the highest reported from a submarine setting (Von Damm, 1995). This clearly sets Tutum Bay apart from deep sea hydrothermal systems and underlines its close relationship to onland hydrothermal systems. In onland systems As is a common constituent in hydrothermal fluids and hydrothermal precipitates, with concentrations in silica sinters of up to 88,000 ppm (Seward and Sheppard, 1986).

The highest As concentrations, however, are found in Fe(III) oxyhydroxide deposits in stream beds and/or soils associated with mine drainage, where concentrations of up to 120,000 ppm have been reported (Leblanc et al., 1996). The strong affinity between Fe(III) oxyhydroxides and As is a blessing in such an environment because As is readily removed from solution and stored. If Fe(III) oxyhydroxide deposition takes place in streams, the concentration of As in solution decreases exponentially with near removal after a few kilometers downstream from the point of contamination (Davis et al., 1989; Leblanc et al., 1996). In Tutum Bay, Fe(III) oxyhydroxide also seems to reduce successfully the input of As into seawater, thus preventing the certain collapse of the surrounding coral reef ecosystem. Compared to the situation onland, arsenic removal in Tutum Bay seems to be perpetual because there the conditions remain oxidizing at all times due to continuous flushing and renewal of seawater. In onland settings, in particular in soils and small streams, reducing conditions are common and promote the stability of As(III) in place of As(V). This leads to lower sorption (retention) and greater leaching of arsenic (e.g., Bowell, 1994). Additional transformation of As(III) to As(V) under slightly reducing conditions can be achieved by bacterial mediation. Ahmann et al. (1994) reported the discovery of a microorganism that gains energy for growth

from reduction of As(III) to As(V) in the absence of oxygen. Reducing conditions during aging of the Fe(III) oxyhydroxide precipitate may also prevent the formation of a discrete As-mineral if the activity of arsenic is insufficient (Figs. 4-9 and 4-11) and, as a result, arsenic is released into solution.

4.5 GEOLOGICAL IMPLICATIONS

Massive sulfides and Fe(III) oxyhydroxides are the principal seafloor deposits associated with hydrothermal activity. Except for a few intra-plate locations, massive sulfides are usually found in deep water, high temperature hydrothermal systems along mid-ocean ridges. Fe(III) oxyhydroxides, on the other hand, are the prominent intra-plate deposits that form in shallow water, low temperature hydrothermal systems in seamount and island-arc environments. Several models have been proposed to explain their formation. All models agree that mixing with seawater is the final step that causes precipitation, although they differ to some degree in explaining the history of the hydrothermal fluid. Rona (1984) suggested that Fe(III) oxyhydroxide deposits could be either the sole product of a low-intensity hydrothermal system or the extremely fractionated endmember phase of a high temperature hydrothermal fluid that has precipitated its metals deeper in the volcanic pile (cf. Puteanus et al., 1991). Puteanus et al. (1991) concluded that they are deposited from a hydrothermal fluid that formed by adsorption of magmatic vapors into seawater. They write: "Initially, magmatic vapors migrating upwards through the hot spot volcano are thought to be absorbed into seawater at comparatively shallow levels to deposit sulfide minerals within the volcanic pile. The Fe oxyhydroxide deposits are the residual low-temperature deposits formed when the spent hydrothermal fluid reached the crest of the seamount". The proposed mechanism for sulfide precipitation is the exsolution of H_2S and CO_2 from the hydrothermal fluid. The problem with this model is that while the mechanism of precipitation is a valid assumption and a process often called upon in the

formation of ore deposits, it also removes most of the Fe^{2+} from solution. The associated increase in pH and drop in temperature, furthermore, hinders the capacity of the hydrothermal fluid to carry substantial amounts of Fe^{2+}. Stoffers et al. (1993) called upon adiabatic boiling as a mechanism to remove the sulfide phase from the hydrothermal fluid and, therefore, separate Fe(III) oxyhydroxides. Boiling is an important process in hydrothermal systems where it controls several physico-chemical parameters and separates a hydrothermal solution into a low chlorinity, vapor phase and a high chlorinity liquid phase (e.g., Butterfield et al., 1990; Delaney and Cosens, 1982; Drummond and Ohmoto, 1985; Seward, 1989; Simmons and Christenson, 1994; Truesdell et al., 1977). Again, boiling compromises the capacity of the hydrothermal fluid to carry substantial amounts of Fe^{2+}.

The Fe(III) oxyhydroxide deposition in Tutum Bay sheds light onto some of the problems noted above. Ambitle Island is in several ways analogous to a seamount with the exception that it is not completely submerged, although its greater part is under water and during its history it may have been longer a seamount than an island. The hydrothermal system here clearly demonstrates the separation into sulfide mineralization, deposited at depth (Licence et al., 1987) and Fe(III) oxyhydroxide mineralization, deposited at the surface. The model that explains the generation of Tutum Bay hydrothermal fluids can also account for elevated iron concentrations necessary for the precipitation of Fe(III) oxyhydroxides and it seems that the absence of sulfur is one of the main factors that would promote the precipitation of a hydroxide phase at the expense of a sulfide mineral.

4.5.1 A short note about mineral exploration

Island arcs, such as the Tabar-Feni arc, are favorable environments for the formation of epithermal ore deposits (e.g., Müller and Groves, 1993; Pichler and Hutchinson, 1993), and identification of anomalous chemical signatures in Fe(III) oxyhydroxides may be used to explore for paleo-hydrothermal systems in ancient island-arc settings. In particular, the

anomalous arsenic concentrations in Tutum Bay Fe(III) oxyhydroxides would be of great interest if found during a geochemical exploration program. Anomalous arsenic concentrations have been linked to more than 20 economically important elements (Boyle and Jonasson, 1973), including the precious metals, Au, Ag and Pt. The definite role of arsenic in the ore forming process is unclear (Parker and Nicholson, 1990), nevertheless the work of Berger and Silberman (1985) and Silberman and Berger (1985) clearly documents its utility as a tracer in delineating areas of epithermal gold mineralization.

4.6 SUMMARY AND CONCLUSIONS

With the exception of the unusually high arsenic values, Tutum Bay Fe(III) oxyhydroxide deposits are in many respects similar to deposits found in much deeper water. Their hydrothermal origin is suggested by a combination of field observations, chemical and mineralogical analyses. Precipitation from the hydrothermal fluid is due to mixing with seawater. Mixing simultaneously increases the pH and Eh, and decreases temperature, all of which favor the precipitation of a Fe(III) oxyhydroxide. Based on measurements of $^{87}Sr/^{86}Sr$ ratios in Fe(III) oxyhydroxide and seawater, precipitation temperatures have been estimated to be between approximately 60 and 90°C. This temperature range is also in good agreement with previous studies of Fe(III) oxyhydroxide precipitation.

Rapid precipitation and subsequent aging, in contact with seawater and/or a mixture of seawater and hydrothermal fluid (seawater >> hydrothermal fluid), is the cause for the observed mineralogy. Rapid precipitation causes protoferrihydrite to be the main mineral phase in Tutum Bay Fe(III) oxyhydroxides. With increasing age and under oxidizing conditions nontronite, gypsum and various As-minerals are formed.

Rare earth element patterns of Fe(III) oxyhydroxides are closely controlled by the hydrothermal fluid and incorporation is without a noticeable fractionation. The absolute

concentration of REEs and selected trace elements (Rb, Tl, Sb and Cs) seems to be controlled by the extend of seawater mixing, as determined by the $^{87}Sr/^{86}Sr$ mixing model.

Arsenic concentrations in Tutum Bay Fe(III) oxyhydroxides are by more than an order of magnitude higher than those from other marine occurrences. The high concentrations are a direct result of the strong sorption ability of the high specific surface material, protoferrihydrite, at a pH of approximately 7 and at sufficient arsenic concentration in the hydrothermal fluid. Arsenic is successfully retained in the Fe(III) oxyhydroxide deposits because oxidizing conditions and high arsenic concentration allow for the formation of discrete arsenic minerals, such as claudetite, arsenic oxide and scorodite.

5. CHANGES IN PHYSICO-CHEMICAL CONDITIONS

The purpose of this short chapter is to qualitatively assess and document the impressive changes in physico-chemical conditions that lead to the distinct mineralogical and chemical zonation in Tutum Bay hydrothermal deposits. Four distinct mineral phases were observed: 1) coarse crystalline aragonite, 2) micro-crystalline aragonite, 3) ferroan calcite, and 4) Fe(III) oxyhydroxide. While they generally occur in the succession coarse aragonite, micro-crystalline aragonite followed by ferroan calcite and Fe(III) oxyhydroxide, other successions have also been observed. In Fig. 5-1 a short period of Fe(III) oxyhydroxide deposition is followed by deposition of micro-crystalline aragonite and again Fe(III) oxyhydroxide. Ferroan calcite is absent in this sequence. The transition between the carbonate and Fe(III) oxyhydroxide phases is sharp and considering an accumulation rate of approximately 1 cm/year, the period of Fe(III) oxyhydroxide deposition may have been as short as 7-8 days.

A direct transition from large pseudo-hexagonal aragonite crystals to Fe(III) oxyhydroxide is documented in Fig. 5-2. This transition is extraordinary in the sense that it happened without the formation of a layer of microcrystalline aragonite, as generally observed (Fig. 3-3). The transition must have been abrupt and quite fast because the crystal faces of the aragonite are still smooth and do not show dissolution or recrystallization features. The relatively thin layer of material indicates a relatively short period of Fe(III) oxyhydroxide accumulation. The sequence of precipitation continues with a layer comprised of a mixture of Fe(III) oxyhydroxide, aragonite and ferroan calcite, the last one followed by a layer of Fe(III) oxyhydroxide and terminated by a layer of aragonite (Sequence a, b, c, d, e in Fig. 5-2b).

A similar sequence is displayed in Fig. 5-3a, a backscatter electron image of a thin section from the same sample. The backscatter electron imaging technique uses the intensity of backscatter electrons to create an image based on density differences: the heavier a mineral or material the brighter its color. Going from right to left the precipitation sequence displayed in Fig. 5-3a is ferroan calcite, Fe(III) oxyhydroxide (Layer A), ferroan calcite and Fe(III)

Fig. 5-1 (a) Stereo microscope photo micrograph of alternating layers of aragonite and Fe(III) oxyhydroxide in sample 4.1 (see also Fig. 3-2). The mineralogical succession is as follows: 1) coarse crystalline aragonite (gray), 2) micro-crystalline aragonite (white), 3) Fe(III) oxyhydroxide (red-brown), 4) micro-crystalline aragonite (white), 5) Fe(III) oxyhydroxide. The scale bar represents 5 mm. (b) Transmitted light photomicrograph of the distinct Fe(III) oxyhydroxide band in micro-crystalline aragonite (see above). Direction of crystal growth is from bottom to top. The Fe(III) oxyhydroxide levels the somewhat jagged crystal ends of the aragonite. Some staining and replacement is evident just below the Fe(III) oxyhydroxide layer. The scale bar represents 200 μm.


a

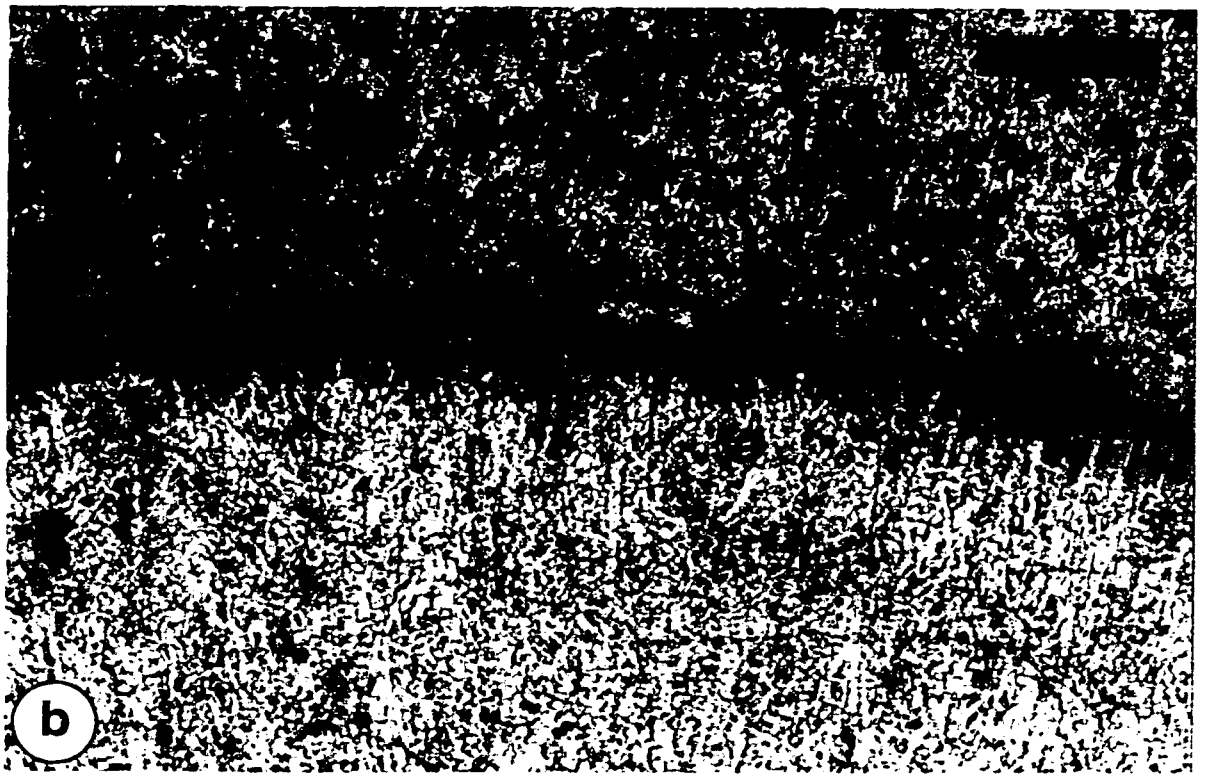
b

Fig. 5-2 (a) Scanning electron microscope secondary electron image of several large pseudo-hexagonal aragonite crystals that are completely covered by later generations of fine grained aragonite and Fe(III) oxyhydroxide. Part of the cover broke lose and exposed the larger pseudo-hexagonal crystal. (b) Magnified image of the rectangular area indicated above. The mineralogical succession is as follows: a) coarse crystalline aragonite, b) Fe(III) oxyhydroxide, c) micro-crystalline aragonite, d) Fe(III) oxyhydroxide and e) micro-crystalline aragonite.

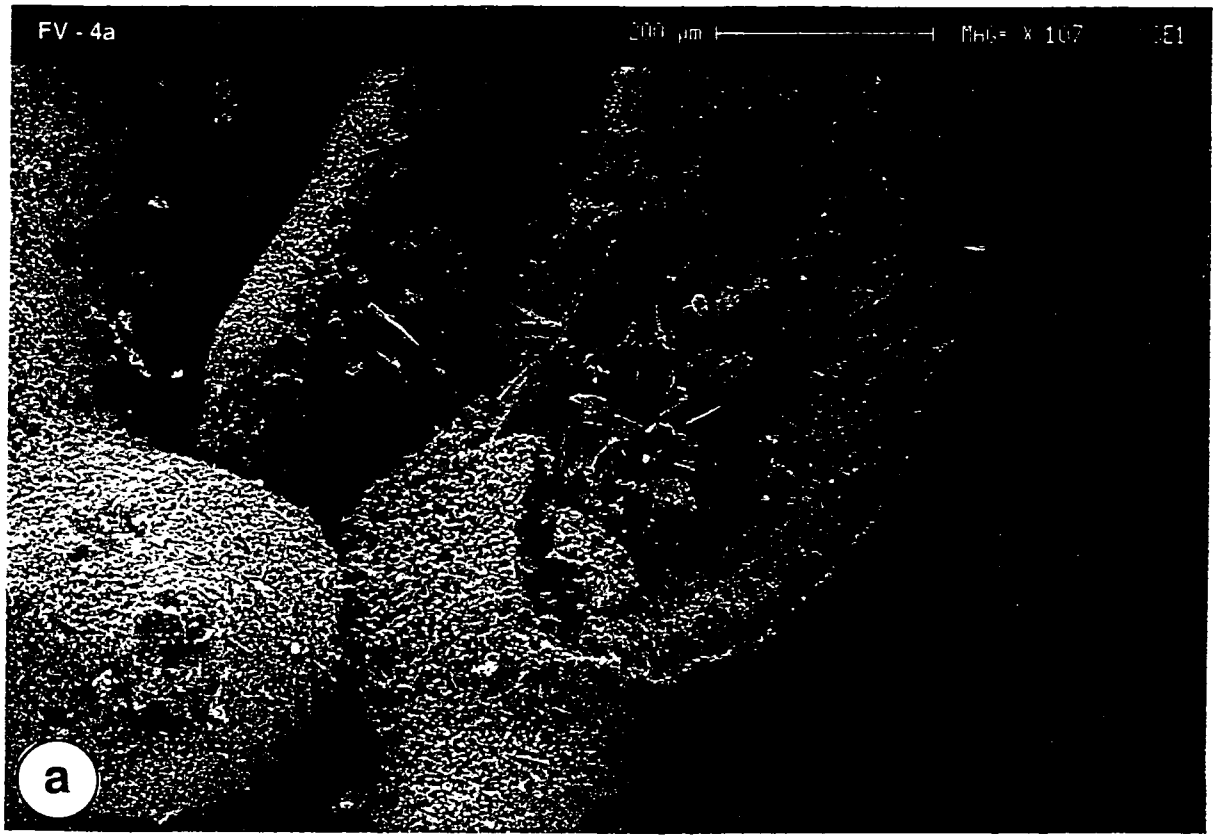
FV - 4a
a

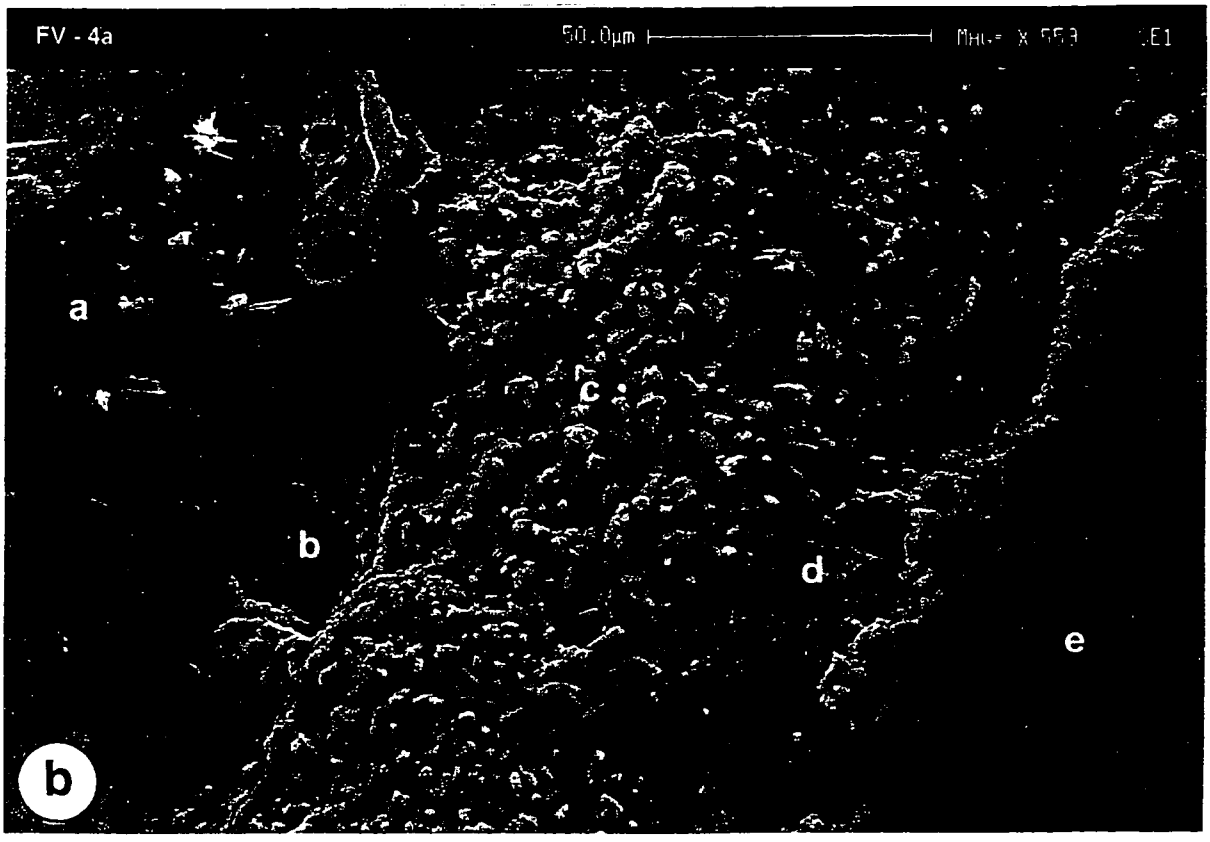
FV - 4a
50.0µm
a
b
c
d
e
b

Fig. 5-3 (a) Scanning electron microscope backscatter electron image of a succession of ferroan calcite (ca) and Fe(III) oxyhydroxide (fe-ox). The direction of mineral accumulation is from the right to the left. Coarse crystalline aragonite is just to the right, outside of the image area. The same area can be seen in transmitted light in Fig. 3-4 (upper arrow). The white circles indicate locations of electron microprobe analyses. (b) Electron microprobe traverse across the succession of Fe(III) oxyhydroxide, ferroan calcite and aragonite (see above). Values for MnO and MgO are multiplied by a factor of 10. Analyses are listed in Table 5-1.

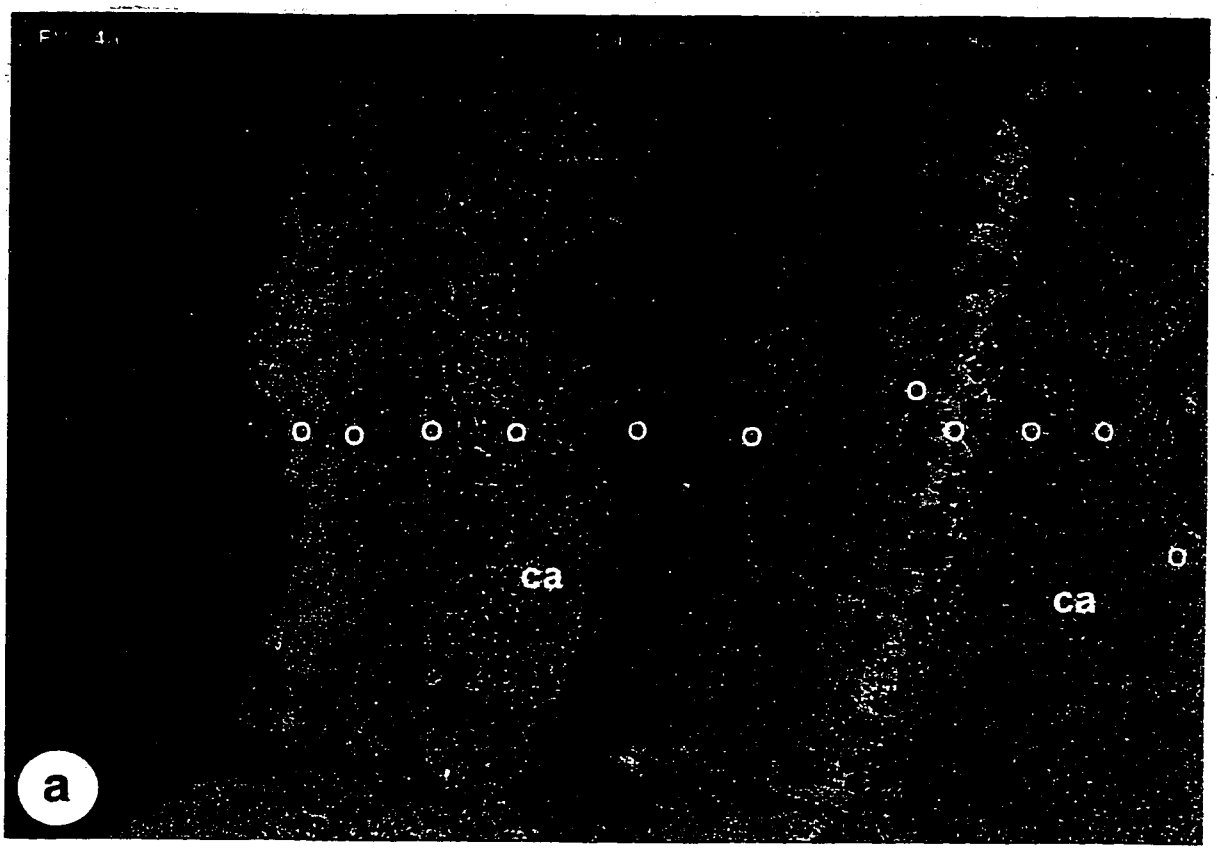
ca
ca
a

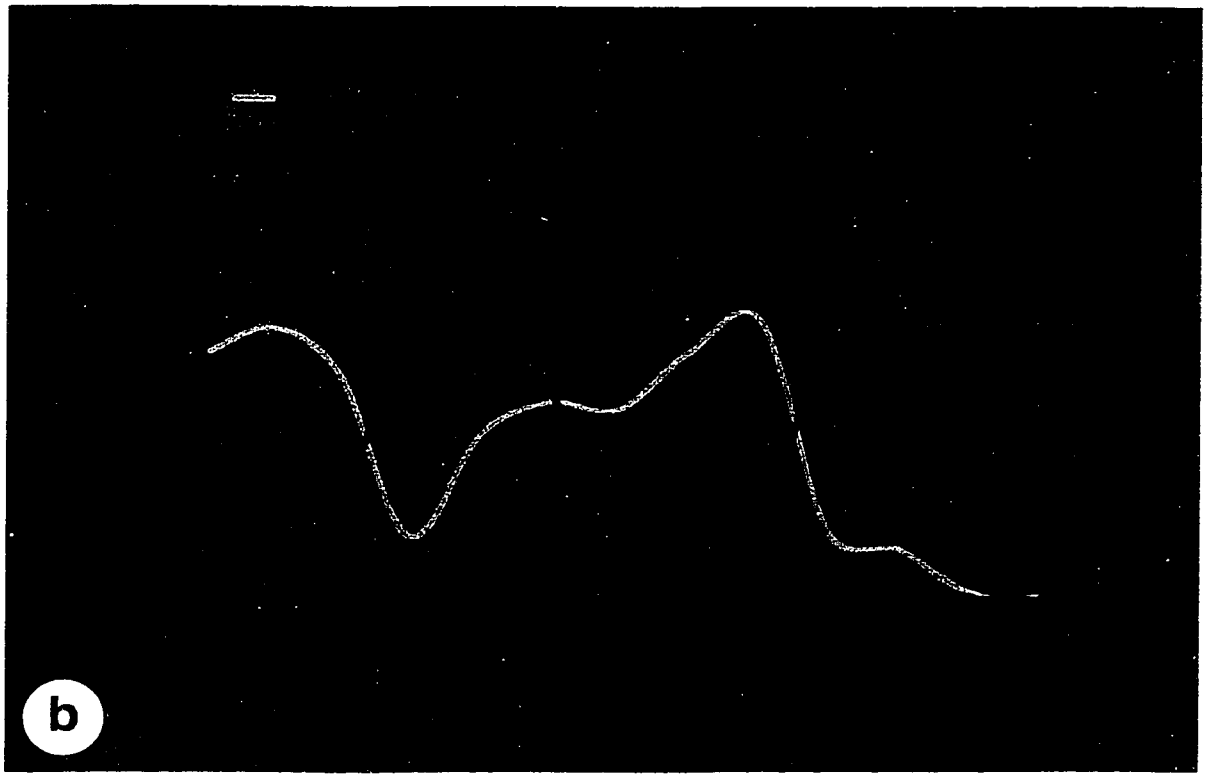
b

TABLE 5-1
MICROPROBE TRAVERSE ACROSS FE(III) OXYHYDROXIDE, FERROAN CALCITE AND ARAGONITE IN SAMPLE FV-4A (FIGS. 3-4 AND 5-3)

No.	Type	CaO	MgO	FeO	MnO	SrO	BaO	ZnO
1	Fe(III) oxyhydroxide	0.46	1.58	27.53	0.02	0.09	0.02	0.29
2	Fe(III) oxyhydroxide	0.36	1.70	30.43	0.21	0.08	0.15	0.00
3	Fe(III) oxyhydroxide	6.59	1.54	24.88	0.81	0.16	0.00	0.47
4	Ferroan calcite	40.89	0.94	6.50	3.56	0.08	0.00	0.00
5	Ferroan calcite & Fe(III) oxyhydroxide	18.82	0.93	18.25	4.19	0.01	0.00	0.00
6	Fe(III) oxyhydroxide	4.53	1.37	22.05	2.37	0.13	0.00	0.00
7	Fe(III) oxyhydroxide	1.22	1.96	21.26	0.70	0.17	0.00	0.00
8	Fe(III) oxyhydroxide	0.45	2.38	27.83	0.19	0.04	0.02	0.22
9	Fe(III) oxyhydroxide	1.02	1.70	31.45	0.33	0.11	0.15	0.08
10	Ferroan calcite	40.77	1.03	7.01	3.31	0.13	0.00	0.06
11	Ferroan calcite	43.83	1.04	5.26	2.23	0.11	0.01	0.07
12	Aragonite	53.41	0.04	0.26	0.20	0.99	0.08	0.06
13	Aragonite	54.50	0.03	0.21	0.05	1.12	0.22	0.16

Note: Analyses performed using a CO_2 routine and reported in wt. %.

oxyhydroxide (Layer B). The shading from light to dark gray in "Layer A" clearly shows the earlier noted lamination present within Fe(III) oxyhydroxides and demonstrates that Fe content is one of the factors responsible. Fe contents are higher in areas of brighter color (Fig. 5-3b and Table 5-1). The microprobe traverse across the Fe(III) oxyhydroxide - carbonate succession also demonstrates the extreme fractionation between Fe and Mn. Ferroan calcite contains more Mn than the Fe(III) oxyhydroxides, which can be explained by changing redox conditions. Ferroan calcite precipitates under slightly reducing conditions and Fe^{2+} and Mn^{2+} are incorporated into its structure substituting for Ca^{2+}. This period is followed by an abrupt change in mineralogy. Conditions must have remained slightly reducing leading to the precipitation of the Fe(III) oxyhydroxide with the highest Fe and lowest Mn concentration (analysis No. 9, Table 5-1). Going to the left within "Layer A", conditions become more and more oxidizing leading to a decrease in Fe and an increase in Mn. The left side of "Layer A" (Fig. 5-3a) most likely represents a hiatus in precipitation. The meandering morphology of the contact between Fe(III) oxyhydroxide and ferroan calcite may indicate a period when redox and venting conditions were in favor of Fe(III) oxyhydroxide dissolution, but not in favor of carbonate precipitation.

The observed changes in mineralogy seem to be a direct response to changes in redox conditions that, in turn, must be closely controlled by the extent of mixing between seawater and hydrothermal fluid. A plot of $^{87}Sr/^{86}Sr$ ratios in aragonite and Fe(III) oxyhydroxides (Fig. 5-4) demonstrates the control of seawater mixing on the observed mineralogy. $^{87}Sr/^{86}Sr$ ratios and, therefore, seawater mixing is always lower for aragonite At more than 11% seawater admixed to the hydrothermal fluid, Fe(III) oxyhydroxide precipitation commences.

If mixing between seawater and hydrothermal fluid is the sole process responsible for the observed mineralogy then the sequence of precipitation would give a clue to changes in the hydrology of the hydrothermal system. A change in discharge rate of the hydrothermal fluid is the only plausible explanation for the observed physico-chemical changes. Without changing

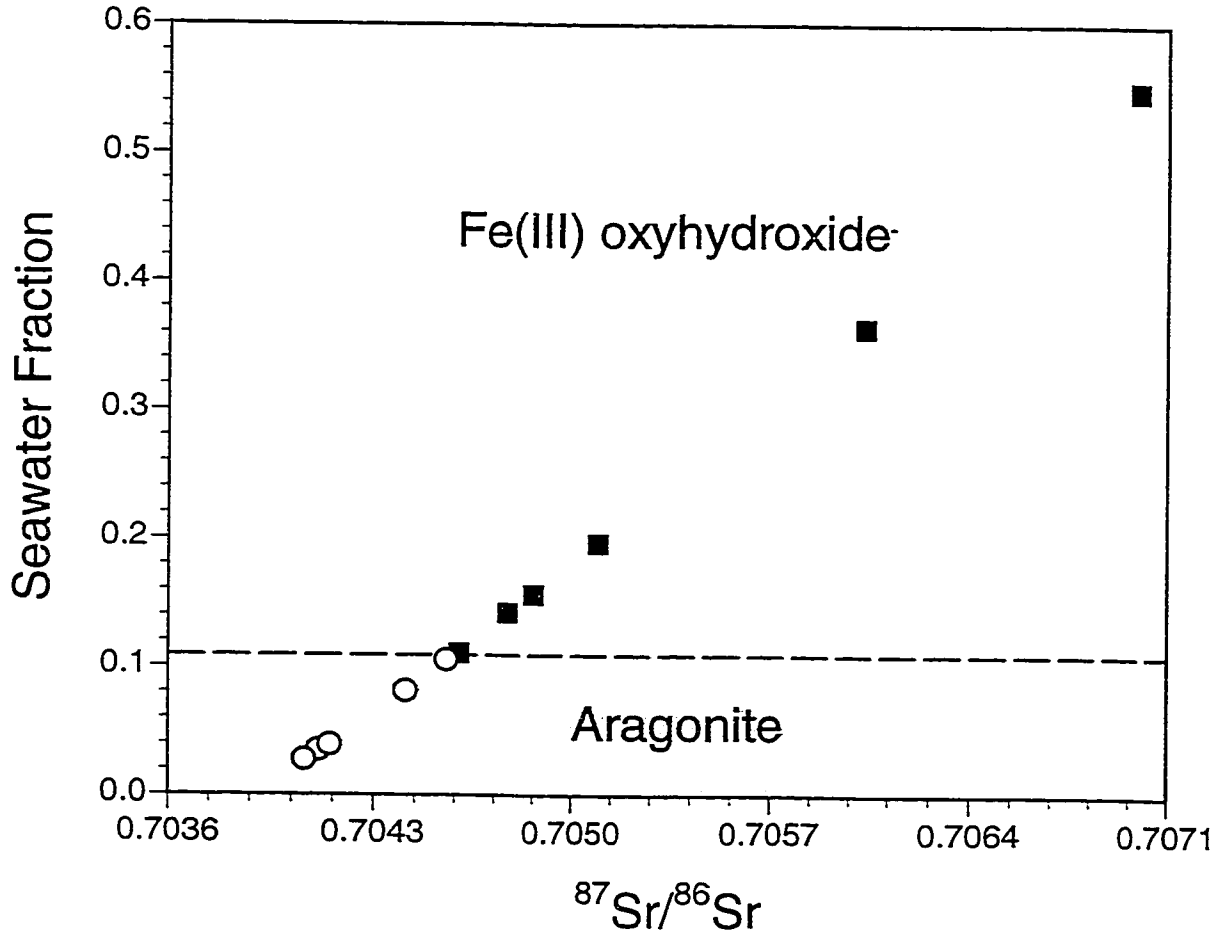

Fig. 5-4 $^{87}Sr/^{86}Sr$ ratios of aragonite (open circles) and Fe(III) oxyhydroxide (filled squares) plotted vs. their respective amount of seawater fraction at the time of precipitation. (cf. Figs. 3-10 and 4-10). The dashed line indicates the boundary between aragonite and Fe(III) oxyhydroxide precipitation. Above 11% seawater addition to the hydrothermal fluid Fe(III) oxyhydroxide precipitates instead of aragonite.

the hydrothermal systems as a whole, supply of groundwater must be the controlling factor to explain a change in discharge rate. Thus extreme changes in local weather conditions may be recorded in Tutum Bay hydrothermal precipitates. Long term monitoring may provide an answer.

6. HYDROTHERMAL FLUID DISSIPATION AND ITS EFFECT ON TUTUM BAY SEAWATER

6.1 INTRODUCTION

In order to investigate the effect of hydrothermal activity on organisms and ambient seawater in Tutum Bay it is necessary to determine the chemical continuity between the hydrothermal fluids and seawater. The discharge from a hydrothermal vent is relatively insignificant when compared to the amount of seawater present in Tutum Bay. Nevertheless, its effect on Tutum Bay seawater is enhanced as a consequence of different chemical composition. This is a process similar to the discharge of industrial emissions from smoke stacks into air. The vertical and horizontal extension of a hydrothermal plume can be mapped by use of hydrographic, optical and chemical tracers, utilizing the difference in chemical composition between plume and seawater.

From studies of hydrothermal plumes over spreading-center axes we know that "black smoker" fluids are rapidly diluted with ambient seawater by factors of 10^4 to 10^5 (Lupton et al., 1985). Subsequently, due to density differences, they generally rise to a level of neutral buoyancy at which they can spread laterally as a distinct hydrographic and chemical layer of up to thousands of kilometers (e.g., Lupton and Craig, 1981).

6.2 ANALYTICAL METHODS, SAMPLING AND RESULTS

Seventy-five (75) seawater samples were collected for chemical analyses throughout the bay at the bottom, in mid water and at the surface at varying distances from vent sites in order to reconstruct the dissipation of the hydrothermal plume and its influence on the seawater composition in Tutum Bay. Samples were taken through a Nalgene® tube that was lowered

from the surface to the depth of sampling. In order to avoid contamination several tube volumes were discarded before taking the actual sample. Horizontal distance from vent sites was determined with ropes and buoys. At the time of sampling no water movement (current) other than that caused by the hydrothermal vents themselves was observed. These samples were filtered to $< 0.45\mu m$ and acidified with ultrapure HNO_3 for later laboratory analyses and stored in high density polyethylene bottles. Si was analyzed by ICP-ES and results are listed in Appendix 1.

Throughout the sampling period several samples of de-ionized water were treated in the same way as the vent samples, i.e., filtered, acidified and filled into high density polyethylene bottles. These samples were later analyzed together with the vent samples in order to check for possible contamination.

The contour maps of the hydrothermal component concentration in Tutum Bay seawater (Figs. 6-1 and 6-2) were constructed using silica as a tracer and assuming conservative behavior and linear mixing. Relative to seawater, silica showed the highest concentration in the hydrothermal fluids (Table 2-5). The hydrothermal component in Tutum Bay seawater was calculated using a simple mass balance equation:

$$C_{TBW} = x\, C_{SW} + y\, C_{HF} \qquad [6\text{-}1]$$

where C_{TBW} is the silica concentration in Tutum Bay seawater, C_{SW} the silica concentration in reference seawater and C_{HF} the silica concentration in the hydrothermal fluid. The contour maps (Figs 6-1 and 6-2) were generated using the computer program Surfer® by Golden Software and kriging was used for interpolation between and extrapolation from data points (Bardossy and Bardossy, 1984).

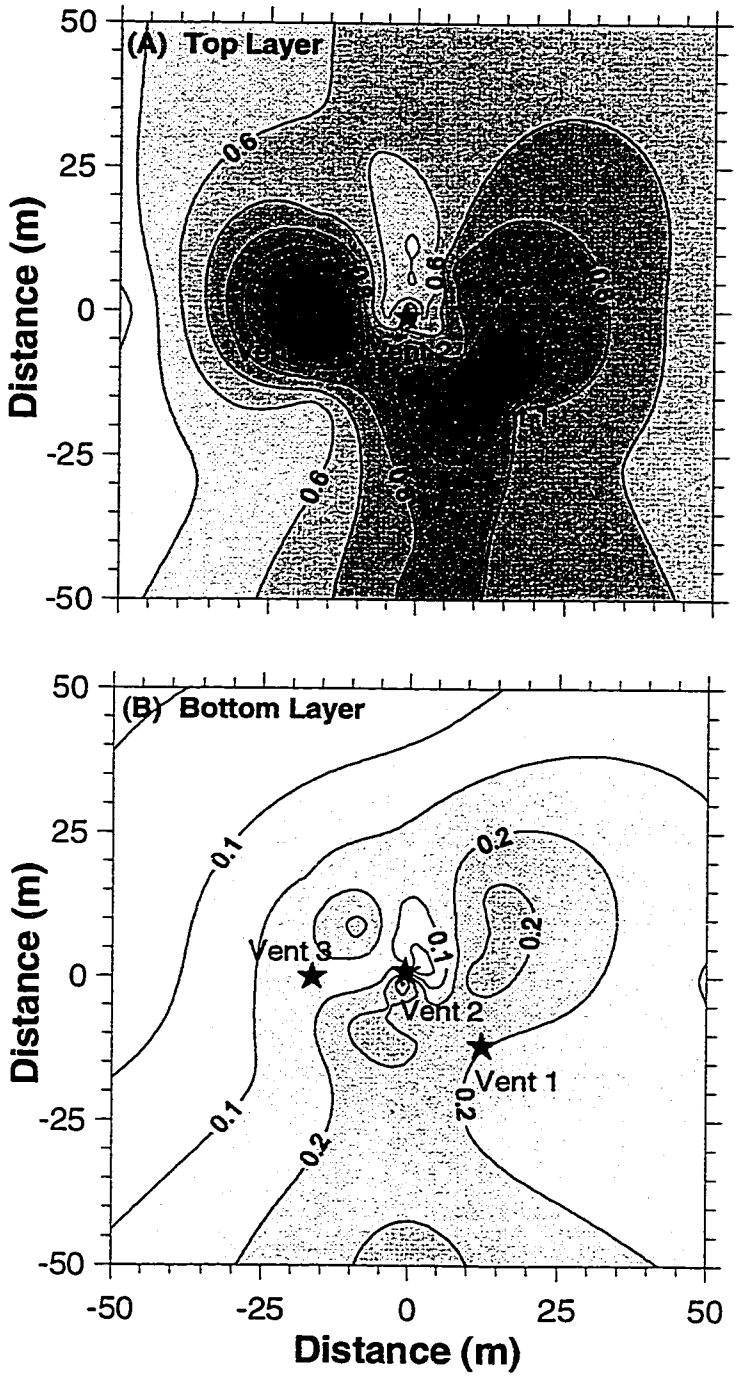

Fig. 6-1 Model of hydrothermal component in (A) surface and (B) bottom water in Tutum Bay in %. The darker colors indicate higher hydrothermal component. The letters E (east), W (west), N (north) and S (south) in (A) indicate the location of the two crossection models in Fig. 6-2.

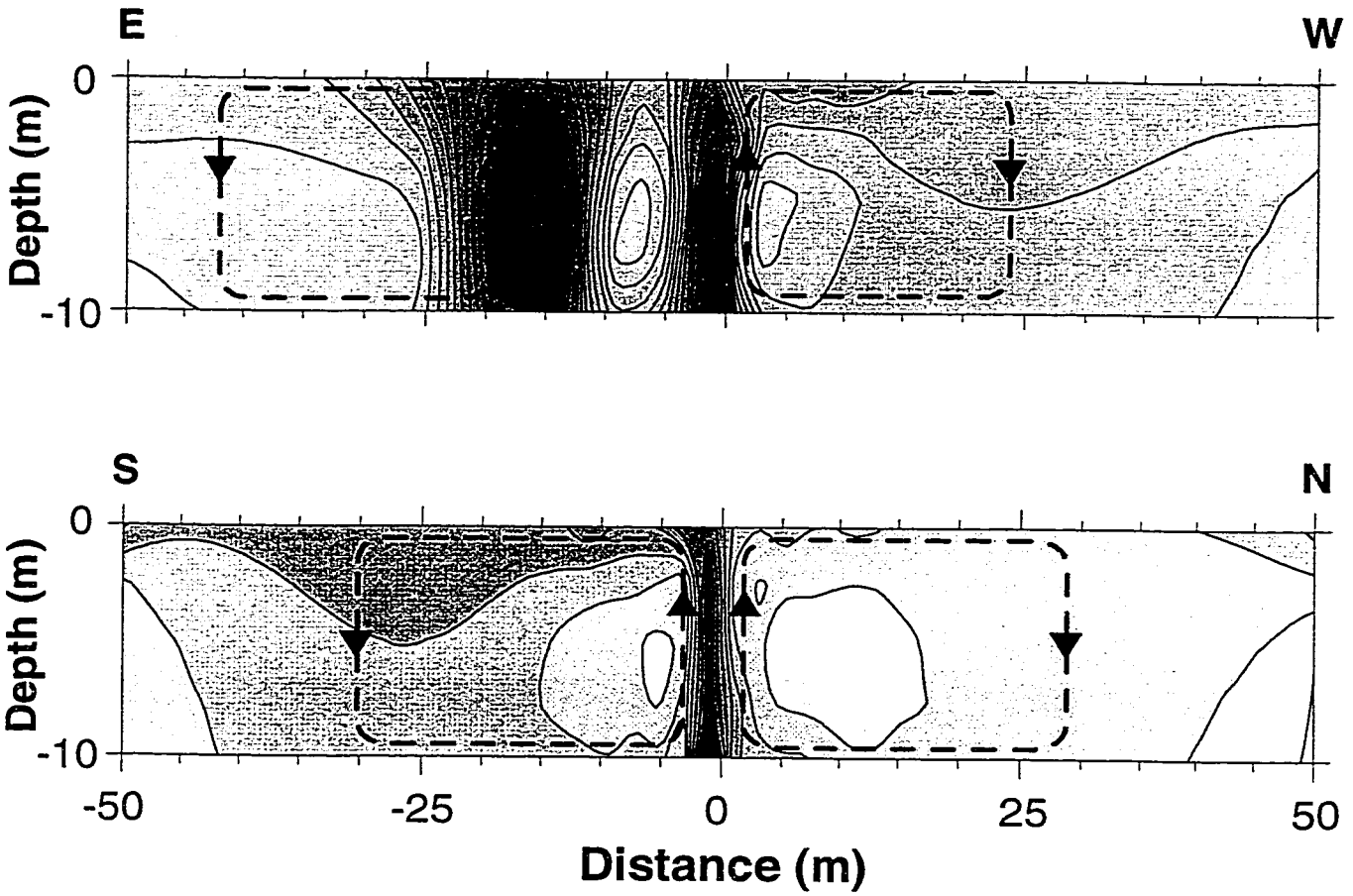

Fig. 6-2 Cross section models of hydrothermal component in Tutum Bay water in E-W and N-S direction. The location of the crossections is indicated in Fig. 6-1. The darker colors indicate higher hydrothermal component. Suggested hydrothermal convection cells are indicated by dashed lines.

6.3 RESULTS AND DISCUSSION

The physico-chemical conditions of plume formation in Tutum Bay are drastically different from those in mid-ocean environments. The temperature gradient in Tutum Bay where ambient seawater is ~ 30°C and hydrothermal fluids are < 100°C is much smaller than the one between seawater ~ -2°C and hydrothermal fluid ~ 350°C at a black smoker. Relative to seawater, Mn is enriched by up to 10^6-fold in most black smoker-type hydrothermal fluids (Von Damm, 1990) and is, therefore, the preferred tracer to map the extension of hydrothermal plumes. At Tutum Bay, however, Mn was not suited as a tracer because the vent fluids are much less enriched and show a significant concentration difference between area A and area B (Table 2-5). The use of Fe as a tracer was discarded on the same basis, which left only Si to construct the plume model.

The bottom water in Tutum Bay shows varying degrees of hydrothermal component and values range from 0.05 and 0.30% (Fig. 6-1). The small area just below vent 2 shows the highest concentrations, but this is an area where hydrothermal fluids seep through the sandy bottom at very low discharge rates. The low concentrations of hydrothermal fluid in the bottom water are not surprising given the physico-chemical conditions of fluid discharge. The vent fluids have a salinity < 3‰, which combined with their discharge temperature of ~ 90°C, makes them buoyant relative to seawater. As a result the hydrothermal fluids quickly rise to the surface (Fig. 1-4) and the surface water shows a hydrothermal component up to 10 times higher in concentrations than the bottom water (Fig. 6-1). Only little mixing occurs with ambient seawater in the immediate proximity of vent orifices. The overall distribution of hydrothermal component is most likely controlled by two processes: 1) diffuse low rate discharge of hydrothermal fluid and 2) the development of hydrothermal convection cells within the bay due to temperature differences (Fig. 6-2).

It is important, however, to realize that the fluid dissipation model presented in Figs. 6-1 and 6-2 are only a snapshot in space and time of a very dynamic system. At times discharge

rates may be much higher or lower resulting in a different concentration of hydrothermal component. Nearshore currents, although none were noticed while sampling, may be present at other times modifying the plume dispersion pattern.

Of potentially poisonous trace metals that are released into Tutum Bay only arsenic has a significantly higher concentration than seawater. In particular, AsIII-compounds are known to have a genotoxic potential (Gebel et al., 1997). The hydrothermal fluids contain extremely high arsenic concentrations of more than 800 ppb and the combined discharge of all vents is estimated to be more than 1500 g of arsenic per day into an area of approximately 50 by 100 m with an average depth of 6 m. These values are the highest arsenic concentration reported from any marine setting, including black smoker fluids from mid-ocean ridges. Despite the amount of arsenic released into the bay, corals, clams and fish do not show a direct response to the elevated values. Fish have been observed to hover over vent orifices bathing in the hydrothermal fluid. The diversity and health of the coral reef is indiscernible from reefs that are not exposed to hydrothermal discharge. The skeletons of scleractinian corals and the shells of *Tridacna gigas* clams do not show elevated concentrations of arsenic or other trace metals when compared to specimens collected from outside Tutum Bay (see Chapter 7).

Two mechanisms efficiently control and buffer the arsenic concentration: (1) dilution by seawater and (2) incorporation in and adsorption on Fe(III) oxyhydroxides that precipitate when the hydrothermal fluids mix with ambient seawater. The hydrothermal fluids have a pH of ~6 and are slightly reducing. Mixing with seawater increases the pH and redox potential and under these conditions As is readily adsorbed by Fe(III) oxyhydroxides (Pierce and Moore, 1980). Subsequent to precipitation, oxidation of As^{3+} to its pentavalent state significantly decreases its reactivity and genotoxicity (Gebel et al., 1997).

It is important to note that whenever it is assumed that changes in the hydrothermal system may have caused a response in the ambient coral reef only increased discharge rate was considered while all other parameters were assumed to remain constant (i.e., temperature, element concentration). That may be sufficient for the purpose of this exploratory study, but it

is important to understand that these parameters may drastically change at times. Higher discharge rates may reduce discharge temperatures if, after heavy rainfalls, increased groundwater recharge dilutes a possible deep chloride fluid already in the subsurface. Increased discharge rates due to volcanic activity, on the other hand, should increase venting temperature and the concentration of dissolved constituents. Tutum Bay offers a natural laboratory where long time monitoring may provide conclusive answers to many coral reef related questions, such as the response to input of potentially poisonous compounds and/or changes in temperature, salinity and carbonate saturation state.

6.4 SUMMARY AND CONCLUSIONS

Compared to seawater, the hydrothermal fluids are depleted in Cl, Br, SO_4, Na, K, Ca, Mg, and Sr and enriched in HCO_3, B, Si, Li, Mn, Fe, Rb, Cs, Sb, Tl and As. Although some elements are significantly enriched, they do not have a clear impact on ambient seawater composition because their concentration is buffered by mixing and uptake into secondary minerals.

Plume dispersion is quite different to that observed above mid-ocean spreading centers. Initial density differences, compositional gradients, temperature gradients and water depth prevent the formation of a buoyant plume. Only the surface water in Tutum Bay carries a clear imprint of the hydrothermal fluids.

7. HYDROTHERMAL EFFECTS ON TUTUM BAY CORALS

7.1 INTRODUCTION

Coral reefs are sensitive ecosystems where complex interactions of biological, climatic, and oceanographic factors influence reef growth. The most important environmental variables are sea level change, carbonate mineral saturation state, temperature, visible light, ultraviolet light, currents, waves, sedimentation rates, salinity, nutrients and anthropogenic stresses (Smith and Buddemeier, 1992). The skeleton and tissue of reef corals contain physical and chemical proxy signals of the surrounding environment. Their applicability as environmental recorders benefited from the discovery of annual density bands (Knutson et al., 1972) that enabled construction of chronologies that are in many ways analogous to those obtained from tree rings. Variations of trace elements and isotopes along their growth axis can thus be used to provide information about changing environmental conditions. For example, the concentrations of trace elements in the aragonite skeleton of corals have been used to investigate the history of anthropogenic metal input into the ocean (e.g., Dodge and Gillbert, 1984; Shen and Boyle, 1987), $\delta^{18}O$ to obtain information about sea surface temperature (SST) and oxygen isotopic composition of seawater (Weber and Woodhead, 1972), and the $\delta^{13}C$ to decipher patterns of light availability associated with the seasonal cycle of insolation, depth and cloudiness to evaluate the symbiotic relationship between corals and their zooxanthellae (e.g., Carriquiry et al., 1994; McConnaughey, 1989a).

Among coral reefs in the proximity to hydrothermal systems (e.g. Heikoop et al., 1996b; Tomascik et al., 1996), the fringing reef around Ambitle Island, Papua New Guinea, is possibly the one, which is subjected to the highest discharge rates of hydrothermal fluids. Isotope and trace element measurements of coral skeletons aim to trace the hydrothermal input into the reef and to determine its possible impact on coral metabolism. A comparable study of organisms living near deep-sea hydrothermal vents, tracing the biological uptake of isotopically

distinct hydrothermal nutrients and the utilization of chemosynthesis as a nutritional strategy, has been published, for example, by Conway et al. (1994).

7.2 SAMPLING AND ANALYTICAL METHODS

One *Tridacna gigas* (T-1) and eight *Porites lobata* samples, C-1 to C-8, were collected throughout Tutum Bay at varying distances from vent sites in April, 1996. All samples were collected from depths between 6-9 m. C-29 is the "non-hydrothermal" reference sample and was collected approximately 10 km north of Tutum Bay (Fig. 1-1). C-4, C-7 and C-8 were sampled as complete coral heads and all other samples represent cores drilled (~2.5 cm Ø) along the main growth axis.

The coral slabs and cores were cut into three pieces along their growth axis. The center piece of approximately 5 mm thickness was x-rayed to obtain growth rate information and subsequently sampled for carbon, oxygen and strontium isotope analyses. Where possible, I sampled approximately the last two years of coral growth by sampling every 1 mm of skeleton along the growth axis using a micro-drill. Samples were only pretreated in areas of extreme organic contamination and were taken over all skeletal elements (corallite walls, septa, etc.). Sample size was approximately 0.3 mg for all samples. See Appendix 2 for more details.

Carbon and oxygen isotope analyses for corals were performed at McMaster University on a VG SIRA II. Precision was tested using an internal coral standard and was 0.04‰ for carbon and 0.03‰ for oxygen. All results are reported in standard delta (δ) notation in per mil (‰) units, relative to the PDB standard. The *Tridacna* sample was treated and prepared identical to the coral samples and analyzed at the G. G. Hatch Isotope Laboratory, University of Ottawa. $^{87}Sr/^{86}Sr$ were measured on a five collector Finnigan MAT 262 solid source mass spectrometer at the Institut für Geologie, Ruhr Universität, Bochum following Buhl et al.

(1991) and Diener et al. (1996). The average of 100 repeat measurements for the NBS 987 standard was 0.710224±0.000008.

Following McConnaughey et al. (1997a), isotopic equilibrium for coral aragonite was calculated using the equations of Romanek et al. (1992) for carbon and Grossman and Ku (1986) for oxygen:

$$\delta^{13}C_{aragonite} = \delta^{13}C_{dissolved\ bicarbonate} + 2.7 \quad [6\text{-}1]$$

and

$$(\delta_C - \delta_w) = 4.75 - 0.23t. \quad [6\text{-}2]$$

δ_C and δ_w are expressed in PDB and SMOW, respectively and t is temperature in °C.

Analyses of carbon-coated, polished sections were performed on the Guelph proton microprobe. Polished sections were prepared from 2 mm thick slabs that were cut with a diamond saw from pieces directly facing the coral slab that was used for isotope analyses. The slabs were sonicated, extensively rinsed with de-ionized water and impregnated with epoxy resin before polishing with aluminum powder. Any skeletal imperfections or micro-borings were clearly visible in reflected light microscopy and avoided during analyses (Allison and Tudhope, 1992).

Analyses were conducted on spots of approximately 5 μm diameter, using a 3 MeV beam and an Al filter in order to attenuate the dominant Ca peak. The instrument constant H was determined using the accurately known Sr and Fe contents of U.S. Geological Survey (USGS) BHVO-1 basalt standard, fused to a glass. Count times were about 6 to 10 min and total element concentrations were evaluated with the GUPIX software package (Maxwell et al., 1989; Maxwell et al., 1995). Sample locations were chosen parallel to the growth axis, directly opposite of areas that were drilled for isotope analyses. Sample numbers for isotope and proton probe spots correspond to each other in such a way that the proton probe point C-1 (1 mm) is

at the same relative location as isotope analyses C-1 (1 mm). See Appendix 2 and 2 for more details.

7.3 RESULTS

7.3.1 Coral growth rates

Density banding is only moderately well developed in these corals and subannual bands are common. This density pattern is likely a result of the relatively uniform equatorial climate. It was, nevertheless, possible to extract growth rate information from these corals (Table 7-1). The listed growth rates are the average of the most recent two years of skeletal deposition and range from 9 to 20 mm per year. There is no significant correlation between coral growth rate and the amount of hydrothermal input experienced by each coral (Figs. 7-1 and 7-2). The low growth rates of sample C-7 likely reflect the fact that it is a juvenile individual. Sample C-1, with the highest growth rate, has a skeletal banding that is distinct from the other samples. Some of the corals receiving the greatest amount of hydrothermal input (C-8 and C-4) have amongst the highest growth rates, while the control coral has the second lowest growth rate of the entire suite. In general, no clear relationship between coral growth and magnitude of hydrothermal input can be recognized. A high density band appeared to be forming at the time of collection in each of the corals. The high density band, therefore, was used as a chronological marker, representing the month of April, when interpreting isotopic records (Fig. 7-3).

TABLE 7-1
AVERAGE ISOTOPIC COMPOSITION, GROWTH RATE, STRONTIUM CONCENTRATION AND HYDROTHERMAL INFLUENCE FOR TUTUM BAY BIOGENIC CARBONATES

Coral Unit	Growth per Year mm	$\delta^{13}C$ ‰ (PDB)	$\delta^{18}O$ ‰ (PDB)	$^{87}Sr/^{86}Sr$	Sr ppm	Hydrothermal Input %
C-1	20	-2.6	-4.8	n.d.	7499	0.08
C-2	12	-2.6	-4.9	n.d.	7923	0.11
C-3	10	-2.7	-4.9	n.d.	7466	0.14
C-4	15	-3.3	-5.6	n.d.	7490	0.16
C-5	10	-1.6	-5.4	0.70917	7549	0.14
C-6	13	-2.3	-5.5	n.d.	7638	0.11
C-7	7	-2.6	-5.4	n.d.	7439	0.15
C-8	13	-4.1	-5.7	0.70918	7594	0.18
C-29	9	-1.1	-5.1	0.70920	7871	0.00
T-1	n.d.	2.1	-1.9	0.70913	1215	0.12

Note: The complete data sets are listed in Appendices 1 and 2; n.d. = not determined; Max. error for strontium isotope values is ±0.000009 2 Standard Errors.

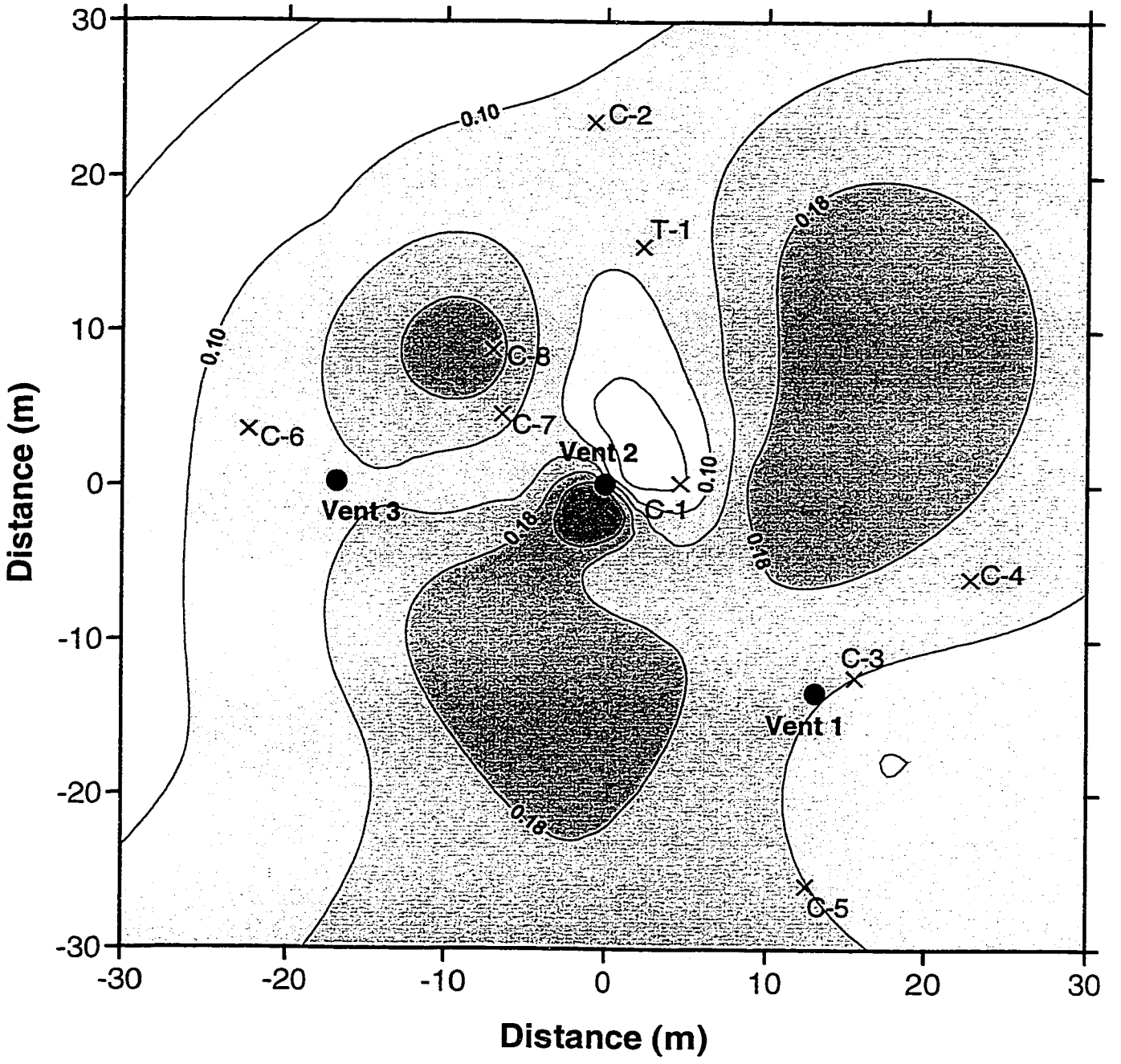

Fig. 7-1 Sample locations for *Tridacna* and coral samples that were collected in Tutum Bay. Locations are indicated (X) and superimposed on the model of hydrothermal component in the bottom water (Fig. 6-1). The darker colors indicate higher hydrothermal component.

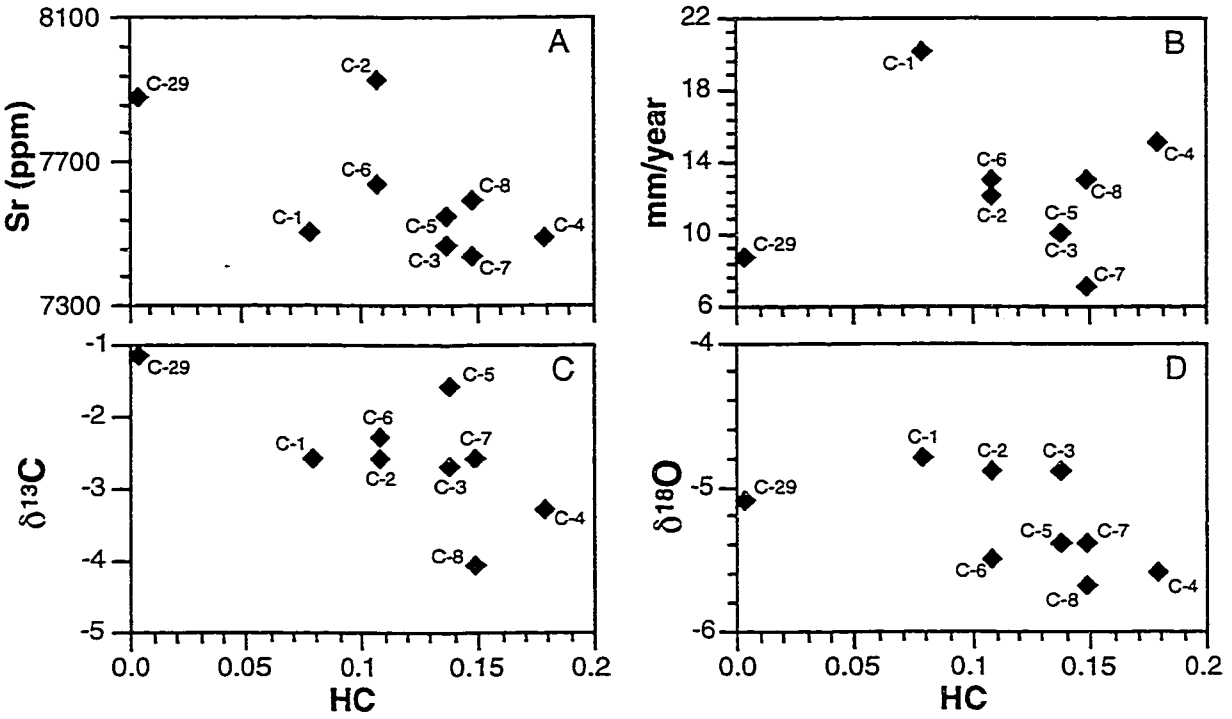

Fig. 7-2 Plot of mean $\delta^{18}O$, $\delta^{13}C$, Sr concentrations and growth rates vs. calculated degree of hydrothermal component (HC) in the Tutum Bay seawater.

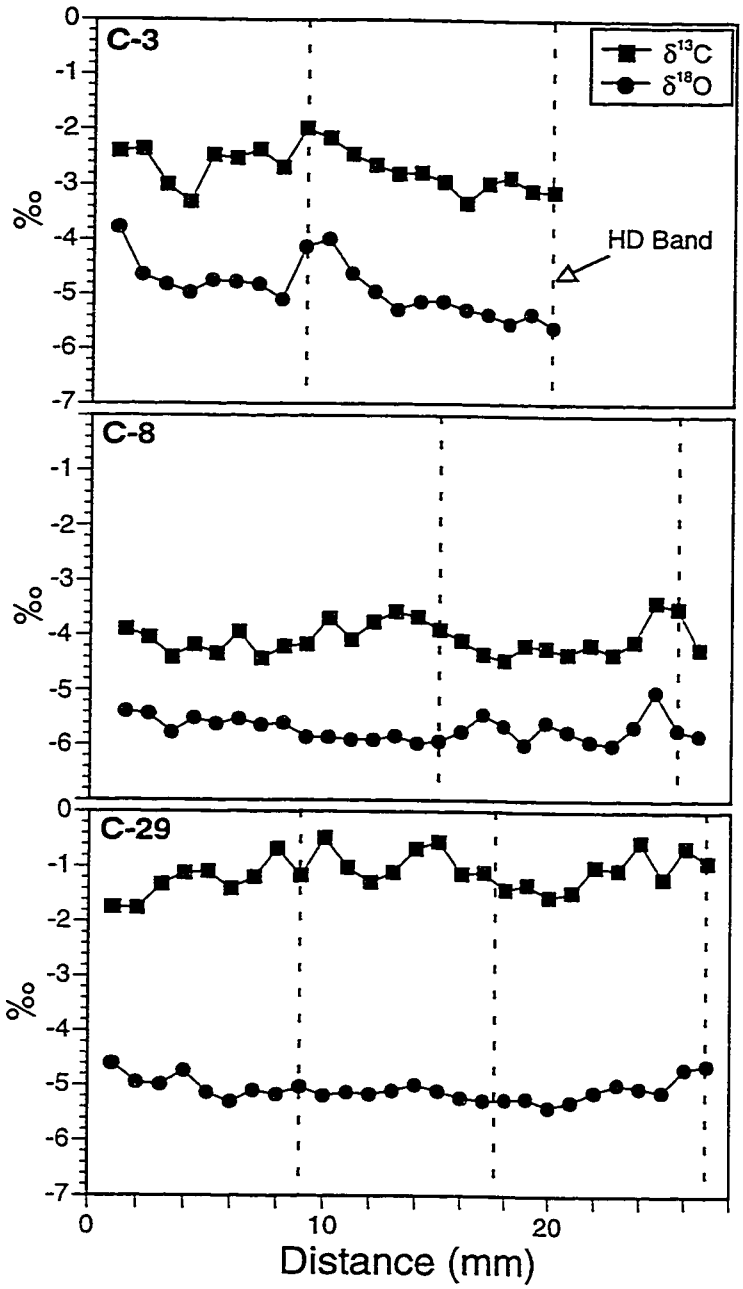

Fig. 7-3 $\delta^{18}O$ and $\delta^{13}C$ values of coral skeletons C-3, C-8 and C-29 ("non-hydrothermal" coral) versus distance from the top of the corallum. Locations of high density bands are indicated (dashed line). The top of the skeleton and each high density band represent primary skeletal deposition during the month of April. The distance between the top of the skeleton and each subsequent high density band, therefore, represents one year of skeletal deposition.

7.3.2 Isotopes

Oxygen and carbon isotope data are presented graphically in Figs. 7-3 and 7-4. Data summaries are provided in Table 7-1 and the whole data set can be found in Appendix 2. $\delta^{13}C$ ranges from -4.5 to -1.0‰ and $\delta^{18}O$ from -6.0 to -3.8‰ for corals from Tutum Bay. The "non-hydrothermal" sample, C-29, has $\delta^{13}C$ values ranging from -1.8 to -0.5‰, and $\delta^{18}O$ values of -5.4 to -4.6‰. The $\delta^{18}O$ values for this specimen are within the range of Tutum Bay corals; $\delta^{13}C$, however, is generally enriched (Fig. 7-4). In $\delta^{18}O$ vs. $\delta^{13}C$ space it can be seen that many of the corals studied plot as nearly distinct fields, representing distinct isotopic signatures (Fig. 7-4 and Appendix 2). There is a significant positive correlation between $\delta^{13}C$ and $\delta^{18}O$ for the entire data set (including C-29; $r=0.33$, $p<0.01$).

Selected examples of isotopic measurements versus distance into the skeleton are shown in Fig 7-3. C-8 represents a coral which receives high amounts of hydrothermal input compared to other samples (Fig. 7-1), C-3 represents a coral growing immediately adjacent to Vent 1 which has the highest hydrothermal discharge (although the benthic waters surrounding this coral have relatively low hydrothermal content), and C-29 displays isotopic data for the control sample. There is only weak evidence for a clear annual cyclicity in these corals. $\delta^{18}O$ generally shows an annual range of approximately 0.5‰ and $\delta^{13}C$ varies about 1‰ in each sample. Only coral C-3 shows a high degree of correlation between $\delta^{18}O$ and $\delta^{13}C$ records ($r=0.79$, $p<0.01$). C-3 also shows the greatest annual range in isotopic variation of the corals studied (Fig. 7-3).

No significant correlation exists between mean $\delta^{18}O$ and either growth or mean $\delta^{13}C$ for the nine corals sampled. A significant correlation for $\delta^{18}O$ with the degree of hydrothermal input, however, does exist if sample C-29 is excluded ($r=-0.712$, $p<0.05$) (Fig. 7-2). Average $\delta^{13}C$ values of Tutum Bay corals show no significant correlation with coral growth rate, but a significant relationship exists with the degree of hydrothermal input if sample C-29 is included in the correlation ($r=-0.673$, $p<0.05$).

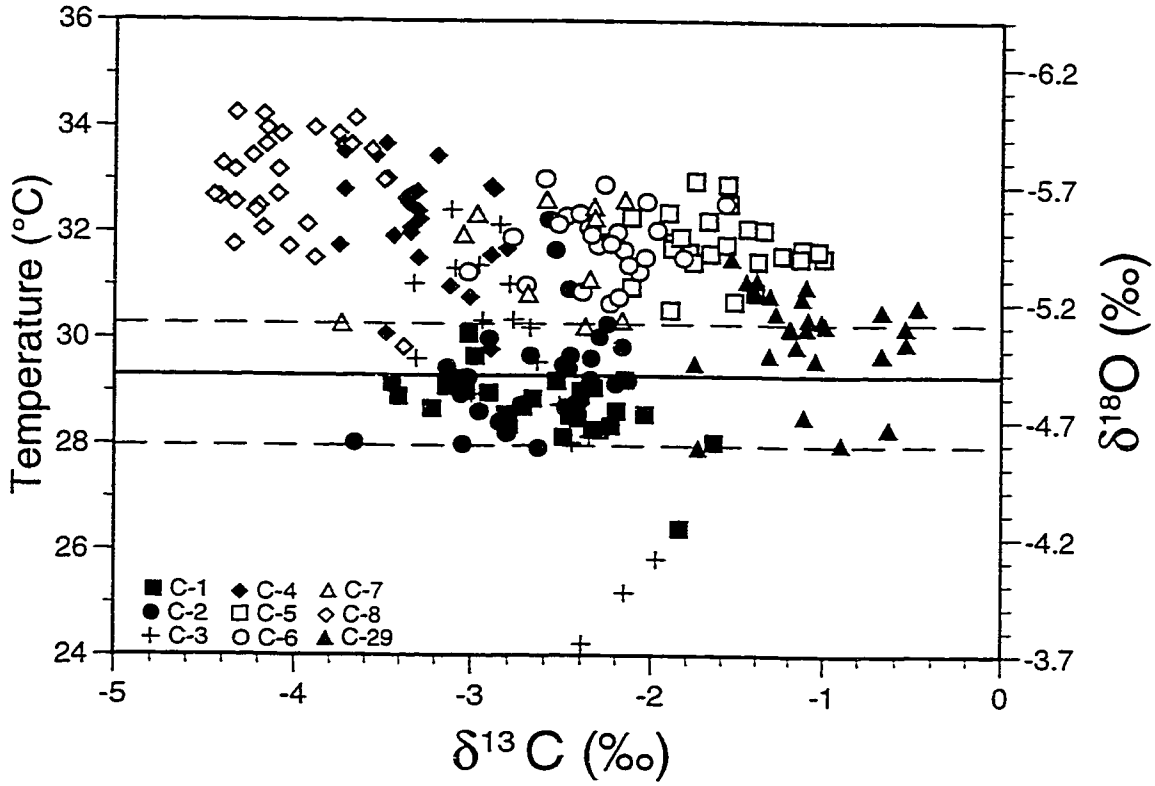

Fig. 7-4 Plot of calculated paleotemperature vs $\delta^{13}C$ for all corals. Dashed lines indicate natural climatic range in temperature at the site and the solid line the temperature at the time of sampling. Values above the upper climatic boundary are thought to result from additional hydrothermal warming. See text for equation and assumptions used in calculating paleotemperatures. Individual corals plot as nearly distinct fields, representing distinct isotopic signatures. The statistical significance is explored in Appendix 3.

Samples that showed either relatively high or low $\delta^{18}O$ and $\delta^{13}C$ values were analyzed for $^{87}Sr/^{86}Sr$. Results for these samples are listed in Table 7-2 and graphically displayed in Fig. 7-5. Ratios range from 0.70914 to 0.70924 and are very close to the values for local seawater 0.70918±0.000009 (Table 2-3). No significant correlation exists between $^{87}Sr/^{86}Sr$ and $\delta^{18}O$ or $\delta^{13}C$. When compared to the "non-hydrothermal" coral sample, both samples from Tutum Bay (C-5 and C-8) show a significantly lower $^{87}Sr/^{86}Sr$ (Fig. 7-5).

The *Tridacna gigas* sample (T-1) experienced hydrothermal influence comparable to coral samples C-2 and C-6. $\delta^{13}C$ and $\delta^{18}O$ values do not correlate and hardly deviate beyond their analytical error (Appendix 2). $\delta^{18}O$ values range from -1.84 to -2.16‰ (mean -1.9‰) and $\delta^{13}C$ range from 1.96 to 2.24‰ (mean 2.1‰). As expected for adult *Tridacna* clams (e.g., Romanek and Grossman, 1989), no annual cyclicity has been observed and, therefore, it is not possible to directly correlate records from T-1 with those from the coral samples. $\delta^{18}O$ growth temperatures were calculated using the temperature equation from Grossman and Ku (1986) and following Romanek and Grossman (1989). Temperature values range from 29.8 to 31.2°C and are in good agreement with the field measurement of 29.3°C and the annual temperature range in the area (Fig. 7-4).

7.3.3 Trace elements

In proton microprobe analyses the LOD (limit of detection) is element specific and count rate dependent and, therefore, can change from analyses to analyses. Detection limits in ppm were: As (1.2-3.4), Ba-16.1-47.1), Br (1.2-2), Co (9.2-15.2), Cr (11.5-24.5), Cu (1.5-2.5), Fe (3.4-6.3), Ga (1.3-3.7), Ge (1.2-3.4), Mn (5.8-12.1), Mo (1.5-3.9), Nb (1.3-4), Ni (1.8-4.3), Pb (3.9-8.7), Rb (1.3-4.3), Se (1.2-3.7), W (4.8-9.6), Y (1.4-4.6), Zn (1.3-9) and Zr (17.4-129.2). At standard experimental conditions, as described above, most elements (Z>22) were below their respective detection limit given acceptable counting times of approximately 10 minutes. Concentrations of As, Co, Cr, Ga, Ge, Mo, Nb, Ni, Pb, Rb, Se,

TABLE 7-2
CARBON, OXYGEN AND STRONTIUM ISOTOPIC COMPOSITION FOR SELECTED SAMPLES FROM TUTUM BAY BIOGENIC CARBONATES

Sample	Point (mm)	$\delta^{13}C$ (‰)	$\delta^{18}O$ (‰)	$^{87}Sr/^{86}Sr$	± 2 Standard Error
C-5	1	-2.11	-5.26	0.70914	0.000009
	13	-1.00	-5.39	0.70916	0.000010
	19	-1.45	-5.51	0.70918	0.000008
	24	-2.35	-5.54	0.70919	0.000013
C-8	1	-3.89	-5.38	0.70914	0.000009
	18	-4.45	-5.65	0.70915	0.000006
	23	-4.33	-5.99	0.70921	0.000010
	25	-3.38	-5.01	0.70921	0.000009
C-29	1	-1.74	-4.60	0.70921	0.000008
	6	-1.40	-5.30	0.70924	0.000009
	26	-0.64	-4.68	0.70919	0.000013
T-1	1	1.96	-1.88	0.70913	0.000008
	10	2.21	-2.09	0.70914	0.000008

Note: The complete data set for oxygen and carbon isotopes is listed in Appendix 1.

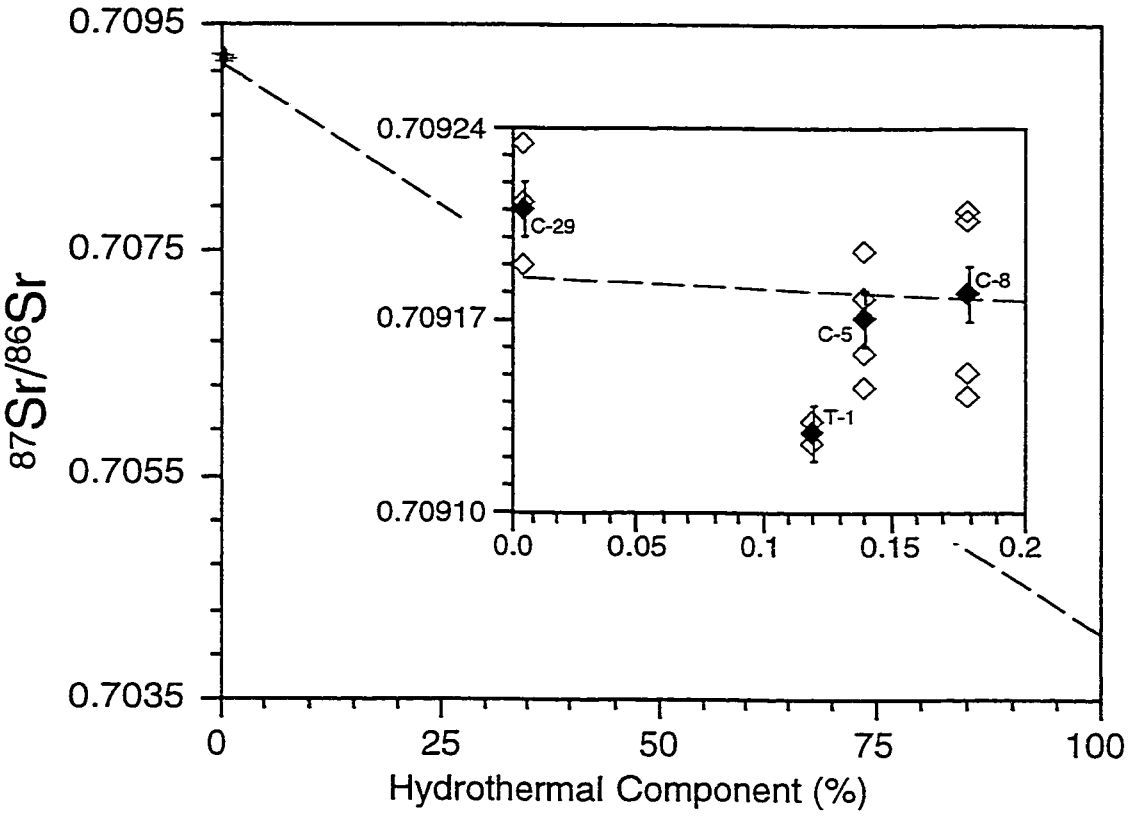

Fig. 7-5 Plot of $^{87}Sr/^{86}Sr$ vs. calculated degree of hydrothermal component (HC) in the Tutum Bay seawater for samples C-29, C-5, C-8 and T-1. The dashed line represents the mixing line for $^{87}Sr/^{86}Sr$ between local seawater (HC=0%) and hydrothermal fluid (HC=100%). The inset graph is a magnification of the area of interest. Here empty diamonds represent the measurements and filled diamonds are the means for individual samples.

W, Y and Zr were always below their respective detection limits. Ba, Br, Cu, Fe, Mn, and Zn were detected in some samples, but due to their scarcity element to element correlation was impracticable. Br was detected in the lower parts of C-8 and throughout C-29. Sr was detected in all samples and its concentration ranged from 6967 to 8236 ppm with a mean of 7642 ppm (n=53, σ=239). The Sr concentration in the control sample C-29 is higher than in most of the corals from Tutum Bay (Table 7-1 and Appendix 3) and Tutum Bay corals do not fall into distinct groups as observed for $\delta^{13}C$ and $\delta^{18}O$.

In the *Tridacna gigas* sample (T-1), Sr was the only element detected. Concentrations ranged from 1111 to 1343 with a mean of 1215 ppm (σ=66). There is a significant correlation between Sr and $\delta^{13}C$ (n=11, r=0.74) and no correlation between Sr and $\delta^{18}O$ (n=11, r=0.04).

7.4 DISCUSSION

7.4.1 Growth rate

It is perhaps not surprising that there is no clear effect of hydrothermal fluids on coral growth rate measurements. While annual temperature and insolation cycles are thought to affect density band formation and annual growth rate, common growth and density patterns may be lacking even between corals within a single reef in which climatic variables are relatively uniform (Lough and Barnes, 1992). Given this natural tendency towards variation in growth parameters within relatively homogeneous environments, it is unlikely that clear relationships would be found within the very heterogeneous system studied here. In general, it is thought that higher ambient temperatures result in higher linear extension rates (e.g., Weber et al., 1975). Although growth rate trends are not clear, samples C-4 and C-8, which experience the most hydrothermal input, do have among the highest growth rates of the corals examined. Coral C-7 also experiences high degrees of hydrothermal input, but is a juvenile sample.

Variations in growth rates cannot be ignored in this study, because they have the potential to affect isotopic signatures (Allison et al., 1996; Heikoop, 1997; McConnaughey, 1989b).

7.4.2 Isotopes

The lack of annual cyclicity in isotope data (Fig. 7-3) possibly reflects buffering of temperature and $\delta^{18}O$ of bay waters by the constant hydrothermal input. Yet, given the lack of cyclicity in the record of coral C-29, it is likely that the relatively uniform isotopic records merely reflect the relatively uniform equatorial climate. Annual temperature variations are only on the order of 2.5 °C (Fig. 7-4). Assuming a temperature dependence of approximately -0.22°C per 1‰ (Carriquiry et al., 1994), the observed annual $\delta^{18}O$ variation in Tutum Bay corals would approximately match this temperature range. Intra- and interannual $\delta^{18}O$ variations in other Papua New Guinea corals have been attributed to variations in the input of isotopically depleted rainfall (Aharon, 1991; Tudhope et al., 1995). Rainfall at this site has a $\delta^{18}O$ value of approximately -5‰. This may be sufficiently depleted relative to seawater to account for some of the observed coral $\delta^{18}O$ variation.

Of greater interest, however, are the distinct isotopic signatures of many of the corals and their correlation with the degree of hydrothermal influence. The $\delta^{18}O$ values for the Tutum Bay corals are within the measured range for shallow water (<10 m) members of the genus *Porites* (e.g., Aharon, 1991; Allison et al., 1996; Carriquiry et al., 1994; Gagan et al., 1994; Klein et al., 1992; Linsley et al., 1994; McConnaughey, 1989b; McConnaughey, 1989a; McCulloch et al., 1994; Patzold, 1984; Quinn et al., 1996; Tudhope et al., 1995; Wellington and Dunbar, 1995). Corals with similar, or even more depleted $\delta^{18}O$ values than Tutum Bay corals, tend to grow in areas with high sea surface temperatures or abundant input of isotopically light rainfall or flood waters (e.g., Gagan et al., 1994; Wellington and Dunbar, 1995).

The $\delta^{13}C$ values of Tutum Bay corals are amongst the most depleted when compared to records from the above referenced studies. Only corals experiencing thermal stress or greatly reduced light availability (photosynthesis) have values as low as those seen in coral C-8 (e.g., Allison et al., 1996; Gagan et al., 1994). Generally, $\delta^{13}C$ values of vent fluid affected corals are distinctly lighter than those of other *Porites* from Papua New Guinea (Tudhope et al., 1995). The "non-hydrothermal" coral (C-29), however, has similar $\delta^{18}O$ and $\delta^{13}C$ values.

For corals collected in such a restricted area, from approximately the same depth, the range in isotopic values is quite large. The fact that some corals plot as distinct fields would seem particularly unusual if environmental conditions were relatively homogenous throughout the bay. It is difficult to compare these results to other published studies because most isotopic work on corals involves longer records from fewer individuals. It is not unusual, however, for corals from a single reef to have distinct isotopic signals, particularly in $\delta^{13}C$ (e.g., Carriquiry et al., 1994).

$\delta^{13}C$ and $\delta^{18}O$ values of the *Tridacna gigas* sample fall within the range reported from other studies (Aharon, 1991).

Variations in $\delta^{18}O$ The main potential sources of variation in $\delta^{18}O$ are displayed in Figure 7-6. Some of the variation could be due to differences in isotopic equilibrium as determined by temperature and $\delta^{18}O$ of the water mass (see eq. [6-2]). Additional variation could also be caused by different growth rates between and within individual corals. Growth rate variations may cause isotopic disequilibrium due to kinetic isotope effects, leading to a simultaneous discrimination against the heavy isotopes of oxygen and carbon during the hydration and hydroxylation of CO_2 during calcification (McConnaughey, 1989b). In general, higher growth rates lead to greater isotopic depletion in both $\delta^{13}C$ and $\delta^{18}O$ of coral skeletons. These kinetic isotope effects, along with metabolic/ photosynthetic effects, are thought to be the source of disequilibrium "vital" effects in coral skeletons (McConnaughey, 1989b).

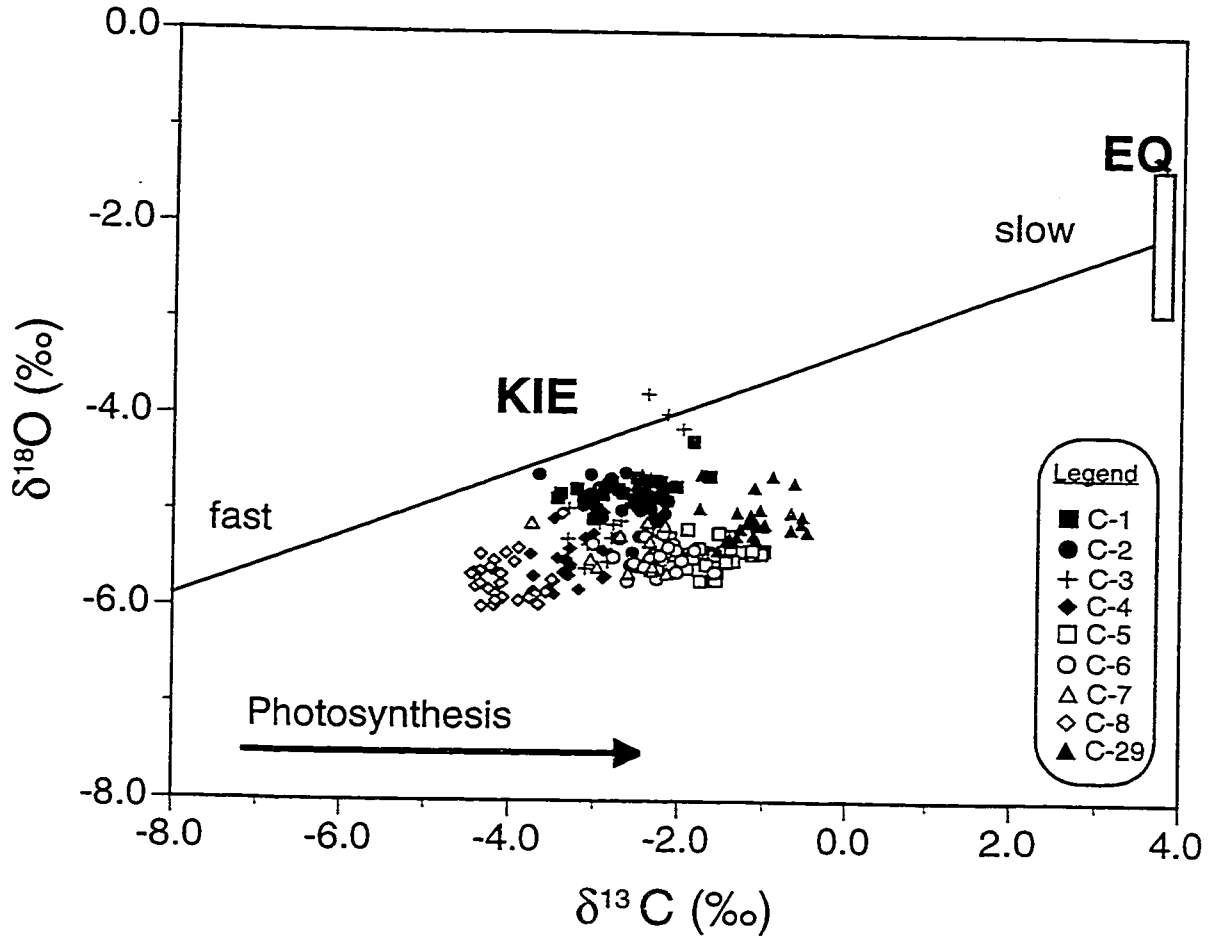

Fig. 7-6 $\delta^{18}O$ vs $\delta^{13}C$ of Tutum Bay (C-1 to C-8) and reference (C-29) corals. Isotopic equilibrium has been calculated using equations given in the text. $\delta^{18}O$ of the water mass has been taken as 0.45‰. The range in oxygen isotopic equilibrium represents a possible temperature range from 27.8 to 33.3°C. The lower value is the lower climatic limit for this site. The upper value represents the upper climatic limit plus three degrees for possible hydrothermal warming of the benthic waters surrounding strongly vent affected corals (see text and Fig. 7-2, for a discussion of the potential magnitude of hydrothermal warming). The range in carbon isotopic equilibrium values represents a possible range in $\delta^{13}C$ of DIC. The upper value is calculated from a measured open ocean seawater DIC value of 1.2‰. The lower value assumes a 10% contribution of hydrothermal fluids with $\delta^{13}C$ of -1‰, giving a minimum value of approximately 1% for DIC of benthic bay waters (i.e. equilibrium should be between 3.7 and 3.9‰). This may greatly exaggerate the impact of hydrothermal fluids on $\delta^{13}C$ of DIC as actual calculated hydrothermal inputs at 0.5 m above the bottom are significantly lower than 10 percent (see Fig. 7-1). Possible causes of isotopic variation are illustrated in this figure: 1) variations in isotopic equilibrium (field marked EQ); 2) coral growth rate (isotopic variation will occur along the trend delineating kinetic isotope effects, KIE); and 3) differential ^{13}C enrichments related to the degree of photosynthesis. Note that most samples plot to the right of the kinetic isotope effect line suggesting net autotrophy.

The most likely cause of the spread in oxygen isotope values between corals is variation in water temperature due to hydrothermal input. Higher temperatures lead to lower values of $\delta^{18}O$ in the aragonite skeleton of corals. In Figure 7-4 the paleotemperature equation for *Porites lobata* of Carriquiry et al. (1994):

$$\delta_c-\delta_w=1.36-0.222*t \qquad [6\text{-}3]$$

was applied to convert $\delta^{18}O$ values into paleotemperatures, using the average $\delta^{18}O$ value of Tutum Bay seawater (δ_w=0.45‰ SMOW) under the assumption that there is no variation due to kinetic isotope effects. Most of the data, including that from C-29, plot either within the average climatic range for this site, or up to four degrees above the climatic maximum. The corals that experienced the most hydrothermal input tend to be the ones with the most elevated paleotemperatures (e.g. C-4 and C-8). Given the lack of variation in $\delta^{18}O$ of the water mass at the time of sampling, the isotopic depletion observed in the most affected corals cannot be easily attributed to different $\delta^{18}O$ values of Tutum Bay waters. Vent waters, however, are depleted in ^{18}O ($\delta^{18}O \sim -5‰$) and some variation may be attributed to this source, particularly for smaller samples growing closer to the substrate.

The overall positive correlation between $\delta^{18}O$ and $\delta^{13}C$ and the general trend of the data towards average isotopic equilibrium could be taken as evidence for strong kinetic isotope effects in the data set (Heikoop, 1997; McConnaughey, 1989b). The lack of correlation between mean $\delta^{18}O$ and growth rate, however, suggests that in the case of skeletal $\delta^{18}O$ at least, these effects may be of secondary importance. $\delta^{18}O$ records in corals are not directly affected by metabolic processes such as photosynthesis and respiration. Evidence that growth rate variations modify the hydrothermal signal to some degree can be found in sample C-3. This coral has relatively heavy values relative to the amount of hydrothermal input experienced (Fig. 7-2) and its slow growth rate may be responsible for the enriched signal. The low

temperature values calculated from subsamples of coral C-3 (Fig. 7-4) may, therefore, also be a result of slow growth.

Calculated paleotemperatures for strongly vent affected corals, however, have to be regarded as maximum values. Lower $\delta^{18}O$ of surrounding seawater and kinetic effects associated with higher growth rates (Table 7-1), likely contribute partially to the observed isotopic depletion (and therefore to higher calculated temperatures).

The small $\delta^{18}O$ variation observed in T-1 is as expected for mature *Tridacna* clams (e.g., Aharon, 1991; Romanek and Grossman, 1989) and the calculated $\delta^{18}O$ paleotemperatures (29.8 to 31.2°C) should be a good estimate of the average seawater temperature in Tutum Bay.

Variations in $\delta^{13}C$ Potential sources of variation in skeletal $\delta^{13}C$ include equilibrium effects, kinetic isotope effects associated with variation in growth rate and metabolic effects associated with the degree of photosynthesis (Fig. 7-6). Of these factors, reduced photosynthesis resulting from thermal stress associated with hydrothermal input is likely to be the most important.

Photosynthesis (P) by zooxanthellae in corals preferentially assimilates the light isotope of carbon (^{12}C) leaving the internal pool from which calcification occurs (internal DIC pool) enriched in ^{13}C. On the other hand, respiration (R) by corals enriches the internal DIC pool in ^{12}C (see reviews in Carriquiry et al., 1994; McConnaughey, 1989b; Swart, 1983). Most of the corals in this study plot to the right of the kinetic isotope line, indicating that they are net autotrophs (P/R >1) (McConnaughey, 1989a). The nearly significant relationship between $\delta^{13}C$ and degree of hydrothermal input (Fig. 7-2) may reflect the effect of hydrothermal fluids on photosynthesis. When compared to sample C-29 and to *Porites* from other locations, the very low $\delta^{13}C$ values of Tutum Bay corals suggest that decreased photosynthesis as a result of coral stress could be an important factor.

Elevated water temperature and/or depressed salinity are common stressors that, depending on the time and degree of exposure, may cause coral death (Coles and Jokiel, 1992; Jokiel and Coles, 1990; Smith and Buddemeier, 1992). Changing discharge rates of the hydrothermal springs and local currents have a great impact on the temperature and salinity regime and, therefore, may affect growth and demise of adjacent corals. As temperatures increase above photosynthetic optimum both photosynthesis and respiration increase. Respiration, however, increases at a faster rate (Swart, 1983) and as a result P/R becomes less than unity and skeletal $\delta^{13}C$ will decrease (Carriquiry et al., 1994; Swart, 1983). It is possible that the higher temperatures experienced by the most strongly affected vent corals, as inferred from oxygen isotopic data, might therefore also indirectly lead to lower values of $\delta^{13}C$. The paleotemperatures shown in Figure 7-4 are beyond the normal upper limit for corals and are high enough to result in coral stress (Jokiel and Coles, 1990). It seems that benthic water/substrate temperatures control reef distribution at this site (i.e. coral cover vs. sand cover), suggesting that thermal stress is an important factor controlling coral health in the bay.

Variations in light availability could also affect the photosynthetic potential. Vent fluids cause a shimmering effect when released into Tutum Bay and cause scattering of downward irradiance. It is conceivable that corals influenced most by vent fluids might receive less irradiance and, hence, exhibit lower photosynthesis and skeletal $\delta^{13}C$.

Equilibrium effects are unlikely to be an important cause of the observed variations. The $\delta^{13}C$ of the DIC (dissolved inorganic carbon) of vent fluids (~ -1‰) is only slightly depleted relative to seawater and the amount of hydrothermal fluid present in Tutum Bay seawater is small. The temperature variations inferred from the oxygen isotopic records should have little direct effect on $\delta^{13}C$ of the coral skeletons. Equilibrium fractionation factors for $\delta^{13}C$ of biogenic aragonite are poorly constrained (Aharon, 1991) and temperature dependence cannot be completely ruled out. If present, however, temperature dependent equilibrium $\delta^{13}C$ variations would be significantly smaller than those for $\delta^{18}O$. The fractionation factors from Romanek et al. (1992) were chosen for equilibrium calculations (Fig. 7-6). Based on their

experiments, Romanek et al. (1992) conclude that the fractionation factor for aragonite-HCO_3^- is constant over the temperature range from 10 to 40°C (see eq. [6-1]).

Kinetic isotope fractionation effects are three times larger for $\delta^{13}C$ than for $\delta^{18}O$ and growth rate differences may be responsible for some of the observed variation. The most affected Tutum Bay corals, however, with some of the most depleted $\delta^{13}C$ values recorded for shallow-water *Porites* (see above), have growth rates that are not significantly higher than those of the corals from studies cited above. The growth rates of the most strongly affected corals are also not significantly higher than some of the least affected Tutum Bay corals (Table 7-1). Growth rate variations, however, may be partially modifying any photosynthetic signal. Coral C-3 is enriched relative to the trend between $\delta^{13}C$ and HC (Fig. 7-2), which may be a function of its slow growth. Similarly, coral C-1 is depleted relative to this trend and has the highest growth of all corals sampled. It seems unusual that the corals with the most hydrothermal input would have amongst the highest growth rates, while stressed by this input. Note, however, that Edinger et al. (in submission) have found that corals growing under stressful eutrophic conditions often have anomalously high growth rates. It is possible that the higher growth rates observed here might reflect a photoadaptation mechanism (i.e. an attempt to maintain as high levels of photosynthesis as possible by growing quicker towards the surface). Also, if high growth rates correspond to high calcification rates in these corals, then increased generation of free protons by calcification might aid in nutrient uptake and promote photosynthesis (McConnaughey and Whelan, 1997).

The overall inverse relationship between both skeletal $\delta^{18}O$ and $\delta^{13}C$ and the degree of hydrothermal input is likely a synergistic combination of direct and indirect effects related to vent activity. Equilibrium effects, growth rate effects and photosynthetic effects all act as described above to cause isotopic depletion in the most vent affected corals. In the case of skeletal $\delta^{18}O$, temperature is likely the most important hydrothermal variable. The stress (higher temperature and lower salinity) induced by the hydrothermal system on the corals is likely the most important factor explaining the $\delta^{13}C$ variations, although growth rate cannot be

completely ruled out. Given the very small hydrothermal contributions to the seawater in the benthic zones of the bay, these results suggest that isotopic records of corals are extremely sensitive indicators of such input.

Strontium Isotopes The $^{87}Sr/^{86}Sr$ in marine carbonates, including coral skeletons is entirely controlled by its ratio in seawater. As discussed above, the multitude of factors that control the fractionation of carbon and oxygen isotopes during precipitation of coral skeletons make it difficult to directly detect vent related isotope signatures. The vent fluids have a significantly lower $^{87}Sr/^{86}Sr$ than local seawater (Table 2-5) and, therefore, Tutum Bay seawater is slightly depleted in ^{87}Sr. This depletion is evident in the $^{87}Sr/^{86}Sr$ of coral skeletons of the samples from Tutum Bay when compared to the "non-hydrothermal" coral (Fig. 7-5).

7.4.3 Trace elements

Neither As, Co, Cr, Ga, Ge, Mo, Nb, Ni, Pb, Rb, Se, W, Y nor Zr were detected during proton probe analyses. This results from low distribution coefficients and low concentration in the hydrothermal fluid (Table 2-2) combined with slightly too high LODs compared to their expected concentration in aragonite (Veizer, 1983). Among the several processes that directly incorporate minor and trace elements into carbonate minerals, substitution for Ca in the $CaCO_3$ structure is the most important. Aragonite preferentially incorporates cations larger than Ca (Sr, Na, Ba, U), while calcite favors the smaller Mg, Fe, Mn, Zn and Cd. Distribution coefficients, however, are generally low and only Mg, Ca, Mn, Br and Y are concentrated preferentially in carbonate rocks (Veizer, 1983).

Based on their own results and other published data, Buddemeier et al. (1981) concluded that the concentration of minor and trace alkaline earth elements in coral skeletons is controlled by calcification. In contrast, the uptake of trace metals seems to be a more complicated process that involves an intimate interplay of biological and inorganic factors.

Given the limited amount of observations, it is not possible to relate the slightly elevated concentrations of Cu, Mn and Fe in some of the corals to the hydrothermal input.

Based on the analyses of 2020 corals, Weber (1973) found that for a given genus skeletal Sr decreases with increasing temperature. Although the Sr values in corals differ from those calculated using an experimentally-determined distribution coefficient (Kinsman and Holland, 1969) they do follow the theoretically predicted trend.

In Tutum Bay three factors, closely related to the discharge of hydrothermal fluids, compete to control the incorporation of Sr into coral skeletons: 1) seawater Sr concentration, 2) temperature, and 3) growth rate. When plotted against hydrothermal component (HC) (Fig. 7-2A) a weak correlation is noticeable. This is expected, considering that the Sr concentration in the hydrothermal fluid is slightly depleted in Sr relative to seawater (Table 2-1 and 2-2) and directly comparable to the lower $^{87}Sr/^{86}Sr$ in Tutum Bay corals when compared to the "non-hydrothermal" sample (Fig. 7-5). In addition, increased venting increases the ambient water temperature, thus causing a lower Sr concentration in coral skeletons (Weber, 1973).

Growth rate variations, however, can mask any correlation between Sr and HC and may be responsible for the only weak correlation in Fig. 7-2A. Sr ions are larger and heavier than those of Ca and during times of high demand (increased growth), the slower diffusing Sr becomes depleted relative to Ca. This may explain the relatively low Sr concentration in sample C-1. C-1 is a sample from the coral that has the highest growth rate and the growth rate related kinetic effect may overprint the HC effect on Sr incorporation. If sample C-1 is excluded from the data set, the Sr values do show a significant Sr-HC (hydrothermal component) correlation (Fig. 7-2).

In the *Tridacna gigas* sample (T-1), Sr values are in good agreement with those expected for marine mollusca (Veizer, 1983). The strong discrimination against substitution for Ca in the $CaCO_3$ structure may explain the absence of minor and trace elements other than Sr. Sr correlates with $\delta^{13}C$, but not with $\delta^{18}O$ indicating that Sr incorporation into the shell is not

temperature dependent. The correlation with $\delta^{13}C$ suggests that biologic factors control Sr incorporation.

7.4.4 Geological significance

In earlier papers (e.g., Heikoop et al., 1996b) the relationship between corals and volcanic/hydrothermal activity was presented. The present study demonstrates that corals are capable of monitoring and (to a certain extent) describing the activity of shallow water hydrothermal venting. The degree to which the hydrothermal signal is preserved in the coral skeletons is astonishing, given the dilution of the discharge in Tutum Bay. Presumably, corals in a more restricted environment, and/or experiencing higher discharge levels, would respond with even more pronounced deviations in stable isotope and Sr values.

Every reef environment is a maze of micro environments. Venting activity will produce very pronounced, distinctive micro-environments (as evidenced by the distinct isotopic character of individual Tutum Bay corals), which has implications for paleoceanographic reconstruction from such settings.

It now appears that hydrothermal events are preserved relatively easily in coral skeletons and the analysis of corals may be another exploration tool available to the economic geologist. Island arcs, such as the Tabar-Feni arc, are favorable environments for the formation of epithermal ore deposits (e.g., Davies and Ballantyne, 1987) and identification of anomalous chemical and isotopic signatures in marine limestone and corals may be used to explore for paleo-hydrothermal systems in ancient island-arcs from tropical regions.

7.5 SUMMARY AND CONCLUSIONS

The hydrothermal input into Tutum Bay, although small at the time of sampling, seems to have a clear impact on the surrounding coral reef. Tutum Bay *Porites lobata* show distinctly different $^{87}Sr/^{86}Sr$, $\delta^{13}C$, $\delta^{18}O$ and Sr records when compared to the "non-hydrothermal" control sample and to other samples from Papua New Guinea. Of the various direct and indirect effects related to vent activity, thermal stress is likely the most important. The hydrothermal vents discharge fluids at a temperature of ~90°C and those corals exposed to the highest hydrothermal influence show the lowest $\delta^{18}O$ and $\delta^{13}C$ signatures. $\delta^{18}O$ values are directly affect by changing water temperature, while the $\delta^{13}C$ values are indirectly affected due to temperature induced changes in coral metabolism and growth rate. Unfortunately, the nature of the hydrothermal discharge in Tutum Bay renders the use of trace elements as recorders of hydrothermal influence nearly impossible. Low trace element concentrations in the vent fluids combined with a small hydrothermal component in the ambient seawater does not cause the uptake of substantial amounts of vent related elements into the coral skeleton. The lower Sr values when compared to the control sample are likely based on a combination of increased growth rate and decreased Sr concentration in ambient seawater due to increased hydrothermal discharge.

8. CONCLUSIONS

Compared to deep sea hydrothermal systems Tutum Bay is unique because there the source of the hydrothermal fluid is meteoric and not seawater. As a result, the physico-chemical conditions in Tutum Bay are much closer to onshore than to deep sea hydrothermal systems, with the exception that Tutum Bay vents discharge into seawater.

Ultimately they are interpreted to be the lateral extension of the vast hydrothermal system present beneath Ambitle Island and their chemical composition is the outcome of a two- or possibly three-step process: (1) Phase separation in the deep reservoir beneath Ambitle Island produces a high temperature vapor that rises upward and subsequently reacts with cooler ground water to form a low pH, CO_2-rich water of approximately 150-160°C. (2) Caused by the steep topography, this CO_2-rich fluid moves laterally towards the margin of the hydrothermal system where it mixes with the marginal upflow of the deep reservoir fluid, producing a dilute chloride water of approximately 165°C. A third step may be the entrainment of minor amounts of ground or seawater during its final ascent. Based on a B-Rb/Cs mixing model it has been estimated that approximately 10% of the deep reservoir fluid reaches the surface.

Extensive deposits of aragonite and Fe(III) oxyhydroxide are present at or just below the seafloor and precipitation from the hydrothermal solution is thought to be caused by a combination of CO_2 degassing and mixing with seawater (aragonite), and mixing with seawater only (Fe(III) oxyhydroxide). The amount of seawater mixing during precipitation was calculated from a $^{87}Sr/^{86}Sr$ mixing model. Aragonite is precipitated up to a maximum seawater fraction of approximately 11%, while above 11% and up to 55% Fe(III) oxyhydroxide is the prominent hydrothermal precipitate. Thus, interlamination of aragonite and Fe(III) oxyhydroxide probably signals abrupt, short-term changes in the physical and/or chemical conditions at and near vents. These changes are most likely directly related to the rate at which Tutum Bay vents discharge.

With the exception of unusually high arsenic values, Tutum Bay Fe(III) oxyhydroxide deposits are in many respects similar to deposits found in much deeper water. Arsenic concentrations in Tutum Bay Fe(III) oxyhydroxides are by more than an order of magnitude higher than those from other marine occurrences. The high concentrations are a direct result of the strong sorption ability of the high specific surface material, protoferrihydrite at a pH of approximately 7 and sufficient arsenic concentration in the hydrothermal fluid. Arsenic is successfully retained in the Fe(III) oxyhydroxide deposits because oxidizing conditions and high arsenic concentration allow for the formation of discrete arsenic minerals, i.e., claudetite, arsenic oxide and scorodite.

Near vent sites, primary pore space in volcaniclastic sediment and in skeletons of dead corals is almost completely occluded by hydrothermal aragonite and Fe(III) oxyhydroxide. The formation and preservation of primary porosity in carbonate platforms that were subject to "normal-marine" depositional and diagenetic processes are fairly well understood and, as a result, the inner shelf, outer shelf and slope are the prime petroleum exploration targets. The occurrence of hydrothermal activity, however, is not confined to any one location within a reef complex and subsurface processes may completely change the reef hydrogeology relative to non-hydrothermal settings. Consequently, early occlusion of pore space may have occurred in areas that are generally thought to have high primary pore space and, therefore, petroleum exploration programs in paleo island arc environments may need to establish carefully temporal and spatial relationships to prove coexistence of abiotic and skeletal carbonate. The determination of $^{87}Sr/^{86}Sr$ in aragonite may provide the necessary answer. Hydrothermal aragonite in Tutum Bay, for example, has a distinctively different isotope composition when compared to "normal" marine carbonate. This implicates marine carbonates that may have accumulated in a similar environment, if the time-dependent variations of $^{87}Sr/^{86}Sr$ are utilized for dating. According to its $^{87}Sr/^{86}Sr$, the coral aragonite from Ambitle Island would have an improbable Late Cretaceous age.

Substantial input of hydrothermal fluids into a reef environment adds to the expected, biological, climatic, and oceanographic factors that influence coral growth and carbonate precipitation in tropical, shallow-water carbonate settings. Ambitle Island, therefore, offers a natural laboratory to evaluate the short- and long-term adaptation and/or mortality of biota related to changes in temperature, salinity and carbonate saturation state.

Every reef environment is a maze of micro environments. Venting activity will produce very pronounced, distinctive micro environments, with implications for paleoceanographic reconstruction from such settings. The hydrothermal input into Tutum Bay, although small at the time of sampling, seems to have a clear impact on the surrounding coral reef. Tutum Bay *Porites lobata* show distinctly different $^{87}Sr/^{86}Sr$, $\delta^{13}C$, $\delta^{18}O$ and Sr records when compared to the "non-hydrothermal" control sample and to other samples from Papua New Guinea. In earlier papers (e.g., Heikoop et al., 1996b) the relationship between corals and volcanic/hydrothermal activity was demonstrated. This study demonstrates that corals are capable of monitoring and (to a certain extent) describing the activity of shallow water hydrothermal venting. The degree to which the hydrothermal signal is preserved in the coral skeletons is astonishing, given the dilution of the discharge in Tutum Bay. Presumably, corals in a more restricted environment, and/or experiencing higher discharge levels, would respond with even more pronounced deviations in stable isotope and Sr values. Of the various direct and indirect effects related to vent activity, thermal stress is likely the most important.

It now appears that hydrothermal events are preserved relatively easily in coral skeletons and the analysis of corals may be another exploration tool available to the economic geologist. Island arcs, such as the Tabar-Feni arc, are favorable environments for the formation of epithermal ore deposits (e.g., Davies and Ballantyne, 1987), and identification of anomalous chemical and isotopic signatures in Fe(III) oxyhydroxides, marine carbonate cements and corals may be used to explore for paleo-hydrothermal systems in ancient island-arcs from tropical regions.

LIST OF REFERENCES

Aharon, P., 1991, Recorders of reef environment histories: stable isotopes in corals, giant clams, and calcareous algae: Coral Reefs, v. 10, p. 71-90.

Ahmann, D., Roberts, A.L., Krumholz, L.R., and Morel, F.M.M., 1994, Microbe grows by reducing arsenic: Nature, v. 371, p. 750.

Allison, N., and Tudhope, A.W., 1992, Nature and significance of geochemical variations in coral skeletons as determined by ion microprobe analysis, Seventh International Coral Reef Symposium: Guam, University of Guam Marine Laboratory, p. 173-178.

Allison, W., Tudhope, A.W., and Fallick, A.E., 1996, Factors influencing the stable carbon and oxygen isotopic composition of *Porites lutea* coral skeletons from Phuket, South Thailand: Coral Reefs, v. 15, p. 43-57.

Alt, J.C., 1988, Hydrothermal oxide and nontronite deposits on seamounts in the Eastern Pacific: Marine Geology, v. 81, p. 227-239.

Alt, J.C., 1993, Low-temperature alteration of basalts from the Hawaiian Arch, Leg 136: Proceedings of the Ocean Drilling Program, Scientific Results, v. 136.

Amundson, R.G., and Kelly, E., 1987, The chemistry and mineralogy of a CO_2 -rich travertine depositing spring in the California Coast Range: Geochimica et Cosmochimica Acta, v. 51, p. 2883-2890.

Anderson, T.F., and Arthur, M.A., 1983, Stable isotopes of oxygen and carbon and their application to sedimentologic and paleoenvironmental problems, *in* Arthur, M.A., Anderson, T.F., Kaplan, I.R., Veizer, J., and Land, L.S., eds., Stable isotopes in sedimentary geology, Volume 10: Columbia, SC, SEPM Short Course, p. 1-151.

Andrews, A.J., 1980, Saponite and celadonite in layer 2 basalts, DSDP Leg 37: Contributions to Mineralogy and Petrology, v. 73, p. 323-340.

Baldi, F., 1994, Microbial transformation of metals in relation to the biogeochemical cycle, *in* Bidoglio, G., and Stumm, W., eds., Chemistry of aquatic systems; local and global

perspectives., Volume 5: Euro Courses. Chemical and Environmental Science: Dordrecht - Boston - London, Netherlands, Kluwer Academic Publishers, p. 121-152.

Bardossy, A., and Bardossy, G., 1984, Comparison of geostatistical calculations with the results of open pit mining at the Iharkut bauxite district, Hungary: a case study: Mathematical Geology, v. 16, p. 173-192.

Barnes, I., Kistler, R.W., Mariner, R.H., and Presser, T.S., 1981, Geochemical evidence on the nature of the basement rocks of the Sierra Nevada, California, U. S. Geological Survey Professional Paper 2181, 13 p.

Berger, B.R., and Silberman, M.L., 1985, Relationships of trace element patterns to geology in hot-spring type precious metal deposits, *in* Berger, B.R., and Bethke, P.M., eds., Geology and Geochemistry of Epithermal Systems, Volume Reviews in Economic Geology 2, Economic Geology, p. 232-248.

Binns, R.A., Scott, S.D., Bogdanov, Y.A., Lisitzin, A.P., Gordeev, V.V., Gurvich, E.G., Finlayson, E.J., Boyd, T., Dotter, L.E., Wheller, G.E., and Muravyev, K.G., 1993, Hydrothermal oxide and gold-rich sulfate deposits of Franklin seamount, western Woodlark Basin, Papua New Guinea: Economic Geology, v. 88, p. 2122-2153.

Bischoff, J.L., 1969, Red Sea geothermal brine deposits: their mineralogy, chemistry, and genesis, *in* Degens, E.T., and Ross, D.A., eds., Hot Brines and Recent Heavy Metal Deposits in the Red Sea: New York, Springer Verlag, p. 368-401.

Bishoff, J.L., and Dickson, F.W., 1975, Seawater basalt interaction at 200°C and 500 bars: implications for the origin of seafloor heavy metal deposits and the regulations of seawater chemistry: Earth and Planetary Science Letters, v. 25, p. 385-397.

Bonatti, E., Kraemer, T., and Rydell, H., 1972, Classification and genesis of iron-manganese deposits, *in* Horn, D.R., ed., Ferro-manganese Deposits on the Ocean Floor: New York, Harriman, Arden House and Lamont-Doherty Geological Observatory, p. 149-166.

Bottinga, Y., 1968, Calculation of fractionation factors for carbon and oxygen isotopic exchange in the system calcite-carbon dioxide-water.: Journal of Physical Chemistry, v. 72, p. 800-808.

Botz, R., Stüben, D., Winckler, G., Bayer, R., Schmitt, M., and Faber, E., 1996, Hydrothermal gases offshore Milos Island, Greece: Chemical Geology, v. 130, p. 161-173.

Bowell, R.J., 1994, Sorption of arsenic by iron oxides and oxyhydroxides in soils: Applied Geochemistry, v. 9, p. 279-286.

Boyle, R.W., and Jonasson, I.R., 1973, The geochemistry of arsenic and its use as an indicator element in geochemical prospecting: Journal of Geochemical Exploration, v. 2, p. 251-296.

Brookins, D.G., 1988, Eh-pH Diagrams for Geochemistry: New York, Springer-Verlag, 178 p.

Browne, P.R.L., 1973, Aragonite deposited from broadlands geothermal drillhole water: New Zealand Journal of Geology and Geophysics, v. 16, p. 927-933.

Bruhn, F., Bruckschen, P., Richter, D.K., Meijer, J., Stephan, A., and Veizer, J., 1995, Diagenetic history of sedimentary carbonates: Constraints from combined cathodoluminescence and trace element analyses by micro-PIXE: Nuclear Instruments and Methods, v. 104, p. 409-414.

Buddemeier, R.W., Schneider, R.C., and Smith, S.V., 1981, The alkaline chemistry of corals, Fourth International Coral Reef Symposium, Volume 2: Manila, p. 81-85.

Buhl, D., Neuser, R.D., Richter, D.K., Riedel, D., Roberts, B., Strauss, H., and Veizer, J., 1991, Nature and nurture: environmental isotope story of the river Rhine: Naturwissenschaften, v. 78, p. 337-346.

Burke, W.H., Denison, R.E., Hetherington, E.A., Koepnick, R.B., Nelson, N.F., and Otto, J.B., 1982, Variation of seawater $^{87}Sr/^{86}Sr$ throughout Phanerozoic time: Geology, v. 10, p. 516-519.

Burns, B., 1997, Vegetation change along a geothermal stress gradient at the Te Kopia steam field: Journal of the Royal Society of New Zealand, v. 27, p. 279-294.

Burton, E.A., 1993, Controls on marine carbonate cement mineralogy: review and reassessment: Chemical Geology, v. 105, p. 163-179.

Butterfield, D.A., Massoth, G.J., McDuff, R.E., Lupton, J.E., and Lilley, M.D., 1990, Geochemistry of hydrothermal fluids from Axial Seamount hydrothermal emissions study vent field, Juan de Fuca Ridge: subseafloor boiling and subsequent fluid-rock interaction: Journal of Geophysical Research, v. 95, p. 12895-12921.

Carpenter, J.H., and Grant, V.E., 1967, Concentration and state of cerium in coastal waters: Journal of Marine Research, v. 25, p. 228-238.

Carpenter, S.J., and Lohmann, K.C., 1992, Sr/Mg ratios of modern marine calcite: Empirical indicators of ocean chemistry and precipitation rate: Geochim. Cosmochim. Acta, v. 56, p. 1837-1849.

Carriquiry, J.D., Risk, M.J., and Schwarcz, H.P., 1994, Stable isotope geochemistry of corals from Costa Rica as proxy indicator of the El Nino/Southern Oscillation (ENSO): Geochimica Cosmochimica Acta, v. 58, p. 335-351.

Chacko, T., Mayeda, T.K., Clayton, R.N., and Goldsmith, J.R., 1991, Oxygen and carbon isotope fractionations between CO_2 and calcite: Geochimica et Cosmochimica Acta, v. 55, p. 2867-2882.

Chang, C.L., 1984, Triangular diagrams for predication of aquifer chemistry: Geothermal Research Council Transactions, v. 8, p. 373-376.

Chao, T.T., and Theobald, J.P.K., 1976, The significance of secondary iron and manganese oxides in geochemical exploration: Economic Geology, v. 71, p. 1560-1569.

Choquette, P.W., and Pray, L.C., 1970, Geologic nomenclature and classification of porosity in sedimentary carbonates: AAPG Bulletin, v. 54, p. 207-250.

Chuck, R.T., 1967, Groundwater resources development on tropical islands of volcanic origin, Int. Conf. Water for Peace, Volume 2: Washington, D. C., p. 963-970.

Churkhov, F.V., Groshkov, A.I., Zirijagin, B.B., Yermilova, L.P., and Balashova, V.V., 1973, Ferrihydrite: International Geology Review, v. 16, p. 1131-1143.

Cioni, R., and D'Amore, F., 1984, A genetic model for the crater fumaroles of Vulcano Island (Sicily, Italy): Geothermics, v. 13, p. 375-384.

Clark, I.D., and Fritz, P., 1997, Environmental isotopes in hydrogeology: Boca Raton, Lewis Publishers, 328 p.

Coles, S.J., and Jokiel, P.L., 1992, Effects of salinity on coral reefs, *in* Connell, D., and Hawker, D., eds., Pollution in Tropical Aquatic Systems: Boca Raton, CRC, p. 125-137.

Conway, N.M., Kennicutt II, M.C., and Van Dover, C.L., 1994, Stable isotopes in the study of marine chemosynthetic-based ecosystems, *in* Lajtha, K., and Michener, R.H., eds., Stable Isotopes in Ecology and Environmental Science: London, Blackwell Scientific Publications, p. 158-186.

Craig, H., 1963, The isotopic geochemistry of water and carbon in geothermal areas, *in* Tongiori, E., ed., Nuclear geology in thermal areas: Spoleto, CNR, p. 17-53.

Craig, H., 1966, Isotopic composition and origin of the Red Sea and Salton Sea geothermal brines: Science, v. 154, p. 1544-1548.

Cremer, M.D., 1995, Geochemistry of hydrothermal deposits from the summit region of Loihi Seamount, Hawaii [M.Sc. thesis]: Honolulu, University of Hawaii.

Dando, P.R., and Leahy, Y., 1993, Hydrothermal activity off Milos, Hellenic Volcanic Arc: BRIDGE News, p. 20-21.

Dandurand, J.L., Gout, R., Hefs, J., Menschel, G., Schott, J., and Usdowski, E., 1982, Kinetically controlled variations of major components and carbon and oxygen isotopes in a calcite-precipitating spring: Chemical Geology, v. 36, p. 299-315.

Davies, R.M., and Ballantyne, G.H., 1987, Geology of the Ladolam gold deposit Lihir Island, Papua New Guinea, Pacific Rim Congress 87: Gold Coast, Australia, Australasian Institute of Mining and Metallurgy, p. 943-949.

Davis, J.A., Fuller, C.C., Rea, B.A., and Claypool-Frey, R.G., 1989, Sorption and coprecipitation of arsenate by ferrihydrite, Water-Rock Interaction: Rotterdam, Balkema, p. 187-189.

Davis, J.A., and Kent, D.B., 1991, Surface complexation modeling in aqueous geochemistry, *in* Hochella, M.F., and White, A.F., eds., Mineral-water Interface geochemistry, Volume 23: Reviews in Mineralogy: Washington, Mineralogical Society of America, p. 177-260.

De Ronde, C.E.J., 1995, Fluid chemistry and isotopic characteristics of seafloor hydrothermal systems and associated VMS deposits: potential for magmatic contributions, *in* Thompson, J.F.H., ed., Magmas, Fluids, and Ore Deposits, Volume 23: Mineralogical Association of Canada Short Course Series: Victoria, Mineralogical Association of Canada, p. 479-509.

Deer, W.A., Howie, R.A., and Zussmann, J., 1992, An introduction to the rock-forming minerals: Essex, Longman Scientific & Technical, 696 p.

Delaney, J.R., and Cosens, B.A., 1982, Boiling and metal deposition in submarine hydrothermal systems: Marine Technology Soceity Journal, v. 16, p. 62-66.

Derochers, A., and Al-Aasm, I.S., 1993, The formation of septarian concretions in Queen Charlotte Islands, B.C.: evidence for microbially and hydrothermally mediated reactions at shallow burial depth: Journal of Sedimentary Petrology, v. 63, p. 282-294.

Diener, A., Ebneth, S., Veizer, J., and Buhl, D., 1996, Strontium isotope stratigraphy of the Middle Devonian: brachiopods and conodonts: Geochimica Cosmochimica Acta, v. 60, p. 639-652.

Dodge, R.E., and Gillbert, T.R., 1984, Chronology of lead pollution contained in banded coral skeletons: Marine Biology, v. 82, p. 9-13.

Drever, J.I., 1982, The geochemistry of natural waters: Englewood Cliffs, Prentice-Hall, 392 p.

Drummond, S.E., and Ohmoto, H., 1985, Chemical evolution and mineral deposition in boiling hydrothermal systems: Economic Geology, v. 80, p. 126-147.

Dzombak, D.A., and Morel, F.M.M., 1990, Surface complexation modeling: Hydrous ferric oxide: New York, Wiley-Interscience.

Ellis, A.J., and Mahon, W.A.J., 1977, Chemistry and Geothermal Systems: New York, Academic Press, 392 p.

Faure, G., 1986, Principles of Isotope Geochemistry: New York, John Wiley & Sons, 589 p.

Fleet, A.J., 1984, Aqueous and sedimentary geochemistry of the rare earth elements, *in* Henderson, P., ed., Rare Earth Element Geochemistry, Volume 2: In Developments in Geochemistry, Elsevier, p. 343-373.

Folk, R.L., 1965, Some aspects of recrystallization in ancient limestones, *in* Pray, L.C., and Murray, R.C., eds., Dolomitization and Limestone Diagensis, Volume 13: Special Publications, Society of Economic Paleontologists and Mineralogists, p. 14-48.

Folk, R.L., 1994, Interaction between bacteria, nannobacteria, and mineral precipitation in hot springs of central Italy: Geographie Physique et Quaternaire, v. 48, p. 233-246.

Fortin, D., Leppard, G.G., and Tessier, A., 1993, Characteristics of lacustine diagenetic iron oxyhydroxides: Geochimica Cosmochimica Acta, v. 57, p. 4391-4404.

Fournier, R.O., 1977, Chemical geothermometers and mixing models for geothermal systems: Geothermics, v. 5, p. 41-50.

Fournier, R.O., 1979, A revised equation for the Na/K geothermometer: Geothermal Research Council Transactions, v. 3, p. 221-224.

Fournier, R.O., 1985, The behavior of silica in hydrothermal solutions, *in* Berger, B.R., and Bethke, P.M., eds., Geology and Geochemistry of Epithermal Systems, Volume Reviews in Economic Geology 2, Economic Geology, p. 45-61.

Fournier, R.O., and Truesdell, A.H., 1973, An empirical Na-K-Ca geothermometer for natural waters: Geochimica et Cosmochimica Acta, v. 37, p. 1255-1275.

Friedman, I., and O'Neil, J.R., 1977, Compilation of stable isotope fractionation factors of geochemical interest, *in* Fleisher, M., ed., Data of Geochemistry, Volume 440-KK: Washington, U.S. Geological Survey Professional Paper, p. 12.

Fritz, P., and Frape, S.K., 1982, Saline groundwaters in the Canadian Shield - a first overview: Chemical Geology, v. 36, p. 179-190.

Gagan, M.K., Chivas, A.R., and Isdale, P.J., 1994, High-resolution records form corals using temperature and mass-spawning chronometers: Earth andPlanetary Science Letters, v. 121, p. 549-558.

Gallahan, W.E., and Duncan, R.A., 1994, Spatial and temporal variability in crystallisation of celadonites within the Troodos Ophiolite, Cyprus: Implications for low-temperature alteration of the oceanic crust: Journal of Geophysical Research, v. 99, p. 3147-3161.

Gebel, T., Christensen, S., and Dunkelberg, H., 1997, Comparative and environmental genotoxicity of antimony and arsenic: Anticancer Research, v. 17, p. 2603-2607.

Giessen, A.A., 1966, The structure of iron (III) oxide hydrate gel: Journal of Inorganic Nuclear Chemistry, v. 28.

Giggenbach, W., 1988, Geothermal solute equilibria. Derivation of Na-K-Mg-Ca geoindicators: Geochimica et Cosmochimica Acta, v. 52, p. 2749-2765.

Giggenbach, W.F., 1982, Carbon-13 exchange between CO_2 and CH_4 under geothermal conditions: Geochimica Cosmochimica Acta, v. 46, p. 159-165.

Giggenbach, W.F., 1991, Chemical techniques in geothermal exploration, *in* D'Amore, F., ed., Application of geochemistry in geothermal reservoir development: Rome, UNITAR/UNDP, p. 252-270.

Giggenbach, W.F., 1992, Isotopic shifts in waters from geothermal and volcanic systems along convergent plate boundaries and their origin: Earth and Planetary Science Letters, v. 113, p. 495-510.

Giggenbach, W.F., 1995a, Variations in the chemical and isotopic composition of fluids discharged from the Taupo Volcanic Zone, New Zealand: Journal of Volcanology and Geothermal Research, v. 68, p. 89-116.

Giggenbach, W.F., 1995b, Composition of fluids in geothermal systems of the Taupo Volcanic Zone, New Zealand, as a function of source magma, International Symposium Water-Rock Interaction, Volume 8: Vladivostok, p. 9-12.

Giggenbach, W.F., 1997, The origin and evolution of fluids in magmatic-hydrothermal systems, *in* Barnes, H.L., ed., Geochemistry of hydrothermal ore deposits: New York, Wiley, p. 737-796.

Giggenbach, W.F., and Goguel, R.L., 1989, Collection and analysis of geothermal and volcanic water and gas discharges, NZ DSIR.

Giggenbach, W.F., Hedenquist, J.W., Houghton, B.F., Otway, P.M., and Allis, R.G., 1989, Research drilling into the volcanic hydrothermal system on White Island, New Zealand: EOS (Transactions, American Geophysical Union), v. 70, p. 98-109.

Giggenbach, W.F., and Matsuo, S., 1991, Evaluation of results from second and third IAVCEI Field Workshops on Volcanic Gases, Mt. Usu, Japan, and White Island, New Zealand: Applied Geochemistry, v. 6, p. 125-141.

Goldberg, E.D., 1961, Chemistry in the oceans, *in* Sears, M., ed., Oceanography, Volume 67, American Association of Advanced Scientific Publications, p. 583-597.

Goldberg, E.D., Koide, M., Schmitt, R.A., and Smith, R.H., 1963, Rare earth distributions in the marine environment: Journal of Geophysical Research, v. 68, p. 4209-4217.

Gonzalez, L.A., and Lohmann, K.C., 1985, Carbon and oxygen isotopic composition of Holocene reefal carbonates: Geology, v. 13, p. 811-814.

Grossman, E.L., and Ku, T.-L., 1986, Oxygen and carbon isotope fractionation in biogenic aragonite: Temperature effects: Chemical Geology, v. 59, p. 59-74.

Gude, A.J., and Sheppard, R.A., 1972, Silhydrite, a new mineral from Trinity County, California: American Mineralogist, v. 57, p. 1053-1065.

HACH Company, 1992. Digital titrator model 16900-01 manual. Loveland, Colorado. 47 pp.

Hall, G.E.M., Vaive, J.E., and McConnell, J.W., 1995, Development and application of a sensitive and rapid analytical method to determine the rare-earth elements in surface waters: Chemical Geology, v. 120, p. 91-109.

Hall, G.E.M., Vaive, J.E., and Pelchat, J.C., 1996, Performance of inductively coupled plasma mass spectrometric methods used in determination of trace elements in surface waters in hydrogeochemical surveys: Journal of Analytical Atomic Spectrometry, v. 11, p. 779-786.

Haskin, L.A., Haskin, M.A., Frey, F.A., and Wildman, T.R., 1968, Relative and absolute terrstrial abundance of the rare earths, *in* Ahrens, L.H., ed., Origin and distribution of the elements, Volume 1: Oxford, Pergamon, p. 889-911.

Hedenquist, J.W., 1990, The thermal and geochemical structure of the Broadlands-Ohaaki geothermal system, New Zealand: Geothermics, v. 19, p. 151-185.

Heikoop, J.M., 1997, Environmental Signals in Coral Tissue and Skeleton: Examples form the Caribbean and Indo-Pacific [Ph.D. thesis]: Hamilton, McMaster University.

Heikoop, J.M., Tsujita, C.J., Risk, M.J., Tomascik, T., and Mah, A.J., 1996a, Modern iron ooids from a shallow-marine volcanic setting: Magengetang, Indonesia: Geology, v. 24, p. 759-762.

Heikoop, J.M., Tsujita, C.J., Risk, M.J., and Tomascik, T., 1996b, Corals as proxy recorders of volcanic activity: evedence from Banda Api, Indonesia: Palaios, v. 11, p. 286-292.

Hein, J.R., Yeh, H.-W., Gunn, S.H., Gibbs, A.E., and Wang, C.-H., 1994, Composition and origin of hydrothermal ironstones from central Pacific seamounts: Geochimica et Cosmochimica Acta, v. 58, p. 179-189.

Hekinian, R., Hoffert, M., Larqué, P., Chemineé, J.-L., Stoffers, P., and Bideau, D., 1993, Hydrothermal Fe and Si oxyhydroxide deposits from South Pacific intraplate volcanoes

and East Pacific Rise axial and off-axial regions: Economic Geology, v. 88, p. 2099-2121.

Henley, R.W., and Ellis, A.J., 1983, Geothermal systems ancient and modern: a geothermical review: Earth-Science Reviews, v. 19, p. 1-50.

Henley, R.W., Truesdell, A.H., and Barton, P.B.J., 1984, Fluid-mineral equilibria in hydrothermal systems, Society of Economic Geologists, 267 p.

Hodkinson, R.A., Cronan, D.S., Varnavas, S., and Perissoratis, C., 1994, Regional geochemistry of sediments from the Hellenic Volcani Arc in regard to submarine hydrothermal activity: Marine Georesources and Geotechnology, v. 12, p. 83-129.

Hoefs, J., 1997, Stable isotope geochemistry: Berlin, Springer, 202 p.

Hovland, M., 1990, Do Carbonate reefs form due to fluid seepage?: Terra Nova, v. 2, p. 8-18.

Johnson, R.W., Perfit, M.R., Chappell, B.W., Jaques, A.L., Shuster, R.D., and Ridley, W.I., 1988, Volcanism in the New Ireland basin and Manus island region: Notes on the geochemistry and petrology of some dredged volcanic rocks from a rifted-arc region, *in* Marlow, M.S., Dadisman, S.V., and Exon, N.F., eds., Geology and offshore resources of Pacific island arcs-New Ireland and Manus region, Papua New Guinea, Volume 9: Houston, Circum-Pacific Council for Energy and Mineral Resources, p. 113-130.

Jokiel, P.L., and Coles, S.J., 1990, Response of Hawaiian and other Indo-Pacific reef corals to elevated temperature: Coral Reefs, v. 8, p. 155-62.

Jones, B., and Renaut, R.W., 1996, Morphology and growth of aragonite crystals in hot-spring travertines at Lake Bogoria, Kenya Rift Valley: Sedimentology, v. 43, p. 323-340.

Jordan, C.F., Jr., and Wilson, J.L., 1994, Carbonate reservoir rocks, *in* Magoon, L.B., and Dow, W.G., eds., The petroleum system-from source to trap, Volume AAPG Memoir 60: Tulsa, Oklahoma, American Association of Petroleum Geologists, p. 141-158.

Kaufman, E.G., Arthur, M.A., Howe, B., and Scholle, P.A., 1996, Widespread venting of methane-rich fluids in late cretaceous (Campanian) submarine springs (Tepee Buttes), Western Intererior seaway, U.S.A.: Geology, v. 24, p. 799-802.

Kharaka, Y.K., and Lico, M.S., 1982, Chemical geothermometers applied to formation waters, Gulf of Mexico and California basins: AAPG Bulletin, v. 66, p. 588-598.

Kharaka, Y.K., and Mariner, R.H., 1989, Chemical geothermometers and their application to formation waters from sedimentary basins, *in* Naeser, N.D., and McCulloch, T.H., eds., Thermal history of sedimentary bsins: methods and case histories: New York, Springer Verlag, p. 99-117.

Kim, S.-T., 1997, Equilbrium and nonequilibrium oxygen isotope effects in synthetic carbonates: Geochimica Cosmochimica Acta, v. 61, p. 3461-3475.

Kinsman, D.J.J., and Holland, H.D., 1969, The coprecipitation of cations with $CaCO_3$ IV. The coprecipitation of Sr^{2+} with aragonite between 16 and 96°C: Geochimica Cosmochimica Acta, v. 33, p. 1-17.

Klein, R., Patzold, J., Wefer, G., and Loya, Y., 1992, Seasonal variations in the stable isotopic composition and the skeletal density pattern of the coral Porites lobata (Gulf of Eilat, Red Sea): Marine Biology, v. 112, p. 259-263.

Klemme, H.D., and Ulmishek, G.F., 1991, Effective petroleum source rocks of the world-stratigraphic distribution and controlling depositional factors: AAPG Bulletin, v. 75, p. 1809-1851.

Knutson, D.W., Buddemeier, R.W., and Smith, S.V., 1972, Coral chronometers: seasonal growth bands in reeef corals: Science, v. 177, p. 270-272.

Koeppenkastrop, D., and De Carlo, E.H., 1992, Sorption of rare-earth elements from seawater onto synthetic mineral particles: An experimental approach: Chemical Geology, v. 95, p. 251-263.

Koeppenkastrop, D., De Carlo, E.H., and Roth, M., 1991, A method to investigate the interaction of rare earth elements in aqueous solution with metal oxides: Journal Radioanalysis and Nuclear Chemistry, v. 152, p. 337-346.

Leblanc, M., Achard, B., Othmann, D.B., Luck, J.M., Bertand-Sarfati, J., and Personne, J.C., 1996, Accumulation of arsenic from acid mine waters by ferruginous bacterial accretions (stromatolites): Applied Geochemistry, v. 11, p. 541-554.

Lee, J.H., and Bryne, R.H., 1993, Complexation of trivalent rare earth elements (Ce, Eu, Gd, Tb, Yb) by carbonate ions: Geochimica Cosmochimica Acta, v. 57, p. 295-302.

Licence, P.S., Terrill, J.E., and Fergusson, L.J., 1987, Epithermal gold mineralization, Ambitle Island, Papua New Guinea, Pacific Rim Congress 87: Gold Coast, Queensland, Australasian Institute of Mining and Metallurgy, p. 273-278.

Linsley, B.K., Dunbar, R.B., Wellington, G.M., and Mucciarone, D.A., 1994, A coral based reconstruction of Intertropical Convergence Zone variability over Central America since 1707: Journal of Geophysical Research, v. 99, p. 9977-9994.

Longman, M.W., 1982, Carbonate diagenesis as a control on stratigraphic traps, Volume 21: Geological Education Course Notes, American Association of Petroleum Geologists, 159 p.

Lorens, R.B., 1981, Sr, Cd, Mn and Co distribution coeficients in calcite as a function of calcite precipitation rate: Geochimica Cosmochimica Acta, v. 45, p. 553-561.

Lough, J.M., and Barnes, D.J., 1992, Comparisons of skeletal density variations in Porites from the central Great Barrier Reef: Journal of Experimental Marine Biology and Ecology, v. 155, p. 1-25.

Lupton, J.E., and Craig, H., 1981, A major helium-3 source at 15°S on the East Pacific Rise: Science, v. 214, p. 13-18.

Lupton, J.E., Delaney, J.R., Johnson, H.P., and Tivey, M.K., 1985, Entrainment and vertical transport of deep-ocean water by buoyant hydrothermal plumes: Nature, v. 316, p. 621-623.

Lyon, G.L., and Hulston, J.R., 1984, Carbon and hydrogen isotopic compositions of New Zealand geothermal gases: Geochimica et Cosmochimica Acta, v. 48, p. 1161-1171.

Manning, B.A., and Goldberg, S., 1997, Adsorption and stability of arsenic(III) at the clay mineral-water interface: Environmental Science & Technology, v. 31, p. 2005-2011.

Maxwell, J.A., Teesdale, W.J., and Campbell, J.L., 1989, The Guelph PIXE software package: Nuclear Instruments and Methods in Physics Research, v. B43, p. 218-230.

Maxwell, J.A., Teesdale, W.J., and Campbell, J.L., 1995, The Guelph PIXE software package II: Nuclear Instruments and Methods in Physics Research, v. B95, p. 407-421.

Mazzullo, S.L., and Harris, P.M., 1992, Mesogenetic dissolution: its role in porosity development in carbonate reservoirs: AAPG Bulletin, v. 76, p. 607-620.

McConnaughey, T., 1989a, ^{13}C and ^{18}O isotopic disequilibrium in biological carbonates: I. Patterns: Geochimica Cosmochimica Acta, v. 53, p. 151-162.

McConnaughey, T., 1989b, ^{13}C and ^{18}O isotopic disequilibrium in biological carbonates: II. In vitro simulation of kinetic isotope effects: Geochimica Cosmochimica Acta, v. 53, p. 163-171.

McConnaughey, T.A., and Whelan, J.F., 1997, Calcification generates protons for nutrient and bicarbonate uptake: Earth-Science Reviews, v. 42, p. 95-117.

McCulloch, M.T., Gagan, M.K., Mortimer, G.E., Chivas, A.R., and Isdale, P., 1994, A high-resolution Sr/Ca and $\delta^{18}O$ coral record from the Great Barrier Reef, Australia and the 1982-1983 El Nino: Geochimica et Cosmochimica Acta, v. 58, p. 2747-2754.

McInnes, B.I.A., and Cameron, E.M., 1994, Carbonated, alkaline metasomatic melts from a sub-arc environment: Mantle wedge samples from the Tabar-Lihir-Tanga-Feni arc, Papua New Guinea: Earth and Planetary Science Letters, v. 122, p. 125-141.

McMurtry, G.M., and Yeh, H.W., 1981, Hydrothermal clay mineral formation of East Pacific Rise and Bauer Basin sediments: Geology, v. 32, p. 189-205.

Merlino, S., 1983, Okenite: the first example of a chain and sheet silicate: American Mineralogist, v. 68, p. 614-622.

Michard, A., 1989, Rare earth element systematics in hydrothermal fluids: Geochimica Cosmochimica Acta, v. 53, p. 745-750.

Millero, F.J., Sotolongo, S., and Izaguirre, M., 1987, The oxidation kinetics of Fe(II) in seawater: Geochimica Cosmochimica Acta, v. 51, p. 793-801.

Moore, C.H., 1989, Carbonate Diagenesis and Porosity: Amsterdam, Elsevier, 338 p.

Morgan, J.J., and Stumm, W., 1964, Colloid-chemical propeties of manganese dioxides: Journal of Colloid Science, v. 9, p. 347-359.

Müller, D., and Groves, D.I., 1993, Direct and indirect associations between potassic igneous rocks, shoshonites and gold-copper deposits: Ore Geology Reviews, v. 8, p. 383-406.

Murnane, R., and Clague, D.A., 1983, Nontronite from a low-temperature hydrothermal system on the Juan de Fuca Ridge: Earth Planet. Sci. Lett., v. 65, p. 343-352.

Murray, J.W., 1979, Iron oxides, *in* Burns, R.G., ed., Marine minerals, Volume 6: Washington, Mineralogical Society of America, p. 47-98.

Nahm, G.-Y., 1966, Geology and groundwater resources of volcanic island, Cheju-do: Geology and Ground-Water Resources, v. 3, p. 109-133.

Nicholson, K., 1992, Geothermal fluids, Springer Verlag, 266 p.

O'Neill, P., 1990, Arsenic, *in* Pacey, G.E., and Ford, J.A., eds., Heavy metals in soils: Glasgow, Blackie, p. 83-99.

Oberdorfer, J.A., and Buddemeier, R.W., 1985, Coral reef hydrogeology, Proceedings of the Fifth International Coral Reef Congress, Volume 3: Tahiti, p. 307-312.

Ohmoto, H., and Rye, R.O., 1979, Isotopes of Sulfur and Carbon, *in* Barnes, H.L., ed., Geochemistry of Hydrothermal Ore Deposits: New York, Wiley, p. 509-567.

Olivarez, A.M., and Owen, R.M., 1989, REE/Fe variations in hydrothermal sediments: Implications for the REE content of seawater: Geochimica et Cosmochimica Acta, v. 53, p. 757-762.

Parker, R.J., and Nicholson, K., 1990, Arsenic in geothermal sinters: determineation and implications for mineral exploration, *in* Harvey, C.C., Browne, P.R.L., Freestone, D.H., and Scott, G.L., eds., 12th NZ Geothermal Workshop: Auckland, Auckland University, p. 35-39.

Parkhust, D.L., 1995, User's guide to PHREEQC - A computer program for speciation, reaction-path, advective-transport, and inverse geochemical calculations: Lakewood, CO, U.S. Department of the Interior.

Patzold, J., 1984, Growth rhythms recorded in stable isotopes and density bands in the reef coral Porites lobata (Cebu, Phillipines): Coral Reefs, v. 3, p. 87-90.

Pichler, T., Hannington, M.D., McInnes, B.I.A., Watkinson, D.H., and Staff, K.a.L.M.C., 1995, Shallow submarine venting in the Tabar-Feni Arc: Mineralogy and geochemistry of hydrothermal precipitates, Geological Association of Canada/Mineralogical Association of Canada Annual Meeting: Victoria, British Columbia, p. A-83.

Pichler, T., and Hutchinson, R.W., 1993, Gold Mineralization in the Marine Environment: A possible Marine Mineral Exploration and Mining Target, 24th Underwater Mining Institute: Estes Park, Colorado.

Pierce, M.L., and Moore, C.B., 1980, Adsorption of arsenite on amorphous iron hydroxide from dilute aqueous solution: Environmental Science & Technology, v. 14, p. 214-216.

Poorter, R.P.E., Varekamp, J.C., Poreda, R.J., van, B.M.J., and Kreulen, R., 1991, Chemical and isotopic compositions of volcanic gases from the East Sunda and Banda arcs, Indonesia: Geochimica et Cosmochimica Acta, v. 55, p. 3795-3807.

Puteanus, D., Glasby, G.P., Stoffers, P., and Kunzendorf, H., 1991, Hydrothermal iron-rich deposits from the Teahitia-Mehitia and Macdonald hot spot areas, Southwest Pacific: Marine Geology, v. 98, p. 389-409.

Quinn, T.M., Taylor, F.W., Crowley, T.J., and Link, S.M., 1996, Evaluation of sampling resolution in coral stable isotope records: a case study using records from New Caledonia and Tarawa: Paleoceanography, v. 11, p. 529-542.

Rad, v., U., Frenzel, G., and Muehe, R., 1990, Origin and alteration of submarine volcanoclastic rocks from the Lau and North Fiji basins: Geolgisches Jahrbuch, v. D 92, p. 341-393.

Renaut, R.W., and Jones, B., 1997, Controls on aragonte and calcite precipitation in hot spring travertines at Chemurkeu, Lake Bogoria, Kenya: Canadian Journal of Earth Sciences, v. 34, p. 801-818.

Rimstidt, J.D., and Barnes, H.L., 1980, The kinetics of silica-water reactions: Geochimica Cosmochimica Acta, v. 44, p. 1683-1699.

Roehl, P.O., and Choquette, P.W., 1985, Carbonate Petroleum Reservoirs: New York, Springer-Verlag, 622 p.

Romanek, C.S., and Grossman, E.L., 1989, Stable isotope profiles of *Tridacna maxima* as environmental indicators: Palaios, v. 4, p. 402-413.

Romanek, C.S., Grossman, E.L., and Morse, J.W., 1992, Carbon isotopic fractionation in synthetic aragonite and calcite; effects of temperature and precipitation rate: Geochimica et Cosmochimica Acta, v. 56, p. 419-430.

Rona, P.A., 1984, Hydrothermal mineralization at seafloor spreading centers: Earth-Science Reviews, v. 20, p. 1-104.

Sandberg, P.A., 1985, Aragonite cements and their occurrence in ancient limestones, *in* Schneidermann, N., and Harris, P.M., eds., Carbonate Cements, Volume 36, Society of Economic Paleontologists and Mineralogists Special Publication, p. 33-57.

Sarano, F., Murphy, R.C., Houghton, B.F., and Hedenquist, J.W., 1989, Preliminary observations of submarine geothermal activity in the vicinity of White Island Volcano, Taupo Volcanic Zone, New Zealand: Journal of the Royal Society of New Zealand, v. 4, p. 449-459.

Schwertmann, U., 1966, Die Bildung von Eisenoxidmineralien: Fortschritte der Mineralogie, v. 46, p. 274-285.

Schwertmann, U., 1970, Der Einfluss einfacher organischer Anionen auf die Bildung von Goethit und Haematit aus amorphen Fe(III) hydroxid: Geoderma, v. 3, p. 207-214.

Schwertmann, U., and Fischer, R.W., 1973, Natural "amorphous" ferric hydroxide: Geoderma, v. 10, p. 237-247.

Sedwick, P., and Stüben, D., 1996, Chemistry of shallow submarine warm springs in an arc-volcanic setting: Vulcano Island, Aeolian Archipelago, Italy: Marine Chemistry, v. 53, p. 146-161.

Seward, T.M., 1989, The hydrothermal chemistry of gold and its implications for ore formation: Boiling and conductive cooling as examples: Economic Geology Monograph, v. 6, p. 398-404.

Seward, T.M., and Sheppard, D.S., 1986, Waimangu geothermal field, *in* Henley, R.W., Hedenquist, J.W., and Roberts, P.J., eds., Guide to active epithermal (geothermal) systems and precious metal deposits of New Zealand: Berlin, Gebrueder Borntraeger, p. 81-91.

Shen, G.T., and Boyle, E.A., 1987, Cadmium in corals as a tracer of historical upwelling and industrial fallout: Nature, v. 328, p. 794-796.

Silberman, M.L., and Berger, B.R., 1985, Relationships of trace element patterns to alteration and morphology in epithermal precious metal deposits, *in* Berger, B.R., and Bethke, P.M., eds., Geology and Geochemistry of Epithermal Systems, Volume Reviews in Economic Geology 2, Economic Geology, p. 203-232.

Simmons, S.F., and Christenson, B.W., 1994, Origins of calcite in a boiling geothermal system: American Journal of Science, v. 294, p. 361-400.

Smith, S.V., and Buddemeier, R.W., 1992, Global change and coral reef ecosystems: , v. 23, p. 89-118.

Speer, J.A., 1983, Crystal chemistry and phase relations of orthorhombic carbonates, *in* Reeder, R.J., ed., Carbonates: Mineralogy and Chemistry, Volume 11: Reviews in Mineralogy: Washington, Mineralogical Society of America, p. 145-189.

Stakes, D.S., and Scheidegger, K.F., 1981, Temporal variations in secondary minerals from Nazca Plate basalts, *in* Kulm, L.D., ed., Nazca Plate: Crustal formation and Andean convergence, Volume Memoir 154, Geological Society of America, p. 109-130.

Stoffers, P., and Botz, R., 1994, Formation of hydothermal carbonate in Lake Tanganyika, East-Central Africa: Chemical Geology, v. 115, p. 117-122.

Stoffers, P., Glasby, G.P., Stüben, D., Renner, R.M., Pierre, T.G., Webb, J., and Cardile, C.M., 1993, Comparative mineralogy and geochemistry of hydrothermal iron-rich crusts from the Pitcairn, Teahitia-Meahitia, and Macdonald hot spot areas of the S.W. Pacific: Marine Georesources and Geotechnology, v. 11, p. 45-86.

Stoffers, P., Singer, A., McMurtry, G.M., Arquit, A., and Yeh, H.-W., 1990, Geochemistry of a hydrothermal nontronite deposit from the Lau Basin, southwest Pacific: Geologisches Jahrbuch, v. D 92, p. 615-628.

Stumm, W., and Morgan, J.J., 1996, Aquatic Chemistry: New York, Wiley-Interscience, 1022 p.

Swan, A.R.H., and Sandilands, M., 1995, Introduction to geological data analysis: Oxford, Blackwell Science, 446 p.

Swart, P.K., 1983, Carbon and oxygen isotope fractionation in scleractinian corals: a review: Earth Science Reviews, v. 19, p. 51-80.

Switzer, D.G., 1997, Recent benthic foraminifera in a shallow hydrothermally vented patch reef off Ambitle Island, Papua New Guinea [B. Sc. Honors thesis]: Ottawa, Carleton University.

Tarutani, T., Clayton, R.N., and Mayeda, T.K., 1969, The effect of polymorphism and magnesium substitution on oxygen isotope fractionation between calcium carbonate and water: Geochimica et Cosmochimica Acta, v. 33, p. 987-996.

Thompson, G., 1991, Metamorphic and hydrothermal processes: basalt-seawater interactions, *in* Floyd, P.A., ed., Oceanic Basalts: Glasgow and London, Blackie, p. 148-173.

Tomascik, T., Van Woesik, R., and Mah, A.J., 1996, Rapid recolonization of a recent lava flow following a volcanic eruption, Banda Islands, Indonesia: Coral Reefs, v. 15, p. 169-175.

Tonani, F., 1970, Geochemical methods of exploration for geothermal energy: Geothermics, v. 2, p. 492-515.

Towe, K.M., and Bradley, W.F., 1967, Mineralogical constitution of colloidal "hydrous ferric oxides": Journal of Colloid and Interface Science, v. 24, p. 384-392.

Truesdell, A.H., Nathenson, M., and Rye, R.O., 1977, The effects of subsurface boiling and dilution on the isotopic composition of Yellowstone thermal waters: Journal of Geophysical Research, v. 82, p. 3694-3703.

Tucker, M.E., and Wright, V.P., 1990, Carbonate Sedimentology: Oxford, Blackwell Scientific Publications, 483 p.

Tudhope, A.W., Shimmield, G.B., Chilcott, C.P., Jebb, M., Fallick, A.E., and Dalgleish, A.N., 1995, Recent changes in the far western equatorial Pacific and their relationship to the Southern Oscillation; oxygen isotope records from massive corals, Papua New Guinea: Earth and Planetary Science Letters, v. 136, p. 575-590.

Usdowski, E., Hoefs, J., and Menschel, G., 1979, Relationship between ^{13}C and ^{18}O fractionation and changes in major element composition in a recent calcite-depositing spring - a model of chemical variations with inorganic $CaCO_3$ precipitation: Earth and Planetary Science Letters, v. 42, p. 267-276.

Varnavas, S.P., and Cronan, D.S., 1991, Hydrothermal metallogenic processes off the islands of Nisiros and Kos in the Hellenic Volcanic Arc: Marine Geology, v. 99, p. 109-133.

Veizer, J., 1983, Chemical diagenesis of carbonate rocks: theory and application of trace element technique, *in* Arthur, M.A., and Anderson, T.F., eds., Stable Isotopes in

Sedimentary Geology, Volume Short Course No. 10, Society of Economic Paleontologists and Mineralogists, p. 3.1-3.100.

Veizer, J., 1989, Strontium isotopes in seawater through time: Annual Reviews Earth and Planetary Science Letters, v. 17, p. 141-167.

Vidal, M.V., Vidal, F.V., and Isaacs, J.D., 1981, Coastal submarine hydrothermal activity off northern Baja California 2. Evolutionary history and isotope geochemistry: Journal of Geophysical Research, v. 86, p. 9451-9468.

Vidal, M.V., Vidal, F.V., Isaacs, J.D., and Young, D.R., 1978, Coastal submarine hydrothermal activity off northern Baja California: Journal of Geophysical Research, v. 83, p. 1757-1774.

Von Bitter, P.H:, Scott, S.D., and Schenk, P.E., 1990, Early Carboniferous low-temperature hydrothermal vent communities from Newfoundland: Nature, v. 344, p. 145-148.

Von Damm, K.L., 1990, Seafloor hydrothermal activity: black smoker chemistry and chimneys: Annual Review of Earth and Planetary Sciences, v. 18, p. 173-204.

Von Damm, K.L., 1995, Controls on the chemistry and temporal variability of seafloor hydrothermal systems, *in* Humphries, S.E., Zierenberg, R.A., Mullineaux, L.S., and Thomson, R.E., eds., Seafloor hydrothermal systems, Volume Geophysical Monograph 91, American Geophysical Union, p. 222-247.

Vuataz, F.-D., and Goff, F., 1986, Isotope geochemistry of thermal and non-thermal waters in the Valles caldera, Jemez Mountains, Northern New Mexico: Journal of Geophysical Research, v. 91, p. 1835-1853.

Vuataz, F.-D., Goff, F., Foulliac, C., and Calvez, J.-Y., 1988, A strontium isotope study of the VC-1 core hole and associated hydrothermal fluids and rocks from Valles Caldera, Jemez Mountains, New Mexico: Journal of Geophysical Research, v. 93, p. 6059-6067.

Wallace, D.A., Johnson, R.W., Chappell, B.W., Arculus, R.J., Perfit, M.R., and Crick, I.H., 1983, Cainozoic volcanism of the Tabar, Lihir, Tanga, and Feni islands, Papua

New Guinea: Geology, whole-rock analyses, and rock-forming mineral compositions, Bureau of Mineral Resources Geology and Geophysics.

Weber, J.N., 1973, Incorporation of strontium into reef coral skeletal carbonate: Geochimica Cosmochimica Acta, v. 37, p. 2173-2190.

Weber, J.N., White, E.W., and Weber, P.H., 1975, Correlation of density banding in coral skeletons with environmental parameters: the basis for interpretation of chronological records preserved in the corallia of corals: Paleobiology, v. 1, p. 137-149.

Weber, J.N., and Woodhead, P.M.J., 1972, Temperature dependence of oxygen-18 concentration in reef coral carbonates: Journal of Geophysical Research, v. 77, p. 463-473.

Weisgerber, G., 1982, Towards a history of copper mining in Archaeology, *in* Muhly, J.D., Maddin, R., and Karageorghis, V., eds., Early Metallurgy in Cyprus: Nicosia, Cyprus, Pierides Foundation, p. 382.

Welhan, J.A., 1988, Origins of methane in hydrothermal systems: Chem. Geol., v. 71, p. 183-198.

Wellington, G.M., and Dunbar, R.B., 1995, Stable isotopic signature of El Nino- Southern Oscillation events in eastern tropical Pacific reef corals: Coral Reefs, v. 14, p. 5-25.

APPENDIX 1

Results of Si analyses that were performed on Tutum Bay seawater. Samples were collected systematically at varying distances from vent sites in order to reconstruct the effect of venting on local seawater composition.

Sample No.	Depth (m)	Distance (m)	Direction	Si (ppm)
1a	0.3	50	W	0.5630
2a	0.3	10	W	1.1363
3a	0.3	5	W	0.7224
4a	0.3	1	S	0.7491
5a	0.3	5	S	1.0645
6a	0.3	11	S	1.1912
7a	0.3	50	S	1.0702
8a	0.3	50	N	0.8787
9a	0.3	12	N	0.6854
10a	0.3	5	N	0.6999
11a	0.3	1	N	0.7923
12a	0.3	1	E	0.8223
13a	0.3	5	E	1.0223
14a	0.3	10	E	1.0727
15a	0.3	50	E	0.8479
16a	0.3	10	NE	1.1057
17a	0.3	20	NE	1.0527
18a	0.3	12	NW	0.9450
19a	0.3	25	NW	0.9152
20a	0.3	25	SW	0.7254
21a	0.3	12	SW	1.1200
22a	0.3	25	SE	0.9712
23a	0.3	10	SE	0.9230
1b	5.0	50	W	0.2563
2b	6.0	10	W	0.2727
3b	4.0	5	W	0.2696
4b	3.5	1	S	0.5610
5b	3.0	5	S	0.4422
6b	3.5	11	S	0.3854
7b	3.0	50	S	0.4032
8b	4.0	50	N	0.1859
9b	3.5	12	N	0.2100
10b	3.0	5	N	0.3830
11b	3.0	1	N	0.2809
12b	4.0	1	E	0.1791
13b	3.5	5	E	0.2590
14b	3.5	10	E	0.2895
15b	2.5	50	E	0.4900
15b	2.5	50	E	0.4900
16b	3.0	10	NE	0.2479
17b	2.5	20	NE	0.4308
18b	4.0	12	NW	0.3541
19b	5.0	25	NW	0.2492
20b	4.5	25	SW	0.2886
21b	4.0	12	SW	0.2910
22b	3.0	25	SE	0.3183
23b	3.0	10	SE	0.3333
1c	10.0	50	W	0.1308
2c	8.5	10	W	0.3117
3c	7.0	5	W	0.3141
4c	6.5	1	S	0.5895
5c	6.0	5	S	0.3390
6c	6.5	11	S	0.4058
7c	7.0	50	S	0.4208
8c	8.0	50	N	0.1627
9c	7.0	12	N	0.2706
10c	6.0	5	N	0.2238
11c	6.5	1	N	0.3121
12c	8.0	1	E	0.2159
13c	7.5	5	E	0.2395
14c	7.0	10	E	0.4182
15c	5.0	50	E	0.2830
16c	6.0	10	NE	0.3295
17c	5.5	20	NE	0.4773
18c	8.0	12	NW	0.4270
19c	10.0	25	NW	0.2848
20c	8.5	25	SW	0.3033
21c	8.0	12	SW	0.4177
22c	6.0	25	SE	0.2833
23c	7.0	10	SE	0.3636
Vent 1	0.3	-	-	1.88
Vent 1	3.0	-	-	1.00
Vent 2	0.3	-	-	0.86
Vent 2	3.0	-	-	3.52
Vent 3	0.3	-	-	2.41
Vent 3	3.0	-	-	5.44

Note: Sample numbers were used as follows: same number indicates the same location, same letter indicates the same depth. Depth is measured in meters from sea level. Distance was measured from the location of vent 2 and in combination with the direction data gives the exact location. For example, sample 15b was collected exactly 50 m east of vent 2 from a depth of 2.5 m below sea level. The samples vent 1 to vent 3 were collected exactly above vent sites.

APPENDIX 2

Results of isotope analyses in δ-notation for *Tridacna gigas* (T-1) and *Porites lobata* (C-1 to C-29) sub-samples from Ambitle Island on the PDB scale. For the corals, sample points are measured parallel to the growth axis from the top of a coral slab. *Tridacna gigas* samples do not necessarily correspond to the same time span as the coral samples.

Sample Point (mm)	C-1 $\delta^{13}C$ ‰	C-1 $\delta^{18}O$ ‰	C-2 $\delta^{13}C$ ‰	C-2 $\delta^{18}O$ ‰	C-3 $\delta^{13}C$ ‰	C-3 $\delta^{18}O$ ‰	C-4 $\delta^{13}C$ ‰	C-4 $\delta^{18}O$ ‰	C-5 $\delta^{13}C$ ‰	C-5 $\delta^{18}O$ ‰	C-6 $\delta^{13}C$ ‰	C-6 $\delta^{18}O$ ‰	C-7 $\delta^{13}C$ ‰	C-7 $\delta^{18}O$ ‰	C-8 $\delta^{13}C$ ‰	C-8 $\delta^{18}O$ ‰	C-29 $\delta^{13}C$ ‰	C-29 $\delta^{18}O$ ‰	T-1 $\delta^{13}C$ ‰	T-1 $\delta^{18}O$ ‰
1	-1.84	-4.26	-3.66	-4.61	-2.39	-3.77	-3.12	-5.27	-2.11	-5.26	-2.71	-5.27	-3.05	-5.49	-3.89	-5.38	-1.74	-4.60	1.96	-1.88
2	-2.20	-4.75	-2.81	-4.65	-2.35	-4.64	-3.30	-5.38	-1.41	-5.24	-2.07	-5.33	-3.74	-5.11	-4.04	-5.43	-1.76	-4.95	1.96	-1.99
3	-1.65	-4.62	-2.96	-4.74	-3.00	-4.82	-3.30	-5.58	-1.25	-5.40	-2.24	-5.20	-2.60	-5.63	-4.40	-5.78	-1.32	-4.99	2.01	-1.80
4	-2.33	-4.84	-2.64	-4.59	-3.31	-4.96	-3.29	-5.55	-1.36	-5.50	-2.19	-5.22	-2.38	-5.10	-4.18	-5.51	-1.12	-4.73	2.09	-1.91
5	-2.42	-4.72	-3.05	-4.61	-2.46	-4.74	-2.81	-5.43	-1.67	-5.41	-2.31	-5.44	-2.33	-5.60	-4.34	-5.62	-1.09	-5.13	2.05	-1.94
6	-2.29	-4.67	-2.43	-4.78	-2.52	-4.77	-2.90	-5.40	-2.12	-5.56	-2.21	-5.47	-2.35	-5.30	-3.94	-5.52	-1.40	-5.30	2.18	-1.83
7	-2.23	-4.68	-2.49	-4.76	-2.36	-4.81	-3.34	-5.49	-1.91	-5.58	-2.49	-5.56	-2.97	-5.57	-4.42	-5.64	-1.19	-5.09	2.13	-1.91
8	-2.50	-4.64	-3.06	-4.81	-2.69	-5.09	-3.31	-5.66	-1.75	-5.71	-2.16	-5.42	-2.70	-5.24	-4.20	-5.60	-0.68	-5.17	2.12	-1.84
9	-2.67	-4.80	-2.17	-5.01	-1.97	-4.13	-3.33	-5.65	-1.58	-5.44	-2.20	-5.49	-2.32	-5.56	-4.16	-5.86	-1.16	-5.02	2.24	-1.87
10	-2.33	-4.67	-2.35	-4.88	-2.15	-3.98	-3.44	-5.48	-1.68	-5.54	-1.82	-5.39	-2.17	-5.13	-3.69	-5.86	-0.48	-5.19	2.22	-2.16
11	-2.15	-4.88	-3.14	-4.93	-2.45	-4.61	-3.72	-5.67	-1.39	-5.37	-2.04	-5.39	-2.15	-5.63	-4.08	-5.90	-1.01	-5.13	2.21	-2.09
12	-2.91	-4.82	-3.02	-4.89	-2.64	-4.95	-3.48	-5.07	-1.13	-5.43	-2.13	-5.36			-3.76	-5.90	-1.28	-5.16		
13	-2.47	-4.73	-2.25	-5.11	-2.80	-5.27	-3.34	-5.51	-1.00	-5.39	-2.35	-5.50			-3.57	-5.84	-1.10	-5.10		
14	-2.72	-4.76	-2.21	-4.86	-2.78	-5.13	-3.37	-5.63	-1.03	-5.42	-2.38	-5.56			-3.66	-5.97	-0.68	-4.99		
15	-2.54	-4.87	-2.34	-4.96	-2.94	-5.12	-2.88	-5.67	-1.14	-5.39	-2.36	-5.51			-3.89	-5.93	-0.55	-5.10		
16	-2.40	-4.83	-2.85	-4.70	-3.32	-5.28	-3.01	-5.22	-1.56	-5.62	-2.40	-5.25			-4.10	-5.75	-1.13	-5.23		
17	-2.04	-4.73	-2.73	-4.77	-2.96	-5.36	-2.90	-5.00	-1.57	-5.70	-2.78	-5.47			-4.34	-5.44	-1.10	-5.27		
18	-3.02	-5.07	-2.13	-4.88	-2.85	-5.52	-2.90	-5.69	-1.79	-5.41	-3.02	-5.33			-4.45	-5.65	-1.41	-5.26		
19	-3.03	-4.83	-2.50	-4.94	-3.09	-5.34	-3.36	-5.62	-1.45	-5.51	-2.34	-5.48			-4.18	-5.98	-1.32	-5.24		
20	-2.98	-4.97	-2.58	-5.55	-3.12	-5.59	-3.75	-5.44	-1.76	-5.37	-2.53	-5.53			-4.22	-5.58	-1.55	-5.39		
21	-2.82	-4.73	-2.46	-4.98			-3.36	-5.64	-1.90	-5.17	-2.23	-5.45			-4.34	-5.75	-1.46	-5.29		
22	-3.07	-4.88	-2.47	-4.92			-3.19	-5.81	-1.53	-5.21	-1.97	-5.50			-4.16	-5.93	-0.99	-5.11		
23	-3.22	-4.76	-2.30	-5.06			-3.48	-5.86	-1.87	-5.45	-1.58	-5.62			-4.33	-5.99	-1.05	-4.96		
24	-2.80	-4.69	-2.91	-5.05			-3.48	-5.72	-2.35	-5.54	-2.03	-5.62			-4.10	-5.65	-0.54	-5.03		
25	-3.41	-4.81	-2.68	-4.98			-3.54	-5.81	-1.88	-5.43	-2.27	-5.69			-3.38	-5.01	-1.20	-5.10		
26	-3.44	-4.86	-2.41	-4.78			-3.72	-5.83	-2.24	-5.45	-2.61	-5.72			-3.50	-5.71	-0.64	-4.68		
27	-3.14	-4.85	-2.55	-5.42			-3.74	-5.86	-1.84	-5.47	-2.41	-5.57			-4.24	-5.81	-0.90	-4.61		
28			-2.47	-5.25																
AVG	-2.62	-4.77	-2.63	-4.91	-2.71	-4.89	-3.31	-5.55	-1.64	-5.44	-2.29	-5.46	-2.61	-5.40	-4.06	-5.70	-1.11	-5.07	2.11	-1.93
MIN	-3.44	-5.07	-3.66	-5.55	-3.32	-5.59	-3.75	-5.86	-2.35	-5.71	-3.02	-5.72	-3.74	-5.63	-4.45	-5.99	-1.76	-5.39	1.96	-2.16
MAX	-1.65	-4.26	-2.13	-4.59	-1.97	-3.77	-2.81	-5.00	-1.00	-5.17	-1.58	-5.20	-2.15	-5.10	-3.38	-5.01	-0.48	-4.60	2.24	-1.80

APPENDIX 3

Means comparison for $\delta^{13}C$, $\delta^{18}O$ and Sr analyzed in corals from Ambitle Island. Column A shows the distribution of values for each sample. The dashed line across the middle is the grand mean. The top and bottom of the diamonds indicate the 95% confidence interval and the line through the middle of a diamond indicates the mean. In order to account for the imbalance in the data set (i.e., the means do not all have the same number of observations), I plotted comparison circles in columns B and C. The radius of a circle is the 95% confidence interval and, therefore, the larger a circle the lesser the number of observations. In order for means to be significantly different, the angle of intersection has to be less than 90°. Column C shows comparison circles that attempt to correct for a statistical Type I error (multiple comparisons) using the Tukey-Kramer test (Swan and Sandilands, 1995).

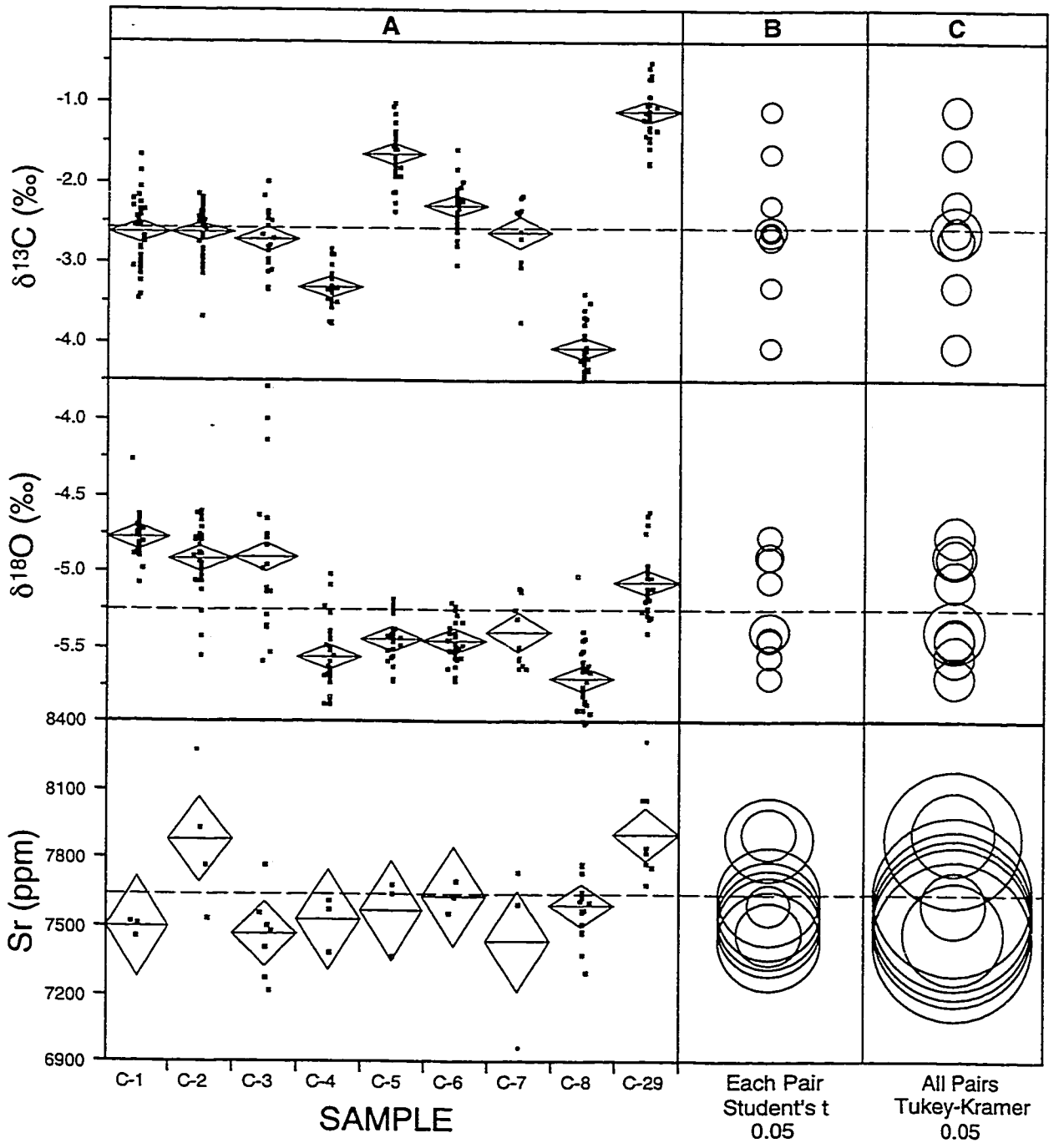
A
B
C
δ13C (‰)
-1.0
-2.0
-3.0
-4.0
δ18O (‰)
-4.0
-4.5
-5.0
-5.5
Sr (ppm)
8400
8100
7800
7500
7200
6900
C-1
C-2
C-3
C-4
C-5
C-6
C-7
C-8
C-29
SAMPLE
Each Pair
Student's t
0.05
All Pairs
Tukey-Kramer
0.05

IMAGE EVALUATION TEST TARGET (QA-3)

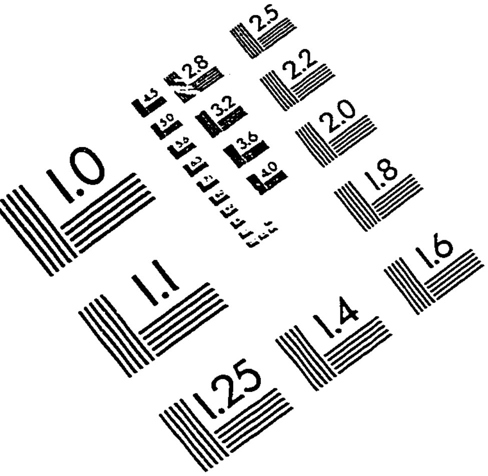

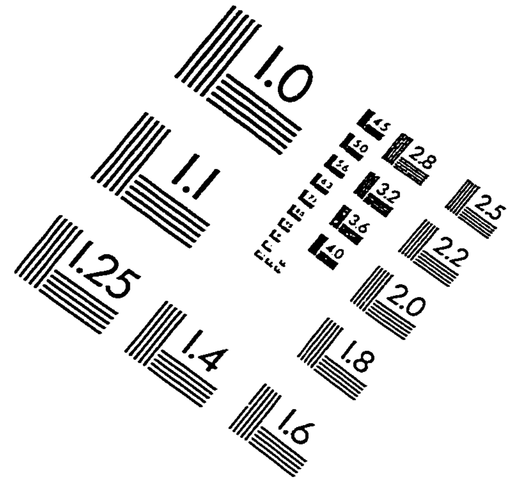

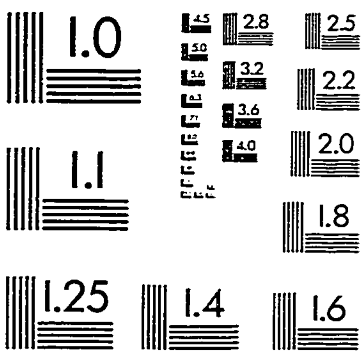

150mm

6"

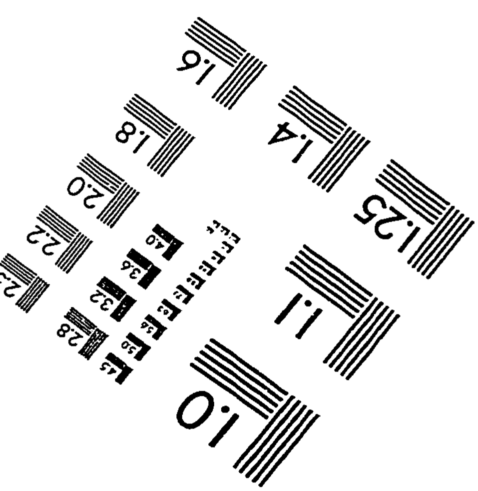

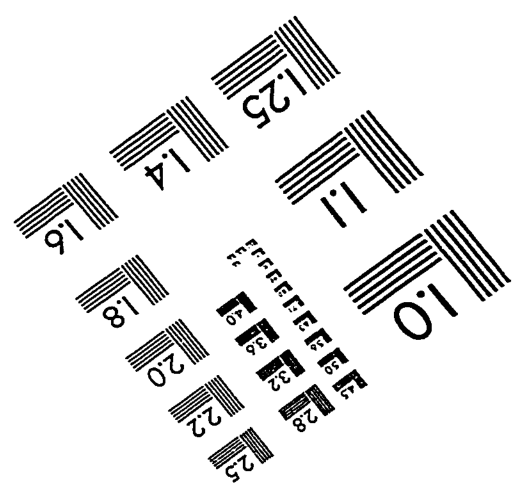

APPLIED IMAGE, Inc
1653 East Main Street
Rochester, NY 14609 USA
Phone: 716/482-0300
Fax: 716/288-5989